Dipl.-Ing. Matthias Karl Scharrer

Statistical Modeling and Optimization of Automotive Lithium-Ion Cells

DOCTORAL THESIS

to achieve the university degree of

Doktor der technischen Wissenschaften

submitted to

Graz University of Technology

Supervisor

Univ.-Prof. Dipl.-Ing. Dr. techn. Daniel Watzenig

Institute of Electrical Measurement and Measurement Signal Processing

Faculty of Electrical and Information Engineering

Graz, March 2021

AFFIDAVIT

I declare that I have authored this thesis independently, that I have not used other than the declared sources/resources, and that I have explicitly indicated all material which has been quoted either literally or by content from the sources used. The text document uploaded to TUGRAZonline is identical to the present doctoral thesis.

Date

Signature

Art is never finished, only abandoned.

— Leonardo da Vinci

I dedicate this work to my parents who have been full of love and support. And waiting.

Abstract

The topic of this thesis is multi-physical modeling and parameter identification of a lithium-ion cell as commonly used in automotive applications and mobile appliances, as well as parameter uncertainties on the basis of measurements with the aim of improving operation strategies and a cell's efficiency.

Lithium-ion cells have become ubiquitous in our everyday life as a means to store electrical energy in mobile applications, but electric cars pose greater challenges. Their popularity has led to increased research focus on efficient control strategies and cell design to improve ecological sustainability and reduce environmental impact.

This work provides an effective methodology to find parameters including their validity ranges to describe cells (and subsequently batteries) better in order to enable the use of high quality models for operation control design.

Literature solves similar tasks, the present work combines four established methods to deliver the best possible results:

First, simulation models with increasing level of detail enable to reproduce and predict the behaviour of battery cells in response to electric excitation, providing a basis for subsequent identification methods. The use of simulation models is paramount, as even precisely manufactured cells do not permit to accurately perform mathematical operations on their resulting measurement data. The type of simulation model used results in a large number of parameters (up to 50) that define the model behaviour.

To gather intelligence about every model parameter's significance, screening methods yield further insight into the relative ranking. As a second step, parameter screening using the Morris-one-at-a-time method provides a ranking of model parameters while efficiently utilizing available computation resources. While this screening yields a merely qualitative result, it outperforms other global sensitivity analysis methods, such as variance decomposition based ones, in terms of runtime (10-100x speedup). In contrast to even faster other one-at-a-time methods it also takes non-linearities and combined effects into account. This information leads to a reduced model or parameter subset to focus identification on.

Depending on the model complexity, direct parameter identification methods are usually infeasible, as they require too many simulations to be run and subsequently take too much time (several days to weeks). Space mapping has proven to be a suitable method for accelerating the optimization process in this context. This surrogate-based technique effectively reduces the number of required simulations. A full cell model using semi-empirical RC-models and a Doyle-Fuller-Newman model could be identified successfully. The rigorous derivation of an adjoint model for the fast and precise gradient calculation improves the run-time reduction further. Yet, the developed method could not be applied to the full range of available measurements.

As an alternative, fast model implementations together with a new hybrid optimization method allow for determining the full parameter set of two complex models, within an hour or a day, respectively. This is a significant advance over the three-week period for

a complete parameter set that had been previously reported in the literature.

Finally, an adaptive Markov chain Monte Carlo method with early or delayed rejection for uncertainty quantification provides a means to sample from the posterior parameter values assuming a standard deviation of the measured cell voltage of 15 mV. This computationally expensive step further enriches the estimated parameter sets by the posterior probability density with a relatively small number of random samples.

While the space mapping approach shows a significant speed-up, a very fast model implementation clearly outperforms the former during parameter identification as well as during uncertainty quantification in terms of computational speed and effectivity.

Keywords: Lithium-Ion, Battery, Optimization, Space Mapping, Uncertainty quantification, Markov-Chain Monte-Carlo Simulation

Zusammenfassung

Thema dieser Arbeit sind die multiphysikalische Modellierung und Parameteridentifikation von Lithium-Ionen-Zellen, wie sie in Fahrzeugen und mobilen Geräten verwendet werden, sowie Parameterunsicherheiten mit dem Ziel, Betriebsstrategien und die Effizienz zu verbessern.

Lithium-Ionen-Zellen sind in unserem Leben allgegenwärtig, um elektrische Energie in mobilen Geräten zu speichern, Elektroautos stellen aber höchste Anforderungen. Ihre Beliebtheit führt zu intensiver Forschung an effizienten Regelstrategien und Zelldesign für mehr Nachhaltigkeit und geringere Umweltbelastung.

Diese Arbeit demonstriert eine effektive Methode, um Parameter einschließlich ihrer Gültigkeitsbereiche zu finden, um Zellen (und damit Batterien) besser beschreiben zu können und die Verwendung hochwertiger Modelle für das Design von Betriebsstrategien zu ermöglichen.

Die Literatur behandelt oft ähnliche Themen; die vorliegende Arbeit kombiniert vier etablierte Methoden, um bestmögliche Ergebnisse zu erzielen:

Simulationsmodelle mit zunehmendem Detaillierungsgrad ermöglichen die Wiedergabe und Prädiktion von Zellverhalten als Reaktion auf elektrische Anregung und bilden so die Basis für nachfolgende Identifizierungsmethoden. Die Verwendung von Modellen ist nötig, da selbst präzise hergestellte Zellen keine genauen mathematischen Operationen an den resultierenden Messdaten erlauben. Der Modelltyp führt zu einer großen Parameterzahl (bis zu 50), die das Modellverhalten definiert.

Screening-Methoden liefern weitere Einblicke in die Reihung der Parameter nach ihrer Bedeutung. Die “Morris-One-at-a-Time”-Methode liefert unter effizienter Nutzung der verfügbaren Rechenressourcen lediglich ein qualitatives Ergebnis. Dabei übertrifft es andere globale Sensitivitätsanalysemethoden, wie z. B. Varianzzerlegung, in Bezug auf die Laufzeit (10-100-fache Beschleunigung). Im Gegensatz zu noch schnelleren “one-at-a-Time”-Methoden werden auch Nichtlinearitäten und kombinierte Effekte berücksichtigt. Dies führt zu einem reduzierten Modell bzw. einer Parameteruntermenge zur Identifikation.

Direkte Parameteridentifikationsmethoden sind für komplexe Modelle normalerweise nicht durchführbar, da sehr viele Simulationen ausgeführt werden müssen und zu viel Zeit (Tage bis Wochen) benötigt wird. “Space Mapping” hat sich in diesem Zusammenhang als geeignete Methode zur Beschleunigung der Optimierung bewährt. Diese Ersatzmodelltechnik reduziert effektiv die Anzahl der erforderlichen Simulationen. Ein Zellmodell mit semi-empirischen “RC”-Modellen sowie ein “Doyle-Fuller-Newman”-Modell konnten erfolgreich identifiziert werden. Die Ableitung eines adjungierten Modells zur schnellen, präzisen Gradientenberechnung reduziert die Laufzeit weiter. Die entwickelte Methode konnte jedoch nicht auf eine umfassende Messung angewendet werden.

Alternativ ermöglichen schnelle Modellimplementierungen sowie eine neue hybride Optimierungsmethode die Bestimmung des vollständigen Parametersatzes zweier kom-

plexer Modelle innerhalb einer Stunde bzw. eines Tages. Dies ist ein signifikanter Fortschritt gegenüber des in der Literatur berichteten Zeitraums von drei Wochen für einen vollständigen Parametersatz.

Schließlich ermöglicht ein adaptives "Markov-Ketten-Monte-Carlo"-Verfahren mit früher oder verzögerter Zurückweisung zur Unsicherheits-Quantifizierung das Abtasten der a-posteriori Verteilung der Parameterwerte unter Annahme einer Standardabweichung der Zellspannung von 15 mV. Dieser rechenintensive Schritt erweitert die geschätzten Parametersätze um Wahrscheinlichkeitsdichten bei einer relativ geringen Zahl an Zufallsstichproben.

Während der "Space-Mapping"-Ansatz eine signifikante Beschleunigung bewirkt, übertrifft eine sehr schnelle Modellimplementierung diese sowohl bei der Parameteridentifikation als auch bei der Unsicherheits-Quantifizierung in Bezug auf Rechengeschwindigkeit und Effektivität deutlich.

Schlagwörter: Lithium-Ionen, Batterie, Optimierung, Space Mapping, Unsicherheits-Quantifizierung, Markov-Ketten Monte-Carlo Simulation

Acknowledgements

I wrote this thesis throughout my work as a researcher in the following funded projects: Klima- und Energiefondsprojekt *ELTOBATT*, as well as the K2-Mobility project *E03-T02 MoLiC*. Thus, I would like to acknowledge financial and technical support of the following companies and organizations: The publication was written at Virtual Vehicle Research GmbH in Graz. Virtual Vehicle Research GmbH has received funding within COMET Competence Centers for Excellent Technologies from BMK, BMDW, the Province of Styria (Dept. 12) and the Styrian Business Promotion Agency (SFG). The Austrian Research Promotion Agency (FFG) has been authorised for the programme management.

In addition, I gratefully acknowledge partial financial support from Climate- and Energy Fund ("Klima- und Energiefonds") as part of the program New Energy 2020 ("NEUE ENERGIEN 2020") of the Federal Province of Styria/Austria for the project *ELTOBATT* in which part of the presented research results were achieved.

Part of the research leading to these results has received funding from the European Union's Seventh Framework Programme (FP7/2007-2013) under Grant Agreements n^0 266090 (SOMABAT), n^0 605170 (TRANSFORMERS) and n^0 608897 (iCOMPOSE).

Eventually, I acknowledge partial financial support from the European Union's Horizon 2020 research and innovation programme under grant agreement n^0 769850 (ASSURED).

During the course of this study, I have received the assistance of many people to whom I am very grateful. First and foremost, I want to thank my advisor, Professor Daniel Watzenig, for supporting me, providing invaluable guidance and advice throughout my studies. Thank You!

Further, I am very grateful for all valuable feedback and cheer-ups from Professor Colin Fox at the *University of Otago* throughout my work on Bayesian inference with real measurements and his willingness to take part in the review and examination committee.

I appreciate the great collaboration with Professor Stefan Volkwein at the *University of Konstanz*, who paved the way for space-mapping with battery models.

I wish to thank Professor Heikki Haario at the *Lahti University of Technology*, for guidance and great collaboration with regard to Bayesian methodology.

I would like to convey my utmost gratitude to Professor George S. Dulikravich for being a perfect host during my short stay at the *Florida International University*, and giving very valuable advice in multiple ways. I would also like to thank Sohail R. Reddy for being a great guy.

I am very grateful to all my friends and colleagues who became friends during a long journey for the great time we had together and for countless fruitful discussions.

Special thanks go to my parents, my wife and my kids for their endless support and love. Your encouragement during both, the good times and the bad times kept me going.

Graz, March 23, 2021

Matthias Karl Scharrer

Contents

1

Introduction

Countries' representatives gathered at the Paris Climate Conference (COP21) in 2015 agreed to increase their efforts to limit climate change. Almost one quarter of current global energy-related and climate change causing greenhouse gas (GHG) emissions are contributed by the growing transport sector. According to the International Energy Agency, limiting effects will require at least 20 % of all road transport vehicles globally to be electrically driven by 2030 (United Nations Framework Convention on Climate Change, 2015).

The automotive industry's choice to store energy in electric vehicles is the lithium-ion battery. Utilizing the battery types used in consumer appliances as a starting point, the batteries have been further improved to fulfill the automotive requirements. In addition, over the last decades also in other areas applications of Li-Ion (Li^+) cells have drastically increased. With the continuous implementation of the Li^+ cells in household appliances, automotive, aerospace and defense industries, accurate modeling and simulation of them is paramount: modeling and simulation enables engineers to vary all design and material parameters in a cell at a very low cost while observing the results almost instantly. For a battery manufacturer, simulations aid in the efficient design of new products, and for a device manufacturer, simulations support their engineering efforts with respect to covering critical operation states (Nyman et al., 2018).

1.1. The Electrochemical Cell

Figure 1.1 by Chawla et al. (2019) shows the fundamental structure and function of a rechargeable Li^+ cell or "*Battery Cell*", commonly shortened to "*Battery*", where the latter technically is but an ensemble of at least two or more battery cells.

A cell comprises three major components:

1. the positive **electrode** — intercalates and deintercalates ions and features electron conductivity.
2. the negative **electrode** — offers similar possibilities as the positive electrode, but at a lower potential.

3. the **electrolyte** — a liquid or solid transport medium that enables charge transfer between the electrodes by means of ions.

By electrochemical oxidation and reduction – "*redox*" – reactions occurring at the two electrodes, chemical energy is set free and electrons are transferred from one active material to the other through an *external* electric circuit. The electrolyte between the electrodes serves as ionic conductor but is an electronic isolator. For safety reasons, to prevent electrodes from a electronic short-circuit, the "*separator*" foil – a permeable membrane – separates both electrodes from one another. During *discharge*, the anode

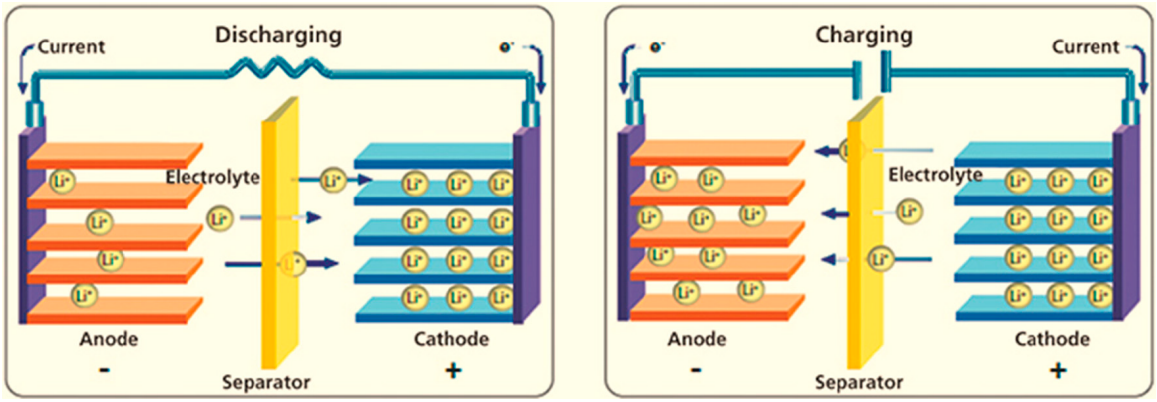

Figure 1.1.: *Basic working principle of a* Li^+ *battery (Chawla et al., 2019)*

is oxidized, Li^+ deintercalate and migrate through the separator and the cathode is reduced, Li^+ intercalate there. At the same time, electrons freed at the anode travel through the external circuit and combine with ions at the cathode again. During charge we apply external power and force Li^+ and electrons to migrate in reverse direction (Linden & Reddy, 2002).

Depending on the application, in the automotive domain in particular, a "*Module*" comprise of a number of cells, which can be connected in series or in parallel. In addition to the cells, a module also contains structural parts, measurement and other simple electric devices. The most dominant rationale to build modules is legal voltage limits and ease of handling, as voltages above 60 V DC require special precautionary measures for further manipulation and processing (Fischer, 2013).

One or more modules combined with the remainder of sensors and controls constitute a battery "*Pack*". In order to operate in a safe range and to control operation in general, a Battery Management System (BMS) accompanies a pack and thus makes it a full battery "*system*". The BMS reads all sensors available from module or pack level to determine all cell voltages, several temperatures, currents at important points and handles the connection and disconnection of the battery system (Plett, 2016).

1.1.1. Related Terminology and Quantities

In this section, we provide a very brief summary to the essential terminology in the context of batteries, that are important for cell specifications, and which will be used throughout the remainder of this work. Unless stated otherwise, all terms are used

to describe characteristics of both, a single battery cell and an entire battery system (Leuthner, 2013; Canova, 2016).

Capacity is the amount of electrical charge that may be retrieved from a power source under specific discharge conditions. The capacity depends on, first and foremost, the type and amount of active materials in the cell, the discharge current, the discharge cut-off voltage, and temperature. The unit of capacity is A s, a cell's capacity is usually rated in A h.

C-Rate describes the rate of charge or discharge current in normalized form and is commonly accepted in the field of battery engineers. The general expression is "C/xx", where the number xx indicates the number of hours to completely discharge the battery at a constant current. So C/20 is the current to be drawn at which the battery voltage will span the complete range within 20 hours, C/1 is the current at which the process will take 1 hour; for higher currents, e.g. "C/1", "C/0.5", "C/0.3333", one would usually write "1 C", "2 C", "3 C", respectively. "1 C" corresponds numerically to the battery nominal capacity. The C-Rate's unit is h^{-1}.

State of Charge (SoC) is a dimensionless value describing the amount of usable charge in the battery at a given point in time and usually expressed as a percentage of the rated capacity – similar to a fuel gauge in a car.

Energy of a cell is calculated according to the product of a capacity and average or nominal discharge voltage. The unit is W s, a cell's energy capacity is usually rated in W h.

Specific Energy relates energy to the mass of the battery and has unit $\mathrm{W\,s\,kg^{-1}}$.

Energy Density relates energy to the geometric volume of the battery and has unit $\mathrm{W\,s\,m^{-3}}$.

Power is the product of current and voltage, e.g. during discharge. It has the unit W.

State of Health (SoH) is a measure of the usable life of a battery cell, i.e. how long the battery will last before it needs to be replaced. Batteries usually slowly degrade both in terms of capacity and power. Battery useful life usually prescribed as point at which the energy (and/or power) capacity has degraded by 20 %.

Efficiency of a $\mathrm{Li^+}$cell is very high, mostly around 95 %. It is defined as the fraction of released energy during discharge compared to the previously stored energy during charge.

Terminal voltage is the voltage that exists between the battery terminals when a load is applied. The terminal voltage varies with the operating conditions of the battery. Its unit is V.

Open Circuit Voltage (OCV) is the difference in potential between the terminals of a cell when the battery is fully rested, i.e. the battery has been subjected to an open circuit for a substantial period of time. The Open Circuit Voltage (OCV) generally depends on the battery charge level and temperature. The unit of the OCV is V.

Internal Resistance indicates an overall resistance within the battery, generally different for charging and discharging, also dependent on the battery charge level. As the internal resistance increases, the battery efficiency decreases and thermal stability is reduced as more of the charging energy is converted into heat. Its unit is Ω.

1.2. Problem statement and Motivation

Accurate modeling and analysis of a battery usually involves the internal states of its cells and modules to be known. These internal states may include abstract quantities, e.g. State of Charge (SoC) and State of Health (SoH), and physical quantities, e.g. potentials, temperature and concentrations. Only very few of these quantities can be measured directly through experimentation; this sparsely available information aids in deducing most of the abstract quantities. For model-based deducing parameters the material properties of a cell are of utmost importance.

This gives rise to the traditional parameter estimation problem. Parameter estimation techniques can be non-intrusive and non-destructive depending on whether the model response can be obtained non-intrusively and non-destructively. Hence, the main question to be answered in this work may be stated as follows: *Given only the voltage, how can the material properties and model parameters of the Lithium-Ion cell model be estimated?*

In practice, for some models one can use standard optimization routines implemented in computational software packages. In the Li-cell modeling case, it is more often highly adapted optimization software. However, since all available data contains measurement errors, the estimated unknowns remain to some degree uncertain.

A natural question then arises: *if measurement noise corrupting the data follows some statistical distribution, what is the distribution of the possible solutions after the estimation procedure?*

1.2.1. State of the Art

Typical high-fidelity simulation models are based on the equations described by Doyle–Fuller–Newman model (DFN) (Newman & Thomas-Alyea, 2004). The DFN is a homogenized system of Partial Differential Equations (PDEs), that typically comprise of more than 50 parameters, a vast majority of which cannot be determined experimentally. This model may be simplified further to a Single–Particle model (SPM) by assuming no electrolyte effects or spatially resolved effects, e.g. varying concentrations in particles within the same electrode. Although this is known to result in less accuracy in general, it is still possible to achieve very high model accuracy by taking the SPM's limitations into account, e.g. currents below 1 C, i.e. the equivalent of a full discharge in more than one hour (Santhanagopalan et al., 2006; Ning & Popov, 2004). Estimating the models parameters based on non-intrusive measurements is a very demanding task and significant effort has been spent on devising algorithms for the identification.

Besides the mechanistic models – DFN and SPM –, a more phenomenological approach is represented by the large class of equivalent circuit models or "RC-models". Computation of electrode and electrolyte kinetics are limited w.r.t. their interpretability, yet RC models are a balanced trade-off between computational speed, required resources and accuracy (F. Pichler & Cifrain, 2014). Although parametrization of RC models is typically done in frequency domain by performing electrochemical impedance spectroscopy, as introduced by Boukamp (1986), we perform parametrization in time domain, similar

to related work in the following paragraphs.

Hu et al. (2012) adopted a Particle Swarm Optimization (PSO)-based global optimization approach. The objective function for the model parameter optimization was defined for model accuracy, measured by the average Root-Mean-Square Error (RMSE) between the test datasets and the output from the optimized models. The optimization was configured to 10 000 iterations, which was considered infeasible for the problem in this work.

Kumar & Bauer (2010) use Multiobjective Genetic Optimization Algorithm (MOGA) to fit a first-order RC-model to data-sheet data. In this case, the parameters of the RC-model are expressed as polynomials of SoC, charge and discharge rates.

In this work, we present a novel approach to parameter identification in coupled 3D cell models. We apply the space mapping based surrogate optimization approach originally devised by Bandler et al. (1994) to a Finite Element Method (FEM) based electric 3D model of a lithium cell, using coupled 0D second-order RC models to model the electrochemical characteristics.

Schmidt et al. (2010) successfully identified 33 DFN parameters using a pattern search algorithm. By utilizing the Fisher information matrix, they devised an automatic model subset selection procedure to focus on identifiable parameters. Speltino et al. (2009) performed parameter identification in a SPM to identify nine parameters. Santhanagopalan et al. (2007) used the Levenberg-Marquardt algorithm to identify five parameters in the DFN and the SPM under constant charge and discharge conditions. Forman et al. (2012) performed parameter identification of 88 parameters using a genetic algorithm. To date, this is the latest attempt in estimating a significant number of parameters in the DFN. Recently, Jin et al. (2018) also performed sensitivity analysis to identify the five most sensitive parameters. They then used Levenberg-Marquardt algorithm to estimate the values of these five parameters. A parallel genetic algorithm was used by Zhang (2013) to identify 29 parameters in the pseudo-two-dimensional (P2D) model. They reported a computing time of 22.3 hours to identify the 29 parameters. Bizeray et al. (2019) identified three parameters in their single particle model. They also identified the independent parameters that can be uniquely, simultaneously estimated in the single particle model. Uddin et al. (2016) estimated a total of three parameters in the DFN model using the differential evolution algorithm.

Previous works cited above have reported solution times ranging from 22 hours up to three weeks. Recently, Reddy et al. (2019) used a hybrid optimization approach to estimate a full set of 44 parameters in the DFN case within 14 hours up to 0.28 % relative error. This work drastically accelerates the parameter estimation of several parameters in the SPMs and DFNs, by making use of several minimization algorithms and continuously switches between them to accelerate convergence and avoid local minima.

First results of the Markov Chain Monte Carlo (MCMC) methodology in the context of Bayesian Inference for Li^+-cell parameter estimation for five parameters under aging influence have been reported by Ramadesigan et al. (2011). In the context of DFN models, they compare Bayesian inference with traditional Gauss-Newton based optimizers for parameter estimation.

Scharrer, Haario, & Watzenig (2014) first presented a thorough analysis of uncertainty quantification of a dynamic pulse profile for a synthetic fitting problem, more generally known as “inverse crime” (Wirgin, 2004).

Tagade et al. (2016) presented a Bayesian calibration framework for estimation of the DFN parameters. In the absence of holistic physical understanding, their framework also quantifies structural uncertainty in the calibrated model to test the validity of new physical phenomena before incorporation in the model, e.g. temperature dependence of lithium plating formation at low temperature.

In this work, we focus on the evaluation of the methodology developed by Scharrer, Haario, & Watzenig (2014) in the context of real measurement data, while providing further improvements. The MCMC sampling developed originally by Metropolis et al. (1953); Hastings (1970) is used for numerical implementation of the proposed framework.

To further improve the acceptance rate of the algorithm and enhance the efficiency of the algorithm, we adopt the Single Component Metropolis- Hastings scheme, presented in the original paper by Metropolis et al. (1953). In Addition, we extend this approach by iteratively adapting the proposal kernel as we proceed in the Markov chain, as introduced by Haario et al. (1999, 2001) and test several stages of proposals as proposed by Haario et al. (2006).

1.3. Significance of the Work/Contribution

This section presents the outline of the thesis and lists contributions and novelties of each chapter in more detail.

Chapter 2 presents a purpose driven framework for modeling of a single cell or a surrogate of a full battery pack on the basis of modeling the effects using a semi-empirical Ansatz down to very detailed electro-chemical modeling taking into account mechanistic effects on a very detailed level or even dual scale inside the cell. Section 2.3 extends the general idea of semi-empirical modelling to the 3D-case of full-cell modelling with spatial resolution. Section 2.4.2 deals with the numerical solution scheme to solve the system of non-linear PDEs that resemble the DFN. Section 2.5 is about simplification of the very detailed electro-chemical system by linearization and covers the mathematical steps to the reformulation.

The most significant achievements in Chapter 2 are

- Stating a model framework to describe the electrical behavior of Li^+ batteries
- Empirical models
- A use case to Model Predictive Control (MPC) in the context of route planning
- Electrochemical models
- Numerical treatment of a system of non-linear PDEs
- Surrogate modeling by linearization of a FEM based PDE system

Chapter 3 deals with the computational techniques to solve the parameter estimation problem and Uncertainty Quantification (UQ). The methods are applicable to the models described earlier in Chapter 2, sometimes interchangeably. Almost all methods presented are not restricted to battery modeling specifically and may as well be used in a general system modeling context. Individual sections may be worked through in sequence to gain insight to models, parameters and uncertainties of parameters. Section 3.1 presents an approach identify the importance of parameters. This parameter screening technique for "*parameter importance ranking*" may be used to identify parameters to be included in a subset for optimization or estimation, e.g. in the case of computationally infeasible optimization problems caused by the number of parameters. In contrast to the standard direct optimization, we present the application of the "*spacemapping*"-technique in Sections 3.2.1 and 3.2.2.

The last part of the chapter comprises of – hybrid – stochastic optimization methods to identify parameters, including the Bayesian methodology for UQ. Section 3.4 recalls the basics of Bayesian inversion theory along with formulations and algorithms to improve the robustness and computational efficiency of the algorithms.

Major outcomes are

- Adopting the spacemapping technique to 3D-extended empirical models
- Rigorous derivation of the optimal control scheme for spacemapped non-linear systems of PDEs
- Numerical treatment of the optimization problem
- Derivation of the adjoint model of system of parabolic PDEs
- Single objective hybrid optimization of a cell model
- Bayesian calibration of a cell model
- Workflow for treating a highly non-linear system

Chapter 4 is titled "Results" and combines the results of the previously defined models in Chapter 2 with the algorithms, screening and solution schemes of Chapter 3. Details for the computational solutions are provided along with a discussion of the presented results.

Valuable contributions of the chapter may be summarized as

- Ranking of model parameters w.r.t. their importance for parameter estimation.
- Accelerated optimization of the parameters for various purposes
- A Bayesian analysis of the forward map
- Analysis of the statistical efficiency of the results
- Robustness of the results w.r.t. the variability of the parameters

1.4. Publications

The author has published the following reviewed journal publications and invited book chapters in the field of battery modeling, surrogate-based and hybrid stochastic optimization, and Bayesian UQ. Figure 1.2 depicts the relations between publications

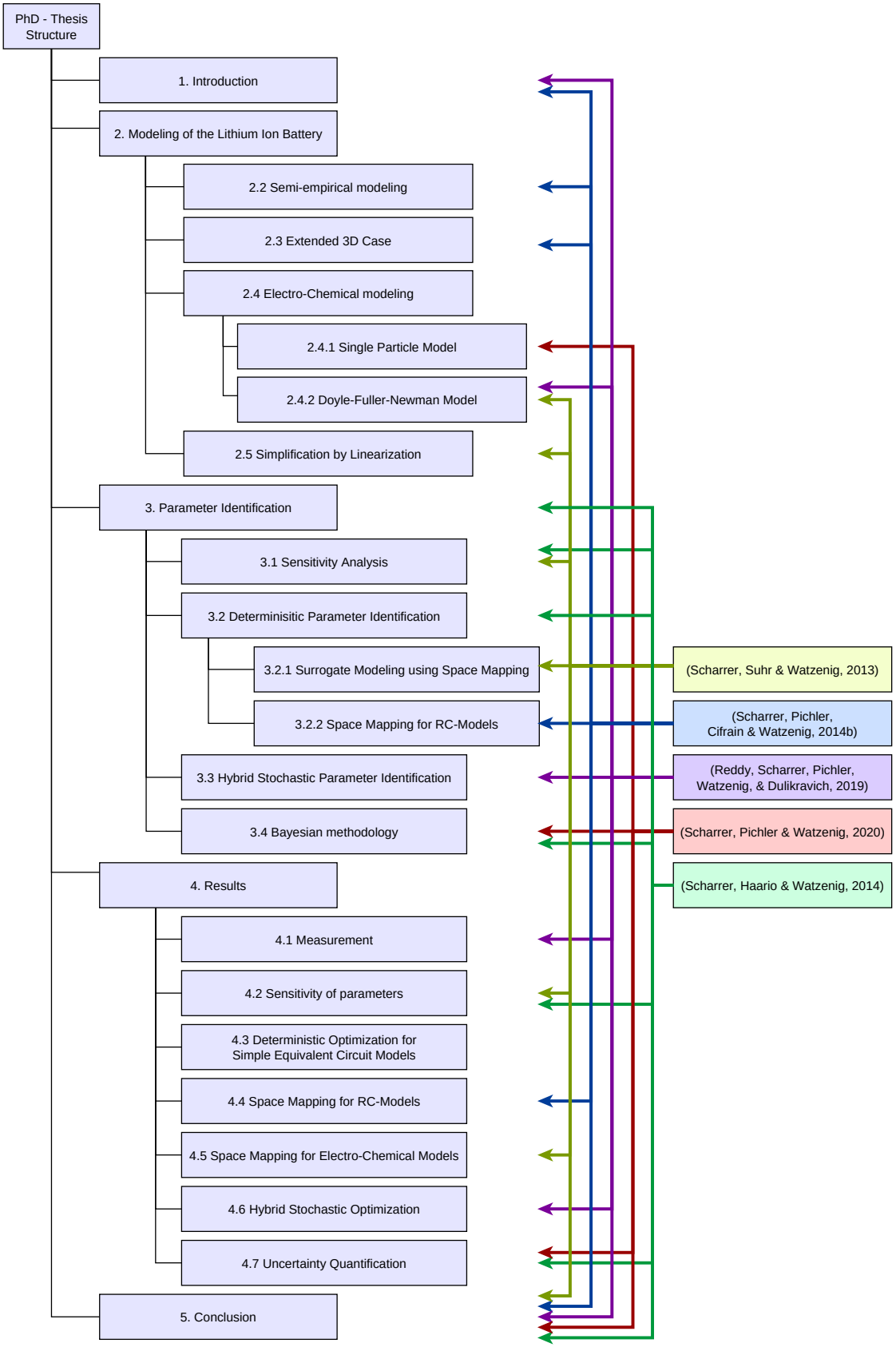

Figure 1.2.: *Publication overview of this PhD-Thesis*

and this thesis graphically. The list below also provides a brief overview of each publication:

- (Scharrer, Haario, & Watzenig, 2014) – this invited book chapter titled "Bayesian Inference for Lithium-Ion Cell Parameter Estimation" deals with an overview of Bayesian parameter estimation. After a brief introduction to the model, parameter selection and modeling of the prior is presented. Finally, results are presented of a synthetic fitting problem solved by a parallel adaptive Markov chain Monte Carlo method. We validate the approach and compare it to realistic noisy data and a separated method.

  This book chapter contributed to this thesis in Section 3.4 and results in 4.7.1.

- (Scharrer, Pichler, Cifrain, & Watzenig, 2014b) – This is the journal version of (Scharrer, Pichler, et al., 2014a). In this article the authors present an approach to estimate parameters in a very efficient way by using a single equivalent circuit model as a surrogate model for a complex 3D model on measurement data. The results of the surrogate model are periodically linked back to the original complex model via the so called space mapping method. The authors validate the approach and compare it to the original problem. As a remarkable result, the authors report the achieved reduction of computational cost by approximately 87 %, which equals a speed up factor of 8. Using high and low fidelity semi-empirical models combined with space mapping is new in the field of electrical modeling of lithium-ion cells. This approach saves much time in parametrization of coupled models while maintaining high quality results for geometrical and thermal optimization of lithium-ion cells.

  This article contributed to this thesis in sections 2.2, 2.3, 3.2.2 and results in Section 4.4.

- (Reddy, Scharrer, Pichler, Watzenig, & Dulikravich, 2019) – This paper aims to solve the parameter identification problem to estimate the parameters in electrochemical models of the Li^+ battery. The parameter estimation framework is applied to the DFN containing a total of 44 parameters. The DFN is fit to experimental data obtained through the cycling of Li-ion cells. The parameter estimation is performed by minimizing the least-squares difference between the experimentally measured and numerically computed voltage curves. The minimization is performed using a state-of-the-art hybridminimization algorithm. The DFN model parameter estimation is performed within 14 h, which is a significant improvement over previous works. Very remarkably, the mean absolute error for the converged parameters is less than 7 mV.

  This article was the main result of collaboration with Sohail Reddy and Professor George S. Dulikravich from Florida International University and it contributes to Section 2.4.2. It is the source of Section 3.3, and the results presented in Section 4.6. The pre-existing "Multiple Objective Hybrid Optimization" framework was adopted for the battery cell parameter estimation problem and applied to two models as joint work.

- (Scharrer, Pichler, & Watzenig, 2021) – This work presents an approach to quantify the uncertainty imposed on the parameters with respect to measurement

errors by using the Markov chain Monte-Carlo sampling methodology. The authors adopt the previously existing methods of Delayed Rejection Adaptive Metropolis and implement it efficiently in a parallel computing framework. Results demonstrate how to efficiently perform statistical inference on high -fidelity models. Furthermore, they enable the assessment of previously performed optimization results on Lithium-Ion cell models.

This forthcoming article – at the time of this writing designated for publishing in the "*Journal of Inverse Problems in Science and Engineering*" (IPSE) – contributed to Section 2.4.1, 3.4 and results in Section 4.7.1.

1.4.1. Other Publications

Besides the reviewed journal publications mentioned above, several other papers related to the thesis have been published and presentations have been given as a result of the work of the author during his time being a Junior and Senior Researcher at the Department of Electrics/Electronis and Software at the VIRTUAL VEHICLE Research Center. The following list provides a brief overview of those publications again with a short summary:

- (Scharrer, Cifrain, & Prochazka, 2011) – This poster presents a new way of implementing the Impedance Spectroscopy (IS) – a very common method for determining the states of electrochemical systems – in the context of the DFN. Simulations of IS spectra are usually based on equivalent-circuit models closely related to measured data. These circuit models often lead to unclear and ambivalent results. To overcome this problem this work concentrates on IS simulation with a PDE based electrochemical model with special focus on lithium-ion cells.
- (Scharrer, Suhr, & Watzenig, 2012) – In this conference paper, for the first time we present the surrogate model optimization approach based on space mapping to reduce computation time. This technique is applied to the parameter estimation problem of an electrochemical cell model by linking a coarse linearized model to the accurate model. We present results of two synthetic fitting problems solved directly and by our surrogate optimization method to validate the approach. As a remarkable result 15 % reduction of computation time for the one dimensional case and 25 % for the two dimensional case were obtained. We discuss a simple measure that doubles the achieved reduction to 48 % for the latter.
- (Scharrer, Suhr, & Watzenig, 2013) – In this conference paper we present the space mapping algorithm adapted to specific properties of a linearized surrogate model. Additionally, gradients of a cost function are calculated utilizing an adjoint model. This technique is applied to the parameter estimation problem of an electrochemical cell. We present results of a synthetic fitting problem solved by our surrogate optimization method. We validate the approach and compare it to using finite differences to approximate derivative information. As a remarkable result, 80 % reduction of computation time for the three dimensional case is obtained.

This conference paper contributed largely to the general description of the electrochemical model in Section 2.4.2 and its simplification by linearization in Section 2.5. Further, it contributed to the derivation of the space mapping algorithm in Section 3.2.1 and results in Section 4.5. Additionaly, this paper contributed the results of the sensitivity analysis presented in Section 4.2.

- (Scharrer, Pichler, Cifrain, & Watzenig, 2014a) – In this conference paper we present an approach to estimate parameters in a very efficient way by using a single equivalent circuit model as a surrogate model on measurement data. This is the original source of the above journal article (Scharrer, Pichler, et al., 2014b).

2

Modeling of the Lithium Ion Battery

The relationship between the variables of a system and the measurable responses of the system to it are described by a mathematical model. Solving such a mathematical model, i.e. the mathematical description of the reaction to the same input is referred to as a *forward problem* or *forward model*.

This chapter starts out with a general formulation of a "*forward model*" in Section 2.1. Section 2.2 presents the so-called "*semi-empirical*" modeling approach on the basis of resistor-capacitor-networks. Introducing spatially resolved resistor-capacitor-networks, Section 2.3 gives a very brief introduction into simple multi-scale modeling and introduces the notion of "*micro*"- and "*macro*"-models.

Eventually, this chapter closes with the introduction of electro-chemical models in Section 2.4, i.e. the simplified SPM and the more complex DFN, where the latter is a multi-scale model again. Due to the complexity of the DFN, Section 2.5 introduces a simplification of the DFN by rigorously deriving a linearized variant of the model.

Section 2.6 summarizes the chapter of the models presented throughout this chapter.

To yield model predictions of high accuracy, however, models must be correctly formulated and calibrated, which is presented in Chapter 3.

2.1. Forward Model in General

In general, we describe a – potentially non-linear – model as

$$\mathbf{y} = f(\mathbf{x}, \theta), \tag{2.1}$$

where $\mathbf{y}$ is the model output, $f(\mathbf{x}, \theta)$ is the model with design variables $\mathbf{x}$ and unknown parameters θ.

The formulation of the model f is typically based on the first principles of physics and chemistry. Solving the forward problem stated by f may require advanced numerical methods, e.g. FEM solution techniques, as well as a large amount of computational power, depending on the complexity and degree of detail of the model.

The properties of electrochemical cells span an enormous range of effects in

- **spatial** dimension – angstroms at the molecular level up to several dozen centimeters at the cell level, as well as
- **temporary** dimension – from nanoseconds at the molecular level to total cell aging, i.e. changes in capacity or dynamic performance in the range of several years or decades.

In general, modeling is characterized by the fact that certain properties and visible and possibly measurable behaviors are replicated on the basis of effects or simulated on the basis of mechanistic principles. In the area of battery modeling, we differentiate between very simple models, which are only supposed to represent the fill level, and the somewhat more complex semi-empirical models, which, in addition to simulating the quasi-stationary behavioral patterns, are also supposed to simulate the short-term, dynamic characteristics. The non-linear relationship between the SoC of the cell and the output voltage quickly becomes apparent, in contrast to the linear behavior that can be observed with simple capacitors.

Known principles of electrochemical models according to Randles (1947) are used to simulate the electrical and electro-thermal dynamics in so called "semi-empirical models", consisting of variations of resistors and capacitors. Semi-empirical models, due to their simplicity, are particularly suitable for carrying out very fast simulations very efficiently. For very accurate replication of the output to input relationships that characterize a simple cell a more sophisticated multi-physical – e.g. electro-chemical – model is required, such as suggested by Newman & Thomas-Alyea (2004).

2.2. Semi-empirical modeling

These simple models can be used particularly well to be coupled with simple thermal models (point masses, lumped models). For this purpose, the currents across the inner resistance or further ohmic resistances are used in particular to characterize the amount of heat generated.

Semi-empirical models comprise a class of equivalent circuit models with an arbitrary number of simple linear elements – resistances, capacitors and inductances – and possibly non-linear elements – Warburg impedances and constant phase elements – of a specific structure. Since there is no spatial distribution of quantities involved in these modeling approaches, they may be referred to as "0D" models that usually result in Ordinary Differential Equations (ODEs) of the order of the number of energy storage elements involved.

In this work, we focus on the former, including a "zero order" RC-model in Section 2.2.1 and a "second order" RC-model in Section 2.2.2. The 2nd order RC-model is later extended to a 3D spatially resolved model in Section 2.3.

2.2.1. Simple Equivalent Circuit Models

The most straight-forward way to model a non-ideal voltage source in general, such as a battery, is to define an *ideal voltage source*, with its output varying depending on the

SoC, and an *inner resistance* in series – see Figure 2.1. This neglects the short-term dynamics of a battery cell, with exception to the immediate voltage drop that follows any change of the input, i.e. current. Although this is a very crude approach to modeling a battery, it is yet very useful in the context of MPC, as used by Scharrer, Messner, & Szymanski (2014); Scharrer et al. (2016).

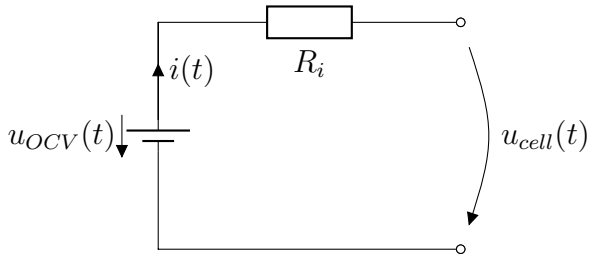

Figure 2.1.: *Schematic drawing of a simple equivalent circuit model.*

In order to enable the necessary variability for the implementation of vehicle models, simple equivalent circuit models used as a place holder for an entire battery in MPC for driving dynamics related optimization, as in the quasi-static system modeling approach facing in backward direction introduced by Guzzella & Amstutz (2005); Guzzella & Sciarretta (2007). For the MPC problem of a specific vehicle velocity demand and gradient of the road, the necessary propulsion force can be derived as described by Scharrer, Messner, & Szymanski (2014).

The battery in this model determines the actual SoC based on the demanded electrical power P_{BT} using maps. Here, a discrimination in charging and discharging operation is necessary. The parameter set of the battery model involves

- the total capacity $Q_{\max}$,
- the map of internal resistance $R_i(\mathrm{SoC}, \mathrm{dir})$ as a function of the SoC and the direction $\mathrm{dir} \in \{+, -\}$ of the current,
- efficiencies $\eta(\mathrm{dir})$ in either direction,
- an OCV lookup table $U_{\mathrm{OCV}}(\mathrm{SoC})$ as a function of the SoC and
- the maximum current $I_{\max}(\mathrm{dir})$ in either direction.

The battery voltage is calculated based on $U_{\mathrm{OCV}}(\mathrm{SoC})$ at the current SoC

$$U_{\mathrm{BT}} = U_{\mathrm{OCV}}(\mathrm{SoC}) \tag{2.2}$$

Out of the battery voltage U_{BT}, the demanded power P_{BT} and the losses at the internal resistance R_i, the battery current I_{BT} can be calculated. Since only the real part of this calculation is from interest, the complex part is eliminated here.

$$I_{\mathrm{BT}} = \eta_{\mathrm{BT}} \cdot \frac{U_{\mathrm{BT}} - \sqrt{U_{\mathrm{BT}}^2 - 4R_{\mathrm{BT}}P_{\mathrm{BT}}}}{2R_{\mathrm{BT}}} \tag{2.3}$$

The current I_{BT} causes a change in the SoC in the current time step. Considering the initial SoC_0, the current SoC value can be calculated

$$\mathrm{SoC} = \frac{-I_{\mathrm{BT}}T_s}{Q_{\max}} + \mathrm{SoC}_0. \tag{2.4}$$

This relationship represents a simple explicitly integrated ODE determining the current SoC as dynamic parameter within the vehicle model. Battery overload happens if $I_{\max}$ is exceeded or if the power demand P_{BT} leads to a voltage drop higher than the battery voltage U_{BT}. In both cases error information is passed on to the superordinate simulation model or optimization system to interrupt the simulation or disregard the results, respectively, see Figure 2.2 for a system overview.

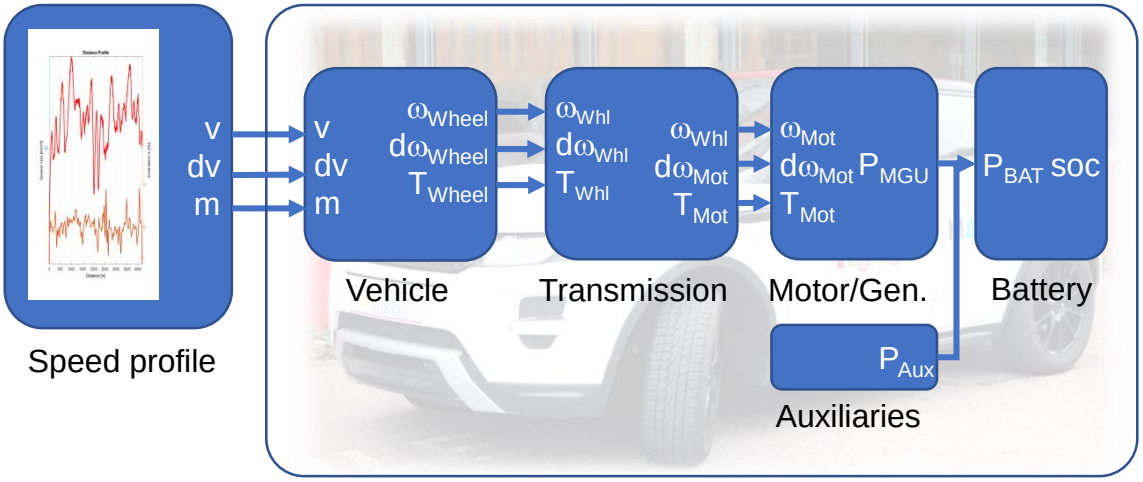

Figure 2.2.: *Structural overview of the models used for model predictive control (Scharrer et al., 2016)*

2.2.2. Equivalent Circuit RC-Models

Equivalent circuit battery models have been studied in literature very well (Greenleaf et al., 2013; Dong et al., 2011; Buller et al., 2005). Usually, they are resistor-capacitor (RC) based models of only a few elements, i.e. 1st, 2nd or 3rd-order RC models are used to describe the dynamic behavior of batteries (Hu et al., 2012). RC models give useful results for the task of phenomenologically describing a cell's or battery's behavior while requiring only little computational effort. However, it is not possible to deduce spatially resolved information from such 0D-models, such as the distribution of current density. This approach is later extended to a more complex 3D FEM model in Section 2.3.

The coarse battery model used in this section is a commonly used (F. Pichler & Cifrain, 2014) equivalent-circuit model as shown in Figure 2.3. In this model, a voltage source yields the OCV as a function of the SoC of the battery.

By definition, the OCV is equal to the terminal voltage of the cell when no current is flowing and the voltage has reached a steady-state point at a specific SoC. The open circuit voltage of the battery can be measured by several methods (Petzl & Danzer, 2013). A resistor R_0 in series to the voltage source replicates the ohmic resistance of the non-ideal voltage source. The dynamic parts of the voltage response are simulated by RC circuits which are parametrized by ohmic resistors R_i parallel to electric capacitors C_i. Depending on the battery, usually two or three equivalent circuits are used in literature (Hu et al., 2012).

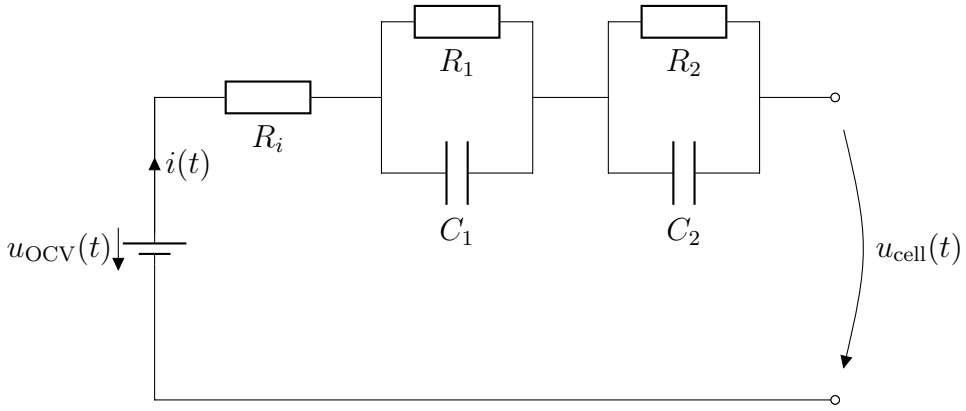

Figure 2.3.: *Schematic drawing of a simple equivalent circuit model.*

In this work, two RC elements are chosen. Due to simplicity and the fact that the SoC is not varied significantly, the OCV is set to the initial measurement voltage and held constant.

The difference between the battery tabs – the cathodic potential ϕ_c and the anodic potential ϕ_a – constitutes the battery voltage. The voltage loop in the circuit is described by

$$\begin{aligned} \phi_c - \phi_a &= U_0 + U_1 + U_2 + U_{\mathrm{OCV}}, \\ &= i_{\mathrm{cell}} R_0 + U_1 + U_2 + U_{\mathrm{OCV}}, \end{aligned} \tag{2.5}$$

where i_{cell} is the current applied to the cell. The dynamic behavior of the i-th RC circuit is deduced by Kirchhoff's law:

$$\begin{aligned} i_{\mathrm{cell}} &= i_{Ri} + i_{Ci} \\ &= U_i/R_i + \frac{\partial UC}{\partial t} \\ &= U_i/R_i + C\frac{\partial U}{\partial t} + \frac{\partial C}{\partial t}U, \end{aligned} \tag{2.6}$$

which eventually yields the ODE

$$R_i C_i \frac{\partial U}{\partial t} = -\left(R_i \frac{\partial C_i}{\partial t} + 1)\right) U_i + R_i i_{\mathrm{cell}}, \tag{2.7}$$

where ignoring the time derivative of the capacitor is a commonly made mistake in fully parametrized RC models, where the parameters change in time.

With respect to the fitting process, the parameters are assumed to be constant over the time of a single measurement profile, which is not altering the temperature or the state of charge of the battery significantly.

So, the final model equations are

$$\phi_c - \phi_a = iR_0 + U_1 + U_2 + U_{\mathrm{OCV}}, \tag{2.8a}$$

$$R_i C_i \frac{\partial U}{\partial t} = -U_i + R_i i_{\mathrm{app}}, \quad i = 1, 2, \tag{2.8b}$$

where the term $\tau_i = R_i C_i$ is commonly referred to as the "*time constant*" of the i-th RC circuit, which, in combination with the resistor, can be used as an alternative parameter set for the circuit. This is very popular because of the intuitive meaning of the time constant. The inner resistance R_0 can be simply calculated from the immediate voltage jump ΔU when a current I is driven through the battery by $R_0 = \Delta U / I$, or fitted to the measurement in order to minimize the residual, where the latter is the chosen approach in this work.

Altogether, the parameter tuple $(R_0, R_1, R_2, \tau_1, \tau_2)$ are subject to the parameter fitting method discussed in Section 3.2.2.

2.3. Extended 3D case

We propose the coupling of equivalent circuits into a high-resolution FEM simulation to model the electric behavior of a lithium-ion pouch cell.

In such a cell, the cell sandwiches formed by layers of aluminium current collector, anode, separator, cathode and copper current collector are stacked on each other in an anti-periodic manner, i.e. cathode and anode always facing towards each other. The stacked block Ω_X thereby consists of several dozens of thin layers. This block is the macroscopic model domain and will be treated as a homogeneous domain that is discretized by 3D FEM as shown in Figure 2.4.

The macroscopic cell behavior is described by a set of PDEs that are derived by homogenization.

There exist various ways of homogenization, several of which are often leading to the same homogenized equations. This work is following the idea of the "*Heterogeneous-Multiscale-Method*" (Weinan et al., 2007) that has already been used for batteries by Kim et al. (2011) and will be sketched very vaguely, in a rather intuitive way here.

For the macroscopic electrical behavior of the battery the surface current density i that is flowing at the current collectors – aluminum and copper layer –, is transformed to a volumetric current source by multiplying it with the electrode surface area per volume $A_{\mathrm{Al/Cu}}$. The surface current density i has to be calculated by a microscopic model as a function of the cathodic and anodic voltages (ϕ_c, ϕ_a) in every macroscopic point. Thus, the inner part of the cell sandwich – anode, separator and cathode – may be replaced by an arbitrary model that replicates this dependency.

The PDE describing the electrical potentials ϕ_c and ϕ_a in the current collector domains, i.e. the aluminum and copper layers Ω_{Al} and Ω_{Cu} is a spatially distributed formulation of Ohm's law given by

$$-\nabla \sigma_{\mathrm{Cu}} \nabla \phi_a = 0, , \quad \text{in } \Omega_{\mathrm{Cu}} \tag{2.9a}$$

$$\sigma_{\mathrm{Cu}} \nabla \phi_a = i, \quad \text{at } \Gamma_{\mathrm{Cu-CS}} \tag{2.9b}$$

$$-\nabla \sigma_{\mathrm{Al}} \nabla \phi_c = 0, \quad \text{in } \Omega_{\mathrm{Al}} \tag{2.9c}$$

$$\sigma_{\mathrm{Al}} \nabla \phi_c = -i, \quad \text{at } \Gamma_{\mathrm{Al-CS}}, \tag{2.9d}$$

where σ_{Al} and σ_{Cu} are electric conductivities of the respective materials and the boundaries Γ_{Al} and Γ_{Cu} are the interfaces between the current collector foils and the

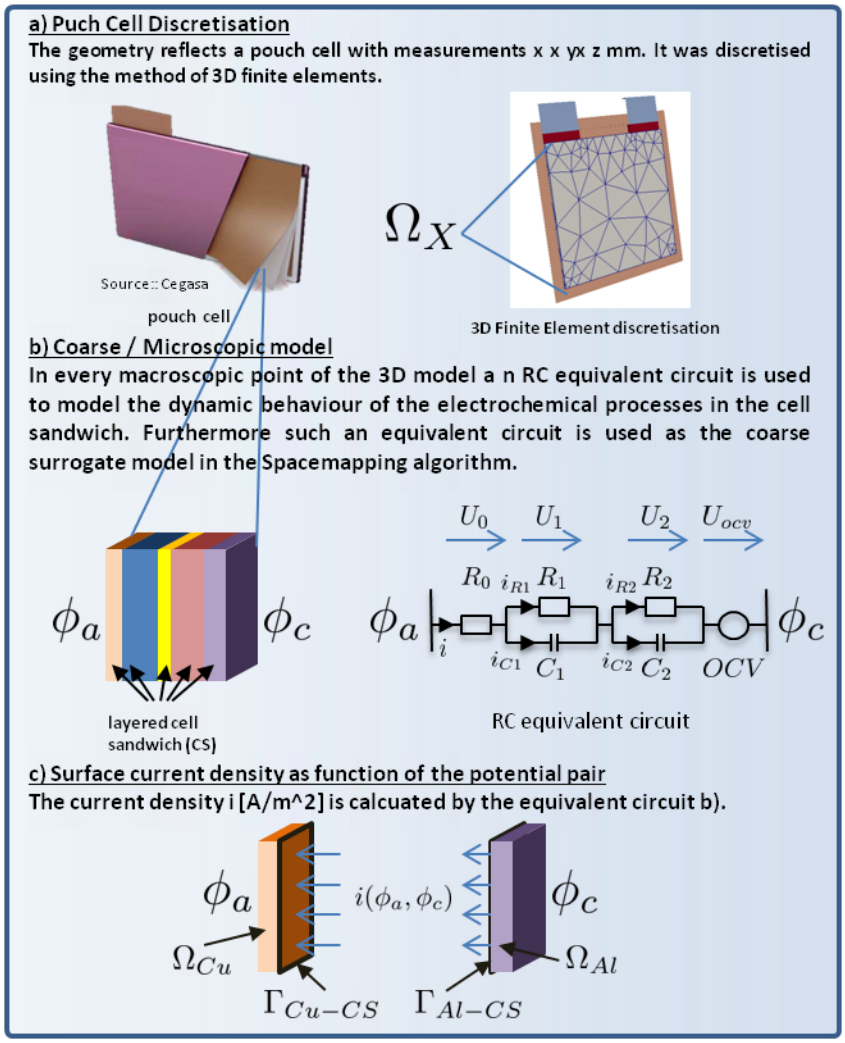

Figure 2.4.: *Schematic overview of the models used for RC-modelling. The microscopic model (bottom line) is used as the coarse model.*

electrodes.

The homogenization of this equations (Kim et al., 2011) yields the potential pair equations

$$-\nabla\sigma_{\text{Al,eff}}\nabla\hat{\phi}_c = A_{\text{Al/Cu}}i, \quad \text{in } \Omega_X \tag{2.10a}$$

$$-\nabla\sigma_{\text{Cu,eff}}\nabla\hat{\phi}_a = -A_{\text{Al/Cu}}i, \quad \text{in } \Omega_X, \tag{2.10b}$$

where $\sigma_{\text{Al,eff}}$ and $\sigma_{\text{Cu,eff}}$ are tensors that describe anisotropic effective conductivities of the homogenized current collectors and the hat on the potentials denotes macroscopic homogenized variables.

In general, the calculation of the effective conductivities is a non-trivial problem that requires the solution of an extra PDE on the microscopic domain called the "*cell problem*" (Hornung, 1996).

In this case, the simple structure of the micro problem, i.e. stacked layers, yields zero

conductivity in the out-of-plane direction perpendicular to the layer planes, as there is no direct connection between the aluminium and copper layers.

The effective in-plane conductivity is calculated by scaling the specific conductivities σ_i of material i by its volume fraction v_i in a unit cell, as they act like a parallel circuit of conductors.

Assuming that the cell's stacked layers are positioned parallel to the xy-plane, this yields a conductivity tensor of

$$\sigma_{i,\text{eff}} = \begin{Bmatrix} \sigma_i \cdot v_i & 0 & 0 \\ 0 & \sigma_i \cdot v_i & 0 \\ 0 & 0 & 0 \end{Bmatrix}. \tag{2.11}$$

The microscopic model that yields the dependency $i = i(\phi_{\text{Al}}, \phi_{\text{Cu}})$ is chosen to be RC-models of second-order – see Section 2.2.2. This is a trade-off between fast evaluation and accurately capturing dynamic behavior of the cell response.

Thus, in every macroscopic point x in the 3D model domain Ω_X the equations (2.8) are solved for the current i depending on the macroscopic potential pair (ϕ_c, ϕ_a). This current is implicitly coupled to the macroscopic equations as the source term.

The equations are implemented and solved with the finite element toolbox ELMER (Lyly et al., 1999), in which a user-defined solver was implemented. It allows to solve for the vector field $(\phi_A, \phi_c, U_1, U_2, i)$ depending on the overall current i_{cell} that is used as the boundary condition at the current collector tabs.

The fitting parameters $(R_0, R_1, R_2, \tau_1, \tau_2)$ are assumed to be constant over the homogenized jelly roll. Therefore, the spatially distributed 3D model described in this section has the same number of fitting parameters as the coarse 0D model described in Section 2.2.2, which is a necessary condition for the space mapping algorithm described in Section 3.2.2.

2.4. Electro-Chemical modeling

A general introduction to the basic functioning principle and the fundamental components of a Li^+cell has been given in Section 1.1. In this section, a more detailed explanation of the physical and chemical transport mechanism is given.

Section 2.4.1 outlines the basic concept of the reduced order model at the level of a single representative particle per electrode, while neglecting any other spatially resolved quantities.

Section 2.4.2 explains the detailed, spatially resolved model of Li^+cells on the basis of the rigorous work of Doyle, Fuller, & Newman (1993).

2.4.1. Single Particle Model

A simple electro-chemical model is represented by the class of SPMs by assuming no electrolyte effects or spatially resolved effects, e.g. varying concentrations in particles

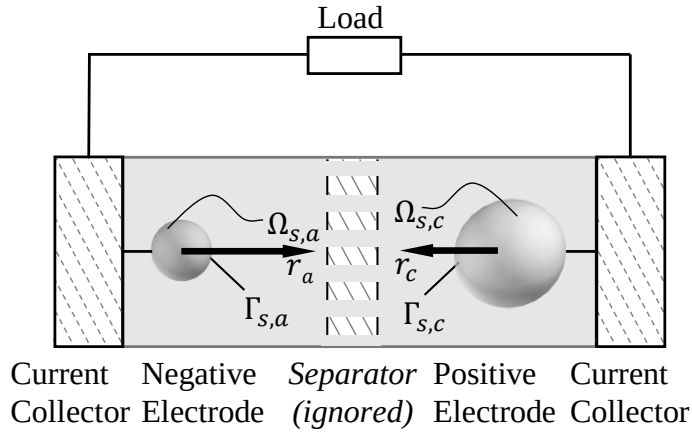

Figure 2.5.: *SPM Problem Domain: The spatial domains are defined as* $\Omega_{s,a}$ *and* $\Omega_{s,c} \subset \mathbb{R}^2$*, and* $R_a, R_c \in \mathbb{R}$*.*

within the same electrode. Although this is known to result in less accuracy in general, it is still possible to achieve very high model accuracy by taking the SPM's limitations into account, e.g. currents below 1 C, i.e. the equivalent of a full discharge in more than one hour (Newman & Thomas-Alyea, 2004; Santhanagopalan et al., 2006; Ning & Popov, 2004).

In this model approach, a SPM is considered as derived by F. Pichler (2018).

Each electrode is represented by a single spherical particle as the limiting factor, whereas all dynamic limitations imposed by the liquid phase are considered negligible except for Ohmic resistance. Figure 2.5 shows the simplified and idealized structure.

The main model equation results in

$$\frac{\partial c_{s,i}}{\partial t} - \frac{1}{r^2}\frac{\partial}{\partial r}\left(D_{s,i} r^2 \frac{\partial c_{s,i}}{\partial r}\right) = 0, \quad \text{in } Q_{s,i} := \Omega_{s,i} \times [0,T], \tag{2.12}$$

where $c_{s,i}$ denotes the concentration of lithium inside the solid, r is the sphere's radial dimension and D_s is the solid diffusion coefficient in electrode i, with $\Omega_{s,i} = [0, R_{s,i}]$. Assuming all electrolyte quantities constant allows us to set the boundary condition to

$$\begin{aligned} D_{s,i}(c)\partial c_{s,i} &= j_{\mathrm{BV},i}\left(\varphi_{s,i}, U_{\mathrm{OCP}}(c_{s,i})\right) \\ &= i_0(c_{s,i})\left(\exp(\alpha\frac{F}{RT}\eta_{s,i}(c_{s,i})) - \exp(-(1-\alpha)\frac{F}{RT}\eta_{s,i}(c_{s,i}))\right), \quad \text{on } \Gamma_{s,i} \end{aligned} \tag{2.13}$$

where the over-potential $\eta_{s,i}$ is defined as

$$\eta_{s,i} = \varphi_{s,i} - U_{\mathrm{OCP}}(c_{s,i}). \tag{2.14}$$

$\varphi_{s,i}$ denotes the electrode potential and $U_{\mathrm{OCP}}(c_{s,i})$ is the open circuit potential of the electrode at a given lithium concentration $c_{s,i}$. The model of $U_{\mathrm{OCP}}(c_{s,i})$ utilized in this

work is based on the Redlich-Kister expansion as introduced by Karthikeyan et al. (2008):

$$U_{\mathrm{OCP}}(\xi) = E_0 + \frac{F}{RT} \ln\left(\frac{(1-\xi)}{\xi}\right) + \frac{F}{RT} \sum_{k=0}^{n} A_k \left((2\xi - 1) - \frac{2\xi k\,(1-\xi)}{(2\xi-1)^{k-1}}\right) \quad (2.15)$$

where $\xi = c_s/c_{total}$ is a measure for the lithiation state of an intercalation electrode. Using the definition of $U_{\mathrm{OCP}}(\xi)$, F. Pichler (2018) derived the exchange current density on the basis of activity functions derived from transition theory:

$$i_0(\xi_s) = k_{\mathrm{BV}} \exp\left(\frac{F}{RT}\left((\xi_s - \alpha)\, U_{\mathrm{OCP}}(\xi_s) - \int_0^{\xi_s} U_{\mathrm{OCP}}(x)\mathrm{d}x\right)\right) \quad (2.16)$$

Again, the assumed constant behavior of the electrolyte quantities permits us to state the conservation of electric charge and current as

$$j_{\mathrm{BV},i} = \frac{I_{\mathrm{app}}}{F\, A_{e,i}}, \quad (2.17)$$

where I_{app} is the applied current to the cell and A_e denotes the electrode cross section area. In addition, we capture the effect of electrolyte losses by an ohmic resistance R_I, such that we may state the cell voltage u_{cell} as the algebraic condition

$$u_{\mathrm{cell}} = I_{\mathrm{app}}\, R_s + \eta_c + \eta_a \quad (2.18)$$

where the cell electrodes' over-potentials $\eta_i = \varphi_{s,i} - U_{\mathrm{OCP}}(c_{s,i})$ are used to simplify the notation.

The output of the SPM is one of two possible steps:

- Evolution of the terminal cell voltage $V(t, I_{\mathrm{app}}; \theta) = u_{\mathrm{cell}}$ for a given current profile I_{app} and a parameter set θ.
- Evolution of the cell current $I(t, u_{\mathrm{cell}}; \theta) = I_{\mathrm{app}}$ for a fixed cell voltage u_{cell}, which is set to match the previous steps final u_{cell}.

The governing equations and boundary conditions for the SPM are numerically implemented using full implicit scheme on the basis of FEM with adaptive time step sizes and the possibility to freeze the time grid to results from a previous evaluation.

2.4.2. Doyle-Fuller-Newman Model

In order to describe the internal dynamic processes in a lithium–ion cell mathematically, an electrochemical model has been realized following the widely used DFN approach (Newman & Thomas-Alyea, 2004). This model can be stated as a system of coupled non–linear partial differential equations in one dimension. A lithium–ion cell with two porous intercalation electrodes (cathode in Ω_c and anode in Ω_a) and an electronically isolating separator in Ω_s in between is considered. For homogenization purpose each electrode is assumed to consist of two phases. The solid phase is assumed to be spherical

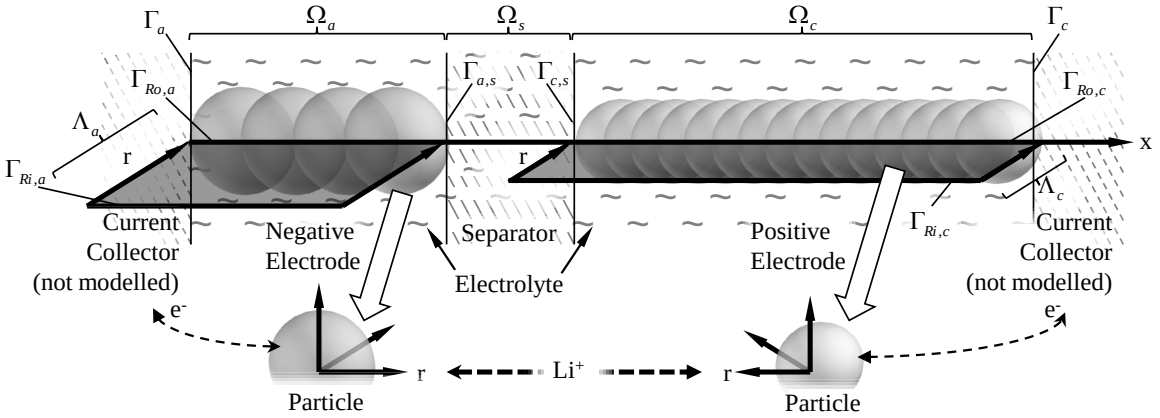

Figure 2.6.: *Problem Domain: The spatial domains are defined as* $\Omega = \Omega_a \cup \Omega_s \cup \Omega_c \subset \mathbb{R}$, $\Omega' = \Omega_a \cup \Omega_c$, $\Lambda_a = \Omega_a \times [0, R_a] \subset \mathbb{R}^2$, $\Lambda_c = \Omega_c \times [0, R_c] \subset \mathbb{R}^2$, $\Lambda = \Lambda_a \cup \Lambda_c$ *and* $R_a, R_c \in \mathbb{R}$.

particles in both cathode (in Λ_c) and anode (in Λ_a), which line up continuously in x direction. The liquid phase modeled in each electrode is electrolyte. In the separator Ω_s we only consider electrolyte, as the solid phase in the separator does not participate in the reactions.

The definitions of the spatial domains may be summarized as:

$$\left.\begin{aligned} \Omega_a &= [a,b] \subset \mathbb{R} \\ \Omega_s &= (b,c) \subset \mathbb{R} \\ \Omega_c &= [c,d] \subset \mathbb{R} \\ \Omega &= \Omega_a \cup \Omega_s \cup \Omega_c \\ \Omega' &= \Omega_a \cup \Omega_c \end{aligned}\right\}, \quad \text{where } a < b < c < d \tag{2.19a}$$

and

$$\Lambda_a = \Omega_a \times [R_{a,0}, R_a] \subset \mathbb{R}^2, \quad \text{where } R_{a,0} < R_a \tag{2.19b}$$

$$\Lambda_c = \Omega_c \times [R_{c,0}, R_c] \subset \mathbb{R}^2, \quad \text{where } R_{c,0} < R_c \tag{2.19c}$$

$$\Lambda = \Lambda_a \cup \Lambda_c \tag{2.19d}$$

with boundaries $\{\Gamma_a, \Gamma_b, \Gamma_c, \Gamma_d, \Gamma_{R,a,0}, \Gamma_{R,a}, \Gamma_{R,c,0}, \Gamma_{R,c}\}$ – as depicted in Figure 2.6 giving a schematic view of the modeled domain. For a final time $T > 0$ we define the space time cylinders $Q_1 := \Omega \times (0,T)$, $Q_1' := \Omega' \times (0,T)$, $Q_a := \Lambda_a \times (0,T)$, $Q_c := \Lambda_c \times (0,T)$ and their respective boundaries $\Sigma_a := \Gamma_a \times (0,T)$, $\Sigma_d := \Gamma_d \times (0,T)$, $\Sigma_{a,d} := \Sigma_a \cup \Sigma_d$, $\Sigma_{b,c} := \Gamma_b \cup \Gamma_c \times (0,T)$, $\Sigma_{R,i} := \Gamma_{R,i} \times (0,T)$, and $\Sigma_{R,i,0} := \Gamma_{R,i,0} \times (0,T)$.

We consider the elliptic-parabolic system similar to the definition in of potential and concentration equations for liquid and solid materials: The governing equations of the one–dimensional cell model considered are defined by system (2.20).

$$-\nabla \cdot (\sigma_s \nabla \varphi_s) = -A_i j_{\mathrm{BV}}^* \text{in } Q_1' \tag{2.20a}$$

$$-\nabla \cdot \left(\kappa_\ell(c_\ell) \nabla \varphi_\ell + \frac{RT}{zF} \kappa_\ell(c_\ell) t_\ell^+ \frac{1}{c_\ell} \nabla c_\ell \right) = A_i j_{\mathrm{BV}}^* \text{in } Q_1 \tag{2.20b}$$

$$\frac{\partial\left(\varepsilon_\ell c_\ell\right)}{\partial t} - \nabla\cdot\left(D_\ell\left(\nabla c_\ell + \frac{zF}{RT}\mu_\ell c_\ell \nabla\varphi_\ell\right)\right) = \frac{A_i}{zF} j^*_{\mathrm{BV}} \text{in } Q_1 \tag{2.20c}$$

$$\frac{\partial c_s}{\partial t} - \frac{1}{r^2}\frac{\partial}{\partial r}\left(D_s r^2 \frac{\partial c_s}{\partial r}\right) = 0 \text{in } Q_2 \tag{2.20d}$$

In the liquid phase the variables are potentials φ_ℓ and concentrations c_ℓ. In the solid phase the variables are split again into potentials φ_s and cathode concentrations c_{sc} as well as anode concentrations c_{sa}. The unknowns are more precisely defined as

$$\varphi_\ell := \varphi_\ell\left(x,t\right), \quad (x,t) \in Q_1 \tag{2.21a}$$

$$\varphi_s := \varphi_s\left(x,t\right), \quad (x,t) \in Q_1' \tag{2.21b}$$

$$c_\ell := c_\ell\left(x,t\right), \quad (x,t) \in Q_1 \tag{2.21c}$$

$$c_{sa} := c_{sa}\left(x,r,t\right), \quad (x,r,t) \in Q_a \tag{2.21d}$$

$$c_{sc} := c_{sc}\left(x,r,t\right), \quad (x,r,t) \in Q_c \tag{2.21e}$$

To shorten the notation, we combine the system variables in an unknowns vector $u := (\varphi_{sa}, \varphi_{sc}, \varphi_\ell, c_\ell, c_{sa}, c_{sc})$. The system variables are defined as time and space dependent $u(\mathrm{x}, t)$ at times $t \in [0,T]$, $T \in \mathbb{R}$ and at space points $x \in \mathbb{R}$ and $(x,r) \in \mathbb{R}^2$, respectively. A comprehensive overview of symbols is given in nomenclature in Chapter A.3.

Since diffusivity and conductivity must be effective values, they are modeled by taking the porosity into account:

$$\sigma_s := \hat{\sigma}_s \varepsilon_s^{\mathrm{brugg}_s}, \tag{2.22a}$$

$$\kappa_\ell := \hat{\kappa}_\ell \varepsilon_\ell^{\mathrm{brugg}_\ell}, \tag{2.22b}$$

$$D_s := \hat{D}_s \varepsilon_s^{\mathrm{brugg}_s}, \tag{2.22c}$$

$$D_\ell := \hat{D}_\ell \varepsilon_\ell^{\mathrm{brugg}_\ell} \tag{2.22d}$$

The Butler–Volmer expression (2.23) couples the system equations (2.20).

$$j^*_{\mathrm{BV}} = \begin{cases} zFk\left(\exp\left(\frac{\alpha zF\eta}{RT}\right) - \exp\left(\frac{-(1-\alpha)zF\eta}{RT}\right)\right) + C_{\mathrm{dl}}\frac{\partial(\varphi_s-\varphi_\ell)}{\partial t} & \text{in } Q' \\ 0 & \text{else} \end{cases} \tag{2.23a}$$

$$\eta = \varphi_s - \varphi_\ell - U_{\mathrm{OCV}}(c_s) \tag{2.23b}$$

Homogenous Neumann conditions are applied at the boundaries except for the outer boundaries of potentials φ_s and concentrations c_s in solid phase:

$$\varphi_s = 0, \quad \text{on } \Sigma_a := \Gamma_a \times [0,T] \tag{2.24a}$$

$$-\sigma_s \nabla\varphi_s = -i\left(t\right), \quad \text{on } \Sigma_c := \Gamma_c \times [0,T] \tag{2.24b}$$

$$-D_s\frac{\partial c_s}{\partial r} = \frac{1}{zF} j^*_{\mathrm{BV}}, \quad \text{on } \Sigma_{Ro} := \Gamma_{Ro,a} \cup \Gamma_{Ro,c} \times [0,T] \tag{2.24c}$$

For (x,t) in Q_1 and (x,r,t) in $Q_a \cup Q_c$ we define the mixed boundary conditions for:

$$-\alpha_1\left(c_\ell;\mu\right)\partial_x\varphi_\ell\left(a,t\right)=-\alpha_1\left(c_\ell;\mu\right)\partial_x\varphi_\ell\left(d,t\right)=0 \tag{2.25a}$$

$$\begin{aligned}&-\alpha_1\left(c_\ell\left(b^-,t\right);\mu\left(b^-\right)\right)\partial_x\varphi_\ell\left(b^-,t\right)+\alpha_2\left(c_\ell\left(b^-,t\right);\mu\left(b^-\right)\right)c_\ell^{-1}\left(b^-,t\right)\partial_x c_\ell\left(b^-,t\right)\\&=-\alpha_1\left(c_\ell\left(b^+,t\right);\mu\left(b^+\right)\right)\partial_x\varphi_\ell\left(b^+,t\right)+\alpha_2\left(c_\ell\left(b^+,t\right);\mu\left(b^+\right)\right)c_\ell^{-1}\left(b^+,t\right)\partial_x c_\ell\left(b^+,t\right)\end{aligned} \tag{2.25b}$$

$$\begin{aligned}&-\alpha_1\left(c_\ell\left(c^-,t\right);\mu\left(c^-\right)\right)\partial_x\varphi_\ell\left(c^-,t\right)+\alpha_2\left(c_\ell\left(c^-,t\right);\mu\left(c^-\right)\right)c_\ell^{-1}\left(c^-,t\right)\partial_x c_\ell\left(c^-,t\right)\\&=-\alpha_1\left(c_\ell\left(c^+,t\right);\mu\left(c^+\right)\right)\partial_x\varphi_\ell\left(c^+,t\right)+\alpha_2\left(c_\ell\left(c^+,t\right);\mu\left(c^+\right)\right)c_\ell^{-1}\left(c^+,t\right)\partial_x c_\ell\left(c^+,t\right)\end{aligned} \tag{2.25c}$$

$$-\alpha_4\left(\mu\right)\partial_x\varphi_s\left(b,t\right)=-\alpha_4\left(\mu\right)\partial_x\varphi_s\left(c,t\right)=0 \tag{2.25d}$$

$$-\alpha_4\left(\mu\right)\partial_x\varphi_s\left(a,t\right)=-\alpha_4\left(\mu\right)\partial_x\varphi_s\left(d,t\right)=-I(t) \tag{2.25e}$$

or

$$\varphi_s\left(d,t\right)=U(t) \tag{2.25f}$$

$$-\alpha_5\left(c_\ell;\mu\right)\,\partial_x c_\ell\left(a,t\right)=-\alpha_5\left(c_\ell;\mu\right)\,\partial_x c_\ell\left(d,t\right)=0 \tag{2.25f}$$

$$\begin{aligned}&-\alpha_5\left(c_\ell\left(b^-,t\right);\mu\left(b^-\right)\right)\,\partial_x c_\ell\left(b^-,t\right)-\alpha_6\left(c_\ell\left(b^-,t\right);\mu\left(b^-\right)\right)\,c_\ell\left(b^-,t\right)\,\partial_x\varphi_\ell\left(b^-,t\right)\\&=-\alpha_5\left(c_\ell\left(b^+,t\right);\mu\left(b^+\right)\right)\,\partial_x c_\ell\left(b^+,t\right)-\alpha_6\left(c_\ell\left(b^+,t\right);\mu\left(b^+\right)\right)\,c_\ell\left(b^+,t\right)\,\partial_x\varphi_\ell\left(b^+,t\right)\end{aligned} \tag{2.25g}$$

$$\begin{aligned}&-\alpha_5\left(c_\ell\left(c^-,t\right);\mu\left(c^-\right)\right)\,\partial_x c_\ell\left(c^-,t\right)-\alpha_6\left(c_\ell\left(c^-,t\right);\mu\left(c^-\right)\right)\,c_\ell\left(c^-,t\right)\,\partial_x\varphi_\ell\left(c^-,t\right)\\&=-\alpha_5\left(c_\ell\left(c^+,t\right);\mu\left(c^+\right)\right)\,\partial_x c_\ell\left(c^+,t\right)-\alpha_6\left(c_\ell\left(c^+,t\right);\mu\left(c^+\right)\right)\,c_\ell\left(c^+,t\right)\,\partial_x\varphi_\ell\left(c^+,t\right)\end{aligned} \tag{2.25h}$$

$$-\alpha_8(c_{sa};\mu)\,\partial_r c_{sa}(x,R_a,t)=\alpha_{14}(\mu)\,j(c_\ell,c_s,\varphi_\ell,\varphi_s;\mu)+\alpha_3(\mu)\,\alpha_{14}(\mu)\,\partial_t(\varphi_s-\varphi_\ell) \tag{2.25i}$$

$$-\alpha_8\left(c_{sa};\mu\right)\,\partial_r c_{sa}\left(x,R_{a,0},t\right)=0 \tag{2.25j}$$

$$-\alpha_8(c_{sc};\mu)\,\partial_r c_{sc}(x,R_c,t)=\alpha_{14}(\mu)\,j(c_\ell,c_s,\varphi_\ell,\varphi_s;\mu)+\alpha_3(\mu)\,\alpha_{14}(\mu)\,\partial_t(\varphi_s-\varphi_\ell) \tag{2.25k}$$

$$-\alpha_8\left(c_{sc};\mu\right)\,\partial_r c_{sc}\left(x,R_{c,0},t\right)=0 \tag{2.25l}$$

In addition, the concentrations are restricted by the following initial conditions:

$$c_\ell\left(x,t=0\right)=c_{\ell,0},\quad\text{in }\Omega \tag{2.26a}$$

$$c_s\left(x,r,t=0\right)=c_{s,0},\quad\text{in }\Lambda \tag{2.26b}$$

The potentials are initialized at rest by the condition $j\left(x,0\right)=0$ consistently. where (2.24a) is defined to provide uniqueness of the system. Obviously, conditions on the outer boundaries – (2.25a) and (2.25f) – can be fulfilled providing that the system

$$-\alpha_1\left(c_\ell;\mu\right)\partial_x\varphi_\ell\left(a,t\right)-\alpha_2\left(c_\ell;\mu\right)c_\ell\left(a,t\right)^{-1}\partial_x c_\ell\left(a,t\right)=0 \tag{2.27a}$$

$$-\alpha_6\left(c_\ell;\mu\right)\,c_\ell\left(a,t\right)\,\partial_x\varphi_\ell\left(a,t\right)-\qquad\alpha_5\left(c_\ell;\mu\right)\,\partial_x c_\ell\left(a,t\right)=0 \tag{2.27b}$$

is regular on both Γ_a and Γ_c, respectively.

We set $V_1=H^1\left(\Omega\right),V_2=\left\{\phi\in H^1\left(\Omega'\right)|\phi\left(a\right)=0\right\},V_i=\left\{(\phi,\psi)\in H^1\left(\Lambda_i\right)\right\}$ and $V=V_1\times V_2\times V_1\times V_a\times V_c$. For convenience we combine the unknows (2.21) in $u=(\varphi_\ell,\varphi_s,c_\ell,c_{sa},c_{sc})\in V$ and call it a *weak solution* to (2.20), if

$$\int_\Omega \Big(\alpha_1(u;\mu)\,\partial_x\varphi_\ell + \alpha_2(u;\mu)\,c_\ell^{-1}\partial_x c_\ell\Big)\,\partial_x\phi - \big(j(u;\mu) + \alpha_3(\mu)\,\partial_t(\varphi_s-\varphi_\ell)\big)\,\phi\,\mathrm{d}x = 0,\quad \forall\phi\in V_1 \tag{2.28a}$$

$$\int_\Omega (\alpha_4(\mu)\,\partial_x\varphi_s\,\partial_x\phi + (j(u;\mu)+\alpha_3(\mu)\,\partial_t(\varphi_s-\varphi_\ell))\,\phi)\,\mathrm{d}x - I\,\phi(\Gamma_c) = 0,\quad \forall\phi\in V_2 \tag{2.28b}$$

$$\int_\Omega \varepsilon_{\ell i}\,\partial_t c_\ell\,\phi + (\alpha_5(u;\mu)\,\partial_x c_\ell + \alpha_6(u;\mu)\,c_\ell\,\partial_x\varphi_\ell)\,\partial_x\phi - \alpha_7(\mu)\,(j(u;\mu)+\alpha_3(\mu)\,\partial_t(\varphi_s-\varphi_\ell))\,\phi\,\mathrm{d}x = 0,\quad \forall\phi\in V_1 \tag{2.28c}$$

$$\iint_{\Lambda_a} (\partial_t c_{sa}\,\phi\,\psi + \alpha_8(u;\mu)\,\partial_r c_{sa}\,\partial_r\psi\,\phi)\,r^2\mathrm{d}r + R_a^2\,\alpha_{14}(\mu)\,(j(u;\mu)+\alpha_3(\mu)\,\partial_t(\varphi_s-\varphi_\ell))\,\psi(\Gamma_{R,a})\,\phi\,\mathrm{d}x = 0,\ \forall(\phi,\psi)\in V_a \tag{2.28d}$$

$$\iint_{\Lambda_c} (\partial_t c_{sc}\,\phi\,\psi + \alpha_8(u;\mu)\,\partial_r c_{sc}\,\partial_r\psi\,\phi)\,r^2\mathrm{d}r + R_c^2\,\alpha_{14}(\mu)\,(j(u;\mu)+\alpha_3(\mu)\,\partial_t(\varphi_s-\varphi_\ell))\,\psi(\Gamma_{R,c})\,\phi\,\mathrm{d}x = 0,\ \forall(\phi,\psi)\in V_c \tag{2.28e}$$

Without further discussion, we assume that for any $\mu\in\mathcal{M}_{\mathrm{ad}}$ the system (2.28) has a unique solution $u(\mu)$. In this case we can define the solution operator $\mathcal{F}:\mathcal{M}_{\mathrm{ad}}\to V$, where $u=\mathcal{F}(\mu)$ is the weak solution to (2.20) for a given $\mu\in\mathcal{M}_{\mathrm{ad}}$.
Depending on the mode of operation we state quantities of interest as either cell voltage

$$U(t) = \varphi_s(d,t) - \varphi_s(a,t),\quad t\in(0,T) \tag{2.29a}$$

or cell current

$$\begin{aligned} I(t) &= \alpha_4(\mu)\partial_x\varphi_s(a,t) = \alpha_4(\mu)\partial_x\varphi_s(d,t)\\ &= \int_{\Omega_a} j\,\mathrm{d}x = -\int_{\Omega_c} j\,\mathrm{d}x,\quad t\in(0,T). \end{aligned} \tag{2.29b}$$

By $\mathcal{M}_{\mathrm{ad}}\subset\mathbb{R}^m$ we introduce the set of admissible parameters. For further clarity, for a given instance $\mu\in\mathcal{M}_{\mathrm{ad}}$ we state μ:

$$\begin{aligned} \mu = \Big\{&\alpha_A,\alpha_K,\varepsilon_{\ell,a},\varepsilon_{\ell,s},\varepsilon_{\ell,c},\tau_{\ell,a},\tau_{\ell,s},\tau_{\ell,c},\varepsilon_{s,a},\varepsilon_{s,c},\sigma_a,\sigma_c,A_{\mathrm{is},a},A_{\mathrm{is},c},C_{\mathrm{dl},a},\\ &C_{\mathrm{dl},c},D_{s,a},D_{s,c},k_a(\vartheta),k_c(\vartheta),R_I,T,c_{\ell,0}(x),c_{sa,0}(x,r),c_{sc,0}(x,r),\\ &t_\ell^+,\kappa_{\ell,A},\kappa_{\ell,B},\kappa_{\ell,C},A_{\mathrm{RK},a,0},\ldots,A_{\mathrm{RK},a,15},A_{\mathrm{RK},c,0},\ldots,A_{\mathrm{RK},c,15},\Big\} \end{aligned} \tag{2.30}$$

where "parameter functions" are to be approximated by polynomials or piecewise polynomial functions. The solution of this system of four non-linearly coupled partial differential equations is done by application of the Finite Element Method with linear test functions for spatial discretization and Backwards Euler Method for time integration. The non-linearity is solved by a damped Newton method. Figure 2.7 shows the states of the full finite element system over time for one parameter set in all unknowns. Only

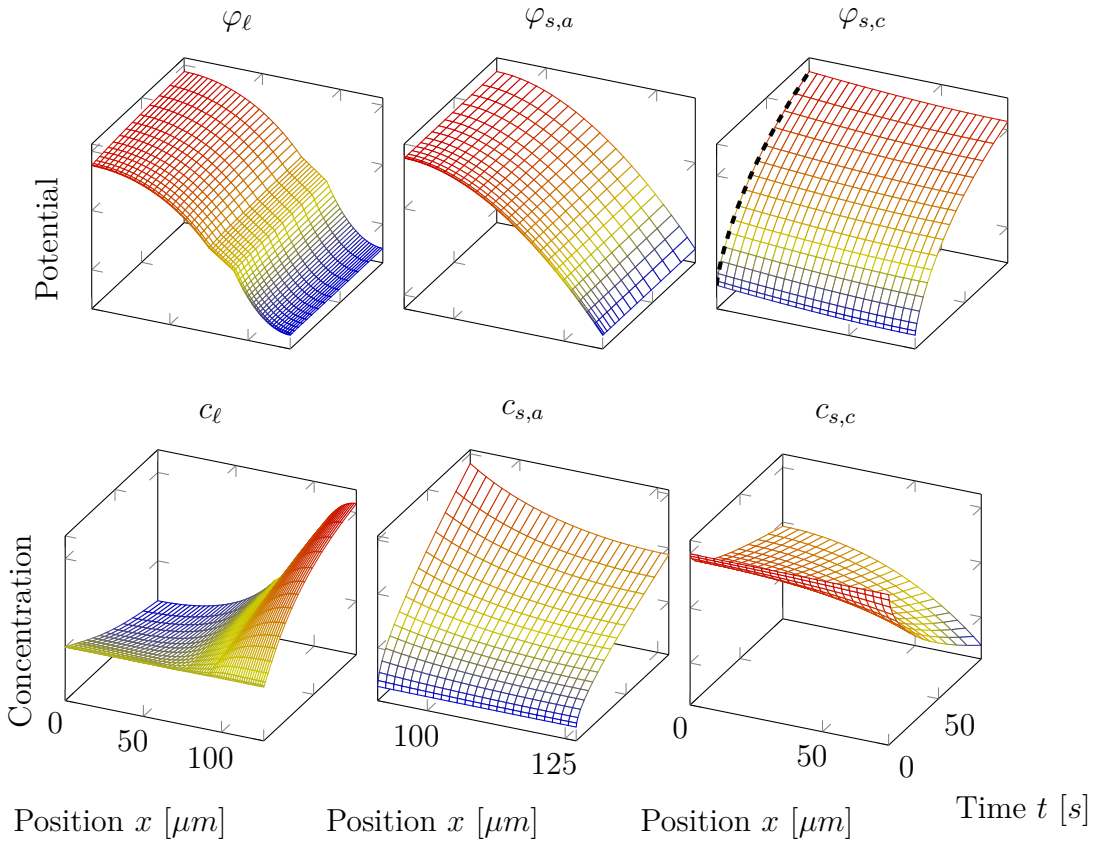

Figure 2.7.: *3D plots of the state u over space and time for the full finite element solution. Initial values and three quarters of the points in time were removed for visibility reasons. The dashed thick line on the top right picture marks the cell voltage results of initial $f(p_0)$ observed in Figure 4.8.*

the solid voltage on one border $\varphi_{s,c}|_{\Gamma_c}$ is used as observed quantity in (3.6). All other information of a real cell would not easily be accessible to measurements without destruction or redesign of the cell.

2.5. Simplification by Linearization

Solution of an optimization problem as described in Chapter 3 is a rather difficult and computationally time consuming task due to the constraining semi linear system (2.20). In this section, we introduce a simplified linear parabolic system of PDEs as a *coarse model*, which provides a much easier and faster solution, but with a loss in accuracy and limitations in usability. Then, in Section 3.2.1 we combine the two models by applying the space mapping approach for surrogate optimization.

Following the approach of Mancini & Volkwein (2011), for a given parameter set $\hat{\mu} \in \mathcal{M}_{\text{ad}}$ and a given solution $\hat{u}$ we want to build a simplified model, i.e. a *coarse model*, out of system (2.20), i.e. the *fine model*, that shows the same or similar behavior in local vicinity to the fine model w.r.t. the parameters and operation modes. Therefore,

we introduce a simplified new system:

$$-\partial_x \left(\alpha_1 \left(\hat{u};\hat{\mu}\right) \partial_x \varphi_\ell + \alpha_2 \left(\hat{u};\hat{\mu}\right) \partial_x c_\ell\right) - \alpha_3 \left(\hat{\mu}\right) \partial_t \left(\varphi_s - \varphi_\ell\right) - j = 0, \tag{2.31a}$$

$$-\partial_x \left(\alpha_4 \left(\hat{\mu}\right) \partial_x \varphi_s\right) + \alpha_3 \left(\hat{\mu}\right) \partial_t \left(\varphi_s - \varphi_\ell\right) + j = 0, \tag{2.31b}$$

$$\begin{aligned} &\varepsilon_{\ell i}\, \partial_t c_\ell - \partial_x \left(\alpha_5 \left(\hat{u};\hat{\mu}\right)\, \partial_x c_\ell + \alpha_6 \left(\hat{u};\hat{\mu}\right)\, \partial_x \varphi_\ell\right) \\ &\quad - \alpha_7 \left(\hat{\mu}\right)\, \alpha_3 \left(\hat{\mu}\right) \partial_t \left(\varphi_s - \varphi_\ell\right) - \alpha_7 \left(\hat{\mu}\right)\, j = 0, \end{aligned} \tag{2.31c}$$

$$\partial_t c_{sa} - r^{-2}\, \partial_r \left(\alpha_8 \left(\hat{u};\hat{\mu}\right)\, r^2\, \partial_r c_{sa}\right) = 0, \tag{2.31d}$$

$$\partial_t c_{sc} - r^{-2}\, \partial_r \left(\alpha_8 \left(\hat{u};\hat{\mu}\right)\, r^2\, \partial_r c_{sc}\right) = 0, \tag{2.31e}$$

where boundary conditions (2.24) and initial conditions (2.26) apply analogously, but boundary conditions differ in their corresponding subequations as follows:

$$\begin{aligned} &-\alpha_1 \left(\hat{u}\left(b^-,t\right);\hat{\mu}\left(b^-\right)\right) \partial_x \varphi_\ell \left(b^-,t\right) + \alpha_2 \left(\hat{u}\left(b^-,t\right);\hat{\mu}\left(b^-\right)\right)\, \partial_x c_\ell \left(b^-,t\right) \\ &= -\alpha_1 \left(\hat{u}\left(b^+,t\right);\hat{\mu}\left(b^+\right)\right) \partial_x \varphi_\ell \left(b^+,t\right) + \alpha_2 \left(\hat{u}\left(b^+,t\right);\hat{\mu}\left(b^+\right)\right)\, \partial_x c_\ell \left(b^+,t\right) \end{aligned} \tag{2.32a}$$

$$\begin{aligned} &-\alpha_1 \left(\hat{u}\left(c^-,t\right);\hat{\mu}\left(c^-\right)\right) \partial_x \varphi_\ell \left(c^-,t\right) + \alpha_2 \left(\hat{u}\left(c^-,t\right);\hat{\mu}\left(c^-\right)\right)\, \partial_x c_\ell \left(c^-,t\right) \\ &= -\alpha_1 \left(\hat{u}\left(c^+,t\right);\hat{\mu}\left(c^+\right)\right) \partial_x \varphi_\ell \left(c^+,t\right) + \alpha_2 \left(\hat{u}\left(c^+,t\right);\hat{\mu}\left(c^+\right)\right)\, \partial_x c_\ell \left(c^+,t\right) \end{aligned} \tag{2.32b}$$

$$\begin{aligned} &-\alpha_5 \left(\hat{u}\left(b^-,t\right);\hat{\mu}\left(b^-\right)\right)\, \partial_x c_\ell \left(b^-,t\right) - \alpha_6 \left(\hat{u}\left(b^-,t\right);\hat{\mu}\left(b^-\right)\right)\, \partial_x \varphi_\ell \left(b^-,t\right) \\ &= -\alpha_5 \left(\hat{u}\left(b^+,t\right);\hat{\mu}\left(b^+\right)\right)\, \partial_x c_\ell \left(b^+,t\right) - \alpha_6 \left(\hat{u}\left(b^+,t\right);\hat{\mu}\left(b^+\right)\right)\, \partial_x \varphi_\ell \left(b^+,t\right) \end{aligned} \tag{2.32c}$$

$$\begin{aligned} &-\alpha_5 \left(\hat{u}\left(c^-,t\right);\hat{\mu}\left(c^-\right)\right)\, \partial_x c_\ell \left(c^-,t\right) - \alpha_6 \left(\hat{u}\left(c^-,t\right);\hat{\mu}\left(c^-\right)\right)\, \partial_x \varphi_\ell \left(c^-,t\right) \\ &= -\alpha_5 \left(\hat{u}\left(c^+,t\right);\hat{\mu}\left(c^+\right)\right)\, \partial_x c_\ell \left(c^+,t\right) - \alpha_6 \left(\hat{u}\left(c^+,t\right);\hat{\mu}\left(c^+\right)\right)\, \partial_x \varphi_\ell \left(c^+,t\right) \end{aligned} \tag{2.32d}$$

$$-\alpha_8 \left(\hat{c}_{sa};\hat{\mu}\right)\, \partial_r c_{sa} \left(x, R_a, t\right) = \alpha_{14} \left(\hat{\mu}\right)\, j + \alpha_3 \left(\hat{\mu}\right)\, \alpha_{14} \left(\hat{\mu}\right)\, \partial_t \left(\varphi_s - \varphi_\ell\right) \tag{2.32e}$$

$$-\alpha_8 \left(\hat{c}_{sc};\hat{\mu}\right)\, \partial_r c_{sc} \left(x, R_c, t\right) = \alpha_{14} \left(\hat{\mu}\right)\, j + \alpha_3 \left(\hat{\mu}\right)\, \alpha_{14} \left(\hat{\mu}\right)\, \partial_t \left(\varphi_s - \varphi_\ell\right) \tag{2.32f}$$

For linearization, the non-linear coupling is expanded in a Taylor series and immediately stopped after the linear term – thus neglecting the error term of second order:

$$j\left(u;\mu\right) \approx j\left(\hat{u};\hat{\mu}\right) + \partial_u j\left(\hat{u};\hat{\mu}\right)^T \left(v - \hat{u}\right) + \partial_\mu j\left(\hat{u};\hat{\mu}\right)^T \left(\lambda - \hat{\mu}\right) \tag{2.33}$$

where $v = \left(\varphi_\ell, \varphi_s, c_\ell, c_{sa}, c_{sc}\right)^T$ and $\lambda \in \mathcal{L}_{\text{ad}}$. By $\mathcal{L}_{\text{ad}} \subset \mathbb{R}^l$ we introduce the set of admissible parameters for the linearized system. Components of the derivatives

$\partial_u j\left(\hat{u};\hat{\mu}\right) = \left(\partial_{\varphi_\ell}\ \partial_{\varphi_s}\ \partial_{c_\ell}\ \partial_{c_{sa}}\ \partial_{c_{sc}}\right) j\left(\hat{u};\hat{\mu}\right)$ can be written as:

$$\begin{aligned}\partial_{\varphi_\ell} j\left(\hat{u};\hat{\mu}\right) = &-\alpha_9\left(\hat{\mu}\right)\ \alpha_{10}\left(\hat{u};\hat{\mu}\right)\ \alpha_{11}\left(\hat{\mu}\right)\ \exp\left(\alpha_{11}\,\eta\left(\hat{u};\hat{\mu}\right)\right) \\ &+\alpha_9\left(\hat{\mu}\right)\ \alpha_{12}\left(\hat{u};\hat{\mu}\right)\ \alpha_{13}\left(\hat{\mu}\right)\ \exp\left(\alpha_{13}\,\eta\left(\hat{u};\hat{\mu}\right)\right)\end{aligned} \tag{2.34a}$$

$$\partial_{\varphi_s} j\left(\hat{u};\hat{\mu}\right) = -\partial_{\varphi_\ell} j\left(\hat{u};\hat{\mu}\right) \tag{2.34b}$$

$$\begin{aligned}\partial_{c_\ell} j\left(\hat{u};\hat{\mu}\right) = &\ \alpha_9\left(\hat{\mu}\right)\ \partial_{c_\ell}\alpha_{10}\left(\hat{u};\hat{\mu}\right)\ \exp\left(\alpha_{11}\,\eta\left(\hat{u};\hat{\mu}\right)\right) \\ &-\alpha_9\left(\hat{\mu}\right)\ \partial_{c_\ell}\alpha_{12}\left(\hat{u};\hat{\mu}\right)\ \exp\left(\alpha_{13}\,\eta\left(\hat{u};\hat{\mu}\right)\right)\end{aligned} \tag{2.34c}$$

$$\begin{aligned}\partial_{c_{si}} j(\hat{u};\hat{\mu}) = &\ \alpha_9(\hat{\mu})\,\psi(\Gamma_{R,i})\left(\partial_{c_{si}}\alpha_{10}(\hat{u};\hat{\mu}) - \alpha_{10}(\hat{u};\hat{\mu})\,\alpha_{11}(\hat{\mu})\,\partial_{c_{si}}U(\hat{u})\right)\exp(\alpha_{11}\,\eta(\hat{u};\hat{\mu})) \\ &-\alpha_9(\hat{\mu})\,\psi(\Gamma_{R,i})\left(\partial_{c_{si}}\alpha_{12}(\hat{u};\hat{\mu}) - \alpha_{12}(\hat{u};\hat{\mu})\,\alpha_{13}(\hat{\mu})\,\partial_{c_{si}}U(\hat{u})\right)\exp(\alpha_{11}\,\eta(\hat{u};\hat{\mu}))\end{aligned} \tag{2.34d}$$

and components of $\partial_\mu j\left(\hat{u};\hat{\mu}\right) = \left(\partial_{A_{is}}\ \partial_k\ \partial_{\alpha_A}\ \partial_{\alpha_K}\ \partial_{U_{coeff}}\right) j\left(\hat{u};\hat{\mu}\right)$ can be written as:

$$\partial_{A_{is}} j\left(\hat{u};\hat{\mu}\right) = zF\,k\left(T\right)\alpha_{10}\left(\hat{u};\hat{\mu}\right)\exp\left(\alpha_{11}\,\eta\left(\hat{u};\hat{\mu}\right)\right) - \alpha_{12}\left(\hat{u};\hat{\mu}\right)\exp\left(\alpha_{13}\,\eta\left(\hat{u};\hat{\mu}\right)\right) \tag{2.35a}$$

$$\partial_k j(\hat{u};\hat{\mu}) = zF\,A_{is}\alpha_{10}(\hat{u};\hat{\mu})\,\exp(\alpha_{11}\,\eta(\hat{u};\hat{\mu})) - \alpha_{12}(\hat{u};\hat{\mu})\,\exp(\alpha_{13}\,\eta(\hat{u};\hat{\mu})) \tag{2.35b}$$

$$\partial_{\alpha_A} j\left(\hat{u};\hat{\mu}\right) = \frac{zF}{RT}\,\alpha_9\left(\hat{\mu}\right)\ \alpha_{10}\left(\hat{u};\hat{\mu}\right)\ \left(\eta\left(\hat{u};\hat{\mu}\right)\right)\exp\left(\alpha_{11}\,\eta\left(\hat{u};\hat{\mu}\right)\right) \tag{2.35c}$$

$$\partial_{\alpha_K} j\left(\hat{u};\hat{\mu}\right) = -\frac{zF}{RT}\,\alpha_9\left(\hat{\mu}\right)\ \alpha_{12}\left(\hat{u};\hat{\mu}\right)\ \left(\eta\left(\hat{u};\hat{\mu}\right)\right)\exp\left(\alpha_{13}\,\eta\left(\hat{u};\hat{\mu}\right)\right) \tag{2.35d}$$

$$\partial_{U_{coeff}} j\left(\hat{u};\hat{\mu}\right) = \partial_{U_{coeff}} U\left(v\right)\ \partial_{\varphi_\ell} j\left(\hat{u};\hat{\mu}\right) \tag{2.35e}$$

where α_{10} and α_{12} are considered constant for now.
For solving (2.31) we utilize the weak form:

$$\begin{aligned}&\int_\Omega \Big(\alpha_1\left(\hat{u};\hat{\mu}\right)\partial_x\varphi_\ell + \alpha_2\left(\hat{u};\hat{\mu}\right)\partial_x c_\ell\Big)\ \partial_x\phi \\ &\quad-\Big(\partial_u\hat{j}^T\,v + \partial_\mu\hat{j}^T\,\lambda + \hat{j}_c + \alpha_3\left(\hat{\mu}\right)\partial_t\left(\varphi_s-\varphi_\ell\right)\Big)\,\phi\,\mathrm{d}x = 0,\quad \forall\phi\in V_1\end{aligned} \tag{2.36a}$$

$$\begin{aligned}&\int_\Omega \alpha_4(\hat{\mu})\partial_x\varphi_s\,\partial_x\phi + \left(\partial_u\hat{j}^T\,v + \partial_\mu\hat{j}^T\,\lambda + \hat{j}_c + \alpha_3(\hat{\mu})\partial_t(\varphi_s-\varphi_\ell)\right)\phi\,\mathrm{d}x - I\,\phi(\Gamma_2) \\ &\quad= 0,\quad \forall\phi\in V_2\end{aligned} \tag{2.36b}$$

$$\begin{aligned}&\int_\Omega \varepsilon_{\ell i}\,\partial_t c_\ell\,\phi + \Big(\alpha_5\left(\hat{u};\hat{\mu}\right)\ \partial_x c_\ell + \alpha_6\left(\hat{u};\hat{\mu}\right)\ \partial_x\varphi_\ell\Big)\ \partial_x\phi \\ &\quad-\alpha_7\left(\hat{\mu}\right)\ \Big(\partial_u\hat{j}^T\,v + \partial_\mu\hat{j}^T\,\lambda + \hat{j}_c + \alpha_3\left(\hat{\mu}\right)\partial_t\left(\varphi_s-\varphi_\ell\right)\Big)\ \phi\,\mathrm{d}x = 0,\quad \forall\phi\in V_1\end{aligned} \tag{2.36c}$$

$$\begin{aligned}&\iint_{\Lambda_a}\Big(\partial_t c_{sa}\,\phi\,\psi + \alpha_8\left(\hat{u};\hat{\mu}\right)\partial_r c_{sa}\,\partial_r\psi\,\phi\Big)\ r^2\mathrm{d}r \\ &+R_a^2\,\alpha_{14}\left(\hat{\mu}\right)\Big(\partial_u\hat{j}^T\,v + \partial_\mu\hat{j}^T\,\lambda + \hat{j}_c + \alpha_3\left(\mu\right)\ \partial_t\left(\varphi_s-\varphi_\ell\right)\Big)\ \psi\left(\Gamma_{R,a}\right)\phi\,\mathrm{d}x = 0, \\ &\quad\forall\left(\phi,\psi\right)\in V_a\end{aligned} \tag{2.36d}$$

$$\begin{aligned}
&\iint_{\Lambda_c} \left(\partial_t c_{sc}\,\phi\,\psi + \alpha_8\left(\hat{u};\hat{\mu}\right)\partial_r c_{sc}\,\partial_r\psi\,\phi\right) r^2 \mathrm{d}r \\
&+ R_c^2\,\alpha_{14}\left(\hat{\mu}\right)\left(\partial_u \hat{j}^T\,v + \partial_\mu \hat{j}^T\,\lambda + \hat{j}_c + \alpha_3\left(\hat{\mu}\right)\,\partial_t\left(\varphi_s - \varphi_\ell\right)\right)\,\psi\left(\Gamma_{R,c}\right)\phi\,\mathrm{d}x = 0, \\
&\quad \forall\,(\phi,\psi) \in V_c
\end{aligned} \tag{2.36e}$$

where $\hat{j}$ refers to $j\left(\hat{u};\hat{\mu}\right)$ and $\hat{j}_c = \hat{j} - \partial_u \hat{j}^T\hat{u} - \partial_\mu \hat{j}^T\hat{\mu}$ for convenience. Again, for a given instance $\lambda \in \mathcal{L}_{\mathrm{ad}}$ we call v a weak solution to (2.31) if (2.36) holds. We assume that for any $\lambda \in \mathcal{L}_{\mathrm{ad}}$ the system (2.36) has a unique solution $v\left(\lambda\right)$ so we can define another solution operator $\mathcal{C} : \mathcal{L}_{\mathrm{ad}} \to V$, where $v = \mathcal{C}\left(\lambda\right)$ is the weak solution to (2.31) for a given $\lambda \in \mathcal{L}_{\mathrm{ad}}$.

Now we define the parameter dependent operator $c := (c_1(y), c_2(y), c_3(y), c_4(y), c_5(y), c_6(y), c_7(y), c_8(y))$ as follows:

$$\begin{aligned}
\left\langle c_1(y),\phi_1\right\rangle_{L^2\left(0,T;V_1'\right),L^2(0,T;V_1)} &= \iint_{Q_1}\left(\alpha_1\partial_x\varphi_\ell + \alpha_2\partial_x c_\ell\right)\,\partial_x\phi_1 \\
&\quad - \left(\partial_u\hat{j}^T\,v + \partial_\mu\hat{j}^T\,\lambda + \hat{j}_c + \alpha_3\partial_t\left(\varphi_s - \varphi_\ell\right)\right)\,\phi_1\,\mathrm{d}x\mathrm{d}t
\end{aligned} \tag{2.37a}$$

$$\begin{aligned}
\left\langle c_2(y),\phi_2\right\rangle_{L^2\left(0,T;V_2'\right),L^2(0,T;V_2)} &= \iint_{Q_1'}\alpha_4\partial_x\varphi_s\,\partial_x\phi_2 \\
&\quad + \left(\partial_u\hat{j}^T\,v + \partial_\mu\hat{j}^T\,\lambda + \hat{j}_c + \alpha_3\partial_t\left(\varphi_s - \varphi_\ell\right)\right)\,\phi_2\,\mathrm{d}x\mathrm{d}t \\
&\quad - \iint_{\Sigma_d} I\,\phi_2\,\mathrm{d}s(x)\mathrm{d}t
\end{aligned} \tag{2.37b}$$

$$\begin{aligned}
\left\langle c_3(y),\phi_3\right\rangle_{L^2\left(0,T;V_1'\right),L^2(0,T;V_1)} &= \iint_{Q_1}\varepsilon_{\ell i}\,\partial_t c_\ell\,\phi_3 + \left(\alpha_5\,\partial_x c_\ell + \alpha_6\,\partial_x\varphi_\ell\right)\,\partial_x\phi_3 \\
&\quad - \alpha_7\,\left(\partial_u\hat{j}^T\,v + \partial_\mu\hat{j}^T\,\lambda + \hat{j}_c + \alpha_3\partial_t\left(\varphi_s - \varphi_\ell\right)\right)\,\phi_3\,\mathrm{d}x\mathrm{d}t
\end{aligned} \tag{2.37c}$$

$$\left\langle c_4(y),\phi_4\right\rangle_H = \left\langle c_\ell(0) - c_{\ell,0},\phi_4\right\rangle_H \tag{2.37d}$$

$$\begin{aligned}
\left\langle c_5(y),\phi_5\right\rangle_{L^2(0,T;V_a'),L^2(0,T;V_a)} &= \iiint_{Q_a}\left(\partial_t c_{sa}\,\phi_5 + \alpha_8\partial_r c_{sa}\,\partial_r\phi_5\right)\,r^2\mathrm{d}r\mathrm{d}x\mathrm{d}t \\
&\quad + \iiint_{\Sigma_a}\alpha_{14}\,\left(\partial_u\hat{j}^T\,v + \partial_\mu\hat{j}^T\,\lambda + \hat{j}_c\right. \\
&\qquad \left. + \alpha_3\,\partial_t\left(\varphi_s - \varphi_\ell\right)\right)\,\phi_5\,r^2\mathrm{d}s(r)\mathrm{d}x\mathrm{d}t
\end{aligned} \tag{2.37e}$$

$$\left\langle c_6(y),\phi_6\right\rangle_H = \left\langle c_{sa}(0) - c_{sa,0},\phi_6\right\rangle_H \tag{2.37f}$$

$$\langle c_7(y), \phi_7 \rangle_{L^2(0,T;V_c'),L^2(0,T;V_c)} = \iiint_{Q_c} (\partial_t c_{sc}\, \phi_7 + \alpha_8 \partial_r c_{sc}\, \partial_r \phi_7)\; r^2 \mathrm{d}r\mathrm{d}x\mathrm{d}t$$
$$+ \iiint_{\Sigma_c} \alpha_{14} \left(\partial_u \hat{j}^T\, v + \partial_\mu \hat{j}^T\, \lambda + \hat{j}_c \right. \tag{2.37g}$$
$$\left. + \alpha_3\, \partial_t \left(\varphi_s - \varphi_\ell\right) \right)\; \phi_7\, r^2 \mathrm{d}s(r)\mathrm{d}x\mathrm{d}t$$

$$\langle c_8(y), \phi_8 \rangle_H = \langle c_{sc}(0) - c_{sc,0}, \phi_8 \rangle_H \tag{2.37h}$$

for $y = (v, \lambda)$. Using the abstract formulation of (2.37), we note that $\langle c\,(v, \lambda)\,, \phi \rangle = 0$ results in $v\,(\lambda)$ for a given λ which is a weak solution to (2.31).

2.6. Summary

In this chapter, various approaches to model Li^+cells and batteries were presented. After discussing the idea of a generalized forward model, semi-empirical models were introduced as a simple but effective means to describe the behavior of a cell at a useful level of detail. An example application of a minimal, simple equivalent circuit models was presented in the context of a MPC system for semi-autonomous driving.

The 0D RC-models where then extended to a 3D case were they serve as an intermediate model in a thermoelectric model of a pouch cell.

Eventually, very detailed microscopic electro-chemical models were presented in the form of the famous DFN and a reduced form thereof, i.e. SPMs. Details for numeric solution of the non-linear PDE-system of the DFN were given and a means of simplification by linearization was presented.

Throughout the chapter, a general notation for common quantities was introduced that allows for a more comprehensible notation in this and successive chapters. Results of the models are presented in Chapter 4.

3

Parameter Identification

The aim of measurements is to retrieve information about the system of interest. In the scope of this work, Li^+ cells in particular do not allow to directly measure quantities of interest. Rather, the measured data depends, in some way, on the quantities of interest. Thus, these quantities are contained in some way in the measurements.

The reverse process of retrieving the data from the measurements, i.e. the problem of trying to reconstruct the quantities that we actually want is called an *inverse problem*. Loosely speaking, an inverse problem is where we observe an *effect* and want to determine the *cause*.

A very specific type of inverse problem is *parameter estimation*. Parameter estimation is not about reconstruction of a continuous input signal, but rather calibration of a mathematical model using measured data with respect to information about the internal parameters.

To recall and extend the generalized model formulation in (2.1), we consider a non–linear model

$$\mathrm{y} = f(\mathrm{x}, \theta) + \varepsilon, \tag{3.1}$$

where in this case y are the obtained measurements, $f(\mathrm{x}, \theta)$ is the model's solution and the measurement error is denoted by ε.

In this chapter, we discuss several approaches to acquire as much information about the internals of $f(\mathrm{x}, \theta)$ as possible while lowering the effort to do so. We start out with *Sensitivity Analysis* in Section 3.1, which proves to be a valuable tool to gain a first sense of the importance of the parameters of the model.

The most widely spread approach for estimating parameters is to adjusting them to match their resulting model output with observations of the equivalent quantity from measurements using the Least Squares (LSQ) criterion or the even more general continuous formulation of a mathematical norm, such as the L^2-Norm. The latter may in turn be approximated by the former to some degree, more closely described in Section 3.2. Section 3.2.1 introduces the "*space mapping*" technique to optimize a complex fine model on the basis of a coarse model by utilizing a linearization of the former. Section 3.2.2 provides a brief summary of a simplified version of the technique for a spatially resolved multi-scale model by using a simple 0D model as a surrogate for parameter estimation.

Section 3.3 shows a solution to the parameter estimation problem using a different paradigm, i.e. stochastic optimization techniques.

Eventually, Section 3.4 introduces a different approach to stochastic parameter optimization on the basis of the Bayesian methodology, which is used to estimate distributions of parameter uncertainties.

While all sections of this chapter provide details about the algorithms used for each of their tasks, implementation details, parameters and results are presented in Chapter 4.

3.1. Sensitivity Analysis

> (Saltelli et al., 2004) *Sensitivity Analysis (SA) is the study of how the variation in the output of a model (numerical or otherwise) can be apportioned, qualitatively or quantitatively, to different sources of variation, and of how the given model depends upon the information fed into it.*

Analysis of the forward model usually requires large computing times, e.g. investigation of its properties, plausibility, scalability, parameter uncertainties and influences as well as validity range.

These studies require up to 50 parameters to be tested. Many internal parameters are difficult to access or not directly measurable. Parameter estimation techniques focus on non-invasive methods only, i.e. without the need to destructively open the cell. These methods estimate parameters by matching predicted cell model output voltages for a given current profile to experimental measurements. To get better insight into the model behavior, a modified "Morris–one–at–a–time" (MOAT) Sensitivity Analysis (SA) parameter screening (Saltelli et al., 2004) was conducted.

The aim of a SA for a mathematical model is to:

- qualitatively identify the input factors that are important for the calibration,
- find interactions between the input factors – if there are any –,
- reduce the dimensions of the input factor space – if possible –, and
- ensure that the model is not ill conditioned.

A general approach to SA may be stated as follows:

Model assumption Before even starting with SA, the expected experimental behavior has to be described, i.e. a model describing a measurable or observable target has to be defined.

Input Space Design Ranges and probability distributions have to be assigned to variable input factors. This may be a very difficult task due to little knowledge at the beginning of the analysis.

Design of Experiments An execution plan comprising varying settings of the input factors has to be created and carried out for the experiments.

Design Execution The previously devised plan has to be executed, i.e. for a computational experiment, the model has to be executed, and the experimental output has to be collected and analyzed. This creates output distributions for the response of interest.

Effect Analysis Eventually, the qualitative or quantitative *effects* of each input factor w.r.t. the output have to be estimated. This should provide further insight to calibrate the model w.r.t. a specific target or iterate the approach by utilizing the knowledge gained and formulating a detailed prior.

SA methods can be grouped into three classes:

- screening,
- local methods and
- global methods.

For the purpose of this thesis, the focus is on screening and global methods.

For a computationally expensive model with a large number of input factors, screening methods may be used to qualitatively rank the input factors by importance w.r.t. their contribution to output variability. Local methods usually focus on so-called "*local sensitivities*"

$$S_\mu := \frac{\partial J}{\partial \mu}, \tag{3.2}$$

where J defines a target function in dependence of the parameters μ. This gives very detailed insight into variance structures, but is very limited to a local vicinity around some working point μ^* for non-linear models.

In global sensitivity analysis, the uncertainty of the output is quantitatively apportioned to the input factors. To turn (3.2) into a global measure, estimating (3.2) on a grid of values covering as much of the parameter space as possible.

The method is based on elementary effects

$$d_i(x) = \left[f(p_1, p_2, \ldots, p_{i-1}, p_i + \Delta, p_{i+1}, \ldots, p_k) - f(\mathrm{p}) \right] / \Delta \tag{3.3}$$

of model responses $f(\mathrm{p})$ for a given parameter set p sampled along *random* trajectories in design space $\mathcal{P}$. The distribution of effects associated with the ith input parameter is denoted by F_i. From this distribution we can deduct qualitative information regarding "overall" influence – by large mean values μ_i of $F_i(d_i)$ – and high dependency on the input – by large spread σ_i of F_i –, i.e. high interaction between parameters or high non–linearity, respectively.

The experimental design matrix $\boldsymbol{X}$ comprises r orientation matrices $\boldsymbol{B}$

$$\boldsymbol{X} = \begin{bmatrix} \boldsymbol{B}_1^* \\ \vdots \\ \boldsymbol{B}_h^* \\ \vdots \\ \boldsymbol{B}_r^* \end{bmatrix}, \tag{3.4}$$

that can be written as

$$\boldsymbol{B}_h^* = (\boldsymbol{J}_{k+1,1} x^* + (\Delta/2)[(2\boldsymbol{B} - \boldsymbol{J}_{k+1,k})\boldsymbol{D}^* + \boldsymbol{J}_{k+1,k}])\boldsymbol{P}^*, \tag{3.5}$$

where $\boldsymbol{J}_{m,n}$ is a $m \times n$-matrix of ones, $\boldsymbol{B}$ is a strictly lower triangular matrix of ones, $\boldsymbol{D}^*$ is a diagonal matrix with diagonal elements randomly chosen as $+1$ or -1 and $\boldsymbol{P}^*$ is a $k \times k$-permutation-matrix

These orientation matrices may be interpreted as *random* trajectories of k steps through the k-dimensional input factor space starting at *random* points. For each of input factor by $r\,(k+1)$ experiments, this yields r *random* samples d_i of elementary effects. For these random samples d_i the mean value μ_i and the standard deviation σ_i are calculated.

Since the monotonicity of the model can not be presumed, it is important to incorporate the absolute value of the measure μ^* of $F_i\,(|d_i|)$ instead of μ – elementary effects could cancel each other out otherwise, see the work of Saltelli et al. (2004).

The mean values μ_i^* and standard deviations σ_i indicate factors that have

- little effect, indicated by small μ_i^* and σ_i,
- linear and additive effects, indicated by small σ_i or
- non-linear effects or strong interaction with other factors, indicated by high μ_i^* and σ_i.

Thus, these simple statistical factors provide very intuitive interpretation of the "overall" measure. They can be ranked by means of their elementary effects, at only the cost of model evaluations, which may be executed without any cross-interaction in an "embarrassingly parallel" way utilizing all available parallel computing infrastructure.

One disadvantage of Morris' method is, that individual interactions among the input factors cannot be estimated. Further, results may vary significantly for poor choice of r or if too many of the experiments fail.

3.2. Deterministic Parameter Identification

In this section we consider the optimal control problem of matching the cell voltage $u_{\text{cell}}(t)$ to a measured profile $\hat{u}_{\text{cell}}$ by determining an optimal parameter set μ^* and a corresponding solution u^*, where $X := V \times \mathcal{M}_{\text{ad}}$ and $(u^*, \mu^*) \in X$. For this purpose we setup a cost functional $J : X \to \mathbb{R}$ to be minimized given by

$$J\,(x) := \frac{1}{2}\int_0^T (u_{\text{cell}} - \hat{u}_{\text{cell}})^2 \,\mathrm{d}t + \frac{1}{2}\sum_{i=1}^{m} \chi_i \left(\mu_i - \mu_i^0\right)^2 \tag{3.6}$$

for $x = (u, \mu)$ subject to the equality constraints of the fine model in (2.28) and to the inequality box constraints

$$\mu_a \leq \mu \leq \mu_b, \tag{3.7}$$

where μ_a and μ_b are tuples of scalar values, χ_i is a regularization parameter and μ^0 is a nominal or initial parameter set satisfying $\mu_a \leq \mu^0 \leq \mu_b$.

Using the non-linear solution operator $\mathcal{F}$ we introduce the reduced cost functional for (3.6):

$$\hat{J}(\mu) := J(\mathcal{F}(\mu), \mu), \quad \text{for } \mu \in \mathcal{M}_{\text{ad}}, \tag{3.8}$$

and the reduced problem

$$\underset{\text{s.t. } \mu \in M_{\text{ad}}}{min} \hat{J}(\mu) \tag{3.9}$$

In the simplest form, we approximate the problem (3.9) by minimizing the – weighted – sum of squares, implicitly setting all $\chi_i = 0$:

$$\hat{J}(\theta) \approx \sum_{i=1}^{n} w_i \left(y_i - f(x_i, \theta)\right)^2. \tag{3.10}$$

Let us consider a linear model with p variables,

$$f(\mathrm{x}, \theta) = \theta_0 + \theta_1 \mathrm{x}_1 + \ldots + \theta_p \mathrm{x}_p, \tag{3.11}$$

with n noisy measurement points $\mathrm{y} = (y_0, y_1, \ldots, y_{n-1})$ at $\mathrm{x}_i = (x_{i,0}, x_{i,1}, \ldots, x_{i,n-1})$.
For easier notation and reading, we rewrite the model in matrix notation

$$\mathrm{y} = \mathrm{X}\theta + \varepsilon, \tag{3.12}$$

where X is often referred to as *design matrix*. The design matrix contains the measured values for the control variables along with a column of ones that represents the intercept term θ_0.
It is easy to derive a direct formula for the LSQ estimator that minimizes

$$\tilde{J}(\theta) = |\mathrm{y} - \mathrm{X}\theta|_2^2. \tag{3.13}$$

Solving this system equal or close to zero leaves us with the *normal equation* if we extend both terms with the transposed design matrix

$$\mathrm{X}^T\mathrm{X}\theta = \mathrm{X}^T\mathrm{y}. \tag{3.14}$$

Eventually, we transform this into the solution for θ utilizing the so-called pseudo-inverse $(\mathrm{X}^T\mathrm{X})^{-1}$

$$\theta^* = \left(\mathrm{X}^T\mathrm{X}\right)^{-1} \mathrm{X}^T\mathrm{y}. \tag{3.15}$$

Since $(\mathrm{X}^T\mathrm{X})$ always yields a square matrix, as long as X constitutes a positive definite square matrix or a rectangular matrix with more rows than columns, equation (3.15) may also lead to a result in the case of overdetermined systems, such as in the case of more data points than parameters.
In practice, for most models, such as the fast models used for MPC in Section 2.2.1 or the slightly more elaborate ones presented in Section 2.2.2, one can use standard optimization routines implemented in computational software packages. In this work we mainly used implementations of matlab software from "MathWorks MATLAB" (1992) including nonlinear least-squares fitting "lsqnonlin" and constrained minimization "fmincon". Furthermore we made use of the implementation of "scipy.optimize.leastsq" of "scipy" scientific python based software by Virtanen et al. (2019).

3.2.1. Surrogate Modeling using Space Mapping

For a given reference parameter set $\hat{\mu} \in \mathcal{M}_{\text{ad}}$ and a resulting solution $\hat{u}(\hat{\mu}) = (\varphi_\ell(\hat{\mu}), \varphi_s(\hat{\mu}), c_\ell(\hat{\mu}), c_{sa}(\hat{\mu}), c_{sc}(\hat{\mu}))$ to the weak form in (2.28), we want to define a space mapping $\mathcal{S} : \mathcal{M}_{\text{ad}} \to \mathcal{L}_{\text{ad}}$ to determine a parameter set λ that minimizes the difference between the coarse model and the fine model.

To more generally formulate the following problems, we introduce a projection of the unknowns v to the cell voltage

$$f(v) := \varphi_s(t), \quad \text{on } \Gamma_d, \forall t \in (0,T), \tag{3.16}$$

Using the projection of (3.16), we rewrite the cost functional of (3.6) using the solution v of the coarse model:

$$J_{\text{Sur}}(z) = \frac{1}{2}\int_0^T (f(v) - \hat{\varphi}_s)^2 \, \mathrm{d}t + \frac{1}{2}\sum_{i=1}^{m} \chi_i (\mu_i - \hat{\mu}_i)^2, \quad \mu \in \mathcal{M}_{\text{ad}}, \tag{3.17}$$

for $z = (v, \mu)$, subject to the box constraints $\mu_a \leq \mu \leq \mu_b$.

Again, we introduce the reduced cost functional corresponding to (3.17) by using the solution operator $\mathcal{C}(\lambda)$ as follows:

$$\hat{J}_{\text{Sur}}(\mu) = \frac{1}{2}\int_0^T (f(\mathcal{C}(\mathcal{S}(\mu))) - \hat{\varphi}_s)^2 \, \mathrm{d}t + \frac{1}{2}\sum_{i=1}^{m} \chi_i (\mu_i - \hat{\mu}_i)^2, \quad \mu \in \mathcal{M}_{\text{ad}}, \tag{3.18}$$

Using the mapping function $\mathcal{S}(\mu)$ and the parameter dependent operator (2.37), we define the corresponding Lagrangian to (3.17) as follows:

$$\mathcal{L}(z, \lambda, p, \xi) := J_{\text{Sur}}(z) + \langle c(v, \lambda), p \rangle_{V',V} + \sum_{i=1}^{l} (\lambda_i - \mathcal{S}(\mu_i)) \, \xi_i \tag{3.19}$$

Without further discussion we assume, that there exist Lagrange multipliers $\bar{p} \in V$ and $\xi \in \mathbb{R}^l$ that permit a unique solution $\bar{z} \in V \times \mathcal{M}_{\text{ad}}$ and $\bar{\lambda} \in \mathcal{L}_{\text{ad}}$ satisfying

$$\nabla_\mu \mathcal{L}\left(\bar{z}, \bar{\lambda}, \bar{p}, \bar{\xi}\right)(\mu - \bar{\mu}) \geq 0, \quad \forall \mu \in \mathcal{M}_{\text{ad}} \tag{3.20a}$$

$$\nabla_v \mathcal{L}\left(\bar{z}, \bar{\lambda}, \bar{p}, \bar{\xi}\right)\tilde{v} = 0, \quad \forall \tilde{v} \in V \tag{3.20b}$$

$$\nabla_\lambda \mathcal{L}\left(\bar{z}, \bar{\lambda}, \bar{p}, \bar{\xi}\right)\lambda = 0, \quad \forall \lambda \in \mathcal{L}_{\text{ad}} \tag{3.20c}$$

Following the *Lagrange formalism* depicted in detail in Section A.3, from (3.20b) we obtain the adjoint system as summarized in (3.21):

$$-\alpha_3 \left(\frac{\partial p_1}{\partial t} - \frac{\partial p_3}{\partial t} + \alpha_7 \frac{\partial p_5}{\partial t} - \alpha_{14} \frac{\partial p_7}{\partial t} \right) - \frac{\partial}{\partial x} \left(\alpha_1 \frac{\partial p_1}{\partial x} + \alpha_6 \frac{\partial p_5}{\partial x} \right) - \frac{\partial \hat{j}}{\partial \varphi_\ell} \left(p_1 - p_3 + \alpha_7 p_5 - \alpha_{14} p_7 \right) = 0, \quad \text{on } Q_1 \tag{3.21a}$$

$$\alpha_3 \left(\frac{\partial p_1}{\partial t} - \frac{\partial p_3}{\partial t} + \alpha_7 \frac{\partial p_5}{\partial t} - \alpha_{14} \frac{\partial p_7}{\partial t} \right) - \frac{\partial}{\partial x} \left(\alpha_4 \frac{\partial p_3}{\partial x} \right) - \frac{\partial \hat{j}}{\partial \varphi_s} \left(p_1 - p_3 + \alpha_7 p_5 - \alpha_{14} p_7 \right) = 0, \quad \text{on } Q_1' \tag{3.21b}$$

$$-\varepsilon_{\ell i} \frac{\partial p_5}{\partial t} - \frac{\partial}{\partial x} \left(\alpha_2 \frac{\partial p_1}{\partial x} + \alpha_5 \frac{\partial p_5}{\partial x} \right) - \frac{\partial \hat{j}}{\partial c_\ell} \left(p_1 - p_3 + \alpha_7 p_5 - \alpha_{14} p_7 \right) = 0, \quad \text{on } Q_1 \tag{3.21c}$$

$$-\frac{\partial p_7}{\partial t} - \frac{1}{r^2} \frac{\partial}{\partial r} \left(r^2 \alpha_8 \frac{\partial}{\partial r} p_7 \right) = 0, \quad \text{on Q} \tag{3.21d}$$

$$\alpha_1 \frac{\partial p_1}{\partial \nu} = \alpha_2 \frac{\partial p_1}{\partial \nu} = 0, \quad \text{on } \Sigma_{\text{ad}} \tag{3.21e}$$

$$-\alpha_4 \frac{\partial p_3}{\partial \nu} = \begin{cases} \bar{\varphi}_s - \hat{\varphi}_s & \text{on } \Sigma_d \\ 0 & \text{else} \end{cases} \tag{3.21f}$$

$$\alpha_5 \frac{\partial p_5}{\partial \nu} = \alpha_6 \frac{\partial p_5}{\partial \nu} = 0, \quad \text{on } \Sigma_{\text{ad}} \tag{3.21g}$$

$$-\alpha_8 \frac{\partial p_7}{\partial \nu} = \begin{cases} \frac{\partial \hat{j}}{\partial c_{si}} \left(p_1 - p_3 + \alpha_7 p_5 - \alpha_{14} p_7 \right) & \text{on } \Sigma_R \\ 0 & \text{on } \Sigma_{R,0} \end{cases} \tag{3.21h}$$

$$p_1(T) - p_3(T) = 0, \quad \text{on } \Omega' \tag{3.21i}$$

$$p_5(T) = 0, \quad \text{on } \Omega \tag{3.21j}$$

$$p_7(T) = 0, \quad \text{on } \Lambda \tag{3.21k}$$

From (3.20c) follows

$$\sum_{i=1}^{l} \bar{\xi}_i \lambda_i - \iint\limits_{Q_1'} -\frac{\partial \hat{j}}{\partial \mu}^T \lambda \left(\bar{p}_1 - \bar{p}_3 + \alpha_7 \bar{p}_5 - \alpha_{14} \bar{p}_7 R^2 \right) \mathrm{d}x\mathrm{d}t = 0, \quad \forall \lambda \in \mathcal{L}_{\text{ad}} \tag{3.22}$$

which implies

$$\bar{\xi}_i = - \iint\limits_{Q_1'} \frac{\partial \hat{j}}{\partial \mu_i} \left(\bar{p}_1 - \bar{p}_3 + \alpha_7 \bar{p}_5 - \alpha_{14} \bar{p}_7 R^2 \right) \mathrm{d}x\mathrm{d}t \tag{3.23}$$

Finally, from (3.20a) we obtain

$$\begin{aligned}&\sum_{i=1}^{m}\left(\chi_i\left(\bar{\mu}_i-\hat{\mu}_i\right)\left(\mu_i-\bar{\mu}_i\right)\right)-\sum_{i=1}^{l}\left(\mathcal{S}'\left(\bar{\mu}_i\right)\left(\mu_i-\bar{\mu}_i\right)\bar{\xi}_i\right)\\&=\sum_{i=1}^{l}\left(\chi_i\left(\bar{\mu}_i-\hat{\mu}_i\right)-\mathcal{S}'\left(\bar{\mu}_i\right)^{\star}\bar{\xi}_i\right)\left(\mu_i-\bar{\mu}_i\right)\geq 0,\quad\forall\mu\in\mathcal{M}_{\mathrm{ad}},\end{aligned}\tag{3.24}$$

where $\mathcal{S}'\left(\bar{\mu}_i\right)^{\star}$ is the adjoint operator to $\mathcal{S}'\left(\bar{\mu}_i\right)$.
It follows that the gradient $\hat{J}'_{\mathrm{Sur}}$ of the reduced cost functional (3.18) is given by:

$$\frac{\partial\hat{J}_{\mathrm{Sur}}\left(\mu\right)}{\partial\mu_i}=\chi_i\left(\mu_i-\hat{\mu}_i\right)-\mathcal{S}'\left(\mu_i\right)^{\star}\xi_i.\tag{3.25}$$

Since the computation of $\mathcal{S}'\left(\mu_i\right)$ is a very difficult task, we utilize Broyden's formula described by Broyden (1965) to compute a local Jacobian Matrix B which we will use to replace the derivative of the mapping function $\mathcal{S}'\left(\mu_i\right)$ and its adjoint $\mathcal{S}'\left(\mu_i\right)^{\star}$.
Evaluation of the mapping function $\mathcal{S}\left(\mu\right)$ itself can be performed by finding the minimum of the cost function

$$J_{\mathrm{SM}}\left(y\right):=\frac{1}{2}\int_0^T\left(f\left(\mathcal{C}\left(\tilde{\lambda}\right)\right)-f\left(\mathcal{F}\left(\hat{\mu}\right)\right)\right)^2\,\mathrm{d}t+\frac{1}{2}\sum_{i=1}^{l}\varrho_i\left(\tilde{\lambda}_i-\hat{\mu}_i\right)^2\tag{3.26}$$

for $y=(v,\lambda)$ subject to the equality constraints of the coarse model in (2.36) and subject to the inequality box constraints

$$\lambda_a\leq\lambda\leq\lambda_b,\tag{3.27}$$

where λ_a and λ_b are tuples of positive scalar values with, ϱ_i is a regularization parameter and $\hat{\mu}$ is the target parameter of the fine model parameter space $\mathcal{M}_{\mathrm{ad}}$ satisfying $\mu_a\leq\hat{\mu}\leq\mu_b$.
Using the linear solution operator $\mathcal{C}$ we again introduce the reduced cost functional for (3.26):

$$\hat{J}_{\mathrm{SM}}\left(\lambda\right):=J\left(\mathcal{C}\left(\lambda\right),\lambda\right),\quad\text{for }\lambda\in\mathcal{L}_{\mathrm{ad}},\tag{3.28}$$

and solution of the reduced problem will in turn result in the evaluation of the mapping function $\mathcal{S}\left(\hat{\mu}\right)$:

$$\lambda=\mathcal{S}\left(\hat{\mu}\right)=\arg\min_{\tilde{\lambda}\in\mathcal{L}_{\mathrm{ad}}}\hat{J}_{\mathrm{SM}}\left(\tilde{\lambda}\right).\tag{3.29}$$

Now we can state the algorithm used to solve the surrogate optimization problem as depicted in Algorithm 1.
By separating the surrogate optimization approach from the computation of the mapping, we can utilize more sophisticated existing optimization procedures, e.g. Gauss-Newton based ones, to improve the convergence behavior of the algorithm. For

Algorithm 1 Gradient-projection based surrogate optimization using space mapping

Input: Choose initial $\mu_0 \in \mathcal{M}_{\text{ad}}$ satisfying $\mu_a \leq \mu_0 \leq \mu_b$; set $\zeta = 10^{-4}, k = 0$, and $B_0 = I$.

1: Determine $u_0(\mu)$ from (2.28) with $\mu = \mu_0$.
2: Evaluate $J(u_0, \mu_0)$ from (3.6).
3: Set the working point of the linearized system $(\hat{u}_0, \hat{\mu}_0) = (u_0, \mu_0)$.
4: Compute $\lambda_0 \leftarrow \mathcal{S}(\mu_0)$ by (3.29). ▷ $\lambda_0 \leftarrow \mu_0$
5: **repeat**
6: Determine $v_k(\lambda_k; \hat{u}_k, \hat{\mu}_k)$ from (2.36).
7: Evaluate $\hat{J}_{\text{Sur}}(\mu_k)$ from (3.18).
8: Compute p_k from (3.21) with $\lambda = \lambda_k, v = v_k$.
9: Evaluate the approximate gradient (3.25) $\hat{J}'_{\text{Sur}}(\mu_k) = I\chi(\mu - \hat{\mu}) - B_k^{\star}(\mu)\,\xi$.
10: Determine a step length parameter $\tau_k > 0$ such that

$$\hat{J}_{\text{Sur}}(\mu_k(\tau_k)) \leq \hat{J}_{\text{Sur}}(\mu_k) - \frac{\zeta}{\tau_k}\|\mu_k(\tau_k) - \mu_k\|_2^2,$$

where $\mu_k(\tau) = \mathcal{R}\left\{\mu_k - \tau \hat{J}'_{\text{Sur}}(\mu_k)\right\} \in \mathcal{M}_{\text{ad}}$.

11: Set $\mu_{k+1} \leftarrow \mu_k(\tau_k)$.
12: Determine $u_{k+1}(\mu)$ from (2.28) with $\mu = \mu_{k+1}$.
13: Evaluate $J(u_{k+1}, \mu_{k+1})$ from (3.6).
14: Shift the working point of the linearized system to $(\hat{u}_{k+1}, \hat{\mu}_{k+1}) = (u_{k+1}, \mu_{k+1})$.
15: Compute $\lambda'_k \leftarrow \mathcal{S}(\mu_k)$ by (3.29).
16: Compute $\lambda_{k+1} \leftarrow \mathcal{S}(\mu_{k+1})$ by (3.29). ▷ $\lambda_{k+1} \leftarrow \mu_{k+1}$
17: Update Jacobian of the mapping using Broyden's formula

$$B_{k+1} \leftarrow B_k + \frac{\mathcal{S}_\delta - B_k\mu_\delta}{\|\mu_\delta\|_2^2}\mu_\delta^T,$$

with $\mu_\delta = \mu_{k+1} - \mu_k$ and $\mathcal{S}_\delta = \lambda_{k+1} - \lambda'_k$.

18: Set $k \leftarrow k + 1$.
19: **until** a certain stopping criterium is fulfilled

▷ *lines 4 and 16 simplify to a direct assignment* $\leftarrow$ *in the case of linearization*

the surrogate optimization we introduce the following approximation of the mapping function $\mathcal{S}(\mu)$:

$$\mathcal{S}(\mu) \approx \bar{\mathcal{S}}(\mu) := B\,(\mu - \hat{\mu}) + \hat{\lambda} \tag{3.30}$$

Using the expression of (3.30) instead of (3.29) forces us to rewrite the surrogate optimization problem (3.18) to

$$\hat{\bar{J}}_{\text{Sur}}(\mu) = \frac{1}{2}\int_0^T \left(f\left(\mathcal{C}\left(\bar{\mathcal{S}}(\mu)\right)\right) - \hat{\varphi}_s\right)^2 \mathrm{d}t + \frac{1}{2}\sum_{i=1}^{m}\chi_i(\mu_i - \hat{\mu}_i)^2, \quad \mu \in \mathcal{M}_{\text{ad}}, \tag{3.31}$$

Using the linearization of (3.30), the algorithm is strongly related to Bakr et al. (2001) and was adopted to the battery optimization problem by Scharrer, Pichler, & Suhr (2012); Scharrer, Suhr, & Watzenig (2012).

Using a linearized version of the fine model as the coarse model results in the additional step of shifting the working point. Taking care of this additional step, the algorithm can be stated as shown in Algorithm 2.

Algorithm 2 Gauss-Newton based Surrogate optimization using space mapping $\mathcal{S}$

Input: Choose initial $\mu_0 \in \mathcal{M}_{\text{ad}}$ satisfying $\mu_a \leq \mu_0 \leq \mu_b$; set $k = 0$, and $B_0 = I$.

1: Determine $u_0(\mu)$ from (2.28) with $\mu = \mu_0$.
2: Evaluate $J(u_0, \mu_0)$ from (3.6).
3: Set the working point of the linearized system $(\hat{u}_0, \hat{\mu}_0) = (u_0, \mu_0)$.
4: Compute $\lambda_0 \leftarrow \mathcal{S}(\mu_0)$ by (3.29). ▷ $\lambda_0 \leftarrow \mu_0$
5: **repeat**
6: Define mapping function according to (3.30)

$$\bar{\mathcal{S}}_k(\mu) := B_k\,(\mu - \mu_k) + \lambda_k$$

7: Compute μ^*_{k+1} for the sub-problem using (3.31):

$$\mu^*_{k+1} \leftarrow \arg\min_{\mu \in \mathcal{M}_{\text{ad}}} \hat{\bar{J}}_{\text{Sur}}(\mu)$$

8: Set $\mu_{k+1} \leftarrow \mu^*_{k+1}$.
9: Determine $u_{k+1}(\mu)$ from (2.28) with $\mu = \mu_{k+1}$.
10: Evaluate $J(u_{k+1}, \mu_{k+1})$ from (3.6).
11: Shift the working point of the linearized system to $(\hat{u}_{k+1}, \hat{\mu}_{k+1}) = (u_{k+1}, \mu_{k+1})$.
12: Compute $\lambda'_k \leftarrow \mathcal{S}(\mu_k)$ by (3.29).
13: Compute $\lambda_{k+1} \leftarrow \mathcal{S}(\mu_{k+1})$ by (3.29). ▷ $\lambda_{k+1} \leftarrow \mu_{k+1}$
14: Update Jacobian of the mapping using Broyden's formula

$$B_{k+1} \leftarrow B_k + \frac{\mathcal{S}_\delta - B_k \mu_\delta}{\|\mu_\delta\|_2^2} \mu_\delta^T,$$

with $\mu_\delta = \mu_{k+1} - \mu_k$ and $\mathcal{S}_\delta = \lambda_{k+1} - \lambda'_k$.
15: Set $k \leftarrow k + 1$.
16: **until** a certain stopping criterium is fulfilled

▷ *lines 4 and 13 simplify to a direct assignment* $\leftarrow$ *in the case of linearization*

Following the ideas of Bakr et al. (1998) and Hintermüller & Vicente (2005), the approach presented in Algorithm 2 can be further globalized and extended by means of the trust–region technique and modification of the Broyden update, as minimization by using the surrogate is our primary goal rather than perfectly solving the space mapping (3.29). To be able to implement the trust–region technique, we rewrite the reduced cost functional (3.18) by making it dependent on λ directly in addition to μ as follows:

$$\hat{J}^*_{\text{Sur}}(\lambda(\mu), \mu) = \frac{1}{2}\int_0^T \left(f\left(\mathcal{C}\left(\lambda(\mu)\right)\right) - \hat{\varphi}_s\right)^2 \mathrm{d}t + \frac{1}{2}\sum_{i=1}^{m} \chi_i \left(\mu_i - \hat{\mu}_i\right)^2, \quad \mu \in \mathcal{M}_{\text{ad}}, \lambda \in \mathcal{L}_{\text{ad}} \tag{3.32}$$

On the basis of Algorithm 2 we can incorporate this ideas as depicted in Algorithm 3.

Algorithm 3 Trust-Region based Surrogate optimization using space mapping $\mathcal{S}$

Input: Choose initial $\mu_0 \in \mathcal{M}_{\text{ad}}$ satisfying $\mu_a \leq \mu_0 \leq \mu_b$; Choose $\gamma_1, \gamma_2, \eta_1 \in (0,1)$; set $k = 0, B_0 = I$ and $\Delta_0 = 1$.

1: Determine $u_0(\mu)$ from (2.28) with $\mu = \mu_0$.
2: Evaluate $J(u_0, \mu_0)$ from (3.6).
3: Set the working point of the linearized system $(\hat{u}_0, \hat{\mu}_0) = (u_0, \mu_0)$.
4: Compute $\lambda_0 \leftarrow \mathcal{S}(\mu_0)$ by (3.29). ▷ $\lambda_0 \leftarrow \mu_0$
5: **repeat**
6: Define mapping function according to (3.30)

$$\bar{\mathcal{S}}_k(\mu) := B_k(\mu - \mu_k) + \lambda_k$$

7: Compute μ^*_{k+1} for the sub-problem using (3.31):

$$\mu^*_{k+1} \leftarrow \arg\min_{\mu \in \mathcal{M}_{\text{ad}}} \hat{\bar{J}}_{\text{Sur}}(\mu), \quad \text{s.t.} \quad \left\|\mu^*_{k+1} - \mu_k\right\| \leq \Delta_k$$

8: Determine $u_{k+1}(\mu)$ from (2.28) with $\mu = \mu^*_{k+1}$.
9: Evaluate $J\left(u_{k+1}, \mu^*_{k+1}\right)$ from (3.6).
10: Shift the working point of the linearized system to $(\hat{u}_{k+1}, \hat{\mu}_{k+1}) = \left(u_{k+1}, \mu^*_{k+1}\right)$.
11: Compute $\lambda'_k \leftarrow \mathcal{S}(\mu_k)$ by (3.29).
12: Compute $\lambda_{k+1} \leftarrow \mathcal{S}\left(\mu^*_{k+1}\right)$ by (3.29). ▷ $\lambda_{k+1} \leftarrow \mu^*_{k+1}$
13: Determine ratio between actual and predicted reduction

$$\rho_k = \frac{\text{ared}\left(\mu_k, \mu^*_{k+1}\right)}{\text{pred}\left(\mu_k, \mu^*_{k+1}\right)} = \frac{\hat{J}^*_{\text{Sur}}(\lambda'_k, \mu_k) - \hat{J}^*_{\text{Sur}}\left(\lambda_{k+1}, \mu^*_{k+1}\right)}{\hat{\bar{J}}_{\text{Sur}}(\mu_k) - \hat{\bar{J}}_{\text{Sur}}\left(\mu^*_{k+1}\right)}$$

14: **if** $\rho_k \geq \eta_1$ **then**
15: Set $\mu_{k+1} \leftarrow \mu^*_{k+1}$.
16: Grow trust–region $\Delta_{k+1} \leftarrow \frac{\Delta_k}{\gamma_2}$
17: Update Jacobian of the mapping using Broyden's formula

$$B_{k+1} \leftarrow B_k + \frac{\tilde{\mathcal{S}}_\delta - B_k \mu_\delta}{\|\mu_\delta\|_2^2} \mu_\delta^T,$$

where $\tilde{\mathcal{S}}_\delta = \mathcal{S}_\delta + \sigma_k \frac{\Delta \hat{J}^*_{\text{Sur}} - \left(\hat{J}'_{\text{Sur}}\right)^T \mathcal{S}_\delta}{\left\|\hat{J}'_{\text{Sur}}\right\|_2^2} \hat{J}'_{\text{Sur}}$, $\mathcal{S}_\delta = \lambda_{k+1} - \lambda'_k$, $\mu_\delta = \mu_{k+1} - \mu_k$
and $\Delta \hat{J}^*_{\text{Sur}} = \hat{J}^*_{\text{Sur}}\left(\lambda_{k+1}, \mu^*_{k+1}\right) - \hat{J}^*_{\text{Sur}}(\lambda'_k, \mu_k)$
18: **else**
19: Keep $\mu_{k+1} \leftarrow \mu_k$
20: Shrink trust–region $\Delta_{k+1} \leftarrow \gamma_1 \Delta_k$
21: Keep $B_{k+1} \leftarrow B_k$
22: Shift back the working point of the linearized system $(\hat{u}_{k+1}, \hat{\mu}_{k+1}) = (u_k, \mu_k)$.
23: **end if**
24: Set $k \leftarrow k + 1$.
25: **until** a certain stopping criterium is fulfilled

▷ *lines 4 and 12 simplify to a direct assignment* $\leftarrow$ *in the case of linearization*

3.2.2. Space Mapping for RC-Models

The system described in the Section 2.3 contains many parameters which cannot be measured directly. To formulate the parameter estimation problem in a general way, we merge the parameter set of interest into the parameter vector $\mathrm{p} \in P_{\mathrm{ad}} \subset \mathcal{R}^m$, where P_{ad} is defined as the admissible parameter set. The basis optimization problem is introduced as

$$\mathrm{p}^* = \arg\min_{\mathrm{p}\in P_{\mathrm{ad}}} H\left(f\left(\mathrm{p}\right)\right), \tag{3.33}$$

where an optimal set of parameters $\mathrm{p}^* \in P_{\mathrm{ad}}$ is sought, which minimizes a merit function H of a model response $f\left(\mathrm{p}\right)$ depending on the parameters p.

Since we focus on parameter estimation based on cell voltages, we set H to compute the difference with respect to a predescribed function $\hat{y}$. We rewrite (3.33) to

$$\mathrm{p}^* = \arg\min_{\mathrm{p}\in P_{\mathrm{ad}}} \left\| w_i \left(y(t_i;\mathrm{p}) - \hat{y}(t_i)\right)\right\|_2^2 \tag{3.34}$$

where we want to minimize the difference between measured cell voltages $\hat{y}$ and computed voltages $f\left(\mathrm{p}\right) = y\left(\cdot;\mathrm{p}\right) = \varphi_s|_{\Gamma_c} - \varphi_s|_{\Gamma_a}$ at predefined times t_i. Variations in time step sizes are taken into account by the weights w_i.

Classical optimization using this objective function yields unacceptable response times, since not only the solution of the system defined in Section 2.3 has to be computed, but additionally the derivative of the objective function with respect to every parameter in our set of interest p has to be estimated. Since this might be intractable for non–linear PDE constraint problems, we revert to numerical gradient estimation by finite differences. As execution time of a single simulation on current hardware may require several minutes to hours – depending on the prescribed input profile – direct evaluation of (3.34) is to be avoided where possible.

3.3. Hybrid Stochastic Parameter Identification

The traditional approach to solve the parameter identification problem involves minimizing the difference between the measured response and predicted response. If the cell voltage curve obtained through experimental measurement is $\hat{u}_{\mathrm{cell}}(t)$ and the cell voltage curve obtained by solving the mathematical model for a given parameter set μ is $u_{\mathrm{cell}}(t;\mu)$, then the correct parameter set μ^* can be estimated by solving the optimization problem given by

$$\begin{aligned}\mu^* &= \arg\min_{\mu\in\mathcal{M}_{\mathrm{ad}}} \hat{J}\left(\mu\right) \\ &= \frac{1}{2}\int_0^T \left(u_{\mathrm{cell}}(t;\mu) - \hat{u}_{\mathrm{cell}}(t)\right)^2 \,\mathrm{d}t\end{aligned} \tag{3.35}$$

The minimization algorithm subsequently updates the parameter set μ to minimize the error norm. It should be mentioned that each computation of that error norm requires the solution of the mathematical model using the given parameter set μ. For this

reason, an algorithm that can efficiently minimize the error with few number of model evaluations is very appealing, such as in Section 3.2. This minimization algorithm must be robust and should be able to avoid local minima. Due to the computational efforts and time necessary in order to solve the mathematical models of both, the SPM and DFN, and due to the non-linearity of the cost-function space, efficiency is another fundamental requirement to the optimization algorithm.

The "*No-Free-Lunch-Theorems*" state that

> (Wolpert & Macready, 1997) *If an algorithm performs well on a certain class of problems then it necessarily pays for that with degraded performance on the set of all remaining problems.*

Conversely, this means that a combination of several optimization algorithms with potentially adversarial properties and fitness w.r.t. problem classes increases the robustness of the holistic algorithm over many problem classes.

For this reason, a recently developed hybrid optimizer is used to solve the above optimization problem, the "Single Objective Hybrid Optimizer (SOHO)" algorithm. The Single Objective Hybrid Optimizer (SOHO) algorithm is capable of combining several different algorithms from deterministic and stochastic optimization domains. The three algorithms used in this work are the single objective variants of the Non-dominant Sorting Genetic Algorithm III (NSGA-III) by Deb & Jain (2014), Non-dominant Sorting Differential Evolution (NSDE) by Robič & Filipič (2005) and Multiobjective Evolutionary Algorithm based on Dominance and Decomposition (MOEA-DD) by Li et al. (2015), since all three of them are commonly known as robust and performing satisfyingly.

The top-level optimization switching strategy works as described below: One of the three previously stated algorithms is selected to initialize the SOHO. The algorithm is operating in iterations until the target objective value, i.e. the error norm, stagnates and does not reduce any further. If the objective value stagnates, a different algorithm is selected randomly from the remaining two. This random selection of algorithms adds a stochastic nature to search process and avoids user bias. Figure 3.1 shows the three algorithms and the switching scheme.

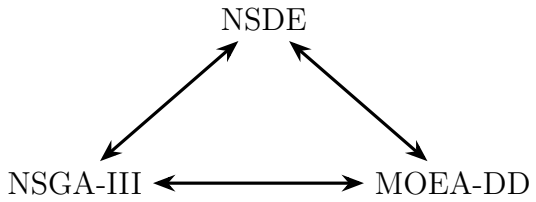

Figure 3.1.: *Algorithms and switching between the algorithms in the SOHO suite.*

This hybridization allows SOHO to avoid or escape local minima and increases the convergence rate to the global minimum.

NSGA-III uses simulated binary crossover (Deb & Agrawal, 1995) and polynomial mutation (Deb, 2001) to perform recombination. The parent parameters to be mated are selected randomly from the entire population set.

NSDE uses the "*rand/1/bin*" (Robič & Filipič, 2005) mutation to perform the recombination where the parents to be mated are randomly selected from population set of unique members.

MOEA-DD also uses the same recombination operators as the NSGA-III algorithm, but selects its parents randomly from the N *best members*.

As previously mentioned, the parameter estimation problem is solved by minimizing the L^2-norm of the difference between the calculated and measured voltage curves. The calculated curve is obtained by solving the mathematical model – SPM or DFN, respectively – while the measured voltage curve has been obtained experimentally – see Section 4.1.

It is worth noting that the so-called "*inverse crime*" (Wirgin, 2004) is avoided in this work since the two voltage curves are obtained using different methods and due to the inherent measurement errors present in the experimentally obtained voltage curve.

3.4. Bayesian methodology

After having optimized parameters as discussed in the preceding sections, there always remains an error between the model results and measurements. All real data is subject to noise and measurement errors, the estimated unknowns according to the above sections are to some degree uncertain.

Noisy data is not the only source of uncertainty in modeling. It may be more challenging to estimate the impact of model bias due to insufficient understanding of the phenomena under study, or just the numerical approximation errors we may have to make to minimize the CPU requirements.

A recent development of the last decades regarding computational models, particularly in the computational science and engineering community, is the focus on UQ methods to estimate model error statistics to describe uncertainties.

3.4.1. Linear Model Error Statistics

For linear models, such as the ones described in (3.11) in Section 3.2 the statistics of parameter estimation or the so-called *uncertainty* can be determined with ease. To obtain the statistics for the estimate, we can compute the covariance matrix $\mathrm{Cov}(\theta^*)$. Under the assumption that the measurement noise is independent and identically distributed (iid), i.e. $\varepsilon \overset{\text{iid}}{\sim} \mathcal{D}\{0, \sigma^2\}$ of some distribution $\mathcal{D}$, the covariance matrix for the measurement is given as $\mathrm{Cov}(\mathrm{y}) = \sigma^2 \mathrm{I}$, where I is the identity matrix. The parameter uncertainty is then characterized by the covariance

$$\mathrm{Cov}(\hat{\theta}) = \sigma^2 (\mathrm{X}^T \mathrm{X})^{-1}. \tag{3.36}$$

The diagonal of the covariance matrix contains the variances of the estimated parameters. If we further assume that the measurement errors are Gaussian, we can also conclude

that the distribution of θ^* is Gaussian, with the covariance matrix as stated by the expressions above.

For non-linear models, no such closed expression is available. In this case, we need to use numerical methods and approximations. The standard strategy in these cases is to linearize the non-linear model and employ the linear theory as stated above. This requires the computation of model parameters' derivatives. The first order derivatives can be assembled into a matrix – the *Jacobian* J with its elements

$$[\mathrm{J}]_{ip} = \frac{\partial f\left(x_i;\theta\right)}{\partial \theta_p}|_{\theta=\theta^*}, \tag{3.37}$$

where θ^* denotes the linearization point of θ at each measurement point x_i. The Jacobian J has a similar function to the design matrix X in the linear case. This means approximative error analysis for non-linear models – assuming iid Gaussian errors with measurement error variance σ^2 –, is given by the covariance matrix

$$\mathrm{Cov}(\theta^*) = \sigma^2(\mathrm{J}^T\mathrm{J})^{-1}. \tag{3.38}$$

The measurement error σ^2 can be estimated using repeated measurements. Replicated measurements are rarely available. In this case, the measurement noise can be estimated using the residuals of the fit, using the "perfect model" assumption that *residuals* $\approx$ *measurement error*. An estimate for the measurement error can be obtained using the Mean Square Error (MSE):

$$\sigma^2 \approx \mathrm{MSE} = \mathrm{RSS}/(n-p), \tag{3.39}$$

where Residual Sum of Squares (RSS) is the fitted value of the least squares function, n is the number of measurements and p is the number of parameters in θ. In other words, the measurement error variance is computed as the average of the squared residuals, adjusted to the actual Degrees of Freedom (DOF), i.e. the number of measurement points reduced by the number of estimated parameters.

3.4.2. General Model Error Statistics

In the case of non-linear models, error estimates of linearized models are valid only in the case of parameter distributions being close to Gaussian distributions due to maximizing the likelihood equals minimizing the sum of the squares of the residuals. However, this cannot be guaranteed. Non-linear model structures usually result in parameter distributions that are far from the results of the linearized versions.

This section introduces a method that – even in the presence of strong non-linearity – enables to explore the true distributions. This exploration is conducted by sampling from the target distributions using the MCMC method devised by Metropolis et al. (1953); Hastings (1970) in spite of not knowing these distributions in advance.

Instead of changing the data, MCMC methods take the uncertainty of data into account by accepting parameters that produce model predictions that fit the data within the noise level of measurements.

The Bayesian approach of MCMC treats the unknown vector of parameters $\boldsymbol{\theta}$ as a *random variable* sampled from a distribution. This manifests itself in $\boldsymbol{\theta}$ being changed rather than repeated measurement of the *same* experiment, which is an infeasible task in the context of batteries and their long-term dynamics and aging effects. In addition, *prior knowledge* may be included naturally in the estimation process.

Again, we consider the non-linear model $y_i = f(x_i; \boldsymbol{\theta}) + \varepsilon_i$, where we assume the errors $\varepsilon_i \overset{\text{iid}}{\sim} \mathcal{N}(0, \sigma^2)$. The vector $\boldsymbol{\theta}$ comprises the unknowns to be estimated by the measured data values y_i.

Assuming $\boldsymbol{\theta}^*$ is known and a perfect, unbiased model $f(\boldsymbol{x}; \boldsymbol{\theta}^*)$, measured values y_i follow the normal distribution centered around $f(x_i, \boldsymbol{\theta}^*)$. As the errors ε_i were assumed to be independent, the distributions of the different measurements y_i, $i = 0, \ldots, n-1$ are independent, and the joint distribution for the measurement vector $\boldsymbol{y} = (y_0, \ldots, y_{n-1})$ is obtained as the product of distributions:

$$\begin{aligned} p\left(\boldsymbol{y}|\theta\right) &= \prod_{i=0}^{n-1} \frac{1}{\sqrt{2\pi\sigma^2}} \exp\left(\frac{-(y_i - f(\boldsymbol{x};\theta))^2}{2\sigma^2}\right) \\ &= \frac{1}{(2\pi\sigma^2)^{n/2}} \exp\left(-\sum_{i=0}^{n-1} \frac{\left(y_i - f\left(\boldsymbol{x};\theta\right)\right)^2}{2\sigma^2}\right), \end{aligned} \tag{3.40}$$

where $p\left(\boldsymbol{y}|\theta\right)$ is the *conditional probability* of $\boldsymbol{y}$ given θ and referred to as *likelihood function*. For numerical reasons, we use log-transform and state the *log-likelihood* function as

$$\begin{aligned} \text{logLH}(\theta) &= p\left(\boldsymbol{y}|\theta\right) \\ &= -\frac{n}{2}\log 2\pi\sigma^2 - \sum_{i=0}^{n-1} \frac{\left(y_i - f\left(\boldsymbol{x};\theta\right)\right)^2}{2\sigma^2}, \end{aligned} \tag{3.41}$$

Using the likelihood function, the Bayes formula can be written as a generalization of the conditional probability in basic probability calculus, as

$$\pi\left(\boldsymbol{\theta}|\boldsymbol{y}\right) = \frac{p\left(\boldsymbol{y}|\boldsymbol{\theta}\right)\pi(\boldsymbol{\theta})}{p(\boldsymbol{y})} = \frac{p\left(\boldsymbol{y}|\boldsymbol{\theta}\right)\pi(\boldsymbol{\theta})}{\int p(\boldsymbol{y}|\boldsymbol{\theta})\pi(\boldsymbol{\theta})\mathrm{d}\theta}. \tag{3.42}$$

In (3.42) we face the problem of computing the integral expression for the so-called *evidence* $p(\boldsymbol{y})$ of the output, i.e. the normalizing constant, which may be an infeasible task in the case of physical models.

3.4.3. Metropolis Random Walk

The most famous MCMC algorithm is the random walk Metropolis algorithm developed by Metropolis et al. (1953). Despite its simplicity, the Metropolis algorithm is very effective: it works by generating candidate parameter values from a *proposal distribution* and then either accepts or rejects the value proposal according to a simple rule. Algorithm 4 shows the Metropolis algorithm in pseudo-code.

Algorithm 4 The random walk Metropolis algorithm (Metropolis et al., 1953)

Input: Choose initial $\mu_0 \in \mathcal{M}_{\text{ad}}$ satisfying $\mu_a \leq \mu_0 \leq \mu_b$

1: **repeat**
2: Choose a new candidate **proposal** $\hat{\theta}$ from a suitable *proposal distribution* $q(.|\mu_n)$, possibly depending on the previous point of the chain.
3: **Accept** the candidate with probability

$$\alpha\left(\theta_n, \hat{\theta}\right) = \min\left(1, \frac{\pi(\hat{\theta})}{\pi(\theta_n)}\right). \tag{3.43}$$

4: **if** accept **then**
5: add the new candidate point to the chain.
6: **else**
7: repeat the previous point in the chain.
8: **end if**
9: Set $n \leftarrow n + 1$.
10: **until** a certain stopping criterium is fulfilled, e.g. $n = N_{\text{iter}}$

Output: a chain of parameter tuples $\boldsymbol{\theta}$ drawn from $\pi(\boldsymbol{\theta}|\boldsymbol{y})$

Instead of estimating the computationally infeasible integral from (3.42), only ratios of π between successive points in the parameter space are required to succeed in Algorithm 4. In addition, it is also possible to specify a *non-informative prior* distribution and still obtain a solution, i.e. providing a *flat prior* bound by box-constraints may already be sufficient.

We use a Gaussian proposal kernel to propose successive values in the Markov chain. The distribution used for the proposal kernel is fundamental to the performance of the entire chain. The key performance criterion is the so-called "*mixing*" of the chain, i.e. how well the chain *spreads* across the entire parameter space. Since in Algorithm 4 the proposal is centered around the previous state, this is referred to as a "random walk" algorithm. The kernel distribution is usually chosen as Gaussian. The covariance of such kernels may be set by trial and error, but to improve, i.e. shorten, the burn-in phase of the MCMC algorithm, we utilize the covariance from linear theory, i.e. for a linear model $y = \boldsymbol{J\theta} + \varepsilon$ with errors $\varepsilon \overset{\text{iid}}{\sim} \mathcal{N}(0, \sigma^2 I)$ follows (3.38), so we initialize the proposal covariance to:

$$C^{(0)} = \text{Cov}(\hat{\boldsymbol{\theta}}) \approx \sigma^2 \left(J^T J\right)^{-1}. \tag{3.44}$$

This holds true for residuals equal to zero or very small residuals. Furthermore, we can use the residuals to estimate the variance σ^2 in (3.44):

$$\sigma^2 \approx \sigma^2_{\text{MSE}} = \frac{\sum_{i=1}^{n} \left(u_{\text{cell}}(t;\boldsymbol{\theta}) - u_{\text{cell}}(t)\right)^2}{n - p}, \tag{3.45}$$

where p is the number of parameters in $\boldsymbol{\theta}$.

Since J in (3.44) is hard to compute analytically correct, we use finite differencing and concurrent computing to quickly estimate the gradient of $u_{\text{cell}}(t;\boldsymbol{\theta})$ with respect to $\boldsymbol{\theta}$ and adopt it into the Jacobian J.

3.4.4. Adaptive Metropolis

One of the fundamental problems of the random-walk MCMC algorithm is the choice of the underlying distribution for the proposal kernel, so that the algorithm converges as quickly as possible. On the one hand, this could be set by choosing the parameters of the Gaussian distribution, as shown in Section 3.4.3. However, the Adaptive MCMC method has emerged as a better choice. The Adaptive MCMC method is based on the previous history of the Markov chain, i.e. the previously migrated list of parameter tuples. Of course, this type of adaptivity is prone to the stochastic process losing its Markov properties, since each instance in the Markov chain no longer depends exclusively on its predecessor, but on a longer range of the previous history.

The adaptivity is based on the adaptation of the covariance matrix of a Gaussian distribution, i.e. the extent and orientation of the distribution in the parameter space adapt to the environment of the target distribution.

Adaptive Metropolis (AM) algorithms were introduced by Haario et al. (2001). Growing parts of the chain are used for the adjustment. As a result, the chain's Markov property is generally lost and the chain's ergodicity can no longer be easily ensured, however, in the case of a growing window size to determine the proposal distribution, statements can be made and proven regarding the ergodicity (Haario et al., 2001).

For the AM method, Algorithm 4 only needs to be extended by a few simple steps. After the "acceptance" step 3, there are ideally two further steps:

- Calculate $C^{(i+1)}$
- Calculate R such that $C^{(i+1)} = R^T R$

For $C_i + 1$ we use an adaptation from the entire chain:

$$C^{(i+1)} = s_d \mathrm{Cov}(\theta_0, \ldots, \theta_t), \quad \text{if } n > n_0 \tag{3.46}$$

where n_0 represents the "initialization time" of adaptivity. That is, as long as $n \leq n_0$ we use the initial covariance C_0, as shown in equation (3.44). The constant s_d is a scaling variable that depends on the dimension of the parameter space. The rule of thumb for the scaling size is $s_d = \frac{2.4^2}{d}$ as stated by Gelman et al. (1996). This should ideally optimize the mixing property of the random walk algorithm if Gaussian distributions are used for likelihood and proposal distribution (Haario et al., 2001).

"Thinning" can be used to prevent excessive volatility in the proposal widths. This means that the adjustment is only made for all n_U iterations and is retained in between.

To calculate the covariance, all samples of the chain are required in the standard formula (3.46). Since MCMC methods typically result in very long chains, all values would have to be kept in memory for this and taken into account during the update. In order to make these calculations more efficient in terms of memory and speed, the calculation of the covariance is carried out via accumulated values and the recurrent relation introduced by Welford (1962).

First part of the algorithm starts at iteration n_0 and estimates the covariance as stated in (3.46). Furthermore, we calculate the chain's average value $\bar{\boldsymbol{\theta}}^{(i+1)}$ and the

accumulative sum of squares of differences $M^{(i+1)}$.

$$\bar{\boldsymbol{\theta}}^{(i+1)} = \frac{1}{i+1} \sum_{t=0}^{i} \boldsymbol{\theta}^{(t)} \tag{3.47a}$$

$$C^{(i+1)} = \mathrm{Cov}\left(\boldsymbol{\theta}^{(0)}, \ldots, \boldsymbol{\theta}^{(N_c)}\right) \tag{3.47b}$$

$$M^{(i+1)} = (i)\, C^{(i+1)}. \tag{3.47c}$$

For every update of the chain after the initialization phase, i.e. after appending a new set $\boldsymbol{\theta}^{(i+1)}$, we need to update the running average $\bar{\boldsymbol{\theta}}^{(i+1)}$ and the running sum of squares of differences $M^{(i+1)}$

$$\bar{\boldsymbol{\theta}}^{(i+1)} = \frac{i\,\bar{\boldsymbol{\theta}^{(t)}} + \boldsymbol{\theta}^{(t+1)}}{t+1} \tag{3.48a}$$

$$M^{(i+1)} = M^{(i)} + \left(\boldsymbol{\theta}^{(t+1)} - \bar{\boldsymbol{\theta}}^{(i+1)}\right)\left(\boldsymbol{\theta}^{(t+1)} - \bar{\boldsymbol{\theta}}^{(i+1)}\right)^{T}. \tag{3.48b}$$

For every adaption update of the proposal kernel, i.e. in the case of thinning for every $i - n_0 \equiv 0 \,(\mathrm{mod}\ n_U)$, the covariance matrix may be quickly estimated by simply computing

$$C^{(i+1)} \leftarrow \frac{M^{(i+1)}}{i}. \tag{3.49}$$

Thus, any overhead time from increasing memory consumption of storing the entire Markov chain may be avoided and the AM algorithm may be executed with no significant influence on the performance even in the case of fast model evaluation.

3.4.5. Parallelism

In his article, Solonen et al. (2012) showed how an effective parallelization of the MCMC algorithm can be implemented for complex, computationally expensive models. Instead of a single, long chain, several adaptive chains are processed in parallel. In order not to lose the Markov property of each individual chain, it is obviously not easily possible to exchange values between the individual chains. Craiu et al. (2009) has shown a simple and effective way that improves the mixing properties of the chains in order to increase each individual chain's efficiency. Information about the entirety of all parameter chains collected so far is gathered at a central point and the information required for improved adaptivity of each individual chain is returned. This means that instead of calculating each individual chain separately from another, the covariance is no longer updated for the individual chain as described in equations (3.46) and (3.49), but at a central point. Figure 3.2 shows the working principle for an example of three parallel chains.

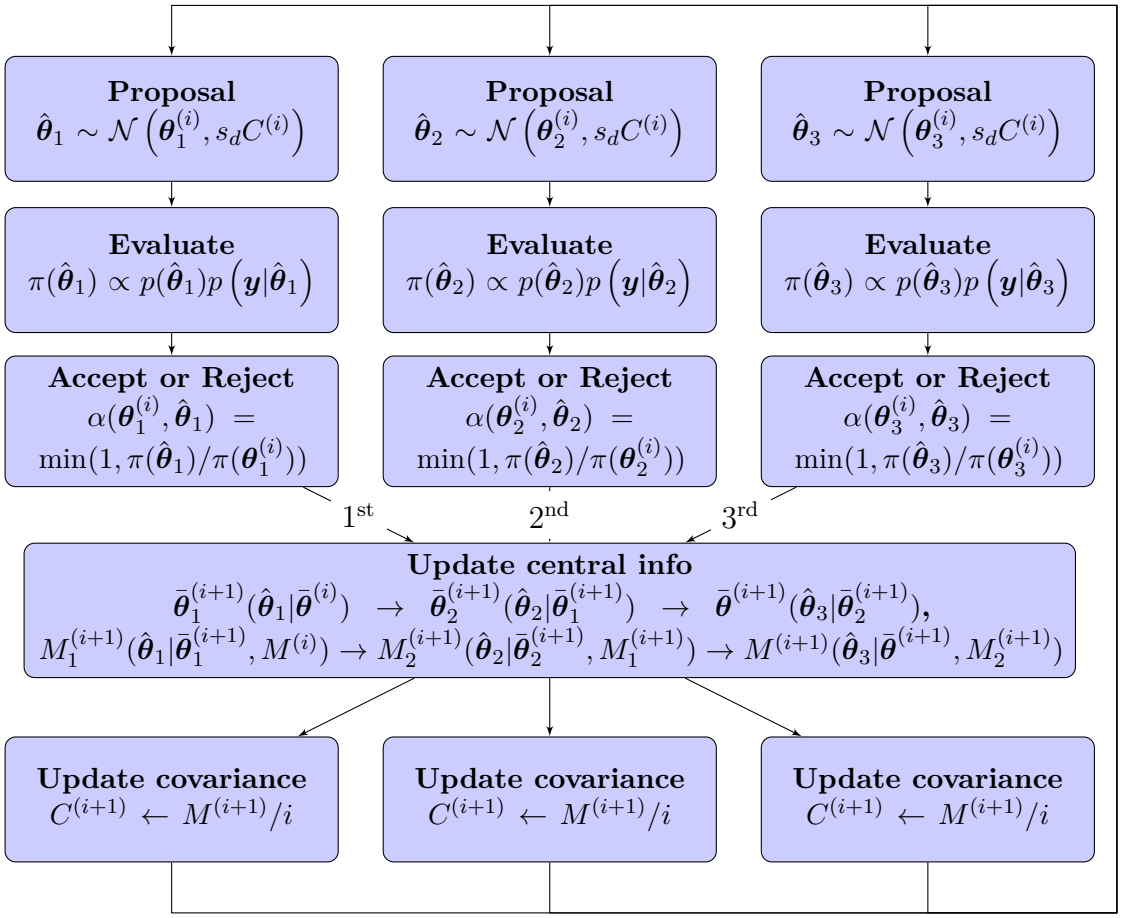

Figure 3.2.: *Adaptive Metropolis algorithm workflow. Here, three chains are shown as an example of how the proposal kernel covariance is adapted using the results from all chains. Proposed samples are denoted by $\hat{\boldsymbol{\theta}}_i$ of chain i. The global update step successively applies information provided of* concurrent *execution in* random *sequence of arrival. Here, a simple $1 \rightarrow 2 \rightarrow 3$ sequence is shown as an example.*

3.4.6. Single Component Adaptive Metropolis

Whereas the algorithms in the sections above describe the update of all parameters at once, this may not always be an ideal strategy. Even in the original article by Metropolis et al. (1953), the chain is updated one component of $\boldsymbol{\theta}$ at a time. This means, each iteration of the algorithm is rather split up into p sub-iterations of updating each parameter in $\boldsymbol{\theta}$ individually. It is important to note that the Markov chain is not branched by this approach, i.e. each of the sub-iterations takes into account the result of the preceding sub-iteration rather than the previous full iteration. While this slows down the sampling process and reduces computational efficiency due to p model evaluations per iteration versus a single model evaluation per iteration, the Single Component (SC) approach has the advantage that for higher numbers of p, the proposal distributions remain simple while not being affected by possible highly complex covariance structures and correlations between parameters. Furthermore, this leads to better mixing in terms of movements in the parameter space due to higher

acceptance rates, while proposals covering the entire parameter set $\boldsymbol{\theta}$ have a very low probability of being accepted.

After the initialization step, the single component algorithm walks through all p parameters of the previous sample $\boldsymbol{\theta}^{(i-1)}$ and modifies one component by drawing a new proposal $\hat{\boldsymbol{\theta}}_j$ from the one-dimensional Gaussian proposal kernel distribution

$$q\left(\cdot|\boldsymbol{\theta}^{(i-1)}\right) \sim \mathcal{N}\left(\boldsymbol{\theta}^{(i-1)}, s_d C_{j,j}^{(i)}\right), \tag{3.50}$$

where $C_{j,j}^{(i)}$ indicates the respective diagonal entry of the current chain's covariance and the dimension dependent scaling parameter $s_d = \frac{2.4^2}{n_d}$, which is 2.4^2 for the single component case (=one dimensional).

For the next step, we accept the proposal with probability

$$\alpha\left(\boldsymbol{\theta}^{(i-1)}, \hat{\boldsymbol{\theta}}_j\right) = 1 \wedge \frac{\pi\left(\hat{\boldsymbol{\theta}}_j\right)}{\pi\left(\boldsymbol{\theta}^{(i-1)}\right)}, \tag{3.51}$$

and on rejection we repeat the point $\boldsymbol{\theta}^{(i-1)}$ as $\boldsymbol{\theta}^{(i)}$ in the chain. In the higher dimensional parameter sets case of the cell model, we notice very low acceptance rates due to high correlation between parameters.

All methods that consider parameters individually and not in their entirety are prone to poor mixing behavior if the parameters are strongly correlated. This is to be expected because the correlations cannot be represented by simple one-dimensional proposal distributions, where movements in the parameter space can only take place along the main axes.

One solution to this problem is a rotation of the parameter space, which could be easily accomplished using the "*Principal Component Analysis (PCA)*" of the Markov chain, which results in transformed new main axes as a linear combination of the existing dimensions. Another advantage of the Principal Component Analysis (PCA) would be the possibility of reducing the number of dimensions and work in a sub-space, which would further improve the performance of the algorithm in any case, since the algorithm would mainly make significant changes in this way.

3.4.7. Single Component Adaptive Metropolis with Delayed Rejection

To further improve the acceptance rate and the efficiency of the algorithm, we apply the concept of Delayed Rejection (DR) as introduced by Tierney & Mira (1999): Instead of directly rejecting a failed proposal, we propose a new parameter set $\hat{\boldsymbol{\theta}}_j^{(1)}$ based on the rejected parameter set and perform a new acceptance check. Obviously, this new check is subject to a modified acceptance probability rate

$$\alpha\left(\boldsymbol{\theta}^{(i-1)}, \hat{\boldsymbol{\theta}}_j, \hat{\boldsymbol{\theta}}_j^{(1)}\right) = 1 \wedge \frac{\pi\left(\hat{\boldsymbol{\theta}}_j^{(1)}\right) q\left(\boldsymbol{\theta}^{(i-1)}|\hat{\boldsymbol{\theta}}_j, \hat{\boldsymbol{\theta}}_j^{1}\right)\left[1-\alpha\left(\hat{\boldsymbol{\theta}}_j^{1}, \hat{\boldsymbol{\theta}}_j\right)\right]}{\pi\left(\boldsymbol{\theta}^{(i-1)}\right) q\left(\hat{\boldsymbol{\theta}}_j^{1}|\hat{\boldsymbol{\theta}}_j, \boldsymbol{\theta}^{(i-1)}\right)\left[1-\alpha\left(\boldsymbol{\theta}^{(i-1)}, \hat{\boldsymbol{\theta}}_j\right)\right]}, \tag{3.52}$$

which accounts for the previous rejection and the modification of the new proposal. In the case of another rejection, this may be iterated for k stages until we reach acceptance or continue with the next step, i.e. processing the remaining parameters of the set.

Due to the virtually infinite availability of computational power, we propose to perform the computation of the stages in parallel for the wall-clock time cost of a single computation and decide about the acceptance on the basis of (3.51) and (3.52) afterwards.

DR was later on combined with AM by Haario et al. (1999, 2001) into the Delayed Rejection Adaptive Metropolis (DRAM) algorithm (Haario et al., 2006). For the original AM, possibly after an initialization period, we periodically update the proposal covariance $C^{(i)}$ centered at the current position of the Markov chain, i.e. at $\theta^{(i)}$, and set it to

$$C^{(i)} = \begin{cases} C^{(0)} & n \leq n_0 \\ s_d \mathrm{Cov}\left(\boldsymbol{\theta}^{(0)}, \ldots, \boldsymbol{\theta}^{(i-1)}\right) & n > n_0 \end{cases} . \tag{3.53}$$

We use the proposal covariance $C^{(i)}$ for the first proposal in each iteration. On rejection, we modify all subsequent proposal covariances $C^{(i),k}$ for stage k as

$$C^{(i),k} = \gamma_k C^{(i)} \tag{3.54}$$

Since the evaluation of (3.52) and subsequent decision about acceptance may be postponed downstream, we propose to perform the computation of all proposals and according model responses for each stage – including the initial evaluation – at the same time using parallel computing. This way, we can make use of available computation resources and cut down the previously reported 2.6-2.9 fold increase of computation times using DRAM Haario et al. (2006) back to close to 1. Effectively, this translates to performing the computation of *all stages* of a *single step* within a *single chain* in parallel for the wall-clock time cost of a *single computation*. The decision about the acceptance of the proposals on the basis of (3.51) and (3.52) may then be made afterwards in an insignificant amount of time.

The complete algorithm incorporating the concepts of

- Adaptivity,
- Single Component proposal sampling,
- Delayed Rejection, and
- Parallelism

is depicted in Algorithm 5.

3.5. Summary

This chapter presents methods of a general workflow to

- gain insight into parameter importance
- identify parameters using fast deterministic surrogate methods
- identify parameters using effective global stochastic optimization

- quantify uncertainties using the Bayesian methodology

for complex, non-linear models, such as Lithium Ion cells and batteries.

The SA methods presented in Section 3.1 provide a brief introduction to a well established method, originally devised by Morris (1991) and further enhanced by Saltelli et al. (2004).

The results of the SA are fundamental to Section 3.2.1, where a novel approach of surrogate modeling is presented with the aim of optimizing a complex model by means of a surrogate coarse model. The main purpose of the space mapping is to accelerate the inversion. Two examples are presented, including

- the electro-chemical model from Section 2.4.2 and
- the extended 3D-RC-model from Section 2.3.

Further, we exploit the properties of linear models and re-formulate the algorithms for space mapping taking into account the shifting of the linearization point.

After discussing the idea of the "*No-Free-Lunch-Theorems*" (Wolpert & Macready, 1997), an introduction to the SOHO algorithm is given. Rather than improving the solution speed, the focus of the SOHO algorithm is to improve the effectivity of the optimization by avoiding getting stuck in local minima.

Finally, the Bayesian methodology for UQ is presented in detail. Several enhancements to the original algorithm by Metropolis et al. (1953) are presented:

- Adaptive Metropolis (AM)
- exploiting parallelism for mixing
- SCAM
- DRSCAM exploiting parallelism for DR.

The DRSCAM offers a possibility to speed up Bayesian inversion methods for a higher dimensional parameter space.

Algorithm 5 SCAM-DR

Input: Choose initial $\boldsymbol{\theta}_0 \in \mathcal{M}_{\text{ad}}$, choose N_{iter}

Set $\boldsymbol{\theta}^{(0)}$ via optimization, one of Section 3
Set σ^2 (3.45)
Compute Jacobian J
Set $C \leftarrow \sigma^2 \left(J^T J\right)^{-1}$ (3.44)
Set sample index $i \leftarrow 0$
while $i \leq N_{\text{iter}}$ **do**
    for $j \in \{1, \ldots, p\}$ **do**
        Advance sample index $i \leftarrow i + 1$
        for $k \in \{0, \ldots, K\}$ **do**
            Sample $z \sim \mathcal{N}(0, 1)$
            Set $\hat{\boldsymbol{\theta}_{j,k}} \leftarrow \boldsymbol{\theta}^{(i-1)} + \mathbf{e}_j \sqrt{\gamma_k s_d C_{j,j}^{(i)}} \cdot z$
            Calculate logLH $\left(\hat{\boldsymbol{\theta}}_{j,k}\right)$ (3.41)
            Calculate acceptance $\alpha_k \left(\boldsymbol{\theta}^{(i-1)}, \hat{\boldsymbol{\theta}}_{j,0}, \ldots, \hat{\boldsymbol{\theta}}_{j,k}\right)$ (3.52)
            Sample $u_\alpha \sim \mathcal{U}[0, 1]$
            Select winning stage
            if $\alpha_k \geq 1$ or $u_\alpha < \alpha_k$ **then**
                add the new candidate point to the chain.
$\boldsymbol{\theta}^{(i)} \leftarrow \hat{\boldsymbol{\theta}}_{j,k}$
                Exit For k loop
            else
                repeat the previous point in the chain.
$\boldsymbol{\theta}^{(i)} \leftarrow \boldsymbol{\theta}^{(i-1)}$
            end if
        end for
        Update Covariance
        if $i = n_0$ **then**
            Set $\bar{\boldsymbol{\theta}}^{(i+1)} \leftarrow \frac{1}{N_c+1} \sum_{t=0}^{N_c} \boldsymbol{\theta}^{(t)}$
            Set $C^{(i+1)} \leftarrow \text{Cov}\left(\boldsymbol{\theta}^{(0)}, \ldots, \boldsymbol{\theta}^{(N_c)}\right)$
            Set $M^{(i+1)} \leftarrow (i-1)\, C^{(i+1)}$
        else if $i - n_0 \equiv 0 \,(\text{mod } n_U)$ **then**
            $C^{(i+1)} \leftarrow \frac{M^{(i+1)}}{i-1}$
        else
            Set $C^{(i+1)} \leftarrow C^{(i)}$
        end if
    end for
end while

Output: a chain of parameter tuples $\boldsymbol{\theta}$ drawn from $\pi(\boldsymbol{\theta}|\boldsymbol{y})$

4

Results

4.1. Measurement

At the VIRTUAL VEHICLE Research Center, a large database of measurements has been generated, on the basis of which the aging properties of cells were examined by Berger (2018); Hrvanovic (2018); Laubichler (2018); A. Pichler (2018). Since most of this work is focused on deducing parameters and models from real measurement data, many measurements were collected from these projects and partly designed and processed in the work cited above. All tests were executed using an Arbin BT-2000 battery testing system and Memmert incubators with Peltier cooling (model IPP600) for maintaining the temperature at 25 °C by forced air cooling.

Throughout this work, mainly voltage data obtained from cycling commercial Panasonic NCR18650B cells is used.

Estimate 80 % **capacity** by applying three times ≈80 % SoC discharge and charge operations between 15 % and 95 % SoC, utilizing OCV points previously acquired for these SoCs

- Each cell is first charged at C/3 rate (C-Rate = 3.35 A) until the voltage reaches 4.113 V followed by a
- constant voltage charge at 4.113 V until the current tapered down to 160 mA (≈C/20 rate), then
- discharged at C/3 rate until 3.498 V again followed by a
- constant voltage discharge at 3.498 V for 40 minutes or until the current dropped to 160 mA, respectively.

This is repeated three times for settling transients and obtaining reproducible results.

Estimate 100 % **capacity** afterwards by two full capacity estimation cycles according to the data-sheet:

- the cell is charged at C/2 rate until 4.2 V,
- constant voltage charged at 4.2 V until the current dropped to C/50 rate and
- discharged at 1 C rate until 2.5 V.

Again, this is repeated twice for settling transients and obtaining reproducible results.

Estimate dynamic behavior — each cell is then charged to 95 % again and

- discharged to a specific SoC level (85 %, 75 %, 65 %, 55 %, 45 %, 35 % or 25 %)
- At each level a set of current pulses are applied such that the dynamic behaviour of the cell is excited as much as possible in the voltage.
  - The pulse sequence subsequently applies C/5, 1.25C and 1.35C pulses in charge (+) and discharge (-) direction for 10s,
  - followed by 15 minutes rest after each pulse
- The pulse sequence ends with a combined 5s-pulse sequence of +C/5, +C/5, -C/5, -C/5, -1.35 C, +1 C with 5 s rest in-between and a
- discrete stair profile of 0.2 C, 0.35 C, 0.5 C, 0.75 C, 1.25 C for 10 s per level

Figure 4.1 shows the entire procedure on one cell as an example.

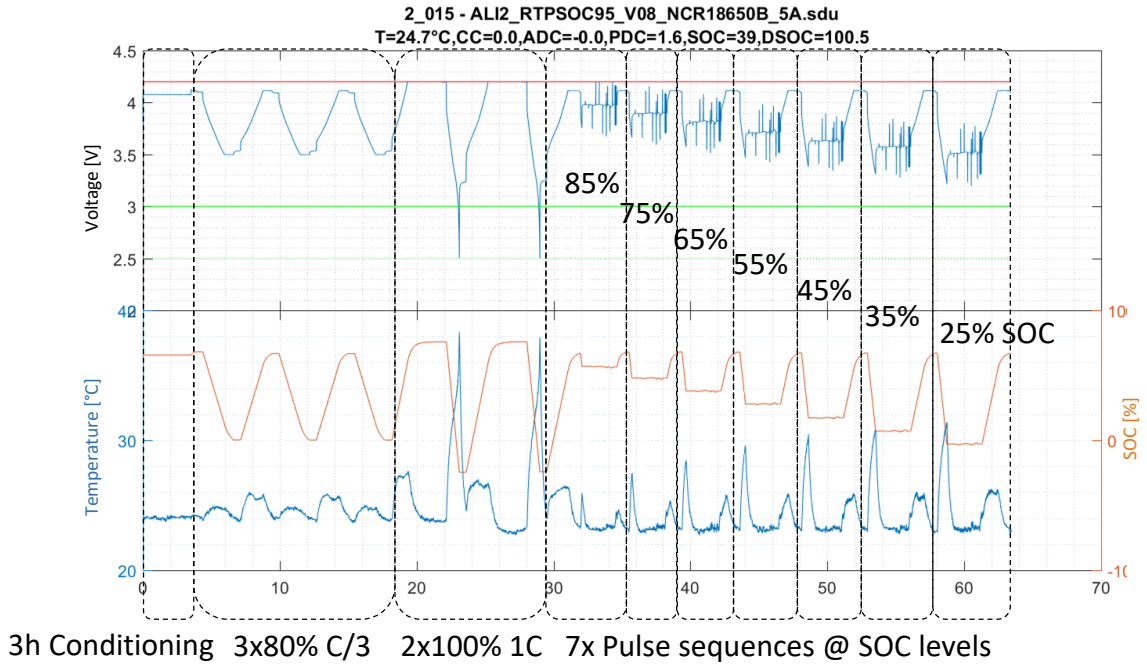

Figure 4.1.: *Reference Test Protocol (RTP) example measurement. The top row shows the cell identifier (2_015) and the cycling program file name. The second row states the average temperature measured, peak discharge current (PDC) as C-rate, time averaged estimated SoC, and the maximum estimated SoC operation window (DSOC). The upper graph displays voltage over time (in hours) and the upper (red) and lower (green) voltage limits of the stationary operation window, which may be exceeded temporarily down to* 2.5 V*, as is the case for the* 100 % *discharge cycles. The lower graph shows Temperature (left axis, blue) and an estimate for the SoC (right axis, orange) over time. Dashed boxes and the bottom-most labels depict the individual phases of the characterization procedure.*

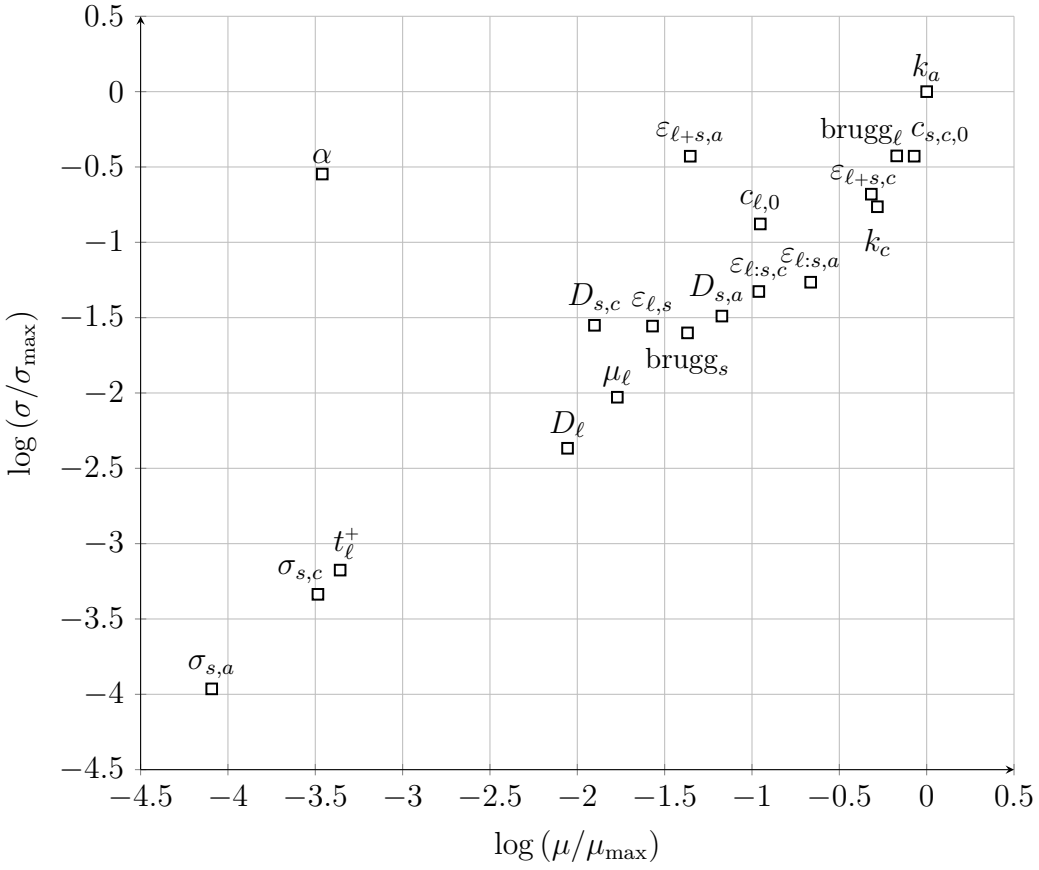

Figure 4.2.: *Results of the "Morris one at a time" global sensitivity analysis*

4.2. Sensitivity of parameters

As input factors to the screening need not necessarily resemble parameters of the model, it was possible to combine dependent parameters pairwise, i.e. the electrolyte volume fractions ε_ℓ and solid volume fractions ε_s in anode and cathode where merged into two factors representing the sum of fractions $\varepsilon_{\ell+s}$ and their ratio $\varepsilon_{\ell:s}$, such that they may not exceed their physical limits.

Figure 4.2 and Table 4.1 show the qualitative ranking order result of the screening experiment for several parameters of interest. It is thus reasonable to assume, that parameter changes for some parameters show minimal effects on the output, e.g. σ_s. Because of the high non-linearity and interaction between parameters indicated by high mean and high spread, k_a and $c_{s,c,0}$ are most likely having high impact on the output.

4.3. Deterministic Optimization for Simple Equivalent Circuit Models

Using the model structure presented in Section 2.2.1, there was a requirement to calibrate the simplistic battery model towards measurements, as there was only very

Table 4.1.: *Global sensitivity analysis results ordered descending by* $(\log(\mu/\mu_{max}))^2 + (\log(\sigma/\sigma_{max}))^2$

Rank	Variable
1.	k_a
2.	$c_{s,c,0}$
3.	brugg_ℓ
4.	$\varepsilon_{\ell+s,a}$
5.	α
6.	$\varepsilon_{\ell+s,c}$
7.	k_c
8.	$c_{\ell,0}$
9.	$\varepsilon_{\ell:s,a}$
10.	$\varepsilon_{\ell:s,c}$
11.	$D_{s,a}$
12.	$D_{s,c}$
13.	$\varepsilon_{\ell,s}$
14.	brugg_s
15.	μ_ℓ
16.	D_ℓ
17.	t_ℓ^+
18.	$\sigma_{s,c}$
19.	$\sigma_{s,a}$

little information about individual cells available, whereas no complete characterization of the battery pack was available due to its prototypical nature. We defined a simple model function $i_{\text{BT}}(\boldsymbol{\mu}, t)$ incorporating the entire model structure depicted in Figure 2.2. The function was designed to match available measurements $\hat{i}_{\text{BT}}(t = k \cdot \triangle T)$ at equidistant time points $k \cdot \triangle T$, which were available from an onboard measurment recording system.

The parameter tuple $\boldsymbol{\mu}$ was chosen to incorporate transform parameters of existing characteristic curves in the QSS-Toolbox of Guzzella & Amstutz (2005).

$$\tilde{R}_i(\text{SoC}) = R_i(\text{SoC}) + \mu_{Ri} \tag{4.1a}$$

$$\tilde{U}_{\text{OCV}}(\text{SoC}) = U_{\text{OCV}}(\text{SoC}) \cdot \mu_{OCVk} + \mu_{OCVd} \tag{4.1b}$$

The entire problem was quickly setup in MATLAB by "MathWorks MATLAB" (1992) and yielded satisfying results after few iterations. The total function evaluation counted up to 32, which translates to less than one hour of computation time on modern work stations.

Considering the deviation from measurements, we define the normalized Root-Mean-Square Error (nRSME) as:

$$\text{nRMSE}\left(y(s), \hat{y}(s)\right) := \frac{1}{\hat{y}_{\max} - \hat{y}_{\min}} \sqrt{\frac{\int_{s_{\min}}^{s_{\max}} \left(y(\sigma) - \hat{y}(\sigma)\right)^2 \mathrm{d}\sigma}{s_{\max} - s_{\min}}}, \tag{4.2}$$

with y being the simulated entity, $\hat{y}$ the corresponding measured entity and s being the distance. The optimized test track simulation results yield – using nRMSE $(\cdot(s), \hat{\cdot}(s))$:

- nRMSE(T_{EM})=8.14 %,
- nRMSE(I_{BT})=8.14 %,
- nRMSE(P_{EM})=12.33 %,
- nRMSE(P_{EG})=40.42 %,

where T_{EM} is the motor torque – in both motor and generator mode –, I_{BT} is the battery pack current, P_{EM} is the motor power, and P_{EG} is the generator power.

Figures 4.3, 4.4 and 4.5 show the results obtained in more detail resolved in time. The deviations in the charge profile are estimated to be caused by deviations in the measured road gradient profile from the real situation, thus under-estimating the required torque in a few situations and over-estimating the gain from recuperation. However, a deviation of approximately 2 % absolute SoC for the final point after a total discharge of approximately 20 %, i.e. from 75 % to 54 %, was considered reasonable and useful for further processing, as depicted by Scharrer, Messner, & Szymanski (2014).

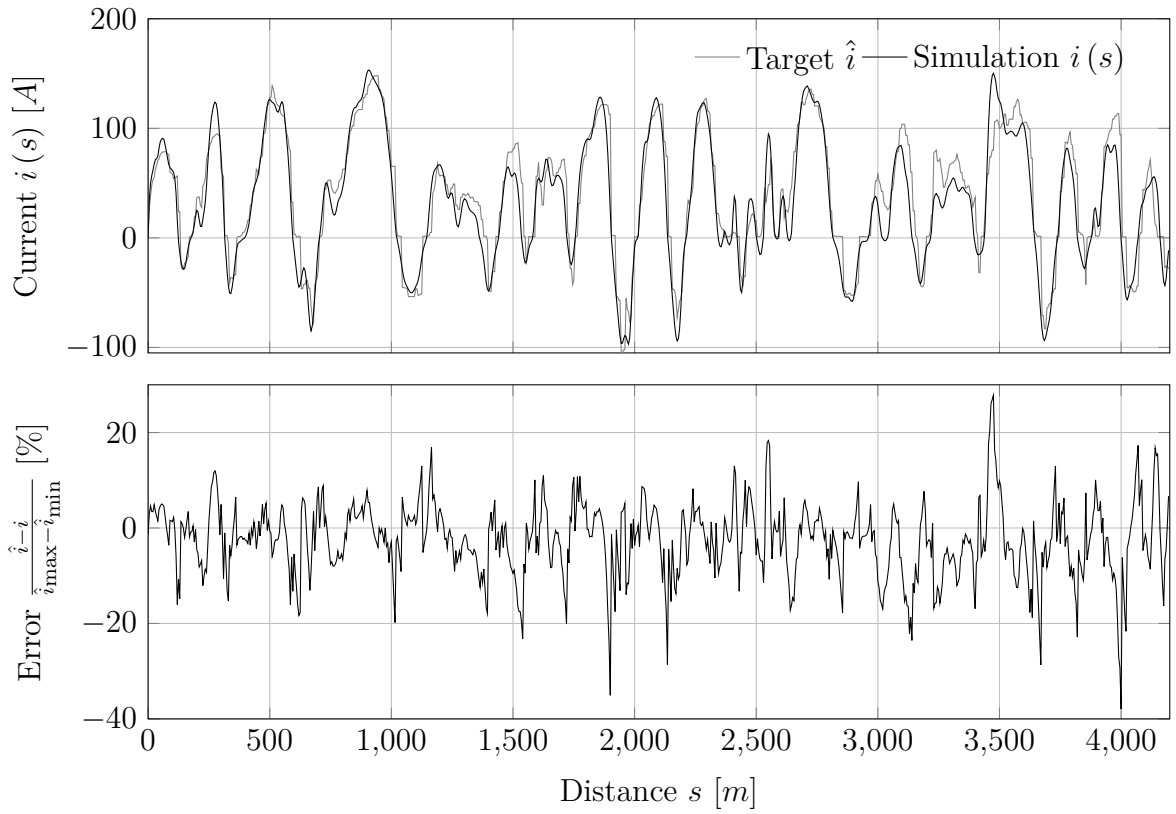

Figure 4.3.: *Model current simulation results versus real electric car based measurements on the test track (Scharrer et al., 2016)*

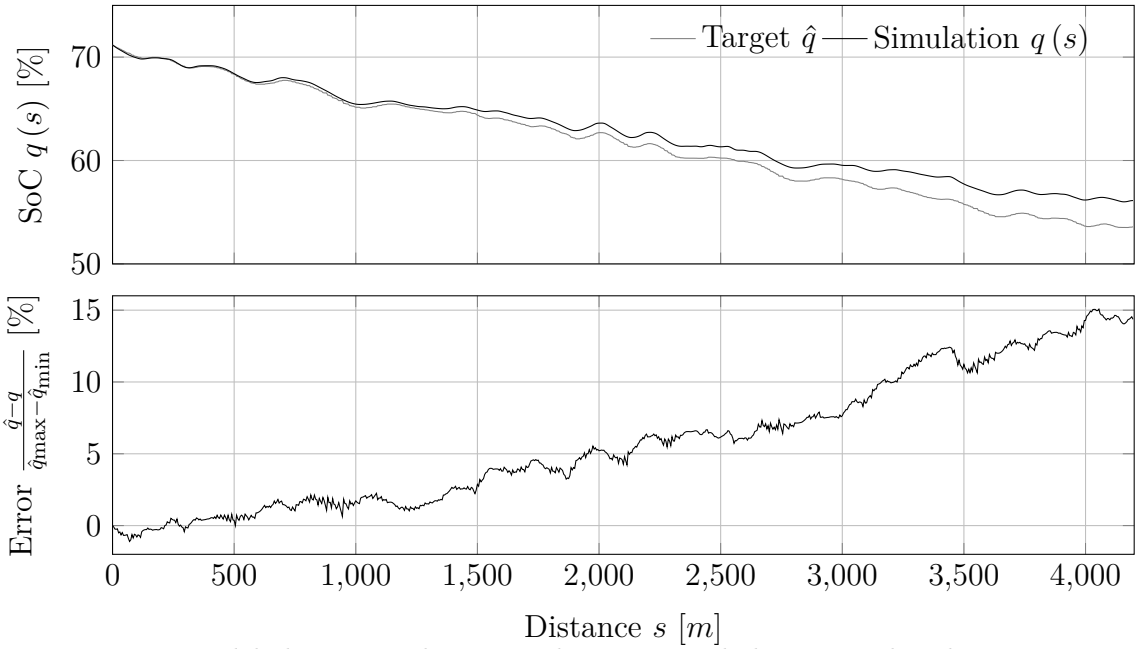

Figure 4.4.: *Model charge simulation results versus real electric car based measurements on the test track (Scharrer et al., 2016)*

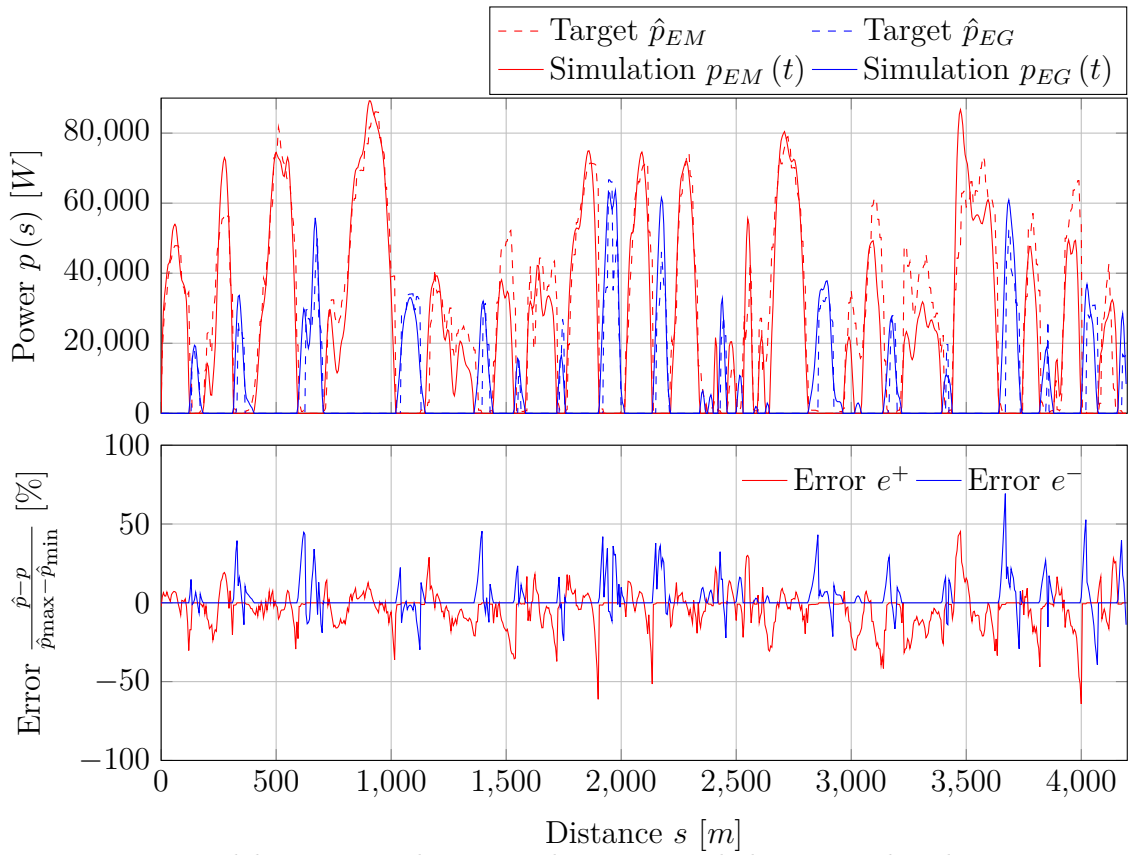

Figure 4.5.: *Model power simulation results versus real electric car based measurements on the test track (Scharrer et al., 2016)*

4.4. Space Mapping for RC-Models

In accordance with Figure 2.4 in Section 3.2.1, we consider the complex Pouch cell 3D FEM-model the *fine model* for the space mapping approach. We restrict the *coarse model* to a plain 0D second-order RC model, which evaluates very fast for the same number of parameters, neglecting the spatial distribution of the fine model. However, the 3D model requires additional material parameters, which are summarized in Table 4.2.

Table 4.2.: *The fixed simulation parameters*

σ_{Al}	v_{Al}	σ_{Cu}	v_{Cu}	$A_{Al/Cu}$
59.1×10^6	3.13 %	37.7×10^6	7.05 %	8×10^3

The optimization system is evaluated on measurement data acquired by applying short pulses to a pouch cell at three temperatures. Then, the speed up attained is compared to the direct fitting procedure without using the surrogate for the same measurements.

The proposed optimization algorithm is applied to the model in order to fit its voltage output to three different measurement curves. These curves are the voltage answers to 1 C current pulses of 25 s at three different temperatures: 10 °C, 25 °C, and 40 °C.

Starting from the same initial guesses for the parameters and having the same stopping criteria in the optimization algorithm the space mapping algorithm is approx. eight times superior to the classic least-squares algorithm w.r.t. to computation times while yielding the same range of fitting error. For the least-squares algorithm the 3D model had to run for 64, 68 and 82 times for the three respective cases. The numbers got reduced to 6, 8 and 9 runs in the space mapping algorithm with additional 388, 637 and 622 runs of the fast surrogate model. Table 4.3 summarizes the detailed numbers and relevant times.

Comparing the results of the coarse and fine model shows very little difference, as depicted in Figure 4.6 for a simple 25 °C pulse case.

The pulses at 10 °C, 25 °C, and 40 °C of the reference cell measurement along with the simulated pulse responses of the best results of direct and surrogate parameter estimation are shown in Figure 4.7. It can be seen, that the results almost coincide, both yielding very accurate results. This is also confirmed by the resulting residuals of the L_2-norm, as shown in Table 4.4.

The fact that the microscopic model in the homogenized 3D model is reflecting the coarse model, is considered to be a big advantage.

The similarity of the model parameters is very beneficial to the space mapping algorithm in that the mapping between the parameter spaces is close to identity, thus reducing the amount of iterations necessary to adjust the space mapping. As an example the Broyden matrix, i.e. the approximation of the linearized space mapping, for the 40 °C

case is

$$B = \begin{Bmatrix} 1.00 & 2.14 \times 10^{-11} & 2.55 \times 10^{-7} & 8.41 \times 10^{-11} & 4.72 \times 10^{-8} \\ 1.01 \times 10^{-11} & 1.00 & 1.87 \times 10^{-7} & 3.55 \times 10^{-10} & -4.51 \times 10^{-8} \\ 1.06 \times 10^{-7} & 2.86 \times 10^{-7} & 1.00 & 9.97 \times 10^{-7} & 1.39 \times 10^{-4} \\ -6.68 \times 10^{-11} & -4.13 \times 10^{-11} & -5.52 \times 10^{-6} & 1.00 & -3.21 \times 10^{-7} \\ 1.07 \times 10^{-7} & -3.55 \times 10^{-7} & 9.17 \times 10^{-2} & -9.20 \times 10^{-5} & 9.72 \times 10^{-1} \end{Bmatrix}$$

in the last iteration. As long as the dimensions of the battery cell taken for measurements are small, this similarity to identity of the Broyden-matrix stay intact for arbitrary microscopic battery models. Having a microscopic model at hand, that is parametrized in the proposed manner, allows for virtual up-scaling and prototyping of batteries in a fast and effective way.

Table 4.3.: *Resulting timing and Speed up*

	Python leastsq	Space mapping	
Optimization	Fine	Fine	Coarse
0	1	2	3
Runs	$64 + 68 + 82$	$6 + 8 + 9$	$388 + 637 + 622$
Time [s]	22293.0	2226.37	518.28
Avg. Time per run [s]	104.17	96.79	0.31
Speedup factor			8.12

Table 4.4.: *L_2-Residuals of the optimization*

Measurement	10 °C	25 °C	40 °C
Direct	8.00×10^{-4}	3.51×10^{-4}	2.00×10^{-4}
Surrogate	7.19×10^{-4}	2.86×10^{-4}	1.78×10^{-4}

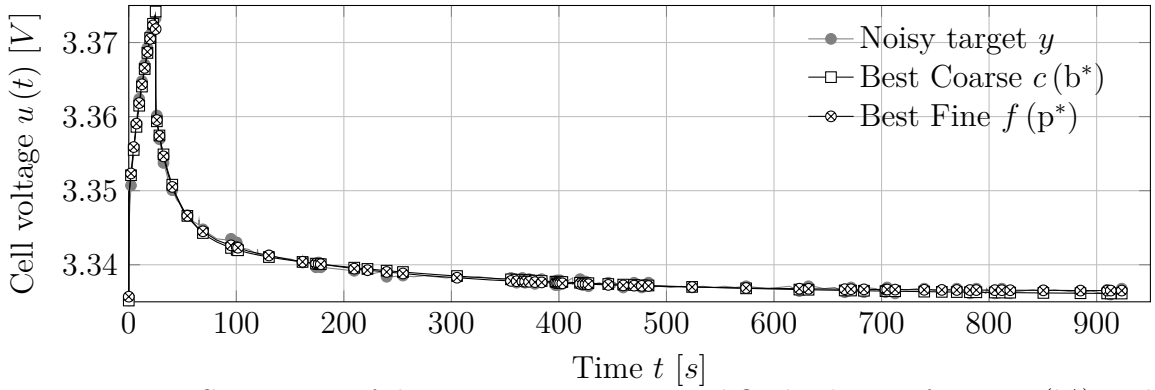

Figure 4.6.: *Comparison of the measurement curve and final voltages of coarse $c\,(\mathrm{b}^*)$ and fine $f(\mathrm{p}^*)$ model response after identification of the parameter set of interest* p. *Measurements and final curves of the fine model are very close.*

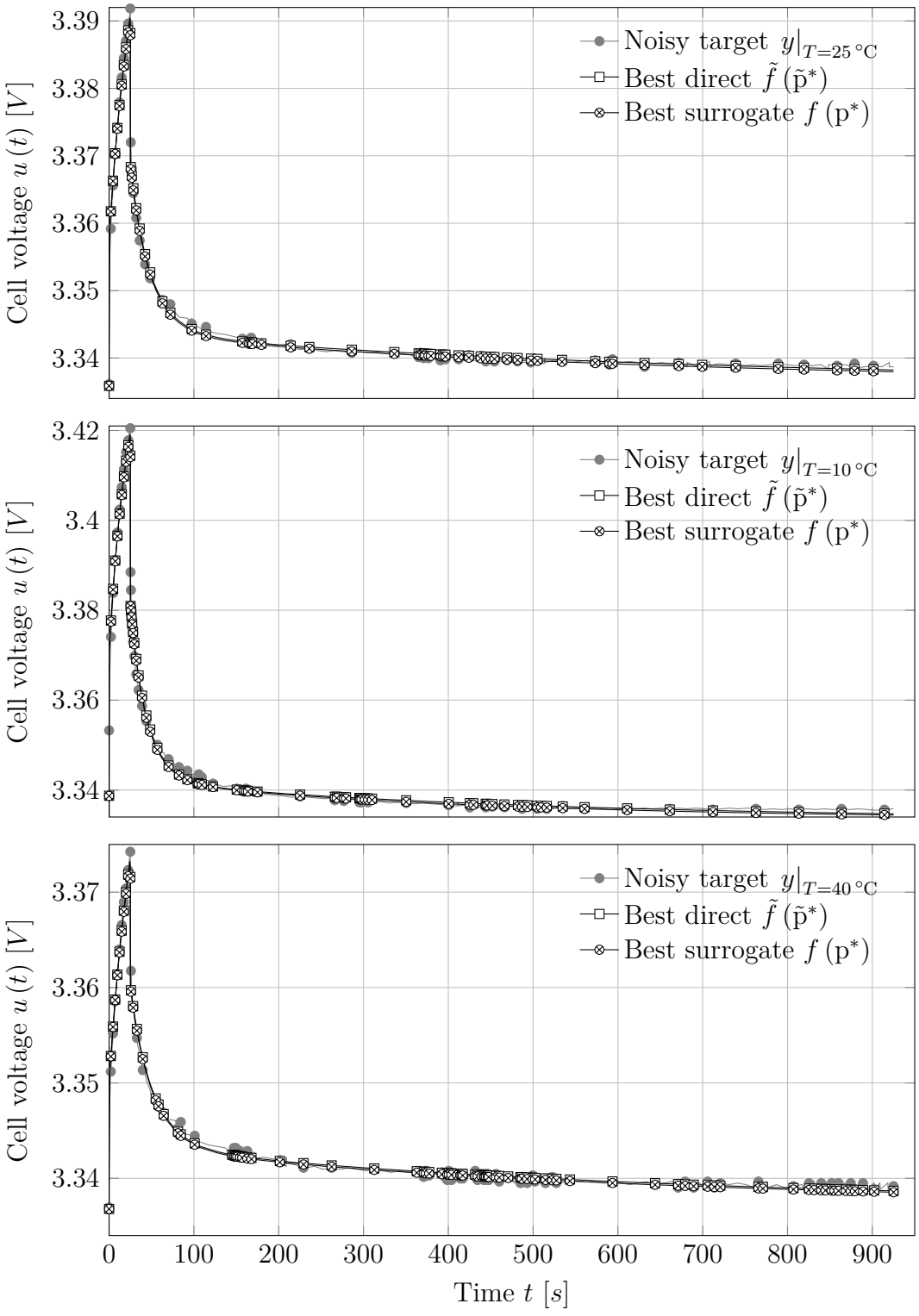

Figure 4.7.: *Comparison of the measurement curve and final voltages of direct* $\tilde{f}\,(\tilde{\mathrm{p}}^*)$ *and surrogate* $f\,(\mathrm{p}^*)$ *model response after identification of the parameter set of interest* p. *Measurements and final curves of the model optimization are very close, results from direct and surrogate optimization almost coincide. This is confirmed by the residual* L_2*-norm shown in Table 4.4*

4.5. Space Mapping for Electro-Chemical Models

After implementing the linearized model as a *surrogate* for optimization, we defined a parameter estimation task for validation of the algorithm. In this section, we present the result of a synthetic parameter estimation task, where parameters of a simulation are recovered starting from another point in parameter space.

Because of long computation times of the constraining non-linear forward problem (2.20), direct optimization of (4.3) is very time consuming, i.e. minutes up to hours depending on the input profile.

Additionally, it is not clear, that the *Nemytskii operator* $\Phi : u(\cdot) \to j_{BV}^{*}(u(\cdot))$ is Fréchet-differentiable, which is a pre-condition to derive necessary optimality conditions. Because the problem is a non-convex optimization problem, it would even be necessary to derive sufficient optimality conditions of second order, too.

Since it may be advisable not to optimize all parameters at once, we introduce the parameter vector $\mathrm{p} \in \mathcal{P}_{\mathrm{ad}} := \{\mathrm{p} \in \mathbb{R}^m | \mathrm{p}_a \leq \mathrm{p} \leq \mathrm{p}_b\}$, where $\mathcal{P}_{\mathrm{ad}}$ is referred to as admissible parameter set.

We define $f(\mathrm{p}) := \varphi_s(x, t; \mathrm{p})$ as the solution of the *fine* model for a parameter set p. By $\bar{\mathrm{p}}$ we refer to the optimal parameters minimizing the cost function defined as:

$$J(\mathrm{p}) := \frac{1}{2} \iint_{\Sigma_c} \left(f(\mathrm{p}) - \hat{\varphi}_s(t)\right)^2 \mathrm{d}s(x)\mathrm{d}t \tag{4.3}$$

subject to $\mathrm{p} \in \mathcal{P}_{\mathrm{ad}}$ and the equality constraints of model (2.20). Since in Section 4.2 it is shown that parameters reaction rate k_c, initial Li^+-concentration in the solid in cathode $c_{s,c,0}$ and the symmetry factor α are most significant, we set $\mathrm{p} := (k_c, c_{s,c,0}, \alpha)^T$ throughout the rest of this section. It is also confirmed by Santhanagopalan et al. (2007) that these parameters are showing highest impact on the results.

Simulation platform was an Intel Core i7 processor at 2.7 GHz 64 Bit equipped with 4 GB RAM running python 2.7 and Matlab 2012b on Windows 7. Implementation of the *fine*, *coarse* and *adjoint* model was done in python using the python scientific library "SciPy" (Virtanen et al., 2019). All optimization problems in this section were solved using the "active-set" algorithm of Matlab's "fmincon" ("MathWorks MATLAB", 1992).

Estimating p was done by an optimization problem as defined in (3.33). The target cell voltage $\hat{\varphi}_s$ and test voltage $\varphi_s(\mathrm{p})$ were generated by simulating a 100 s short charge pulse of C/2 rate load starting from 50 % SoC.

The reference value was set to $\bar{\mathrm{p}} = (1 \times 10^{-7}\,\mathrm{mol\,m^{-2}\,s^{-1}}, 8567\,\mathrm{mol\,m^{-3}}, 0.5)$, the overall optimization starting point was set to $\mathrm{p}_0 = (7 \times 10^{-8}\,\mathrm{mol\,m^{-2}\,s^{-1}}, 8000\,\mathrm{mol\,m^{-3}}, 0.35)$. The limits of admissible parameters were equally set to

$$\mathrm{p}_a = (1 \times 10^{-8}\,\mathrm{mol\,m^{-2}\,s^{-1}}, 5000\,\mathrm{mol\,m^{-3}}, 0.25) \tag{4.4a}$$

and

$$\mathrm{p}_b = (1 \times 10^{-6}\,\mathrm{mol\,m^{-2}\,s^{-1}}, 12\,000\,\mathrm{mol\,m^{-3}}, 0.75) \tag{4.4b}$$

for both the *fine* $\mathcal{P}_{\text{ad}}$ and *coarse* $\mathcal{B}_{\text{ad}}$ parameter spaces.
Considering the optimization algorithm we applied an additional scaling

$$\tilde{\mathrm{p}} \leftarrow (\mathrm{p} - \mathrm{p}_a)\,(\mathrm{p}_b - \mathrm{p}_a)^{-1}\,. \tag{4.5}$$

To avoid estimating parameters of a model by using *exactly* the same model, we chose different spatial discretization to obtain a cell voltage curve $\tilde{\varphi}_s$, see Table 4.5. In addition, we applied Gaussian white noise of zero mean and very high standard deviation $\sigma = 0.5\,\mathrm{mV}$ to obtain the target cell voltage curve $\hat{\varphi}_s\,(t_i) = \tilde{\varphi}_s\,(t_i) + e\,(t_i)$ at discrete time points t_i.

Table 4.5.: *Comparison of Degrees of Freedom (DOF) between the target model and the inverted models –* coarse*,* adjoint *and* fine *– used for parameter estimation.*

Region	Target model	Inverted models
Ω_a	90×3	26×3
Ω_s	40×2	9×2
Ω_c	200×3	26×3
Λ_a	100×90	31×26
Λ_c	100×200	31×26
Total DOF	29950	1786

The stopping criterion of Algorithm 2 was set to test the absolute the function value

$$J\,(\mathrm{p}_i) < \varepsilon_a = 10^{-4}. \tag{4.6}$$

Stopping criteria of the sub problems in steps 7 and 10 where set to test the absolute function value

$$J_{\cdot}\,(\cdot) < \varepsilon_a = 10^{-10} \tag{4.7}$$

and the norm of the step size

$$\|\delta \mathrm{p}\| < \varepsilon_\delta = 10^{-8}. \tag{4.8}$$

A comparison of resulting voltage curves can be found in Figure 4.8. Note, that the final values of $f\,(\mathrm{p}^*_{FD})$ could only be reached by lowering the upper boundary of $c_{s,c,0}$ from $12\,000\,\mathrm{mol\,m^{-3}}$ to $9000\,\mathrm{mol\,m^{-3}}$. The residuals and iteration numbers of the adjoint based and finite differences based algorithm are presented in Table 4.6. The average simulation time of the non-linear model was $12.9\,\mathrm{s} \pm 2.118\,\mathrm{s}$. Average simulation times of the linearized model was $4.2\,\mathrm{s} \pm 0.238\,\mathrm{s}$, which results in a speed up factor of about three.

In a first attempt, the average simulation time of the adjoint model was $14.5\,\mathrm{s} \pm 6.627\,\mathrm{s}$. The high value and standard deviation of the latter can be explained by the bad conditioning of the systems to be solved. Although the system in Section 2.5 and (3.21) in Section 3.2.1 are similar, the changes in the coupling and the boundary conditions

seem to have a very high impact on the solution quality. Whereas the linear and non-linear systems can be solved by direct LU-decomposition, the adjoint system had to be changed to iterative preconditioned stabilized bi–conjugate gradient solver with a very low residual tolerance of 1×10^{-10} to reduce numerical oscillation. But compared to the finite difference based optimization, the number of linear system evaluations during adjoint based optimization could be reduced from 249 to 83 while introducing additional 33 evaluations of the adjoint system. This still results in a reduction of run time from 1145 s down to 915 s, i.e. by $\approx 20\,\%$.

After applying techniques from non-dimensionalization and scaling to the models, i.e. the non-linear fine system, the linear coarse system and the linear adjoint one – see Section A.1 –, the average simulation time of the adjoint model dropped to $4.89\,\mathrm{s} \pm 0.22\,\mathrm{s}$. In addition, the number of evaluations could be further reduced to 74, while the number of adjoint system evaluations reduced to 31. This effort also led to significant drop in linear model evaluation time to $3.11\,\mathrm{s} \pm 0.24\,\mathrm{s}$. The total execution time of the algorithm dropped to 458 s, which is a reduction of $\approx 40\,\%$.

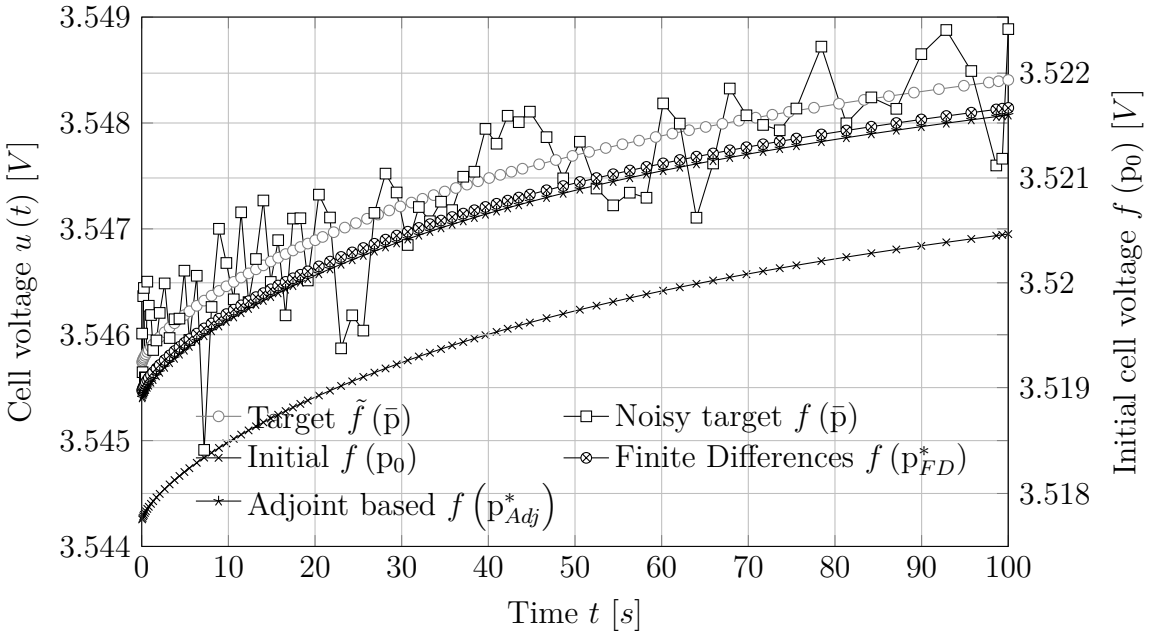

Figure 4.8.: *Comparison of the initial voltage curve, synthetic target voltages and final voltages after estimation of the parameter set of interest* p. *Target curve and final curves of finite differences based approach and adjoint based approach are very close - see residuals in Table 4.6.*

Table 4.6.: *Results of the adjoint based (adj) and finite differences (fd) based space mapping iterations*

iter i	$c^i_{s,c,0}$	k^i_c	α^i	Runtime	residuum	surrogate iterations	mapping iterations
adj_0	8000	$7 \cdot 10^{-8}$	0.35	19 s	$7.81 \cdot 10^{-2}$	–	–
adj_1	8062	$1.02 \cdot 10^{-7}$	0.48	311 s	$4.26 \cdot 10^{-3}$	10	7
adj_2	8090	$1.01 \cdot 10^{-7}$	0.49	671 s	$3.28 \cdot 10^{-3}$	7	3
adj_3	8094	$9.66 \cdot 10^{-8}$	0.49	915 s	$2.77 \cdot 10^{-5}$	6	4
fd_0	8000	$7 \cdot 10^{-8}$	0.35	16 s	$7.81 \cdot 10^{-2}$	–	–
fd_1	7861	$1.18 \cdot 10^{-7}$	0.5	298 s	$4.09 \cdot 10^{-3}$	9	10
fd_2	7826	$1.16 \cdot 10^{-7}$	0.51	761 s	$2.76 \cdot 10^{-3}$	7	3
fd_3	7843	$1.11 \cdot 10^{-7}$	0.51	1145 s	$2.39 \cdot 10^{-5}$	7	3

4.6. Hybrid Stochastic Optimization

The minimization described in this section is performed using the SOHO algorithm as presented in Section 3.3. The SOHO algorithm's search for the parameters is targeting the values that best minimizes this L^2-norm (3.35).

This was performed for both, the DFN and the SPM on the basis of a high-performance implementation devised by F. Pichler (2018). The parameters to be optimized as well as their lower and upper bounds specified for each of the parameters in each of the two models are given in Table 4.7. It should be mentioned that the bounds on each variable are conservative and very wide. This is to mimic the lack of prior knowledge about the parameters. The initial values of each parameter were randomly selected using the algorithm by Sobol (1967). All optimization efforts in this section were initialized with the NSDE algorithm. Due to the large admissible range for most parameters, the optimization algorithm should first efficiently search a large parameter space "*exploration*" but then must focus its search on a smaller region "*exploitation*" where there is a better chance of finding the global minimum.

Forman et al. (2012) tried to fulfill these conflicting objectives by dividing the optimization problem into a global optimization run followed by local optimization run. Solving two separate optimization problems individually, apparently increases the computational cost and time.

The SOHO algorithm makes efficient use of the recombination operators to solve both optimization modes in the same procedure.

The crossover (Deb & Agrawal, 1995) and mutation distribution indices (Deb, 2001), $\eta_{\text{crossover}}$ and η_{mutation}, respectively, control the proximity of the new candidate solution to its parents. A higher value of each index leads to a solution that is closer to its parents. The balancing between global exploration and local exploitation is controlled by adjusting the distribution indices as a function of generations. Each distribution index is linearly increased from a value of 1 to 50 throughout the generations. This

Table 4.7.: *Parameter ranges used to define the SPM and the DFN for SOHO and their admissible range*

			SPM		DFN	
	Average computing time		2.04 s		62.7 s	
#	Parameter	Symbol	min	max	min	max
1	Electrode Area	A_E	–	–	0	2
2	Cathode Tortuosity	τ_c	–	–	0	1
3	Anode Tortuosity	τ_a	–	–	0	1
4	Separator Tortuosity	τ_s	–	–	0	1
5	Separator Porosity	ε_s	–	–	0	1
6	Separator Resistance	R_s	0	1	0	1
7	Anode initial SoC	$\xi_{a,0}$	0	1	0	1
8	Cathode Particle Radius	r_c	10^{-8}	10^{-5}	10^{-8}	10^{-5}
9	Anode Particle Radius	r_a	10^{-8}	10^{-5}	10^{-8}	10^{-5}
10	Cathode Diffusion Coefficient	D_c	0	1	0	1
11	Anode Diffusion Coefficient	D_a	0	1	0	1
12	Cathode Reaction Rate	k_c	−20	100	−20	100
13	Anode Reaction Rate	k_a	−20	100	−20	100
14	Cathode Active Mass	m_c	0	0.051	0	0.051
15	Anode Active Mass	m_a	0	0.033	0	0.033
16–30	Cathode i^{th} RK Coefficients	$A_{c,i}$	−8	8	−8	8
31–44	Anode i^{th} RK Coefficients	$A_{a,i}$	−8	8	−8	8

leads to a more global search at the beginning which then gradually turns into a local search.

The SOHO algorithm was run for a total of 1000 generations, although in all cases, the minimum was found in less than 500 generations. The SOHO algorithm is parallelized in a master-slave arrangement. The master node performs all optimization computation – recombination, selection, etc. – while each slave node solves the mathematical model. A total of 100 parallel runs, i.e. 100 slave nodes, are used throughout the work described in this section.

It should be mentioned that the solution of the SPM and the DFN model was terminated if either

- the time step became less than 1×10^{-6} s or
- the maximum allowable working time was exceeded.

The maximum allowable time was set as approx. *twice* the average computing time – see Table 4.7. This greatly reduces computing time as runs with infeasible parameter combinations that lead to extremely small time steps or diverging solution steps are preemptively stopped from blocking the entire population from advancing.

These termination criteria add an additional degree of non-linearity and discontinuity to the cost function space. It also adds several "flat" regions where the gradient is zero.

For this reason, a gradient based method will find it very difficult to converge to the correct values of the model parameters. The SOHO algorithm is not affected by any of these function space modifications.

4.6.1. SOHO for SPM

The parameter estimation to fit the voltage curve given in Figure 4.1 is first performed using the simpler SPM. A total of 39 parameters defined the SPM model. Figure 4.9 shows the measured voltage and the estimated voltage obtained using the converged values of the 39 parameters.

Apparently, the two voltage curves are very similar. Figure 4.9 shows that charge and discharge peaks from the two curves coincide well. The converged result shown in Figure 4.9 was obtained after 160 000 function evaluations or 1600 iterations of the optimization. Remarkably, even the simpler electro-chemical model is able to accurately represent the experimental results.

It should be mentioned that the estimated set of parameters is able to accurately match experimental data for the entire time from zero to 212 202 s, i.e. close to 2.5 days. Figure 4.9 also shows that the estimated SPM can simulate both slow charging and discharging cycles as well as rapid dynamic pulsing. As previously mentioned,

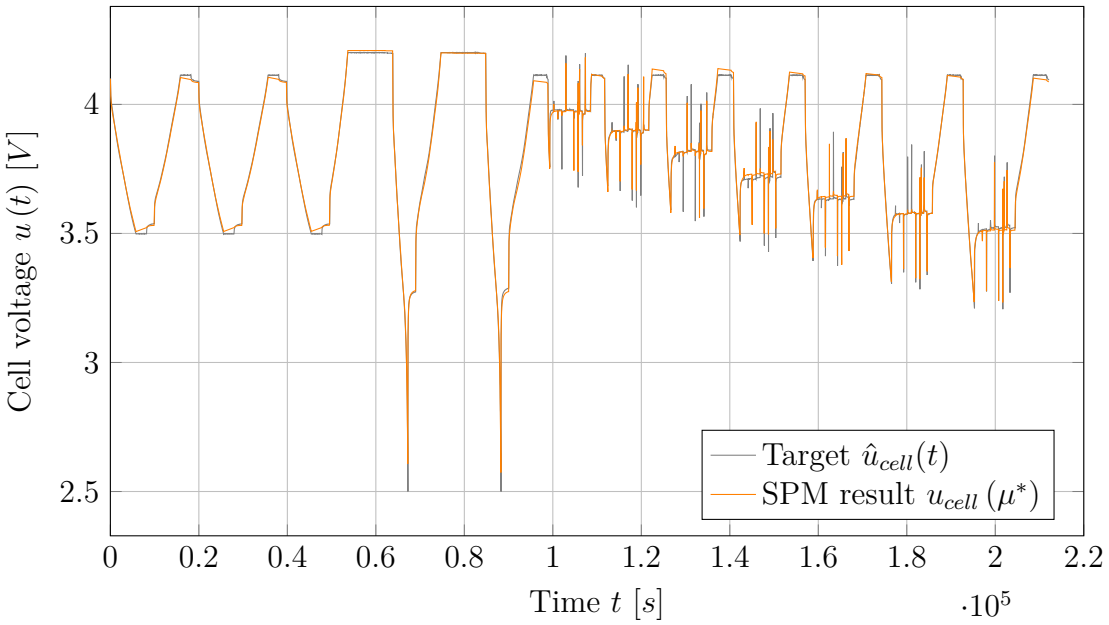

Figure 4.9.: *Measured and estimated voltage response obtained using the converged SPM.*

the hybrid characteristic of the SOHO algorithm increases the convergence rate of the parameter estimation. Figure 4.10 shows the convergence history for the single particle model estimation problem. The residual drastically decreases within the first 200 iterations, i.e. 20 000 model evaluations. Investigating the best set of parameters at any point along the convergence history gives an insight into the error distribution.

The histograms in the sub-figures show such error probability distributions at three different locations. It can be seen that even parameter sets in the early regions of the convergence history (Case 1) have majority of the errors within 50 mV. In the best case (Case 3), the majority of the errors are within 25 mV. This shows that the SOHO algorithm can identify robust parameter sets that produce satisfactory results in a few number of model evaluations. The error statistic and the convergence information

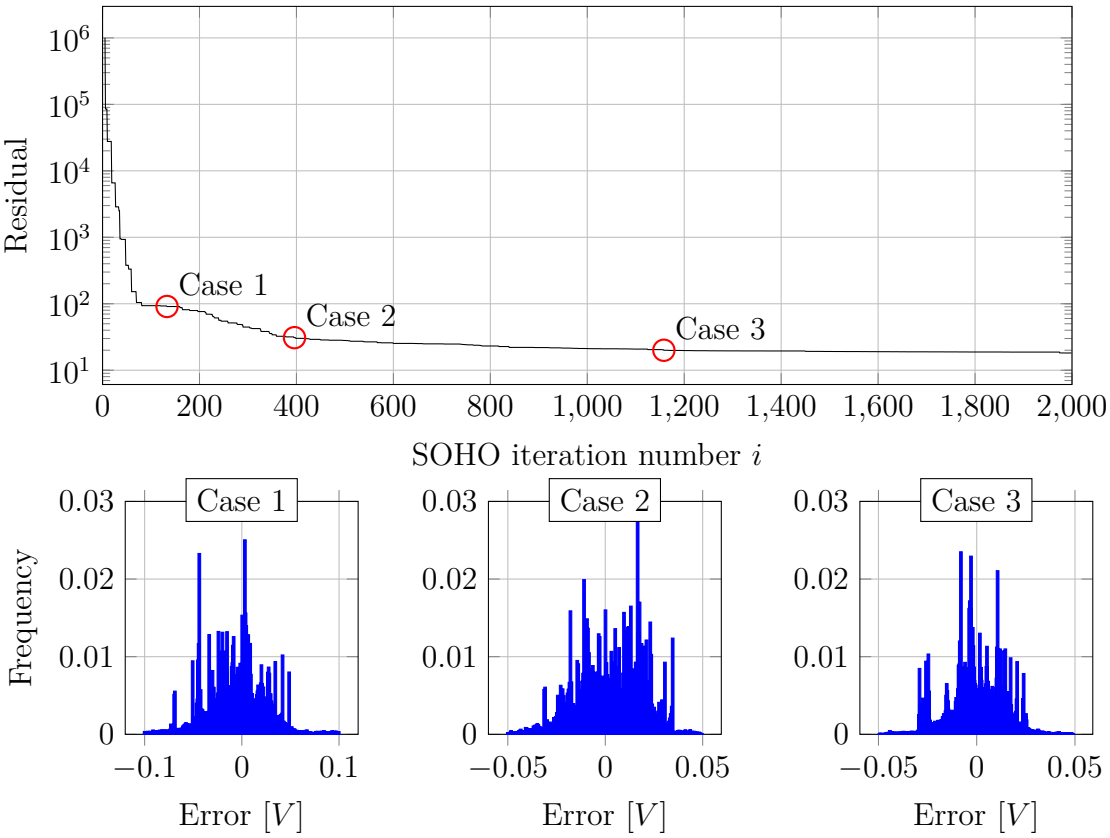

Figure 4.10.: *Parameter estimation residual convergence of the SPM showing: top) the convergence history of the SOHO algorithm, Cases 1, 2 & 3 show the error probability distributions of each example case detail.*

of the three selected cases are shown in Table 4.8. It shows that even in Case 1, the average error is within an acceptable margin. In the case of minimum residual (Case 3), it can be seen that the single particle model estimation was performed in less that one hour with very good accuracy.

4.6.2. SOHO for DFN

Previous results show that the SPM is able to accurately model the battery response. For certain cases, the SPM might not be able to accurately represent the Li^+cell dynamics and a more complete model, such as the DFN, might be required. For this reason, the parameter estimation problem is also solved with the DFN model.

The DFN was defined using a total of 44 parameters. Figure 4.11 shows the estimated

Table 4.8.: *Error statistics of the three cases selected cases in the SPM parameter estimation problem*

	Case 1	Case 2	Case 3
Evaluations to convergence	133	396	1158
Approximate time to convergence [s]	404	1203	3520
Mean absolute error [mV]	24.78	15.02	9.61
Standard deviation of absolute error [mV]	22.55	12.07	8.04

voltage and measured voltage using the 44 converged parameters. Like in the SPM model, it can be seen that the results of the DFN model are similar to those measured. Again, the charge and discharge peaks coincide well for the entire time range. Figure 4.12

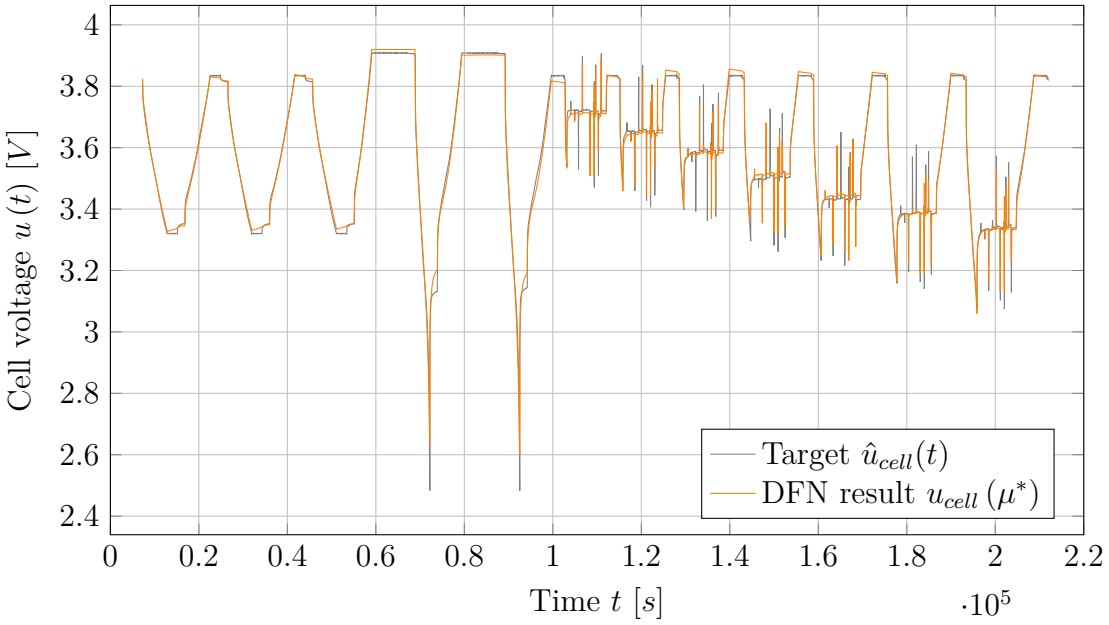

Figure 4.11.: *Measured and estimated voltage response obtained using the converged DFN.*

shows the convergence history for the DFN estimation problem. Here, the residual is seen to sharply decrease within the first 100 iterations. This can be attributed to the better representation of the physical model by the DFN over the SPM. The sub-figures at the bottom show such error probability distributions at three different locations along the convergence history. It can be seen that even parameter sets in the early regions of the convergence history (Case 1) already show the majority of the errors within 50 mV, with a significant number of them centered close to the 0 mV region. In Case 3, the majority of the errors are within 25 mV. Comparing Figure 4.11 and Figure 4.9 shows that the results of the DFN model show a higher probability near 0mV region. Again, this may be attributed to the better suitability of the DFN to capture the electro-chemical dynamics.

The error statistic and the convergence information of the three selected cases of the Newman model are shown in Table 4.9. Comparing Table 4.8 and Table 4.9 show

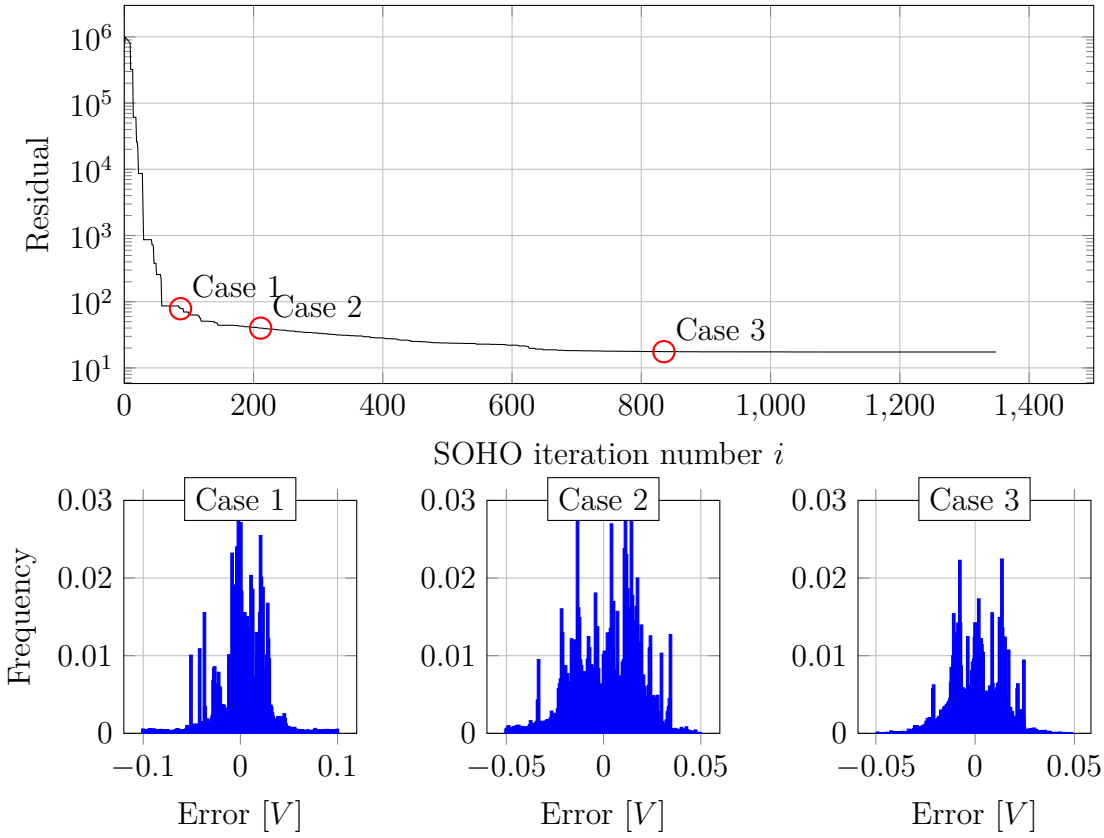

Figure 4.12.: *Parameter estimation residual convergence of the DFN showing: top) the convergence history of the SOHO algorithm, Cases 1, 2 & 3 show the error probability distributions of each example case detail.*

that all three cases for the DFN result in a lower average error and lower standard deviation. Table 4.9 shows that the computing time of the DFN is approximately 30 times larger than the computing time for the SPM. Despite this, the SOHO algorithm is able to estimate the parameters in the DFN in less than one day. This is a significant improvement in convergence time over the previous studies, which took approximately three weeks to obtain converged results. It should be mentioned that the computing time for the DFN used by Forman et al. (2012) (63 seconds) is similar to the DFN used in this work.

Table 4.9.: *Error statistics of the three cases selected cases in the DFN parameter estimation problem*

	Case 1	Case 2	Case 3
Evaluations to convergence	87	211	835
Approximate time to convergence [s]	5455	13330	52354
Mean absolute error [mV]	18.91	15.82	6.47
Standard deviation of absolute error [mV]	24.49	10.95	7.16

4.6.3. Sensitivities of the results

In previous works, e.g. by Forman et al. (2012) and Jin et al. (2018), sensitivity analysis has been used to identify a subset of parameters that influence the model response the most. The parameter identification is then performed only on this subset. Due to the non-linearity and discontinuity of the solution space, the sensitivity analysis in this section is limited to the converged local region.

The local sensitivity is deduced using the local scaled sensitivity coefficients, S where

$$S_\mu := \frac{\partial J}{\partial \mu}, \tag{4.9}$$

is the sensitivity of the cost function J to parameter μ. The sensitivity of the RSS with respect to each parameter μ is calculated.

Figure 4.13 show the absolute value of the scaled sensitivity coefficients in the SPM and DFN models, respectively. It can be seen that the SPM is most sensitive to the OCV offset for the cathode as it directly impacts the offset of the entire solution of the model. Comparing the sensitivities in Figure 4.13 top and bottom, it can be seen that the solution of the DFN is significantly more sensitive than the SPM model. The trends, however, are similar between the two models. Again, the higher order Redlich-Kister coefficients are of the more sensitive terms. The DFN model is most sensitive to cathode reaction rate and cathode active mass, in this order, which directly coincides with the results presented in Section 4.2.

Again, it should be mentioned that the sensitivity analysis in this section is locally based and that other regions of the parameter space most likely will indicate different levels of sensitivity to each parameter.

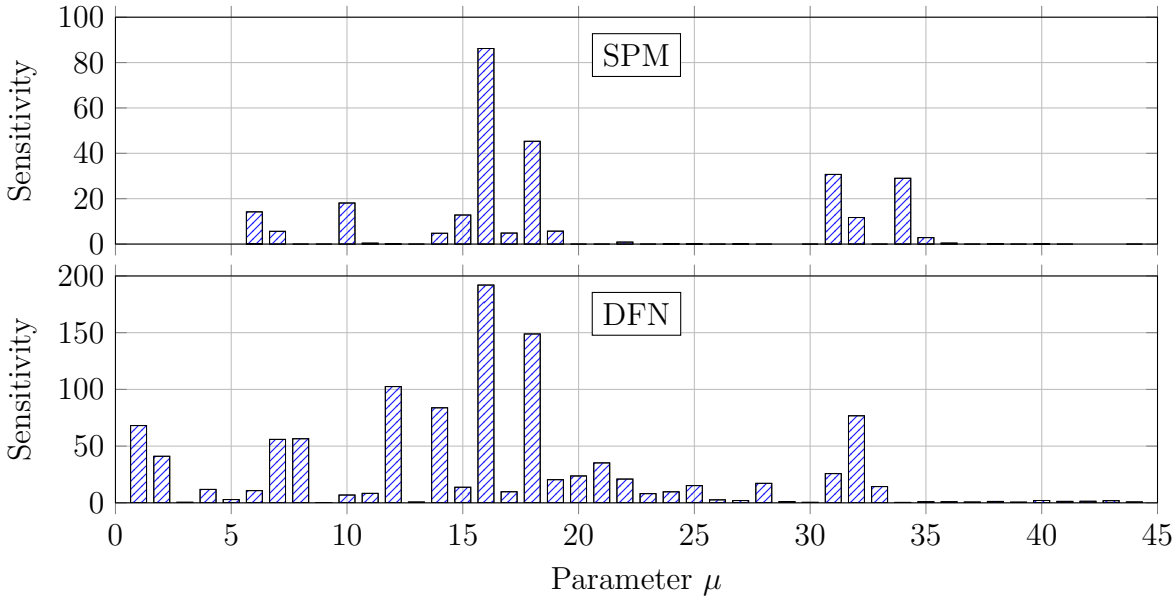

Figure 4.13.: *Local sensitivity coefficients around the converged parameters of the SPM and DFN.*

4.7. Uncertainty Quantification

This section contains two studies using the discussed approaches from Section 3.4. Section 4.7.1 introduces the topic of dynamic pulse based parameter estimation of an implementation of the DFN. This approach takes advantage of the parameter structure and focuses on the five most important dynamic parameters of the model. Several tweaks are applied to improve computational and statistical efficiency, i.e. parallel Adaptive Metropolis – see Section 3.4.5 – and "*early stopping*" of model evaluations as soon as it becomes clear that the results would be rejected. As a proof of concept, this approach did not include physical measurement data but rather synthetic data generated from the same model beforehand, including artificial noise to simulate measurement deviations.

Then, Section 4.7.2 contains the results of the "*Single Component Adaptive Metropolis with Delayed Rejection*" SCAM-DR investigation of a SPM. While this approach did not make use of parallel chains, it makes use of available parallel computation power in terms of concurrent model evaluation for delayed rejection. In addition, results presented are produced on the basis of a fast implementation of the SPM by F. Pichler (2018) and measurement data, as presented in Section 4.3.

Each section includes the required details about the respective problem setting and any specific implementation details.

4.7.1. UQ for DFN

UQ using MCMC requires a very generic set of steps:

1. Modeling of the Prior
2. Posterior Sampling
3. Investigating the statistical efficiency
4. Evaluation of measures taken to improve computation time

All items of this set are presented in their respective sub-section further out this section. The model used in this section is the same as presented in Section 2.4.2

4.7.1.1. Modeling of the Prior

For the sake of brevity, we assume the static influence, e.g. OCV and initial concentrations, to be completely separable from dynamic influence, e.g. diffusion and kinetic rates – as confirmed by e.g. Speltino et al. (2009). They describe identifying parameters of a SPM of battery dynamics in two steps: In the *first step*, the equilibrium potential function of the cathode is identified from OCV measurements, assuming an equilibrium potential function of the anode from the relevant literature. The *second step* involves performing dynamic tests to estimate the remaining model parameters.

For estimating the data, we define a minimalistic input program $i(t)$ that we apply to both measurement and simulation, as shown in Table 4.10.

Table 4.10.: *Input program applied: A discharge pulse from 55 % state of charge (SOC) to ≈ 45 %*

step	Description
0	Initialize the cell to 55 % SOC
1	Discharge at 5 C constant current for 72 s to ≈ 45 % SOC
2	Rest at zero current for 600 s

We arrive at measurements $\mathbf{y} = \{y_i\}$ at time points t_i, which are related to the change of the cell voltage. We introduce the reduced parameter vector $\boldsymbol{\theta} \in \mathcal{P} := \{\boldsymbol{\theta} \in \mathbb{R}^m | \boldsymbol{\theta}_a \leq \boldsymbol{\theta} \leq \boldsymbol{\theta}_b\}$. For a parameter set $\boldsymbol{\theta}$, simulation yields $f(t_j; \boldsymbol{\theta})$ at time points $t_j \leq T$, which are controlled by an adaptive time stepping algorithm, that aims to give local "close–to–linear" behavior for internal states w.r.t. time .

We assume that the observed voltages do not coincide exactly with the true ones of the battery at measured points, but rather that they are subject to Gaussian noise with variance σ^2 – see the observation model in (3.12) in Section 3.2.

Since we do not know much about the parameter set, we choose the parameters in $\boldsymbol{\theta}$, as depicted in Table 4.11. Since the magnitudes of the parameters span a wide range, we introduce $\tilde{\boldsymbol{\theta}}$ as the transformed parameter vector with logarithmic scaling applied.

Since early tests revealed high correlation between k_a and k_c, we introduced a combined factor of $k_{a:c} := k_a/k_c$ instead of k_a. For the transformed parameters, we assume an uninformative, *flat* prior. For the update, we use a random walk proposal kernel using Gaussian distribution initialized to $R_0 = 0.001\tilde{\boldsymbol{\theta}}_0$. The measurement noise deviation and noise in (3.40) were set at $\sigma = 10^{-3}$V, which is considered a realistic value.

Table 4.11.: *Reduced parameter set under test: The table shows initial values $\boldsymbol{\theta}_0$, lower bounds $\boldsymbol{\theta}_a$, upper bounds $\boldsymbol{\theta}_b$, the applied scaling and the target values of the parameters.*

Name	Initial value $\boldsymbol{\theta}_0$	Lower bounds $\boldsymbol{\theta}_a$	Upper bounds $\boldsymbol{\theta}_b$	Scaling $\tilde{\boldsymbol{\theta}}(\boldsymbol{\theta})$	Target $\bar{\boldsymbol{\theta}}$
$D_{s,c}$	4.0×10^{-16}	10^{-18}	10^{-13}	$\log_{10}(\boldsymbol{\theta} \times 10^{18})$	4.0×10^{-17}
$D_{s,a}$	4.5×10^{-14}	10^{-15}	10^{-9}	$\log_{10}(\boldsymbol{\theta} \times 10^{15})$	4.5×10^{-13}
D_ℓ	6.0×10^{-10}	10^{-15}	10^{-8}	$\log_{10}(\boldsymbol{\theta} \times 10^{15})$	4.0×10^{-11}
μ_ℓ	1.0×10^{-5}	10^{-12}	1	$\log_{10}(\boldsymbol{\theta})$	0.1
k_c	9.0×10^{-5}	10^{-9}	10^{-2}	$\log_{10}(\boldsymbol{\theta} \times 10^{9})$	9.0×10^{-4}
k_a/k_c	5.0	10^{-2}	10^{2}	$\log_{10}(\boldsymbol{\theta} \times 10^{2})$	1

4.7.1.2. Posterior Variability of Parameters

Due to the high stiffness of the model, the first run of a sampling chain is performed for parameters $\boldsymbol{\theta}_0$ using adaptive time step sizes. The resulting time points t_j are saved for later reuse in subsequent model evaluations.

The sampling is performed similar to the way proposed by Solonen et al. (2012). It is done in parallel independent chains using Metropolis with adaptive proposal distributions $q(\hat{\theta}|\theta_n) \sim \mathcal{N}(\boldsymbol{\theta}_n, R_n^2)$. The proposal deviation is set $R_n = R_0$ for $n < 20$ and for $n \geq 20$, it is updated to $R_n = \text{chol}(\text{Cov}(\boldsymbol{\theta}_{\text{start}}, \ldots, \boldsymbol{\theta}_{\text{chains}_n})) + \epsilon_\Sigma$. The computation of the Covariance across all available samples starting from some index "start" is performed in a dedicated server, which is the only connection between the chains. To increase adaptivity, "start" grows from 0 by 0.49 per new parameter set per chain. To ensure that R_n does not vanish, we add $\epsilon_\Sigma = 0.001 R_0$. Because of the "flat" prior and symmetric proposals, the acceptance α becomes

$$\alpha\left(\theta_n, \hat{\theta}\right) = \min\left(1, \frac{\pi(\hat{\theta})}{\pi(\theta_n)}\right). \tag{4.10}$$

To further speed up computation, the idea of "*Early Rejection (ER)*" was adopted, which was first applied by Beskos et al. (2006) and Papaspiliopoulos & Roberts (2008). First, a random number $e \in (0, 1)$ is chosen. Simulation is then executed stepwise, and in every time step t_j

$$e < \prod_{k=1}^{j} \frac{L(y_k|f(t_k; \boldsymbol{\theta}_{k+1}))}{L(y_k|f(t_k; \boldsymbol{\theta}_k))} \tag{4.11}$$

is evaluated, and the simulation is aborted as soon as the condition is violated.

As target value $\mathbf{y}$, we chose a *simulated measurement* by running the model at the target parameters $\bar{\boldsymbol{\theta}}$. To avoid "*inverse crime*", the reference model $\bar{f}\left(\bar{\boldsymbol{\theta}}\right)$ was evaluated at different points in time $t_i \neq t_j$ than the model $f\left(\boldsymbol{\theta}\right)$.

Three tests were performed to evaluate the sampling algorithm:

- *Parallel simulation without noise* – The simulation was performed in six parallel chains. The start parameters were set to $\boldsymbol{\theta}_0$. All chains were stopped at the same time after they had reached a little more than 20000 evaluations. The first 10000 samples per chain were discarded as a "burn–in" period to allow π (i.e. the distribution of the Markov chain) to reach equilibrium distribution.
- *Parallel simulation with noise* – The start parameters were set to $\bar{\boldsymbol{\theta}}$, random Gaussian noise was applied to the target voltage with standard deviation $\sigma = 10^{-3}$V. The simulation was performed in five parallel chains. The simulation was aborted after all chains had reached a little more than 2500 evaluations. The first 1000 samples per chain were discarded as a "burn–in" period.
- *Individual simulation with noise* – Although settings were the same as for the parallel simulation with noise, this simulation was performed in three chains with no connection.

Figure 4.14 shows the results of the input profile $i\left(t\right)$ as defined in Table 4.10 and the results for the target, as well as the best evaluation of the simulation without noise. The two voltage curves almost coincide by visual inspection. This is also confirmed by the L_2-norm evaluating to 4.9296×10^{-4}, which is computed by projecting the simulation curve linearly onto the target curve's time points and executing the trapezoidal rule of the squared differences at these points. The statistics of the estimated parameters and

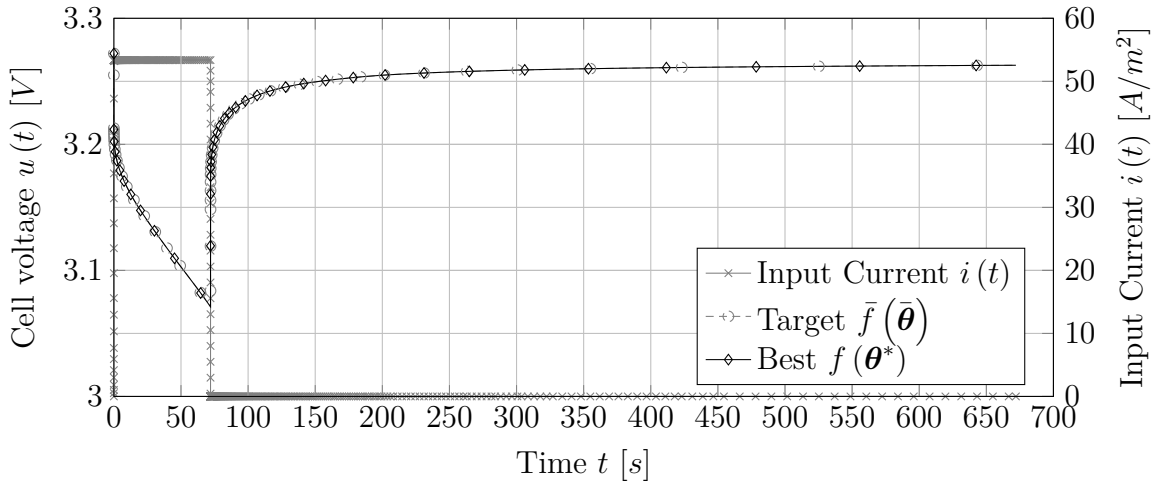

Figure 4.14.: *Comparison of the synthetic target voltages and final voltages after estimation of the parameter set of interest* $\boldsymbol{\theta}$

Table 4.12.: *Results of the uncertainties: Abbreviations are:* #A *Parallel chains without noise,* #B *Parallel chains with noise,* #C,#D,#E *individual chains with noise,* Ref *Target parameters* $\bar{\boldsymbol{\theta}}$

	$\tilde{D}_{s,c}$	$\tilde{D}_{s,a}$	$\tilde{D}_{\ell}$	$\tilde{\mu}_{\ell}$	$\tilde{k}_c$	$\tilde{k}_{a:c}$
#A	1.601±0.002	2.662±0.019	4.604±0.016	−1.025±0.063	5.957±0.075	1.994±0.078
#B	1.603±0.002	2.666±0.018	4.592±0.015	−0.969±0.056	6.044±0.093	1.908±0.096
#C	1.603±0.002	2.662±0.016	4.603±0.005	−1.003±0.003	5.960±0.008	1.996±0.008
#D	1.603±0.002	2.665±0.017	4.590±0.015	−0.962±0.058	6.038±0.08	1.915±0.082
#E	1.605±0.002	2.648±0.011	4.598±0.015	−1.001±0.057	6.025±0.09	1.928±0.093
Ref	1.602±0	2.653±0	4.602±0	−1.000±0	5.954±0	2.000±0

uncertainties are displayed in Table 4.12.

Figure 4.15 shows the posterior distributions of the parameters. Although the noiseless test was expected to show very little standard deviation, it is remarkable that the error made by interpolation of the values at time points from t_j to t_i seems to dominate the results. Furthermore, it is evident, that the individual chains do not to sample from the entire distribution, as the statistics show very little deviation from the starting point. This can also be seen in the scatter plots in Figure 4.16. Samples of the parallel chains cover large areas in the plots, whereas samples of the individual chain cover a slightly smaller part only and in a more dense fashion.

Figure 4.16 also reveals the strong dependence between D_{ℓ} and μ_{ℓ}, and k_c and k_a, respectively. These strong correlations and the shape of the posterior distributions also indicate the logarithmic scaling and selection of $k_{a:c}$ instead of k_a. Direct sampling of all factors without the transformation and combination applied would have lead to statistical and computational inefficiency.

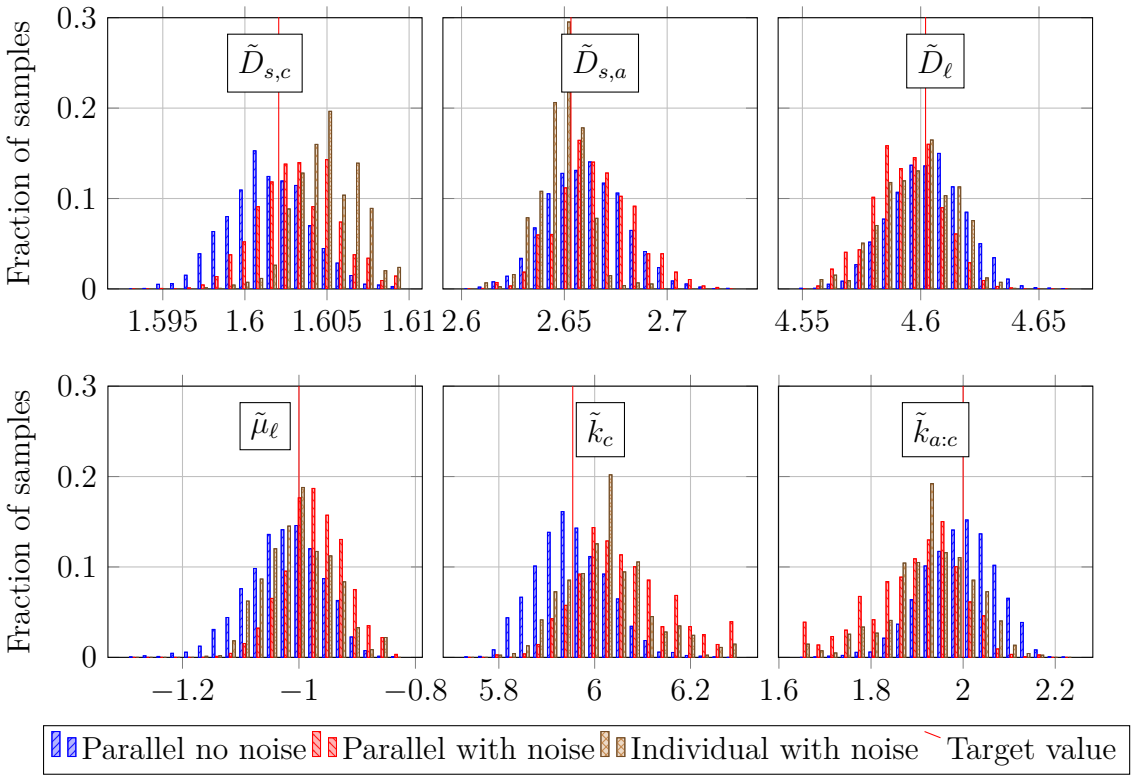

Figure 4.15.: *Results of model posterior*

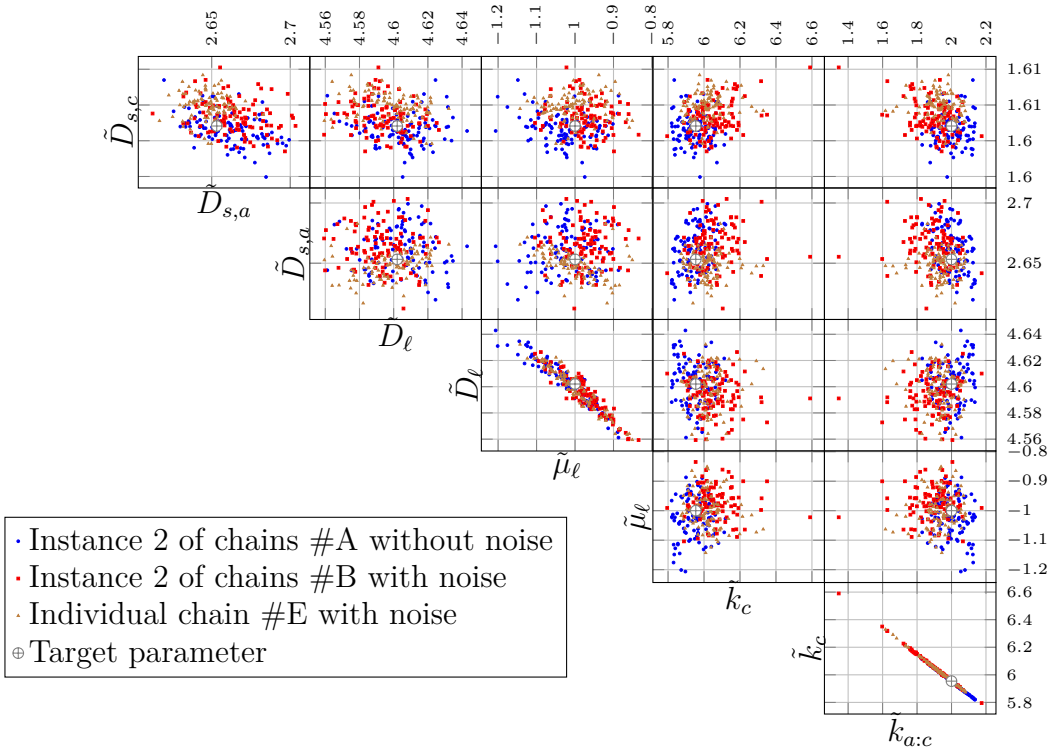

Figure 4.16.: *2D scatter plots showing pairwise correlation between the parameters in* $\boldsymbol{\theta}$

Table 4.13.: *Results of the Integrated Autocorrelation Times τ*

MCMC	τ-$\tilde{D}_{s,c}$	τ-$\tilde{D}_{s,a}$	τ-$\tilde{D}_{\ell}$	τ-$\tilde{\mu}_{\ell}$	τ-$\tilde{k}_{c}$	τ-$\tilde{k}_{a:c}$
#A-1	51.3	56.6	46.7	45.5	55.5	55.7
#A-2	67.1	49.4	52.7	55.3	48.6	48.8
#A-3	65.8	49.4	54.2	56.9	45.7	46.3
#A-4	67.5	44.6	53.7	48.2	55.6	56
#A-5	77.8	53.5	63.8	63	62.3	62.7
#A-6	45.1	45.4	60.4	60.3	53.6	53.8
#B-1	30.9	39.4	49.5	50	33.5	33.3
#B-2	35.4	41.8	45.2	54	55	54.6
#B-3	40	37.1	43.2	43.5	44.3	44.4
#B-4	40.7	28.4	41.2	40	31.9	32.2
#B-5	41.8	35.3	47.7	53.8	36.4	35.5
#C	26.1	21.3	28.6	25.5	19.5	18.9
#D	26.8	31.9	39.2	45.3	33.7	34.6
#E	30.5	54.4	49.2	53.5	26.1	26.3

4.7.1.3. Statistical efficiency

To assess the statistical efficiency, we use the measure of integrated autocorrelation time (iACT). The iACT gives the number of updates of the MCMC algorithm to give one effective independent sample. It was estimated for the posterior distributions by estimating the autocorrelation functions (ACFs) for all parameters. Ideally, the ACF for a stationary time series with little or no serial dependence reach zero quickly for increasing lag. Since the example ACFs in Figure 4.17 exhibit similar behavior, we conclude that only little serial dependence is present in the chains. To finally compute the iACT from the ACF, we utilize the method proposed by Geyer (1992). This method makes use of the pairwise summation of the ACF at consecutive lags and thus yields useful overestimates of the iACT – see Table 4.13. The number of updates to give one effective independent sample τ ranges between 19 and 78. The effective sample numbers of the implemented MCMC algorithms vary between 1.3 % and 5 % of the real sample numbers. This makes the algorithms useful, but still slow, as a single sample evaluation takes a long time.

4.7.1.4. Computational issues

In (4.11), we described the applied reduction of work load during the sample evaluation. ER had a very high impact on the parallel chains without noise. Due to the nature of the model, it is possible to stop many evaluations at a very early stage because of extreme deviations in the output or numerical issues that may arise, since not every possible parameter combination is feasible. The effective work load could be reduced by 67.7 %, i.e. three times as many samples could be evaluated than using the regular approach.

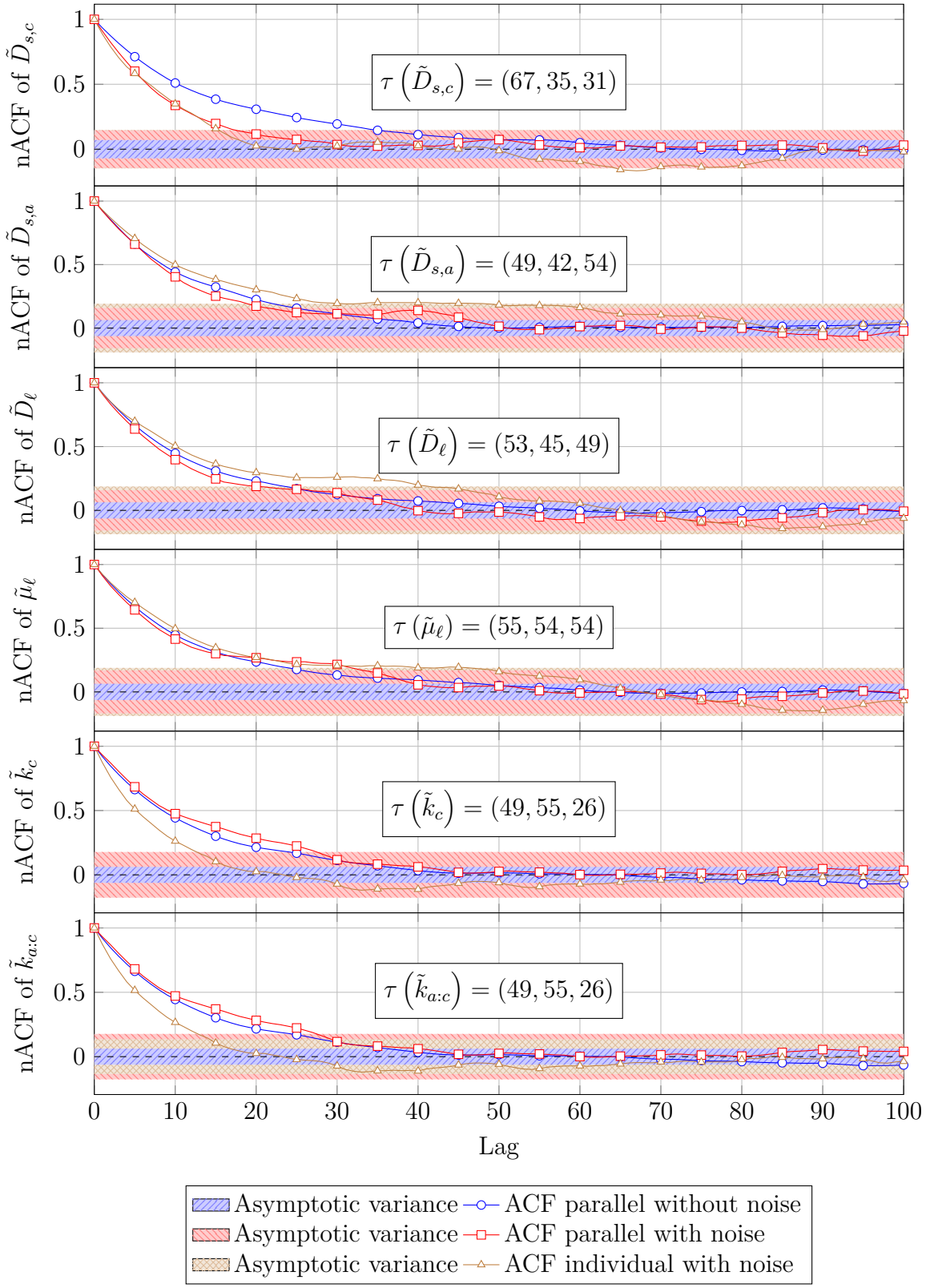

Figure 4.17.: *Estimated normalized Autocorrelation Function (nACF) for the MCMC simulations (The 95 % confidence intervals from the estimated asymptotic variance are superimposed with shaded patterns).*

4.7.2. UQ for SPM

The division in this section follows the same system as in the previous section. In contrast to the previous section, results presented here are produced on the basis of a very fast implementation of the SPM by F. Pichler (2018). The measurement data presented Section 4.1 was used as a realistic target for the algorithms.

It is worth to note that this section may be considered the logical successor to Section 4.6.1.

4.7.2.1. Modeling of the Prior

The SPM in this section is uniquely identified by 44 parameters, which are listed in Table 4.14 along with their respective boundaries. The parameters to be investigated are:

- the inner resistance,
- diffusion coefficients (anode and cathode),
- reaction rates (anode and cathode), and
- active mass (anode and cathode),
- the initial lithiation of the anode, as well as
- the offset of the U_{OCP}-curve in the cathode.

A total of 15 terms in the Redlich-Kister expansion are used to define the U_{OCP}-curves in each electrode, i.e. both anode and cathode. The first RK-coefficient in the anode $A_{a,0}$ is but always set to zero due to linear dependency to $A_{c,0}$. Furthermore, particle radii, material densities and specific capacities are held constant at all times, as they are considered material related constants. This parameter set is subject to parameter estimation, for further uncertainty quantification, we restrict the set of parameters by not including higher order RK-coefficients. Thus, the total number of parameters is 39 for the parameter estimation step at the beginning and 9 for the subsequent uncertainty quantification subject to box constraints, i.e. 28 RK-coefficients are retained at their previously estimated values. Both radius parameters were fixed to the result of the preceding optimization step, as the effect seen on the resulting voltage cannot be attributed separately to diffusion and radius. The starting point for the sampling algorithm is taken from the identification framework.

For better numerical treatment and restriction, as well as taking into account the interdependence of parameters, we apply a transform $\tilde{\boldsymbol{\theta}}(\cdot)$ on the parameters $\boldsymbol{\theta}$ on the basis of knowledge gained in Section 4.7.1.1. Due to the wide range of possible magnitudes of diffusion coefficients and kinetic rates in literature – 8 to 14 orders of magnitude, respectively –, we apply logarithmic scaling to these parameters from the framework point of view. The remainder of the parameters was scaled by their estimated characteristic value.

$$\theta_1 = \tilde{D}_c = \log \frac{D_c}{R_c^2 10^{-6}} \tag{4.12}$$

Table 4.14.: *SPM Model parameter values and ranges used to define the UQ*

Parameter	Symbol	Value
Cathode Diffusion Coefficient	D_c/r_c	$\in (10^{-6}, 10^{-3})$
Anode Diffusion Coefficient	D_a/r_a	$\in (10^{-6}, 10^{-3})$
Anode initial SoC	$\xi_{a,0}$	$\in (0.9, 1.0)$
Inner Resistance	R_s	$\in (0.03, 0.07)$
Cathode Active Mass	m_c	$\in (0.02, 0.052)$
Anode Active Mass	m_a	$\in (0.01, 0.034)$
Cathode Reaction Rate	$\log k_c$	$\in (-20, -1)$
Anode Reaction Rate	$\log k_a$	$\in (-23, 10)$
Cathode OCV offset	$A_{c,0}$	$\in (3, 4)$
Cathode Particle Radius	r_c	$1.08118042 \cdot 10^{-6}$
Anode Particle Radius	r_a	10^{-7}
Cathode active material density	ρ_c	4450
Anode active material density	ρ_a	2260
Cathode specific capacity	C_c	278.9052
Anode specific capacity	C_a	371.9112
Cathode 1$^{\text{st}}$ RK Coefficient	$A_{c,1}$	$-6.21419312054 \cdot 10^{-1}$
Cathode 2$^{\text{nd}}$ RK Coefficient	$A_{c,2}$	$-4.30301784249 \cdot 10^{-2}$
Cathode 3$^{\text{rd}}$ RK Coefficient	$A_{c,3}$	$-1.22016011635 \cdot 10^{-1}$
Cathode 4$^{\text{th}}$ RK Coefficient	$A_{c,4}$	$-3.08693161534 \cdot 10^{-2}$
Cathode 5$^{\text{th}}$ RK Coefficient	$A_{c,5}$	$-4.58298788314 \cdot 10^{-1}$
Cathode 6$^{\text{th}}$ RK Coefficient	$A_{c,6}$	$1.22050353718 \cdot 10^{-2}$
Cathode 7$^{\text{th}}$ RK Coefficient	$A_{c,7}$	$-5.72484625463 \cdot 10^{-1}$
Cathode 8$^{\text{th}}$ RK Coefficient	$A_{c,8}$	$1.33488740252 \cdot 10^{-1}$
Cathode 9$^{\text{th}}$ RK Coefficient	$A_{c,9}$	$-1.73067297349 \cdot 10^{-1}$
Cathode 10$^{\text{th}}$ RK Coefficient	$A_{c,10}$	$1.04461741237 \cdot 10^{-1}$
Cathode 11$^{\text{th}}$ RK Coefficient	$A_{c,11}$	$6.08053240235 \cdot 10^{-1}$
Cathode 12$^{\text{th}}$ RK Coefficient	$A_{c,12}$	-1.18509766977
Cathode 13$^{\text{th}}$ RK Coefficient	$A_{c,13}$	$-5.76553869814 \cdot 10^{-2}$
Cathode 14$^{\text{th}}$ RK Coefficient	$A_{c,14}$	$2.26556461121 \cdot 10^{-2}$
Anode OCV offset	$A_{a,0}$	0
Anode 1$^{\text{st}}$ RK Coefficient	$A_{a,1}$	$-2.18795896469 \cdot 10^{-1}$
Anode 2$^{\text{nd}}$ RK Coefficient	$A_{a,2}$	$1.54704347227 \cdot 10^{-2}$
Anode 3$^{\text{rd}}$ RK Coefficient	$A_{a,3}$	$-2.09151367314 \cdot 10^{-3}$
Anode 4$^{\text{th}}$ RK Coefficient	$A_{a,4}$	$-1.30135546857 \cdot 10^{-1}$
Anode 5$^{\text{th}}$ RK Coefficient	$A_{a,5}$	$-3.42650622958 \cdot 10^{-2}$
Anode 6$^{\text{th}}$ RK Coefficient	$A_{a,6}$	$8.28638329842 \cdot 10^{-1}$
Anode 7$^{\text{th}}$ RK Coefficient	$A_{a,7}$	$-2.38642439510 \cdot 10^{-1}$
Anode 8$^{\text{th}}$ RK Coefficient	$A_{a,8}$	-2.24879248192
Anode 9$^{\text{th}}$ RK Coefficient	$A_{a,9}$	1.43322197461
Anode 10$^{\text{th}}$ RK Coefficient	$A_{a,10}$	2.41299229653
Anode 11$^{\text{th}}$ RK Coefficient	$A_{a,11}$	$-9.80092577782 \cdot 10^{-1}$
Anode 12$^{\text{th}}$ RK Coefficient	$A_{a,12}$	-2.25153043555
Anode 13$^{\text{th}}$ RK Coefficient	$A_{a,13}$	$-1.15378028002 \cdot 10^{-2}$
Anode 14$^{\text{th}}$ RK Coefficient	$A_{a,14}$	1.24600653963

$$\theta_2 = \tilde{D}_a = \log \frac{D_a}{R_a^2 10^{-6}}$$
$$\theta_3 = \tilde{\xi}_{a,0} = \frac{\xi_{a,0}}{0.95}$$
$$\theta_4 = \tilde{R}_s = \frac{R_s}{0.05}$$
$$\theta_5 = \tilde{m}_c = \frac{m_c}{0.036}$$
$$\theta_6 = \tilde{m}_a = \frac{m_a}{0.022}$$
$$\theta_7 = \tilde{k}_c = \log k_c + 10.5$$
$$\theta_8 = \tilde{k}_{a:c} = \log k_a - \log k_c$$
$$\theta_9 = \tilde{A}_{c,0} = \frac{A_{c,0}}{3.5}$$

The prior uncertainty in these parameters is given as an uninformative flat prior in the transformed parameter space in a maximum possible bounding box, as shown in Table 4.14. The measurement uncertainty is specified as $\sigma = 0.015\,\mathrm{V}$, which exceeds the equipment uncertainty of 0.02 % FSR, translating to approximately $\sigma_e = 0.000\,29\,\mathrm{V}$.

For the test example, 4 731 957 samples were drawn from the posterior distribution using effective sampling after a burn-in period of 3600 samples, i.e. after four adaptation steps of the proposal distribution. Figure 4.18 shows the evolution of the log-likelihood function of the entire chain. There is no sign of a change in the trend of the likelihood, equilibrium is reached.

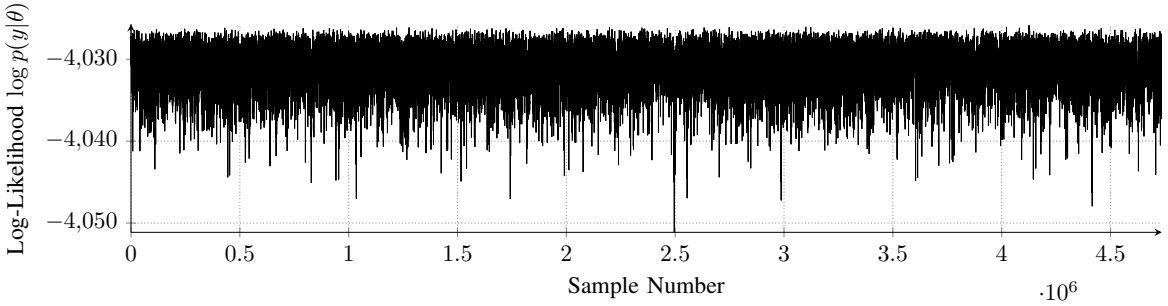

Figure 4.18.: *Results of the log-Likelihood of the sampled MCMC simulations (after burn-in).*

For every sample, 15 evaluations of the model are performed in parallel selecting γ_k according to (3.54). We freely choose $\gamma_k = 2^k$ for $k \in \{0, 4, 3, \ldots, -9, -10\}$ to enable wider spread of proposed samples.

The sampling is performed with an adaptive proposal distribution of Variance $C_{j,j}^{(0)}$ for 900 samples and updated every 900 samples afterwards.

4.7.2.2. Posterior Variability of Parameters

MCMC sampling does not explore the entire posterior, therefore, to the best of our knowledge, assuming to have found the global optimum after applying the hybrid optimization method of Reddy et al. (2019) and sample from the distribution in its vicinity.

Figure 4.19 shows the sampled probability distributions of the marginal distribution per parameter in $\boldsymbol{\theta}$ from the sampled posterior. The sampled posterior distributions show significant shapes compared to the uninformative (flat) prior. As expected due to the uninformative prior, the maximum values (modes) of the PDFs in Figure 4.19, i.e. the maximum a posteriori values, coincide well with the previous optimization results presented in Section 4.6.1, i.e. the maximum likelihood up to scale. The mismatch of the mode and the optimization result of the parameter $\tilde{k}_{a:c}$ and the wide spread of the distribution, although cut at the upper boundary of the box constraints, indicate its insignificance on the model output.

Although the procedure from the optimization step in Section 4.6.1 resulted in a single usable parameter set, it is remarkable that there exists strong correlation between several parameters, e.g. between $\tilde{\xi}_{a,0}$, $\tilde{A}_{c,0}$, $\tilde{m}_{a,c}$ and $\tilde{m}_{a,a}$ there exists a reasonable relationship, as each of these parameters offsets the output cell voltage in a very similar way. Figure 4.20 partially confirms this by showing a rotated ellipsoidal distribution in the scatterplots of $\tilde{\xi}_{a,0}$ versus $\tilde{m}_{a,c}$, $\tilde{m}_{a,a}$ and $\tilde{A}_{c,0}$, respectively, and other pairwise combinations among this set of four parameters. Furthermore, Figure 4.20 shows a very strong correlation between $\tilde{R}_s$ and $\tilde{k}_c$. Both parameters contribute to the full cell's overpotential depending on the applied current I_{app}, as can be seen from equations (2.13), (2.16), (2.17) and (2.18). Eventually, we report the results of the estimated values and their respective 95 %-confidence intervals in Table 4.15, taking into account the iACT presented in the next section.

4.7.2.3. Statistical efficiency

To assess the statistical efficiency, we use the measure of iACT. The iACT yields the number of successive updates of the MCMC algorithm that yield one effective independent sample. It is estimated for the posterior distributions by estimating the ACF for all parameters. Ideally, the ACFs for a stationary time series with little or no serial dependence reach zero quickly for increasing lag. We present the ACFs in Figure 4.21 for a maximum lag of 800. Since the functions exhibit the expected dropping behavior, we conclude that strong serial dependence is present in the chain, but this may be reduced by skipping the number of samples resulting from computing the iACT from the ACF.

To finally compute the iACT from the ACF, we utilize the method proposed by Geyer (1992) again. This method makes use of the pairwise summation of the ACF at consecutive lags and thus yields useful overestimates of the iACT. The number of updates to yield independent samples from the chain ranges between 16 and 760. The effective sample numbers of the implemented MCMC algorithms vary between 0.03 % and 0.7 % of the sampling iteration numbers. This makes the algorithms useable, but

very costly in terms of computation time. Despite the small number of independent samples, Table 4.15 shows a very tight region of confidence for each parameter that is well below 0.5 % of each respective parameter.

The algorithm was evaluated on an Intel Xeon CPU E5-2630 v3 at 2.40 GHz with 15 parallel evaluations for the DR part leading to a single sample in the chain. All samples in the chain resulted in an average model evaluation time of 0.36 s on the basis of the implementation in F. Pichler (2018).

Table 4.15.: *SPM sample results and* 95 % *confidence intervals*

Parameter	Initial Value	Resulting Mean	95 % Interval
Cathode Diffusion Coeff. $\tilde{D}_{s,c}$	2.201828	2.2019	$\pm 1.054 \cdot 10^{-4}$
Anode Diffusion Coeff. $\tilde{D}_{s,a}$	1.914624	1.9144	$\pm 1.102 \cdot 10^{-4}$
Anode initial SoC $\tilde{\xi}_{a,0}$	0.989519	0.98954	$\pm 2.028 \cdot 10^{-5}$
Inner Resistance $\tilde{R}_s$	0.711943	0.71386	$\pm 4.782 \cdot 10^{-4}$
Cathode Active Mass $\tilde{m}_c$	0.597076	0.59709	$\pm 7.961 \cdot 10^{-5}$
Anode Active Mass $\tilde{m}_a$	0.652706	0.65283	$\pm 1.904 \cdot 10^{-4}$
Cathode Reaction Rate $\tilde{k}_c$	−2.9707	−2.957	$\pm 2.394 \cdot 10^{-3}$
Anode Reaction Rate $\tilde{k}_{a:c}$	11	6.6442	$\pm 1.377 \cdot 10^{-2}$
Cathode OCV offset $\tilde{A}_{c,0}$	1.05888	1.05888	$\pm 1.981 \cdot 10^{-5}$

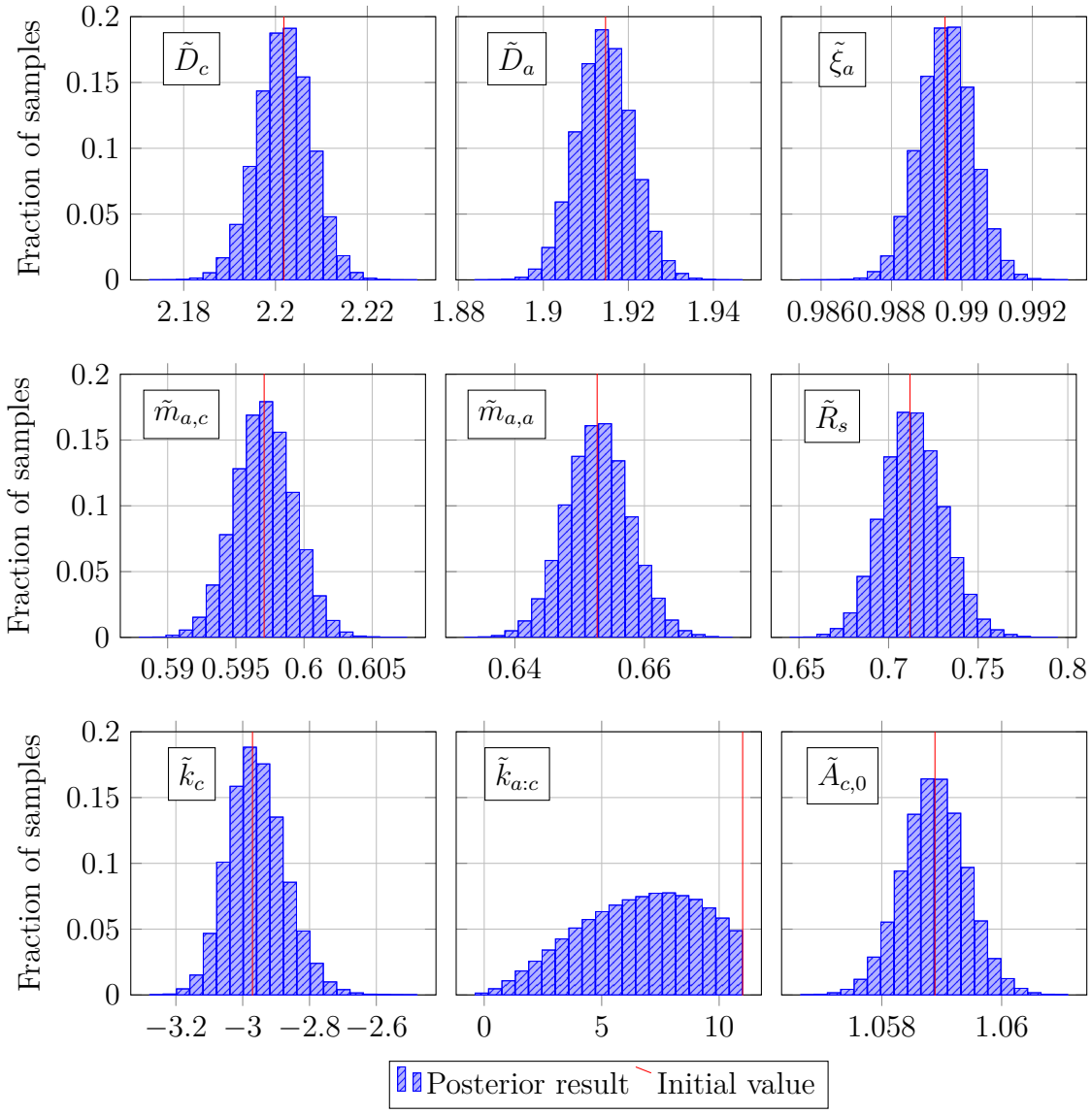

Figure 4.19.: *Sampled model posterior distribution*

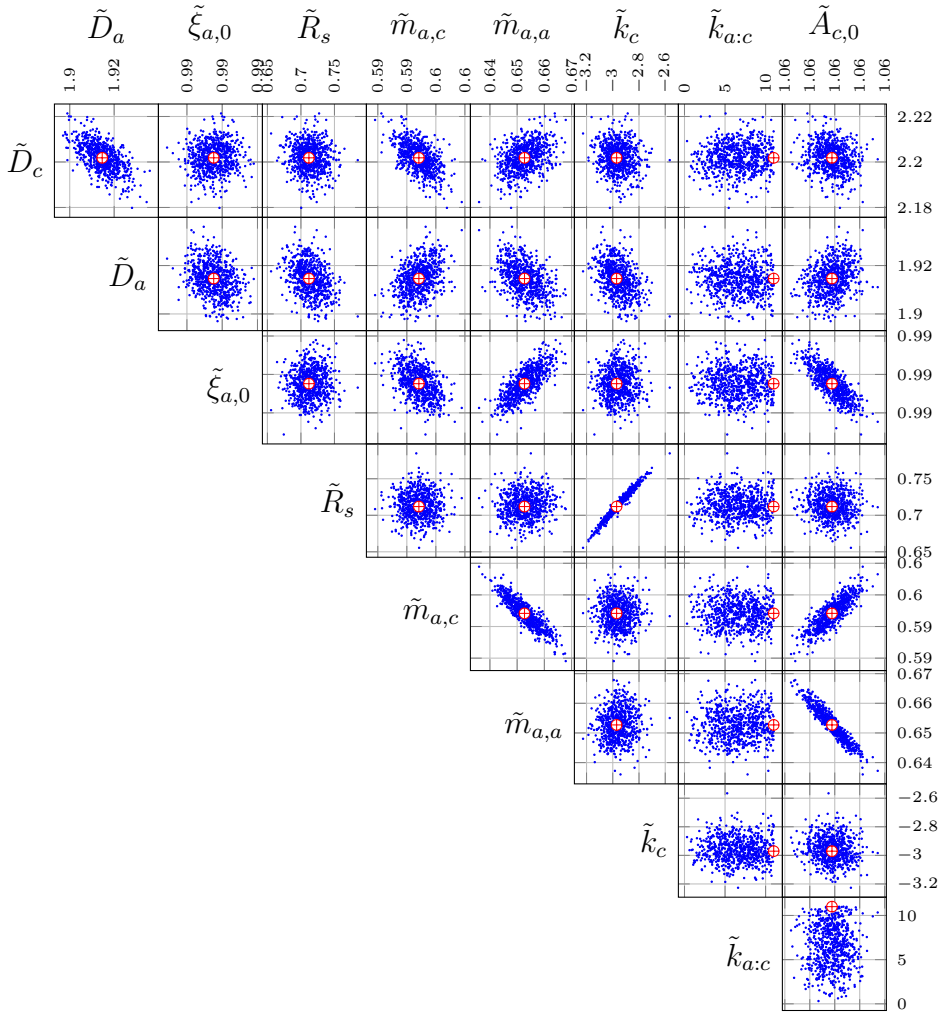

Figure 4.20.: *2D scatter plots showing pairwise correlation between the parameters in* $\boldsymbol{\theta}$*. Each element of the matrix shows a scatter plot of a pair of parameters labelled at their respective row and column of the matrix with one element of the parameter set.*

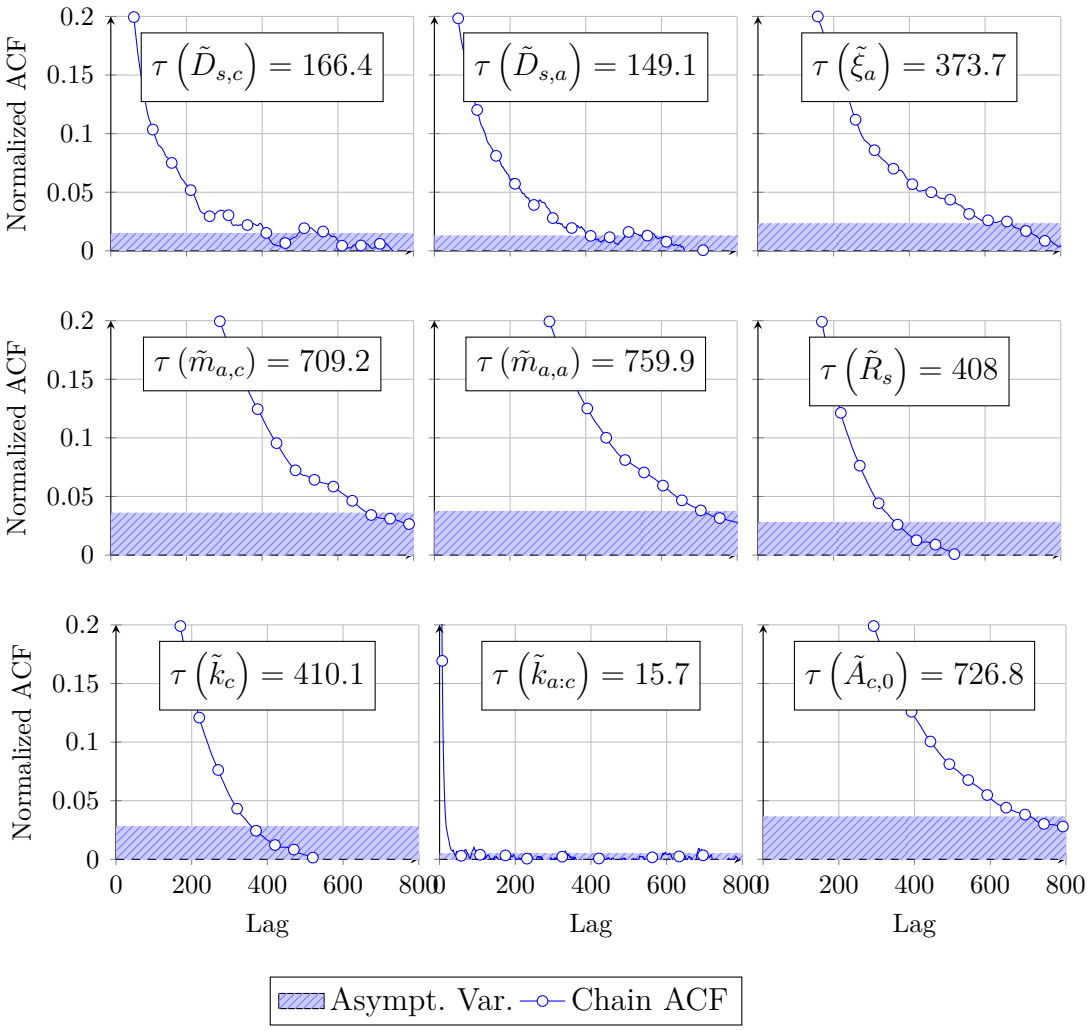

Figure 4.21.: *Estimated Autocorrelation Function (ACF) for the MCMC simulations (The 95 % confidence intervals from the estimated asymptotic variance are superimposed with shaded patterns).*

5

Conclusion

In this work, approaches for efficient and effective modeling of complex coupled systems of PDEs, their parameter identification and Bayesian uncertainty quantification are presented and demonstrated using the example of a variety of automotive lithium-ion cell models. These subject areas are also reflected in the title of the work itself.

Overall, this thesis provides contributions to

- Numerical techniques,
- Sensitivity analysis,
- Optimization algorithms,
- Uncertainty Quantification.

The fundamentals of mathematical modeling of Lithium-Ion cells, which provides the foundations of this thesis, are presented in Chapter 2. The field of mathematical modeling of batteries is a rather recent and very active research field. There exist a range of semi-empirical models that very well manage to capture the behavior of a cell on the basis of only few abstract parameters. More sophisticated models, as introduced by Doyle et al. (1993), provide a very attractive trade-off of complexity and mechanistic understanding of fundamental processes in a cell. The attractiveness of the approach lies in the great insight that these models provide and the perspective of incorporating aging effects and manufacturing influences, which results in a wide range of not-yet-standardized model formulations. Five model variants are presented, which provide fast evaluation for each of their respective purpose. These models are used in the later part of the thesis combined with the developed optimization methods.

The major new part of Chapter 3, the surrogate modeling of the previously defined models is described and the space mapping for optimization of each pair of coarse and fine models is discussed. The rigorous formulation of the optimization problem of the non-linear electro-chemical model is derived by utilizing the linearized model. This work shows the application of the space mapping approach to speed up estimation of the parameters. This happens through substituting model evaluations by the response of a fast surrogate model, i.e. a linearized version of the battery model. Afterwards, the obtained parameters are mapped back from the tangent space into the original model's parameter space by an iteratively refined mapping function. The use of the linearized version as a *coarse* model and the adapted space mapping algorithm have been stated.

Further, a consistent formulation of the adjoint model is derived to solve the problem of missing gradients of the optimization problem in a single model evaluation.

Using modern High-Performance Computing implementations of the electro-chemical models permit optimization using stochastic algorithms. In this approach, the problem of false convergence in local minima is mitigated by commonly known global optimization techniques. Thus, the recently developed SOHO algorithm loosens the dependency on parameter starting point locations and manages to establish sensible results in reasonable time.

Finally, Chapter 3 presents a Bayesian inference framework, where all parameters are treated as random variables. Several MCMC algorithms are presented, which provide enhancements over the original Metropolis algorithm w.r.t. statistical efficiency, computational speed and applicability. In addition, implementation details are given to bootstrap the algorithms and additional considerations w.r.t. the application.

All of the algorithms devised in this chapter are tested in the last part of Chapter 4 and improvements in terms of efficiency and results could be achieved.

Chapter 4 combines the models of Chapter 2 with the computational optimization techniques developed in Chapter 3. Results of a SA are presented, followed by results of applying the space mapping technique to optimize parameters on the basis of the SA results. Two variants of the previously presented MCMC algorithms are presented with regard to one variant of the electro-chemical models each.

As a first outcome, SA results from applying the MOAT global parameter screening yield knowledge about the parameter sensitivities of a complex electro-chemical model. Based on the results, three parameters are selected for validation of the space mapping algorithm. The validation of the algorithm happens through applying it on a synthetic fitting problem in three dimensions, where parameters of a simulation are recovered starting from a different point in the parameter space. The gradient estimation of the optimization sub-problems is compared between finite differences and using the adjoint system. In addition, further numerical treatment of the adjoint system is presented to facilitate and speed up the solution of the overarching problem.

In addition, successful application of the space mapping algorithm to FEM-based electric 3D model of a lithium cell using coupled 0D second-order RC models is presented. This is done by substituting model evaluations by the response of a fast surrogate model, i.e. a single second-order RC model. The obtained parameters are mapped into the original model's parameter space by an iteratively refined mapping function. Results of the algorithm compared to the straight forward direct approach applied to three pulse measurements at different temperatures are given. Comparison results indicate a remarkable reduction in computational effort of approximately 87 %, i.e. a speed up factor of 8, while maintaining very high accuracy of the results. Surrogate-based optimization with space mapping has proven to be of great help in the parameter identification process, bearing in mind that for typical battery models not only three different temperatures are chosen in order to parametrize the equivalent-circuits.

The second part demonstrates the efficient solution of the parameter identification problem to match the voltage obtained from both, the SPM and the DFN, and from experimental measurements. A total of 39 and 44 parameters are used to define the

SPM and DFN, respectively. The minimization of the error between computed and measured voltage is performed using an efficient Single Objective Hybrid Optimizer (SOHO) algorithm. The parameters of the SPM are identified within *one hour* while the parameters of the DFN are identified within *one day*. Both models yield an average error and standard deviation below 10 mV, which is a remarkable result. A posteriori sensitivity analysis is performed on the converged parameters of both models and the degree of sensitivity of each parameter identified.

The last part of Chapter 4 shows the applicability of parameter estimation and uncertainty quantification of lithium-ion cells by Bayesian model inversion using the MCMC sampling approach. In this context, estimating dynamic parameters and their uncertainties in the DFN is focused. Modeling of the prior and the set-up of the algorithm is done in a very general way, applicable to a wide range of complex models. Due to the complexity of the model, a parallelized approach was devised and implemented, including "Early Stopping" as an additional means of reducing computing times. The results of applying the algorithm against synthetic measurements were compared and the statistical efficiency was presented by investigating the iACT.

The analysis of the statistics and the iACT indicate a sharp distribution and a higher statistical efficiency for individual chains. Only the scatter plots reveal the inferior sample coverage of the posterior in the individual chain case. This highlights the advantage of using parallel chains.

A more realistic example was presented in the last section. This section demonstrates the applicability of the MCMC sampling approach on the basis of real measurement data. Due to the complexity of the model, the approach implements "*Delayed Rejection*" in parallel and "*adaptivity*" as a means of improving the statistical and computational efficiency.

Output of this framework is the parameters of the lithium-ion cell model with quantified uncertainties. Marginal distribution and 2D-scatter plots are given to report the results of the sampling. The statistical efficiency is reported by investigating the integrated auto-correlation time. The proposed approach is shown to be appropriate for investigating the dynamic properties of lithium-ion cells in the presence of noise.

5.1. Outlook

Even though this thesis contributes a number of new views, results and techniques to the field, there emerges a wide range of prospective future work.

Modeling of Lithium-Ion cells is an ongoing and very active field of research. Recent advances have been made to combine results of even more detailed models on the basis of Molecular Dynamics (MD) and Density Functional Theory (DFT) to model interphase and transport effects on a molecular level. On the other hand, long term aging effects are subject to research projects with the aim to establish a single model formulation that incorporates them along with short-term dynamics. Hence, the most crucial open problem, that requires further work, is to harmonize the models and establish one standardized formulation that incorporates the mentioned effects.

Remaining tasks for further investigation in the context of Chapter 2 may be summarized as

- Model reduction and performance improvements of electro-chemical models to be incorporated in MPC.
- Other model reduction techniques of systems of PDEs to devise a faster coarse model
- Incorporation of proper thermal dynamic behavior into the model
- Incorporation of mechanical stresses
- Transform into frequency domain

There exist various ways of model reduction, such as the Direct Realization Algorithm (DRA), Proper Orthogonal Decomposition (POD) and Machine Learning (ML), that seem promising tools to cut down computational requirements, that would possibly enable implementation of the more complex models in the context of MPC in embedded systems. Also, after making some first steps with POD, this appears to be very well suited for use in the context of space mapping in combination with an adjoint model, as the latter may also be represented by a transform of the POD system.

On the other hand, increasing the complexity of the model apparently is unavoidable, as the incorporation of proper thermo-dynamic behavior is a key cornerstone to enable accurate aging mechanics in simulation.

As frequency domain based IS is a very established tool to estimate parameters for semi-empirical RC-models, it is reasonable to assume that a similar approach could be followed for electro-chemical models as well. In particular, the complex impedance that is acquired for a IS offers a unique mapping between model results and measurements, as there exists a clear Euclidean distance measure in the complex plane, as opposed to the simple sum of squared differences in the time domain case.

With respect to the sensitivity analysis, the following points seem sensible future tasks:

- Radial enhanced sampling for uniformity,
- Full variance decomposition for global sensitivity analysis.

Although sensitivity analysis has been performed already, Radial enhanced sampling for uniformity (ReSU) appears to be a very promising technique to perform the parameter ranking task by reducing the required number of model evaluations even further. This would provide an interesting result for validation of the MOAT-result or possibly even improve it. On the other hand, full variance decomposition could serve the same purpose by utilizing the virtually unlimited amounts of available cloud-computing power with very high reliability. In addition to the validation, this could also yield results regarding the correlation of (quasi-)stationary and dynamic effects and influences.

Another issue for improving the MCMC methods is given by

- Asymptotically exact MCMC
- Approximation and sampling using the tensor train decomposition.
- Full parameter investigation

Similar to the space mapping approach in the deterministic case, replacing the forward model with a surrogate decouples the required number of model evaluations from the

length of the MCMC chain, and thus could vastly reduce the overall cost of inference (Conrad, 2014).

In a similar sense, tensor train decomposition seems to be a very promising recent development, that builds on constructing a tensor-train approximation to the target probability density function, which effectively provide a low-rank surrogate. First results show, that the tensor-train method outperforms the DRAM by orders-of-magnitude (Dolgov et al., 2018).

A very detailed sampling result has already been achieved, nevertheless a result w.r.t. the full parameter set is still pending. However, additional work has to be performed to investigate the correlation between (quasi-)stationary and dynamic effects and influences, such as the OCV and the total active mass of lithium.

A

Appendix

A.1. Scaling of the System

Due to problems with solving the adjoint system described in Section 3.2.1, it became clear that the "dual" nature of the adjoint system in a numerical sense led to a "mix-up" of all system variables in their respective domains. In other words, while the original system described as an operator in (2.37) shows only little connection between variables, mainly connected by the linearized Butler-Volmer derivative $\partial_u \hat{j}$, the adjoint system in (3.21) shows a tight interaction between all adjoint variables p_i in *every* equation. Thus, small values in the 1D-domains are added to and subtracted from very high values in the 2D-domains of particle concentrations, due to their high sensitivities, and numerical quantization noise is amplified throughout the computations leading to divergent solutions. Switching from direct to iterative solvers could mitigate the effects, but to further avoid this behavior, several improvements to the original system have been devised and adopted in the linear and the adjoint system.

We start by defining *independent* variables in space and time – x, r, t, respectively – and transform their associated derivatives. Choosing x_c as a scaling factor in spatial dimensions, this results in:

$$\hat{x} = \frac{x}{x_c} \Rightarrow x = x_c \hat{x} \tag{A.1a}$$

$$\frac{\partial}{\partial x} = \frac{1}{x_c}\frac{\partial}{\partial \hat{x}} = \frac{1}{x_c}\hat{\nabla}, \quad \text{to ease reading} \tag{A.1b}$$

$$\hat{r} = \frac{r}{x_c} \Rightarrow r = x_c \hat{r} \tag{A.1c}$$

$$\frac{\partial}{\partial r} = \frac{1}{x_c}\frac{\partial}{\partial \hat{r}} \tag{A.1d}$$

By choosing a single, spatial scale factor of x_c rather than introducing separate factors, e.g. r_c for r, we may define a single scaling factor for time t, also depending on space,

as known from literature (Langtangen & Pedersen, 2016).

$$\hat{t} = \frac{t}{\frac{x_c^2}{D_{\text{ref}}}} \Rightarrow t = \frac{x_c^2}{D_{\text{ref}}}\hat{t} \tag{A.2a}$$

$$\frac{\partial}{\partial t} = \frac{D_{\text{ref}}}{x_c^2}\frac{\partial}{\partial \hat{t}} \tag{A.2b}$$

Further, we introduce a reference value for scaling material parameters:

$$\hat{D}_s = \frac{D_s}{D_{\text{ref}}} \tag{A.3a}$$

$$\hat{\sigma}_{s,i} = \frac{\sigma_{s,i}}{\sigma_{\text{ref}}} \tag{A.3b}$$

$$\hat{\kappa} = \frac{\kappa}{\kappa_{\text{ref}}} \tag{A.3c}$$

Note, that the parameters for σ_s depend on the electrode i such that it can compensate for different values in each domain.

Eventually, we introduce scaling for the concentrations c_s and c_ℓ, as part of the *dependent* variables.

$$\hat{c}_s = \frac{c_s}{c_{\text{ref}}} \tag{A.4a}$$

$$\hat{c}_\ell = \frac{c_\ell}{c_{\text{ref}}} \tag{A.4b}$$

Again, there is a common reference shared between solid and liquid concentrations to simplify derivation and implementation.

Substituting each occurrence in the original system (2.20) leads to:

$$-\hat{\nabla}\cdot\left(\hat{\sigma}_{s,i}\hat{\nabla}\varphi_s\right) = -\frac{x_c^2}{\sigma_{\text{ref},i}}A_i j_{\text{BV}}^*, \quad \text{in } \hat{Q}_1' \tag{A.5a}$$

$$-\hat{\nabla}\cdot\left(\hat{\kappa}_\ell(\hat{c}_\ell c_{\text{ref}})\hat{\nabla}\varphi_\ell + \frac{RT}{zF}\hat{\kappa}_\ell(\hat{c}_\ell c_{\text{ref}})t_\ell^+\frac{1}{\hat{c}_\ell}\hat{\nabla}\hat{c}_\ell\right) = \frac{x_c^2}{\kappa_{\text{ref},i}}A_i j_{\text{BV}}^*, \quad \text{in } \hat{Q}_1 \tag{A.5b}$$

$$\frac{\partial\left(\varepsilon_\ell\hat{c}_\ell\right)}{\partial\hat{t}} - \hat{\nabla}\cdot\left(\hat{D}_\ell\left(\hat{\nabla}\hat{c}_\ell + \frac{zF}{RT}\mu_\ell\hat{c}_\ell\hat{\nabla}\varphi_\ell\right)\right) = \frac{x_c^2}{D_{\text{ref}}}\frac{A_i}{zF}j_{\text{BV}}^*, \quad \text{in } \hat{Q}_1 \tag{A.5c}$$

$$\frac{\partial\hat{c}_s}{\partial\hat{t}} - \frac{1}{\hat{r}^2}\frac{\partial}{\partial\hat{r}}\left(\hat{D}_s\hat{r}^2\frac{\partial\hat{c}_s}{\partial\hat{r}}\right) = 0, \quad \text{in } \hat{Q}_2 \tag{A.5d}$$

subject to boundary conditions:

$$\hat{\varphi}_s = 0, \quad \text{on } \Sigma_a := \Gamma_a \times [0,T] \tag{A.6a}$$

$$-\hat{\sigma}_s\hat{\nabla}\varphi_s = \frac{-x_c}{\sigma_{\text{ref}}}i\left(t\right), \quad \text{on } \hat{\Sigma}_c := \hat{\Gamma}_c \times [0,T] \tag{A.6b}$$

$$-\hat{D}_s\frac{\partial\hat{c}_s}{\partial\hat{r}} = \frac{-x_c}{c_{\text{ref}}D_{\text{ref}}}\frac{1}{zF}j_{\text{BV}}^*, \quad \text{on } \hat{\Sigma}_{Ro} := \hat{\Gamma}_{Ro,a} \cup \hat{\Gamma}_{Ro,c} \times [0,T] \tag{A.6c}$$

A.2. Discretization of the Linear System

To spatially discretize the system, we start by replacing the test functions ϕ and ψ in (2.36) by compact test functions ϕ_i and ψ_k

$$\begin{aligned}&\int_\Omega \Big(\alpha_1\left(\hat{u};\hat{\mu}\right)\partial_x\varphi_\ell + \alpha_2\left(\hat{u};\hat{\mu}\right)\partial_x c_\ell\Big)\ \partial_x\phi_i \\ &\quad - \Big(\partial_u\hat{j}^T\, v + \partial_\mu\hat{j}^T\,\lambda + \hat{j}_c + \alpha_3\left(\hat{\mu}\right)\partial_t\left(\varphi_s-\varphi_\ell\right)\Big)\ \phi_i\,\mathrm{d}x = 0,\end{aligned} \tag{A.7a}$$

$$\begin{aligned}&\int_\Omega \alpha_4\left(\hat{\mu}\right)\partial_x\varphi_s\,\partial_x\phi_i + \Big(\partial_u\hat{j}^T\, v + \partial_\mu\hat{j}^T\,\lambda + \hat{j}_c + \alpha_3\left(\hat{\mu}\right)\partial_t\left(\varphi_s-\varphi_\ell\right)\Big)\ \phi_i\,\mathrm{d}x \\ &\quad - I\,\phi_i\left(\Gamma_c\right) = 0,\end{aligned} \tag{A.7b}$$

$$\begin{aligned}&\int_\Omega \varepsilon_{\ell i}\,\partial_t c_\ell\,\phi_i + \Big(\alpha_5\left(\hat{u};\hat{\mu}\right)\ \partial_x c_\ell + \alpha_6\left(\hat{u};\hat{\mu}\right)\ \partial_x\varphi_\ell\Big)\ \partial_x\phi_i \\ &\quad - \alpha_7\left(\hat{\mu}\right)\ \Big(\partial_u\hat{j}^T\, v + \partial_\mu\hat{j}^T\,\lambda + \hat{j}_c + \alpha_3\left(\hat{\mu}\right)\partial_t\left(\varphi_s-\varphi_\ell\right)\Big)\ \phi_i\,\mathrm{d}x = 0,\end{aligned} \tag{A.7c}$$

$$\begin{aligned}&\iint_{\Lambda_a}\Big(\partial_t c_{sa}\,\phi_i\,\psi_k + \alpha_8\left(\hat{u};\hat{\mu}\right)\partial_r c_{sa}\,\partial_r\psi_k\,\phi_i\Big)\ r^2\mathrm{d}r \\ &+ R_a^2\,\alpha_{14}\left(\hat{\mu}\right)\ \Big(\partial_u\hat{j}^T\, v + \partial_\mu\hat{j}^T\,\lambda + \hat{j}_c + \alpha_3\left(\mu\right)\ \partial_t\left(\varphi_s-\varphi_\ell\right)\Big)\ \psi_k\left(\Gamma_{R,a}\right)\phi_i\,\mathrm{d}x = 0\end{aligned} \tag{A.7d}$$

$$\begin{aligned}&\iint_{\Lambda_c}\Big(\partial_t c_{sc}\,\phi_i\,\psi_k + \alpha_8\left(\hat{u};\hat{\mu}\right)\partial_r c_{sc}\,\partial_r\psi_k\,\phi_i\Big)\ r^2\mathrm{d}r \\ &+ R_c^2\,\alpha_{14}\left(\hat{\mu}\right)\ \Big(\partial_u\hat{j}^T\, v + \partial_\mu\hat{j}^T\,\lambda + \hat{j}_c + \alpha_3\left(\hat{\mu}\right)\ \partial_t\left(\varphi_s-\varphi_\ell\right)\Big)\ \psi_k\left(\Gamma_{R,c}\right)\phi_i\,\mathrm{d}x = 0\end{aligned} \tag{A.7e}$$

In the next step, we apply the method of Galerkin, i.e. we substitute the unknowns by a linear combination of the basis functions:

$$\begin{aligned}\varphi_\ell\left(x,t\right) &= \left(\sum_j \hat{\varphi}_{\ell,j}\left(t\right)\ \phi_j\left(x\right)\right),\ \varphi_s\left(x,t\right) = \left(\sum_j \hat{\varphi}_{s,j}\left(t\right)\ \phi_j\left(x\right)\right), \\ c_\ell\left(x,t\right) &= \left(\sum_j \hat{c}_{\ell,j}\left(t\right)\ \phi_j\left(x\right)\right),\end{aligned}$$

$$\begin{aligned}c_{sa}\left(x,r,t\right) &= \left(\sum_j \phi_j\left(x\right)\ \hat{c}_{sa,j}\left(r,t\right)\right) = \left(\sum_j \phi_j\left(x\right)\ \sum_l \psi_l\left(r\right)\ \hat{c}_{sa,j,l}\left(t\right)\right), \\ c_{sc}\left(x,r,t\right) &= \left(\sum_j \phi_j\left(x\right)\ \hat{c}_{sc,j}\left(r,t\right)\right) = \left(\sum_j \phi_j\left(x\right)\ \sum_l \psi_l\left(r\right)\ \hat{c}_{sc,j,l}\left(t\right)\right) \quad \text{and} \\ \hat{v}_j\left(t\right) &= \begin{pmatrix}\hat{\varphi}_{\ell,j}\left(t\right)\\ \hat{\varphi}_{s,j}\left(t\right)\\ \hat{c}_{\ell,j}\left(t\right)\\ \hat{c}_{sa,j,l}\left(t\right)\\ \hat{c}_{sc,j,l}\left(t\right)\end{pmatrix}\end{aligned}$$

wherein all unknowns are combined.

$$\begin{aligned}
&\int_{\Omega} \alpha_1\left(\hat{u};\hat{\mu}\right)\left(\sum_j \hat{\varphi}_{\ell,j}\left(t\right)\,\partial_x\phi_j\right)\,\partial_x\phi_i + \alpha_2\left(\hat{u};\hat{\mu}\right)\left(\sum_j \hat{c}_{\ell,j}\left(t\right)\,\partial_x\phi_j\right)\,\partial_x\phi_i \\
&\quad - \sum_j \left(\partial_u\hat{j}^T\,\hat{v}_j\left(t\right) + \alpha_3\left(\hat{\mu}\right)\partial_t\left(\hat{\varphi}_{s,j}\left(t\right) - \hat{\varphi}_{\ell,j}\left(t\right)\right)\right)\phi_j\,\phi_i\,\mathrm{d}x = \\
&\qquad \int_{\Omega}\left(\partial_\mu\hat{j}^T\,\lambda + \hat{j}_c\right)\,\phi_i\,\mathrm{d}x,
\end{aligned} \tag{A.8a}$$

$$\begin{aligned}
&\int_{\Omega} \alpha_4\left(\hat{\mu}\right)\left(\sum_j \hat{\varphi}_{s,j}\left(t\right)\,\partial_x\phi_j\right)\,\partial_x\phi_i \\
&\quad + \sum_j \left(\partial_u\hat{j}^T\,\hat{v}_j\left(t\right) + \alpha_3\left(\hat{\mu}\right)\partial_t\left(\hat{\varphi}_{s,j}\left(t\right) - \hat{\varphi}_{\ell,j}\left(t\right)\right)\right)\phi_j\,\phi_i\,\mathrm{d}x = I\,\phi_i\left(\Gamma_c\right) \\
&\qquad - \int_{\Omega}\left(\partial_\mu\hat{j}^T\,\lambda + \hat{j}_c\,\phi_i\right)\,\mathrm{d}x,
\end{aligned} \tag{A.8b}$$

$$\begin{aligned}
&\int_{\Omega} \varepsilon_{\ell i}\,\partial_t\left(\sum_j \hat{c}_{\ell,j}\left(t\right)\,\phi_j\right)\,\phi_i \\
&\quad + \alpha_5\left(\hat{u};\hat{\mu}\right)\left(\sum_j \hat{c}_{\ell,j}\left(t\right)\,\partial_x\phi_j\right)\,\partial_x\phi_i + \alpha_6\left(\hat{u};\hat{\mu}\right)\left(\sum_j \hat{\varphi}_{\ell,j}\left(t\right)\,\partial_x\phi_j\right)\,\partial_x\phi_i \\
&\qquad - \alpha_7\left(\hat{\mu}\right)\sum_j \left(\partial_u\hat{j}^T\,\hat{v}_j\left(t\right) + \alpha_3\left(\hat{\mu}\right)\partial_t\left(\hat{\varphi}_{s,j}\left(t\right) - \hat{\varphi}_{\ell,j}\left(t\right)\right)\right)\phi_j\,\phi_i\,\mathrm{d}x = \\
&\qquad \int_{\Omega}\alpha_7\left(\hat{\mu}\right)\,\left(\partial_\mu\hat{j}^T\,\lambda + \hat{j}_c\right)\,\phi_i\,\mathrm{d}x,
\end{aligned} \tag{A.8c}$$

$$\begin{aligned}
&\iint_{\Lambda_a}\left(\partial_t\left(\sum_{j,l}\phi_j\,\psi_l\,\hat{c}_{sa,j,l}\left(t\right)\right)\,\phi_i\,\psi_k + \alpha_8\left(\hat{u};\hat{\mu}\right)\partial_r\left(\sum_{j,l}\phi_j\,\psi_l\,\hat{c}_{sa,j,l}\left(t\right)\right)\,\partial_r\psi_k\,\phi_i\right)\,r^2\mathrm{d}r \\
&\quad + R_a^2\,\alpha_{14}\left(\hat{\mu}\right)\sum_j\left(\partial_u\hat{j}^T\,\hat{v}_j\left(t\right) + \alpha_3\left(\hat{\mu}\right)\partial_t\left(\hat{\varphi}_{s,j}\left(t\right) - \hat{\varphi}_{\ell,j}\left(t\right)\right)\right)\,\psi_k\left(\Gamma_{R,a}\right)\,\phi_j\,\phi_i\,\mathrm{d}x = \\
&\qquad - \int_{\Omega}\left(R_a^2\,\alpha_{14}\left(\hat{\mu}\right)\,\left(\partial_\mu\hat{j}^T\,\lambda + \hat{j}_c\right)\psi_k\left(\Gamma_{R,a}\right)\,\phi_i\right)\,\mathrm{d}x,
\end{aligned} \tag{A.8d}$$

$$\begin{aligned}
&\iint_{\Lambda_c}\left(\partial_t\left(\sum_{j,l}\phi_j\,\psi_l\,\hat{c}_{sc,j,l}\left(t\right)\right)\,\phi_i\,\psi_k + \alpha_8\left(\hat{u};\hat{\mu}\right)\partial_r\left(\sum_{j,l}\phi_j\,\psi_l\,\hat{c}_{sc,j,l}\left(t\right)\right)\,\partial_r\psi_k\,\phi_i\right)\,r^2\mathrm{d}r \\
&\quad + R_c^2\,\alpha_{14}\left(\hat{\mu}\right)\sum_j\left(\partial_u\hat{j}^T\,\hat{v}_j\left(t\right) + \alpha_3\partial_t\left(\hat{\varphi}_{s,j}\left(t\right) - \hat{\varphi}_{\ell,j}\left(t\right)\right)\right)\,\phi_j\,\psi_k\left(\Gamma_{R,c}\right)\phi_i\,\mathrm{d}x = \\
&\qquad - \int_{\Omega}\left(R_c^2\,\alpha_{14}\left(\hat{\mu}\right)\,\left(\partial_\mu\hat{j}^T\,\lambda + \hat{j}_c\right)\psi_k\left(\Gamma_{R,c}\right)\,\phi_i\right)\,\mathrm{d}x,
\end{aligned} \tag{A.8e}$$

Now we identify three parts of the system, i.e. a *Mass matrix* M, that consists of coefficients of the terms that contain time derivatives of the unknowns, a *Stiffness matrix* K that consists of coefficients to all other terms that include unknowns and

a *Right hand side vector* R that contains all constant values. For computing the Unknowns $\hat{v}$, we denote the elements of the identified block matrices:

$$M_{1,1}^{i,j} = \int_{\Omega_E} \alpha_3\left(\hat{\mu}\right)\, \phi_j\, \phi_i \,\mathrm{d}x \tag{A.9a}$$

$$M_{1,2}^{i,j} = -M_{1,1}^{i,j} \tag{A.9b}$$

$$M_{2,1}^{i,j} = -\int_{\Omega_E} \alpha_3\left(\hat{\mu}\right)\, \phi_j\, \phi_i \,\mathrm{d}x \tag{A.9c}$$

$$M_{2,2}^{i,j} = -M_{2,1}^{i,j} \tag{A.9d}$$

$$M_{3,1}^{i,j} = \int_{\Omega_E} \alpha_3\left(\hat{\mu}\right)\, \alpha_7\left(\hat{\mu}\right)\, \phi_j\, \phi_i \,\mathrm{d}x \tag{A.9e}$$

$$M_{3,2}^{i,j} = -M_{3,1}^{i,j} \tag{A.9f}$$

$$M_{3,3}^{i,j} = \int_{\Omega_E} \varepsilon_{\ell i}\, \phi_j\, \phi_i \,\mathrm{d}x \tag{A.9g}$$

$$M_{4,1}^{i,j,k} = -\int_{\Omega_E} R_a^2\, \alpha_3\left(\hat{\mu}\right)\, \alpha_{14}\left(\hat{\mu}\right)\, \psi_k\left(\Gamma_{R,a}\right)\, \phi_j\, \phi_i \,\mathrm{d}x \tag{A.9h}$$

$$M_{4,2}^{i,j,k} = -M_{4,1}^{i,j,k} \tag{A.9i}$$

$$M_{4,4}^{i,j,k,l} = \iint\limits_{\Lambda_{a,E}} \psi_l\, \psi_k\, r^2 \mathrm{d}r\, \phi_j\, \phi_i \,\mathrm{d}x \tag{A.9j}$$

$$M_{5,1}^{i,j,k} = -\int_{\Omega_E} R_c^2\, \alpha_3\left(\hat{\mu}\right)\, \alpha_{14}\left(\hat{\mu}\right)\, \psi_k\left(\Gamma_{R,c}\right)\, \phi_j\, \phi_i \,\mathrm{d}x \tag{A.9k}$$

$$M_{5,2}^{i,j,k} = -M_{5,1}^{i,j,k} \tag{A.9l}$$

$$M_{5,5}^{i,j,k,l} = \iint\limits_{\Lambda_{c,E}} \psi_l\, \psi_k\, r^2 \mathrm{d}r\, \phi_j\, \phi_i \,\mathrm{d}x \tag{A.9m}$$

for the *Mass Matrix* and

$$K_{1,1}^{i,j} = \int_{\Omega_E} \alpha_1\left(\hat{u};\hat{\mu}\right)\, \partial_x\phi_j\, \partial_x\phi_i \,\mathrm{d}x \tag{A.10a}$$

$$K_{1,3}^{i,j} = \int_{\Omega_E} \alpha_2\left(\hat{u};\hat{\mu}\right)\, \partial_x\phi_j\, \partial_x\phi_i \,\mathrm{d}x \tag{A.10b}$$

$$K_{2,2}^{i,j} = \int_{\Omega_E} \alpha_4\left(\hat{\mu}\right)\, \partial_x\phi_j\, \partial_x\phi_i \,\mathrm{d}x \tag{A.10c}$$

$$K_{3,1}^{i,j} = \int_{\Omega_E} \alpha_6\left(\hat{u};\hat{\mu}\right)\, \partial_x\phi_j\, \partial_x\phi_i \,\mathrm{d}x \tag{A.10d}$$

$$K_{3,3}^{i,j} = \int_{\Omega_E} \alpha_5\left(\hat{u};\hat{\mu}\right)\, \partial_x\phi_j\, \partial_x\phi_i \,\mathrm{d}x \tag{A.10e}$$

$$K_{4,4}^{i,j,k,l} = \iint\limits_{\Lambda_{a,E}} \alpha_8\left(\hat{u};\hat{\mu}\right) \partial_r\psi_l\, \partial_r\psi_k\, r^2 \mathrm{d}r\, \phi_j\, \phi_i \,\mathrm{d}x \tag{A.10f}$$

$$K_{5,5}^{i,j,k,l} = \iint\limits_{\Lambda_{c,E}} \alpha_8\left(\hat{u};\hat{\mu}\right) \partial_r\psi_l\, \partial_r\psi_k\, r^2 \mathrm{d}r\, \phi_j\, \phi_i \,\mathrm{d}x \tag{A.10g}$$

for the *Stiffness Matrix* and

$$K^{\prime i,j}_{1,1} = -\int_{\Omega_E} \partial_{\varphi_\ell}\hat{j}\,\phi_j\,\phi_i\,\mathrm{d}x \tag{A.11a}$$

$$K^{\prime i,j}_{1,2} = -\int_{\Omega_E} \partial_{\varphi_s}\hat{j}\,\phi_j\,\phi_i\,\mathrm{d}x \tag{A.11b}$$

$$K^{\prime i,j}_{1,3} = -\int_{\Omega_E} \partial_{c_\ell}\hat{j}\,\phi_j\,\phi_i\,\mathrm{d}x \tag{A.11c}$$

$$K^{\prime i,j,k,l}_{1,4} = -\int_{\Omega_E} \partial_{c_{sa}}\hat{j}\,\phi_j\,\phi_i\,\mathrm{d}x \tag{A.11d}$$

$$K^{\prime i,j,k,l}_{1,5} = -\int_{\Omega_E} \partial_{c_{sc}}\hat{j}\,\phi_j\,\phi_i\,\mathrm{d}x \tag{A.11e}$$

$$K^{\prime i,j}_{2,1} = \int_{\Omega_E} \partial_{\varphi_\ell}\hat{j}\,\phi_j\,\phi_i\,\mathrm{d}x \tag{A.11f}$$

$$K^{\prime i,j}_{2,2} = \int_{\Omega_E} \partial_{\varphi_s}\hat{j}\,\phi_j\,\phi_i\,\mathrm{d}x \tag{A.11g}$$

$$K^{\prime i,j}_{2,3} = \int_{\Omega_E} \partial_{c_\ell}\hat{j}\,\phi_j\,\phi_i\,\mathrm{d}x \tag{A.11h}$$

$$K^{\prime i,j,k,l}_{2,4} = \int_{\Omega_E} \partial_{c_{sa}}\hat{j}\,\phi_j\,\phi_i\,\mathrm{d}x \tag{A.11i}$$

$$K^{\prime i,j,k,l}_{2,5} = \int_{\Omega_E} \partial_{c_{sc}}\hat{j}\,\phi_j\,\phi_i\,\mathrm{d}x \tag{A.11j}$$

$$K^{\prime i,j}_{3,1} = -\int_{\Omega_E} \alpha_7\left(\hat{\mu}\right)\,\partial_{\varphi_\ell}\hat{j}\,\phi_j\,\phi_i\,\mathrm{d}x \tag{A.11k}$$

$$K^{\prime i,j}_{3,2} = -\int_{\Omega_E} \alpha_7\left(\hat{\mu}\right)\,\partial_{\varphi_s}\hat{j}\,\phi_j\,\phi_i\,\mathrm{d}x \tag{A.11l}$$

$$K^{\prime i,j}_{3,3} = -\int_{\Omega_E} \alpha_7\left(\hat{\mu}\right)\,\partial_{c_\ell}\hat{j}\,\phi_j\,\phi_i\,\mathrm{d}x \tag{A.11m}$$

$$K^{\prime i,j,k,l}_{3,4} = -\int_{\Omega_E} \alpha_7\left(\hat{\mu}\right)\,\partial_{c_{sa}}\hat{j}\,\phi_j\,\phi_i\,\mathrm{d}x \tag{A.11n}$$

$$K^{\prime i,j,k,l}_{3,5} = -\int_{\Omega_E} \alpha_7\left(\hat{\mu}\right)\,\partial_{c_{sc}}\hat{j}\,\phi_j\,\phi_i\,\mathrm{d}x \tag{A.11o}$$

$$K^{\prime i,j,k}_{4,1} = \int_{\Omega_E} R_a^2\,\alpha_{14}\left(\hat{\mu}\right)\,\psi_k\left(\Gamma_{R,a}\right)\,\partial_{\varphi_\ell}\hat{j}\,\phi_j\,\phi_i\,\mathrm{d}x \tag{A.11p}$$

$$K^{\prime i,j,k}_{4,2} = \int_{\Omega_E} R_a^2\,\alpha_{14}\left(\hat{\mu}\right)\,\psi_k\left(\Gamma_{R,a}\right)\,\partial_{\varphi_s}\hat{j}\,\phi_j\,\phi_i\,\mathrm{d}x \tag{A.11q}$$

$$K^{\prime i,j,k}_{4,3} = \int_{\Omega_E} R_a^2\,\alpha_{14}\left(\hat{\mu}\right)\,\psi_k\left(\Gamma_{R,a}\right)\,\partial_{c_\ell}\hat{j}\,\phi_j\,\phi_i\,\mathrm{d}x \tag{A.11r}$$

$$K^{\prime i,j,k,l}_{4,4} = \int_{\Omega_E} R_a^2\,\alpha_{14}\left(\hat{\mu}\right)\,\psi_k\left(\Gamma_{R,a}\right)\,\partial_{c_{sa}}\hat{j}\,\phi_j\,\phi_i\,\mathrm{d}x \tag{A.11s}$$

$$K^{\prime i,j,k}_{5,1} = \int_{\Omega_E} R_c^2\,\alpha_{14}\left(\hat{\mu}\right)\,\psi_k\left(\Gamma_{R,c}\right)\,\partial_{\varphi_\ell}\hat{j}\,\phi_j\,\phi_i\,\mathrm{d}x \tag{A.11t}$$

$$K^{\prime i,j,k}_{5,2} = \int_{\Omega_E} R_c^2\,\alpha_{14}\left(\hat{\mu}\right)\,\psi_k\left(\Gamma_{R,c}\right)\,\partial_{\varphi_s}\hat{j}\,\phi_j\,\phi_i\,\mathrm{d}x \tag{A.11u}$$

$$K'^{i,j,k}_{5,3} = \int_{\Omega_E} R_c^2\, \alpha_{14}\left(\hat{\mu}\right)\, \psi_k\left(\Gamma_{R,c}\right)\, \partial_{c_\ell}\hat{j}\, \phi_j\, \phi_i \,\mathrm{d}x \tag{A.11v}$$

$$K'^{i,j,k,l}_{5,5} = \int_{\Omega_E} R_c^2\, \alpha_{14}\left(\hat{\mu}\right)\, \psi_k\left(\Gamma_{R,c}\right)\, \partial_{c_{sc}}\hat{j}\, \phi_j\, \phi_i \,\mathrm{d}x \tag{A.11w}$$

for the linearization parts of the *Stiffness Matrix*. We denote the elements of the *Right hand side vector* as:

$$R_1^i = \int_{\Omega_E} \left(\partial_\mu \hat{j}^T\, \lambda + \hat{j} - \partial_u \hat{j}^T \hat{u} - \partial_\mu \hat{j}^T \hat{\mu}\right)\, \phi_i \,\mathrm{d}x \tag{A.12a}$$

$$R_2^i = I\, \phi_i\left(\Gamma_c\right) - \int_{\Omega_E} \left(\partial_\mu \hat{j}^T\, \lambda + \hat{j} - \partial_u \hat{j}^T \hat{u} - \partial_\mu \hat{j}^T \hat{\mu}\right)\, \phi_i \,\mathrm{d}x \tag{A.12b}$$

$$R_3^i = \int_{\Omega_E} \alpha_7\left(\hat{\mu}\right)\, \left(\partial_\mu \hat{j}^T\, \lambda + \hat{j} - \partial_u \hat{j}^T \hat{u} - \partial_\mu \hat{j}^T \hat{\mu}\right)\, \phi_i \,\mathrm{d}x \tag{A.12c}$$

$$R_4^{i,k} = -\int_{\Omega_E} R_a^2\, \alpha_{14}\left(\hat{\mu}\right)\, \left(\partial_\mu \hat{j}^T\, \lambda + \hat{j} - \partial_u \hat{j}^T \hat{u} - \partial_\mu \hat{j}^T \hat{\mu}\right) \psi_k\left(\Gamma_{R,a}\right)\, \phi_i \,\mathrm{d}x \tag{A.12d}$$

$$R_5^{i,k} = -\int_{\Omega_E} R_c^2\, \alpha_{14}\left(\hat{\mu}\right)\, \left(\partial_\mu \hat{j}^T\, \lambda + \hat{j} - \partial_u \hat{j}^T \hat{u} - \partial_\mu \hat{j}^T \hat{\mu}\right) \psi_k\left(\Gamma_{R,c}\right)\, \phi_i \,\mathrm{d}x \tag{A.12e}$$

For a parabolic, linear system, the initial value problem can be stated as:

$$\begin{aligned} \partial_t \hat{v} &= A\, \hat{v} \\ \hat{v}\left(t_0\right) &= \hat{v}_0 \end{aligned} \tag{A.13}$$

In this sense, the full parabolic, linear system can be given in general as

$$M\, \partial_t \hat{v} + \left(K + K'\right)\, \hat{v} = R \tag{A.14}$$

showing the block matrix structure, it can be stated more clearly as

$$\begin{aligned} &\begin{pmatrix} M_{1,1} & M_{1,2} & \mathbf{0} & \mathbf{0} & \mathbf{0} \\ M_{2,1} & M_{2,2} & \mathbf{0} & \mathbf{0} & \mathbf{0} \\ M_{3,1} & M_{3,2} & M_{3,3} & \mathbf{0} & \mathbf{0} \\ M_{4,1} & M_{4,2} & \mathbf{0} & M_{4,4} & \mathbf{0} \\ M_{5,1} & M_{5,2} & \mathbf{0} & \mathbf{0} & M_{5,5} \end{pmatrix} \frac{\partial \hat{v}}{\partial t} \\ &+ \left(\begin{pmatrix} K_{1,1} & \mathbf{0} & K_{1,3} & \mathbf{0} & \mathbf{0} \\ \mathbf{0} & K_{2,2} & \mathbf{0} & \mathbf{0} & \mathbf{0} \\ K_{3,1} & \mathbf{0} & K_{3,3} & \mathbf{0} & \mathbf{0} \\ \mathbf{0} & \mathbf{0} & \mathbf{0} & K_{4,4} & \mathbf{0} \\ \mathbf{0} & \mathbf{0} & \mathbf{0} & \mathbf{0} & K_{5,5} \end{pmatrix} \right. \\ &\left. + \begin{pmatrix} K'_{1,1} & K'_{1,2} & K'_{1,3} & K'_{1,4} & K'_{1,5} \\ K'_{2,1} & K'_{2,2} & K'_{2,3} & K'_{2,4} & K'_{2,5} \\ K'_{3,1} & K'_{3,2} & K'_{3,3} & K'_{3,4} & K'_{3,5} \\ K'_{4,1} & K'_{4,2} & K'_{4,3} & K'_{4,4} & \mathbf{0} \\ K'_{5,1} & K'_{5,2} & K'_{5,3} & \mathbf{0} & K'_{5,5} \end{pmatrix} \right) \hat{v} = \begin{pmatrix} R_1 \\ R_2 \\ R_3 \\ R_4 \\ R_5 \end{pmatrix} \end{aligned} \tag{A.15}$$

Remark: Indices of the high dimensional components $M_{y,x}^{i,j,k,l}$ have to be mapped to the matrix entries $M_{y,x}^{i+kN^{dx},j+lN^{dx}}$, $M_{y,x}^{i,j,k} \to M_{y,x}^{i+kN^{dx},j}$ – for $K_{y,x}$ analogously – and $R_y^{i,k} \to R_y^{i+kN^{dx}}$. The entries of the upper right traingle of the linearization part are mapped $K'^{i,j,k,l}_{y,x} \to K'^{i,j+lN^{dx}}_{y,x}$ for a single k at the Borders $\Gamma_{R,i}$ – entries for a different k are dismissed.
Let $\hat{v}^k$ denote an approximate solution of (A.14) at a time

$$t = k\,\Delta t, \quad \forall k \in [0, \ldots, K-1] \tag{A.16}$$

given by a time discretization of resolution Δt, then we approximate

$$\partial_t \hat{v} \approx \frac{\hat{v}^{k+1} - \hat{v}^k}{\Delta t} \tag{A.17}$$

For solving the system (A.14) we apply the implicit Euler method

$$(M + \Delta t\, K)\ \hat{v}^{k+1} = \Delta t\, R + M\, \hat{v}^k, \tag{A.18}$$

such that the method is of order 1. Technically, a blended Θ-Method was implemented, but explicit Euler methods were considered inadequate due to the high stiffness of the system, as the potential equations lead to zero eigenvalues in the mass matrix which lead to oscillations.

A.3. Derivation of the Adjoint System

In this section we elaborate in detail on the derivation of the adjoint system as used in Section 3.2.1. By means of the Langrangian function $\mathcal{L}$ we apply the *formal Lagrange method* as described by Tröltzsch (2010). This method is based on the exact Lagrangian principle, but it differs in that the differential operators $-\triangle$ and ∂_ν are written only formally and all multipliers are considered functions without specifying their corresponding spaces explicitly. By assuming square integrability of state, multipliers and their respective derivatives we avoid the use of more general functionals and write L^2 scalar products.

Let us start by defining the cost functional:

$$J(v,\lambda) := \frac{1}{2}\iint\limits_{\Sigma_d} (\varphi_s - \hat{\varphi}_s)^2 \,\mathrm{d}s(x)\mathrm{d}t + \frac{1}{2}\sum_{i=1}^{l} \chi_i \left(\lambda_i - \hat{\mu}_i\right)^2 \tag{A.19}$$

subject to the linearized system defined in (2.31) and (2.32) and the box constraints

$$\lambda_a \leq \lambda \leq \lambda_b \tag{A.20}$$

Remark: For the sake of shortness we omitted the dependencies on space and time. By $\hat{\varphi}_s$ we refer to some predefined values that may have been computed by (2.20) or measurements. The *regularization factors* $\chi_i \geq 0 \in \mathbb{R}^l$ will be discussed later. Finally, $\hat{\mu}_i$ refers to a starting value to initialize the optimization.

We denote the Lagrangian function $\mathcal{L}$ associated to the problem:

$$\begin{aligned}
\mathcal{L} := \mathcal{L}(v,\lambda,p) = J(v,\lambda) &- \iint\limits_{Q_1} -\frac{\partial}{\partial x}\left(\alpha_1 \frac{\partial \varphi_\ell}{\partial x} + \alpha_2 \frac{\partial c_\ell}{\partial x}\right) p_1 \,\mathrm{d}x\mathrm{d}t \\
&- \iint\limits_{Q_1'} \Big(-\frac{\partial \hat{j}}{\partial u}^T v - \frac{\partial \hat{j}}{\partial \mu}^T \lambda - \hat{j}_c - \alpha_3 \frac{\partial(\varphi_s - \varphi_\ell)}{\partial t}\Big) p_1 \mathrm{d}x\mathrm{d}t - \iint\limits_{\Sigma_{ad}} \left(\alpha_1 \frac{\partial \varphi_\ell}{\partial \nu} + \alpha_2 \frac{\partial c_\ell}{\partial \nu}\right) p_2 \mathrm{d}s\mathrm{d}t \\
&- \iint\limits_{Q_1'} \left(-\frac{\partial}{\partial x}\left(\alpha_4 \frac{\partial \varphi_s}{\partial x}\right) + \frac{\partial \hat{j}}{\partial u}^T v + \frac{\partial \hat{j}}{\partial \mu}^T \lambda + \hat{j}_c + \alpha_3 \frac{\partial(\varphi_s - \varphi_\ell)}{\partial t}\right) p_3 \,\mathrm{d}x\mathrm{d}t \\
&- \iint\limits_{\Sigma_{ad}} \left(\alpha_4 \frac{\partial \varphi_s}{\partial \nu} - i\right) p_4 \,\mathrm{d}s\mathrm{d}t - \iint\limits_{\Sigma_{bc}} \left(\alpha_4 \frac{\partial \varphi_s}{\partial \nu}\right) p_4 \,\mathrm{d}s\mathrm{d}t - \iint\limits_{Q_1} \left(\varepsilon_{\ell i} \frac{\partial c_\ell}{\partial t} - \frac{\partial}{\partial x}\left(\alpha_5 \frac{\partial c_\ell}{\partial x}\right.\right. \\
&\left.\left. + \alpha_6 \frac{\partial \varphi_\ell}{\partial x}\right)\right) p_5 \,\mathrm{d}x\mathrm{d}t - \iint\limits_{Q_1'} -\alpha_7 \left(\frac{\partial \hat{j}}{\partial u}^T v + \frac{\partial \hat{j}}{\partial \mu}^T \lambda + \hat{j}_c + \alpha_3 \frac{\partial(\varphi_s - \varphi_\ell)}{\partial t}\right) p_5 \,\mathrm{d}x\mathrm{d}t
\end{aligned} \tag{A.21}$$

$$
\begin{aligned}
&- \int_{\Omega} \varepsilon_{\ell i} \left(c_{\ell}\left(0\right) - c_{\ell,0} \right) p_5 \,\mathrm{d}x - \iint\limits_{\Sigma_{ad}} \left(\alpha_5 \frac{\partial c_{\ell}}{\partial \nu} + \alpha_6 \frac{\partial \varphi_{\ell}}{\partial \nu} \right) p_6 \,\mathrm{d}s\mathrm{d}t \\
&- \iiint\limits_{Q} \left(\frac{\partial c_{si}}{\partial t} - \frac{1}{r^2} \frac{\partial}{\partial r} \left(\alpha_8 \, r^2 \frac{\partial c_{si}}{\partial r} \right) \right) p_7 \, r^2 \mathrm{d}r\mathrm{d}x\mathrm{d}t \\
&- \iint\limits_{\Lambda} \left(c_{si}\left(0\right) - c_{si,0} \right) p_7 \, r^2 \mathrm{d}r\mathrm{d}x - \iiint\limits_{\Sigma_{R,0}} \left(\alpha_8 \frac{\partial c_{si}}{\partial \nu} \right) p_8 \, r^2 \mathrm{d}s(r)\mathrm{d}x\mathrm{d}t \\
&- \iiint\limits_{\Sigma_R} \left(\alpha_8 \frac{\partial c_{si}}{\partial \nu} + \alpha_{14} \left(\frac{\partial \hat{j}}{\partial u}^T v + \frac{\partial \hat{j}}{\partial \mu}^T \lambda + \hat{j}_c + \alpha_3 \frac{\partial \left(\varphi_s - \varphi_{\ell} \right)}{\partial t} \right) \right) p_8 \, r^2 \mathrm{d}s(r)\mathrm{d}x\mathrm{d}t,
\end{aligned}
$$

where ν denotes the exterior normal to its respective boundary.
In the second step, we partially integrate each term in (A.21) containing derivatives. Applying Green's Identity twice w.r.t. space

$$
\begin{aligned}
\int_{\Omega} \triangle f \, \phi \,\mathrm{d}x &= \int_{\Sigma} \partial_{\nu} f \, \phi \,\mathrm{d}s(x) - \int_{\Omega} \nabla f \, \nabla \phi \,\mathrm{d}x \\
&= \int_{\Sigma} \partial_{\nu} f \, \phi \,\mathrm{d}s(x) - \int_{\Sigma} f \, \partial_{\nu} \phi \,\mathrm{d}s(x) + \int_{\Omega} f \, \triangle \phi \,\mathrm{d}x
\end{aligned}
\tag{A.22}
$$

or perform partial integration once w.r.t. time, respectively,

$$
\int_0^T \partial_t f \, \phi \,\mathrm{d}t = \left(f \, \phi \right)\left(T\right) - \left(f \, \phi \right)\left(0\right) - \int_0^T f \, \partial_t \phi \,\mathrm{d}t. \tag{A.23}
$$

Thus, (A.21) is equivalent to the following:

$$
\begin{aligned}
\mathcal{L} = J\left(v, \lambda\right) &- \iint\limits_{\Sigma_{ad}} - \left(\alpha_1 \frac{\partial \varphi_{\ell}}{\partial \nu} + \alpha_2 \frac{\partial c_{\ell}}{\partial \nu} \right) p_1 + \left(\alpha_1 \varphi_{\ell} + \alpha_2 c_{\ell} \right) \frac{\partial p_1}{\partial \nu} \,\mathrm{d}s(x)\mathrm{d}t \\
&- \iint\limits_{Q_1} - \left(\frac{\partial}{\partial x} \left(\alpha_1 \frac{\partial p_1}{\partial x} \right) \varphi_{\ell} + \frac{\partial}{\partial x} \alpha_2 \frac{\partial p_1}{\partial x} c_{\ell} \right) \mathrm{d}x\mathrm{d}t \\
&- \int_{\Omega'} - \alpha_3 \left(\left(\varphi_s - \varphi_{\ell} \right)\left(T\right) p_1(T) - \left(\varphi_s - \varphi_{\ell} \right)\left(0\right) p_1(0) \right) \mathrm{d}x - \iint\limits_{Q_1'} \alpha_3 \left(\varphi_s - \varphi_{\ell} \right) \frac{\partial p_1}{\partial t} \mathrm{d}x\mathrm{d}t \\
&- \iint\limits_{Q_1'} \left(- \frac{\partial \hat{j}}{\partial u}^T v - \frac{\partial \hat{j}}{\partial \mu}^T \lambda - \hat{j}_c \right) p_1 \,\mathrm{d}x\mathrm{d}t - \iint\limits_{\Sigma_{ad}} \left(\alpha_1 \frac{\partial \varphi_{\ell}}{\partial \nu} + \alpha_2 \frac{\partial c_{\ell}}{\partial \nu} \right) p_2 \,\mathrm{d}s(x)\mathrm{d}t \\
&- \iint\limits_{\Sigma_{ad} \cup \Sigma_{bc}} - \alpha_4 \frac{\partial \varphi_s}{\partial \nu} p_3 + \alpha_4 \varphi_s \frac{\partial p_3}{\partial \nu} \,\mathrm{d}s(x)\mathrm{d}t - \iint\limits_{Q_1'} - \frac{\partial}{\partial x} \left(\alpha_4 \frac{\partial p_3}{\partial x} \right) \varphi_s \,\mathrm{d}x\mathrm{d}t \\
&- \int_{\Omega'} \alpha_3 \left(\left(\varphi_s - \varphi_{\ell} \right)\left(T\right) p_3(T) - \left(\varphi_s - \varphi_{\ell} \right)\left(0\right) p_3(0) \right) \mathrm{d}x - \iint\limits_{Q_1'} - \alpha_3 \left(\varphi_s - \varphi_{\ell} \right) \frac{\partial p_3}{\partial t} \,\mathrm{d}x\mathrm{d}t
\end{aligned}
\tag{A.24}
$$

$$
\begin{aligned}
&- \iint\limits_{Q_1'} \left(\frac{\partial \hat{j}}{\partial u}^T v + \frac{\partial \hat{j}}{\partial \mu}^T \lambda + \hat{j}_c \right) p_3 \,\mathrm{d}x\mathrm{d}t - \iint\limits_{\Sigma_{ad}} \left(\alpha_4 \frac{\partial \varphi_s}{\partial \nu} - i \right) p_4 \,\mathrm{d}s(x)\mathrm{d}t \\
&- \iint\limits_{\Sigma_{bc}} \alpha_4 \frac{\partial \varphi_s}{\partial \nu} \, p_4 \,\mathrm{d}s(x)\mathrm{d}t - \int_\Omega \varepsilon_{\ell i} \left(c_\ell(T)\, p_5(T) - c_\ell(0)\, p_5(0) \right) \mathrm{d}x - \iint\limits_{Q_1} -\varepsilon_{\ell i}\, c_\ell \frac{\partial p_5}{\partial t} \,\mathrm{d}x\mathrm{d}t \\
&- \iint\limits_{\Sigma_{ad}} -\left(\alpha_5 \frac{\partial c_\ell}{\partial \nu} + \alpha_6 \frac{\partial \varphi_\ell}{\partial \nu} \right) p_5 + \left(\alpha_5 c_\ell + \alpha_6 \varphi_\ell \right) \frac{\partial p_5}{\partial \nu} \,\mathrm{d}s(x)\mathrm{d}t \\
&- \iint\limits_{Q_1} -\left(\frac{\partial}{\partial x} \left(\alpha_5 \frac{\partial p_5}{\partial x} \right) c_\ell + \frac{\partial}{\partial x} \left(\alpha_6 \frac{\partial p_5}{\partial x} \right) \varphi_\ell \right) \mathrm{d}x\mathrm{d}t \\
&- \int_{\Omega'} -\alpha_3\alpha_7 \left((\varphi_s - \varphi_\ell)(T)\, p_5(T) - (\varphi_s - \varphi_\ell)(0)\, p_5(0) \right) \mathrm{d}x \\
&- \iint\limits_{Q_1'} \alpha_3\alpha_7 \left(\varphi_s - \varphi_\ell \right) \frac{\partial p_5}{\partial t} \,\mathrm{d}x\mathrm{d}t - \iint\limits_{Q_1'} -\alpha_7 \left(\frac{\partial \hat{j}}{\partial u}^T v + \frac{\partial \hat{j}}{\partial \mu}^T \lambda + \hat{j}_c \right) p_5 \,\mathrm{d}x\mathrm{d}t \\
&- \int_\Omega \varepsilon_{\ell i} \left(c_\ell(0) - c_{\ell,0} \right) p_5 \,\mathrm{d}x - \iint\limits_{\Sigma_{ad}} \left(\alpha_5 \frac{\partial c_\ell}{\partial \nu} + \alpha_6 \frac{\partial \varphi_\ell}{\partial \nu} \right) p_6 \,\mathrm{d}s(x)\mathrm{d}t \\
&- \iint\limits_{\Lambda} \left(c_{si}(T)\, p_7(T) - c_{si}(0)\, p_7(0) \right) r^2 \mathrm{d}r\mathrm{d}x - \iiint\limits_{Q} -c_{si} \frac{\partial p_7}{\partial t} r^2 \mathrm{d}r\mathrm{d}x\mathrm{d}t \\
&- \iiint\limits_{\Sigma_{R,0} \cup \Sigma_R} \alpha_8 \left(-\frac{\partial c_{si}}{\partial \nu} p_7 + c_{si} \frac{\partial p_7}{\partial \nu} \right) r^2 \mathrm{d}s(r)\mathrm{d}x\mathrm{d}t - \iiint\limits_{Q} -\frac{1}{r^2} \frac{\partial}{\partial r} \left(r^2 \alpha_8 \frac{\partial}{\partial r} p_7 \right) c_{si} r^2 \mathrm{d}r\mathrm{d}x\mathrm{d}t \\
&- \iint\limits_{\Lambda} \left(c_{si}(0) - c_{si,0} \right) p_7\, r^2 \mathrm{d}r\mathrm{d}x - \iiint\limits_{\Sigma_{R,0}} \alpha_8 \frac{\partial c_{si}}{\partial \nu} \, p_8\, r^2 \mathrm{d}s(r)\mathrm{d}x\mathrm{d}t \\
&- \iiint\limits_{\Sigma_R} \left(\alpha_8 \frac{\partial c_{si}}{\partial \nu} + \alpha_{14} \left(\frac{\partial \hat{j}}{\partial u}^T v + \frac{\partial \hat{j}}{\partial \mu}^T \lambda + \hat{j}_c \right) \right) p_8\, r^2 \mathrm{d}s(r)\mathrm{d}x\mathrm{d}t \\
&- \iint\limits_{\Gamma_{R,i}} \alpha_3\alpha_{14} \left((\varphi_s - \varphi_\ell)(T)\, p_8(T) - (\varphi_s - \varphi_\ell)(0)\, p_8(0) \right) r^2 \mathrm{d}s(r)\mathrm{d}x \\
&- \iiint\limits_{\Sigma_R} -\alpha_3\alpha_{14} \left(\varphi_s - \varphi_\ell \right) \frac{\partial p_8}{\partial t} \, r^2 \mathrm{d}s(r)\mathrm{d}x\mathrm{d}t
\end{aligned}
$$

The Lagrange method prescribes the variational inequality, i.e.

$$
D_v \mathcal{L} \left(\bar{v}, \bar{\lambda}, p \right) (v - \bar{v}) \geq 0 \quad \forall v \in V, \text{ such that } v(0) = v_0. \tag{A.25}
$$

Here $\bar{v}$ and $\bar{\lambda}$ denote the optimal state and the optimal control, respectively. Using the initial condition $v(t=0) = v_0$ and defining $\tilde{v} := (v - \bar{v})$, from (A.25) we obtain

$$
D_v \mathcal{L} \left(\bar{v}, \bar{\lambda}, p \right) \tilde{v} \geq 0 \quad \forall \tilde{v} \in V, \text{ such that } \tilde{v}(0) = 0, \tag{A.26}
$$

Remark: Note that starting from (A.26) for the rest of this section, by v we refer to the substituted states $\tilde{v}$!

Because (A.26) has to hold for either v and $-v$, it constrains the problem such that the necessary first order optimality condition yields the weak formulation of the adjoint system

$$D_v\mathcal{L}\left(\bar{v},\bar{\lambda},p\right)\, v = 0, \quad \forall v \in V, \text{ such that } v\left(0\right) = 0. \tag{A.27}$$

In addition, from the box constraints in (A.20) follows the second variational inequality:

$$D_\lambda\mathcal{L}\left(\bar{v},\bar{\lambda},p\right)\, \left(\lambda - \bar{\lambda}\right) \geq 0, \quad \forall \lambda \in \mathcal{L}_{ad}. \tag{A.28}$$

Evaluating the variational inequality in (A.25) for the *Fréchet derivative* $D_\lambda\mathcal{L}$ yields

$$\begin{aligned} D_\lambda\mathcal{L}\left(\bar{v},\bar{\lambda},p\right)\left(\lambda - \bar{\lambda}\right) = \sum_{i=1}^{l} \chi_i \left(\bar{\lambda}_i - \hat{\mu}_i\right)\, \left(\lambda_i - \bar{\lambda}_i\right) - \iint\limits_{Q_1'} -\frac{\partial\hat{j}}{\partial\mu}^T \left(\lambda - \bar{\lambda}\right) p_1 \mathrm{d}x\mathrm{d}t \\ - \iint\limits_{Q_1'} \frac{\partial\hat{j}}{\partial\mu}^T \left(\lambda - \bar{\lambda}\right)\, p_3\, \mathrm{d}x\mathrm{d}t - \iint\limits_{Q_1'} -\alpha_7 \frac{\partial\hat{j}}{\partial\mu}^T \left(\lambda - \bar{\lambda}\right)\, p_5\, \mathrm{d}x\mathrm{d}t \\ - \iiint\limits_{\Sigma_R} \alpha_{14} \frac{\partial\hat{j}}{\partial\mu}^T \left(\lambda - \bar{\lambda}\right)\, p_8\, r^2 \mathrm{d}s(r)\mathrm{d}x\mathrm{d}t \end{aligned} \tag{A.29}$$

Applying the *Fréchet derivative* to (A.24) w.r.t. each respective unknown, using $v\left(0\right) = 0$ from (A.27) and the rule that *the derivative of a linear continous operator is the operator itself*, we arrive at (A.30).

$$D_{\varphi_\ell}\mathcal{L}\left(\bar{v},\bar{\lambda},p\right)\, \varphi_\ell = - \iint\limits_{\Sigma_{ad}} -\alpha_1 \frac{\partial\varphi_\ell}{\partial\nu}\, p_1 + \alpha_1\varphi_\ell \frac{\partial p_1}{\partial\nu}\, \mathrm{d}s(x)\mathrm{d}t \tag{A.30a}$$

$$- \iint\limits_{Q_1} -\frac{\partial}{\partial x}\alpha_1 \frac{\partial p_1}{\partial x}\varphi_\ell\, \mathrm{d}x\mathrm{d}t - \int_{\Omega'} -\alpha_3\left(-\varphi_\ell\right)\left(T\right) p_1(T)\, \mathrm{d}x - \iint\limits_{Q_1'} \alpha_3\left(-\varphi_\ell\right)\, \frac{\partial p_1}{\partial t}\, \mathrm{d}x\mathrm{d}t$$

$$- \iint\limits_{Q_1'} -\frac{\partial\hat{j}}{\partial\varphi_\ell}\, \varphi_\ell\, p_1\, \mathrm{d}x\mathrm{d}t - \iint\limits_{\Sigma_{ad}} \alpha_1 \frac{\partial\varphi_\ell}{\partial\nu}\, p_2\, \mathrm{d}s(x)\mathrm{d}t - \int_{\Omega'} \alpha_3\left(-\varphi_\ell\right)\left(T\right) p_3(T)\, \mathrm{d}x$$

$$- \iint\limits_{Q_1'} -\alpha_3\left(-\varphi_\ell\right)\, \frac{\partial p_3}{\partial t}\, \mathrm{d}x\mathrm{d}t - \iint\limits_{Q_1'} \frac{\partial\hat{j}}{\partial\varphi_\ell}\, \varphi_\ell\, p_3\, \mathrm{d}x\mathrm{d}t$$

$$- \iint\limits_{\Sigma_{ad}} -\alpha_6 \frac{\partial\varphi_\ell}{\partial\nu}\, p_5 + \alpha_6\varphi_\ell \frac{\partial p_5}{\partial\nu}\, \mathrm{d}s(x)\mathrm{d}t - \iint\limits_{Q_1} -\frac{\partial}{\partial x}\alpha_6 \frac{\partial p_5}{\partial x}\varphi_\ell\, \mathrm{d}x\mathrm{d}t$$

$$- \int_{\Omega'} -\alpha_3\alpha_7\left(-\varphi_\ell\right)\left(T\right) p_5(T)\, \mathrm{d}x - \iint\limits_{Q_1'} \alpha_3\alpha_7\left(-\varphi_\ell\right)\, \frac{\partial p_5}{\partial t}\, \mathrm{d}x\mathrm{d}t$$

$$- \iint\limits_{Q_1'} -\alpha_7 \frac{\partial\hat{j}}{\partial\varphi_\ell}\, \varphi_\ell\, p_5\, \mathrm{d}x\mathrm{d}t - \iint\limits_{\Sigma_{ad}} \alpha_6 \frac{\partial\varphi_\ell}{\partial\nu}\, p_6\, \mathrm{d}s(x)\mathrm{d}t - \iiint\limits_{\Sigma_R} \alpha_{14} \frac{\partial\hat{j}}{\partial\varphi_\ell}\, \varphi_\ell\, p_8\, r^2 \mathrm{d}s(r)\mathrm{d}x\mathrm{d}t$$

$$- \iint\limits_{\Gamma_{R,i}} \alpha_3\alpha_{14}\left(-\varphi_\ell\right)\left(T\right) p_8(T)\, r^2 \mathrm{d}s(r)\mathrm{d}x - \iiint\limits_{\Sigma_R} -\alpha_3\alpha_{14}\left(-\varphi_\ell\right)\, \frac{\partial p_8}{\partial t}\, r^2 \mathrm{d}s(r)\mathrm{d}x\mathrm{d}t,$$

$$D_{\varphi_s}\mathcal{L}\left(\bar{v},\bar{\lambda},p\right)\,\varphi_s = \iint\limits_{\Sigma_d}(\bar{\varphi}_s-\hat{\varphi}_s)\,\varphi_s\,\mathrm{d}s\mathrm{d}t - \int_{\Omega'}-\alpha_3\varphi_s(T)\,p_1(T)\,\mathrm{d}x \tag{A.30b}$$
$$- \iint\limits_{Q_1'}\alpha_3\varphi_s\,\frac{\partial p_1}{\partial t}\,\mathrm{d}x\mathrm{d}t - \iint\limits_{Q_1'}-\frac{\partial\hat{j}}{\partial\varphi_s}\,\varphi_s\,p_1\,\mathrm{d}x\mathrm{d}t - \iint\limits_{\Sigma_{ad}\cup\Sigma_{bc}}-\alpha_4\frac{\partial\varphi_s}{\partial\nu}\,p_3+\alpha_4\varphi_s\,\frac{\partial p_3}{\partial\nu}\,\mathrm{d}s(x)\mathrm{d}t$$
$$- \iint\limits_{Q_1'}-\frac{\partial}{\partial x}\alpha_4\frac{\partial p_3}{\partial x}\varphi_s\,\mathrm{d}x\mathrm{d}t - \int_{\Omega'}\alpha_3\varphi_s(T)\,p_3(T)\,\mathrm{d}x - \iint\limits_{Q_1'}-\alpha_3\varphi_s\,\frac{\partial p_3}{\partial t}\,\mathrm{d}x\mathrm{d}t$$
$$- \iint\limits_{Q_1'}\frac{\partial\hat{j}}{\partial\varphi_s}\,\varphi_s\,p_3\,\mathrm{d}x\mathrm{d}t - \iint\limits_{\Sigma_{ad}}\alpha_4\frac{\partial\varphi_s}{\partial\nu}\,p_4\,\mathrm{d}s(x)\mathrm{d}t - \iint\limits_{\Sigma_{bc}}\alpha_4\frac{\partial\varphi_s}{\partial\nu}\,p_4\,\mathrm{d}s(x)\mathrm{d}t$$
$$- \int_{\Omega'}-\alpha_3\alpha_7\varphi_s(T)\,p_5(T)\,\mathrm{d}x - \iint\limits_{Q_1'}\alpha_3\alpha_7\varphi_s\,\frac{\partial p_5}{\partial t}\,\mathrm{d}x\mathrm{d}t - \iint\limits_{Q_1'}-\alpha_7\,\frac{\partial\hat{j}}{\partial\varphi_s}\,\varphi_s\,p_5\,\mathrm{d}x\mathrm{d}t$$
$$- \iiint\limits_{\Sigma_R}\alpha_{14}\,\frac{\partial\hat{j}}{\partial\varphi_s}\,\varphi_s\,p_8\,r^2\mathrm{d}s(r)\mathrm{d}x\mathrm{d}t - \iint\limits_{\Gamma_{R,i}}\alpha_3\alpha_{14}\varphi_s(T)\,p_8(T)\,r^2\mathrm{d}s(r)\mathrm{d}x$$
$$- \iiint\limits_{\Sigma_R}-\alpha_3\alpha_{14}\varphi_s\,\frac{\partial p_8}{\partial t}\,r^2\mathrm{d}s(r)\mathrm{d}x\mathrm{d}t,$$

$$D_{c_\ell}\mathcal{L}\left(\bar{v},\bar{\lambda},p\right)c_\ell = -\iint\limits_{\Sigma_{ad}}-\alpha_2\frac{\partial c_\ell}{\partial\nu}p_1+\alpha_2c_\ell\frac{\partial p_1}{\partial\nu}\mathrm{d}s(x)\mathrm{d}t - \iint\limits_{Q_1}-\frac{\partial}{\partial x}\alpha_2\frac{\partial p_1}{\partial x}c_\ell\mathrm{d}x\mathrm{d}t \tag{A.30c}$$
$$- \iint\limits_{Q_1'}-\frac{\partial\hat{j}}{\partial c_\ell}\,c_\ell\,p_1\,\mathrm{d}x\mathrm{d}t - \iint\limits_{\Sigma_{ad}}\alpha_2\frac{\partial c_\ell}{\partial\nu}\,p_2\,\mathrm{d}s(x)\mathrm{d}t - \iint\limits_{Q_1'}\frac{\partial\hat{j}}{\partial c_\ell}\,c_\ell\,p_3\,\mathrm{d}x\mathrm{d}t$$
$$- \int_{\Omega}\varepsilon_{\ell i}c_\ell(T)\,p_5(T)\,\mathrm{d}x - \iint\limits_{Q_1}-\varepsilon_{\ell i}\,c_\ell\,\frac{\partial p_5}{\partial t}\,\mathrm{d}x\mathrm{d}t - \iint\limits_{\Sigma_{ad}}-\alpha_5\frac{\partial c_\ell}{\partial\nu}\,p_5+\alpha_5c_\ell\,\frac{\partial p_5}{\partial\nu}\,\mathrm{d}s(x)\mathrm{d}t$$
$$- \iint\limits_{Q_1}-\frac{\partial}{\partial x}\alpha_5\frac{\partial p_5}{\partial x}c_\ell\,\mathrm{d}x\mathrm{d}t - \iint\limits_{Q_1}-\alpha_7\,\frac{\partial\hat{j}}{\partial c_\ell}\,c_\ell\,p_5\,\mathrm{d}x\mathrm{d}t - \iint\limits_{\Sigma_{ad}}\alpha_5\,\frac{\partial c_\ell}{\partial\nu}\,p_6\,\mathrm{d}s(x)\mathrm{d}t$$
$$- \iiint\limits_{\Sigma_R}\alpha_{14}\,\frac{\partial\hat{j}}{\partial c_\ell}\,c_\ell\,p_8\,r^2\mathrm{d}s(r)\mathrm{d}x\mathrm{d}t,$$

$$D_{c_{si}}\mathcal{L}\left(\bar{v},\bar{\lambda},p\right)\,c_{si} = -\iint\limits_{Q_1'}-\frac{\partial\hat{j}}{\partial c_{si}}\,c_{si}\,p_1\,\mathrm{d}x\mathrm{d}t - \iint\limits_{Q_1'}\frac{\partial\hat{j}}{\partial c_{si}}\,c_{si}\,p_3\,\mathrm{d}x\mathrm{d}t \tag{A.30d}$$
$$- \iint\limits_{Q_1'}-\alpha_7\,\frac{\partial\hat{j}}{\partial c_{si}}\,c_{si}\,p_5\,\mathrm{d}x\mathrm{d}t - \iint\limits_{\Lambda}c_{si}(T)\,p_7(T)\,r^2\mathrm{d}r\mathrm{d}x - \iiint\limits_{Q}-c_{si}\,\frac{\partial p_7}{\partial t}\,r^2\mathrm{d}r\mathrm{d}x\mathrm{d}t$$
$$- \iiint\limits_{\Sigma_{R,0}\cup\Sigma_R}\alpha_8\left(-\frac{\partial c_{si}}{\partial\nu}\,p_7+c_{si}\,\frac{\partial p_7}{\partial\nu}\right)\,r^2\mathrm{d}s(r)\mathrm{d}x\mathrm{d}t - \iiint\limits_{Q}-\frac{1}{r^2}\frac{\partial}{\partial r}r^2\alpha_8\frac{\partial}{\partial r}p_7\,c_{si}\,r^2\mathrm{d}r\mathrm{d}x\mathrm{d}t$$

$$-\iiint_{\Sigma_{R,0}} \alpha_8 \frac{\partial c_{si}}{\partial \nu} p_8 r^2 \mathrm{d}s(r)\mathrm{d}x\mathrm{d}t - \iiint_{\Sigma_R} \left(\alpha_8 \frac{\partial c_{si}}{\partial \nu} + \alpha_{14} \frac{\partial \hat{j}}{\partial c_{si}} c_{si}\right) p_8 r^2 \mathrm{d}s(r)\mathrm{d}x\mathrm{d}t.$$

Now we consider the special case when $v \in X_1 := C_0^\infty(Q_1) \times C_0^\infty(Q_1') \times C_0^\infty(Q_1) \times C_0^\infty(Q_a) \times C_0^\infty(Q_c)$. Under this assumption the parts containing $v(T)$, v and $\partial_\nu v$ vanish on $\Omega, \Lambda, \Gamma_{R,i}$ and $\Sigma := \Sigma_{a,d} \cup \Sigma_{b,c} \cup \Sigma_R \cup \Sigma_{R,0}$, respectively.
By applying (A.27) in (A.30) under assumption $v \in X_1$ we obtain

$$\begin{aligned}
&-\iint_{Q_1} -\frac{\partial}{\partial x}\left(\alpha_1 \frac{\partial p_1}{\partial x}\right)\varphi_\ell \,\mathrm{d}x\mathrm{d}t - \iint_{Q_1'} \alpha_3(-\varphi_\ell)\,\frac{\partial p_1}{\partial t}\,\mathrm{d}x\mathrm{d}t - \iint_{Q_1'} -\frac{\partial \hat{j}}{\partial \varphi_\ell}\,\varphi_\ell\, p_1\,\mathrm{d}x\mathrm{d}t \qquad \text{(A.31a)}\\
&\quad - \iint_{Q_1'} -\alpha_3(-\varphi_\ell)\,\frac{\partial p_3}{\partial t}\,\mathrm{d}x\mathrm{d}t - \iint_{Q_1'} \frac{\partial \hat{j}}{\partial \varphi_\ell}\,\varphi_\ell\, p_3\,\mathrm{d}x\mathrm{d}t - \iint_{Q_1} -\frac{\partial}{\partial x}\left(\alpha_6 \frac{\partial p_5}{\partial x}\right)\varphi_\ell\,\mathrm{d}x\mathrm{d}t\\
&\quad - \iint_{Q_1'} \alpha_3\alpha_7(-\varphi_\ell)\,\frac{\partial p_5}{\partial t}\,\mathrm{d}x\mathrm{d}t - \iint_{Q_1'} -\alpha_7 \frac{\partial \hat{j}}{\partial \varphi_\ell}\,\varphi_\ell\, p_5\,\mathrm{d}x\mathrm{d}t\\
&\quad - \iiint_{\Sigma_R} \alpha_{14}\left(\frac{\partial \hat{j}}{\partial \varphi_\ell}\,\varphi_\ell\, p_8 + \alpha_3 \varphi_\ell \frac{\partial p_8}{\partial t}\right) r^2 \mathrm{d}s(r)\mathrm{d}x\mathrm{d}t = 0,
\end{aligned}$$

$$\begin{aligned}
&-\iint_{Q_1'} \alpha_3\varphi_s \frac{\partial p_1}{\partial t}\,\mathrm{d}x\mathrm{d}t - \iint_{Q_1'} -\frac{\partial \hat{j}}{\partial \varphi_s}\,\varphi_s\, p_1\,\mathrm{d}x\mathrm{d}t - \iint_{Q_1'} -\frac{\partial}{\partial x}\left(\alpha_4 \frac{\partial p_3}{\partial x}\right)\varphi_s\,\mathrm{d}x\mathrm{d}t \qquad \text{(A.31b)}\\
&\quad - \iint_{Q_1'} -\alpha_3\varphi_s \frac{\partial p_3}{\partial t}\,\mathrm{d}x\mathrm{d}t - \iint_{Q_1'} \frac{\partial \hat{j}}{\partial \varphi_s}\,\varphi_s\, p_3\,\mathrm{d}x\mathrm{d}t - \iint_{Q_1'} \alpha_3\alpha_7\varphi_s \frac{\partial p_5}{\partial t}\,\mathrm{d}x\mathrm{d}t\\
&\quad - \iint_{Q_1'} -\alpha_7 \frac{\partial \hat{j}}{\partial \varphi_s}\,\varphi_s\, p_5\,\mathrm{d}x\mathrm{d}t - \iiint_{\Sigma_R} \alpha_{14}\left(\frac{\partial \hat{j}}{\partial \varphi_s}\,\varphi_s\, p_8 - \alpha_3\varphi_s \frac{\partial p_8}{\partial t}\right) r^2 \mathrm{d}s(r)\mathrm{d}x\mathrm{d}t = 0,
\end{aligned}$$

$$\begin{aligned}
&-\iint_{Q_1} -\frac{\partial}{\partial x}\left(\alpha_2 \frac{\partial p_1}{\partial x}\right) c_\ell \,\mathrm{d}x\mathrm{d}t - \iint_{Q_1'} -\frac{\partial \hat{j}}{\partial c_\ell}\, c_\ell\, p_1\,\mathrm{d}x\mathrm{d}t - \iint_{Q_1'} \frac{\partial \hat{j}}{\partial c_\ell}\, c_\ell\, p_3\,\mathrm{d}x\mathrm{d}t \qquad \text{(A.31c)}\\
&\quad - \iint_{Q_1} -\varepsilon_{\ell i}\, c_\ell \frac{\partial p_5}{\partial t}\,\mathrm{d}x\mathrm{d}t - \iint_{Q_1} -\frac{\partial}{\partial x}\left(\alpha_5 \frac{\partial p_5}{\partial x}\right) c_\ell\,\mathrm{d}x\mathrm{d}t - \iint_{Q_1'} -\alpha_7 \frac{\partial \hat{j}}{\partial c_\ell}\, c_\ell\, p_5\,\mathrm{d}x\mathrm{d}t\\
&\quad - \iiint_{\Sigma_R} \alpha_{14} \frac{\partial \hat{j}}{\partial c_\ell}\, c_\ell\, p_8\, r^2 \mathrm{d}s(r)\mathrm{d}x\mathrm{d}t = 0,
\end{aligned}$$

$$-\iiint_{Q} -c_{si} \frac{\partial p_7}{\partial t}\, r^2 \mathrm{d}r\mathrm{d}x\mathrm{d}t - \iiint_{Q} -\frac{1}{r^2}\frac{\partial}{\partial r}\left(r^2 \alpha_8 \frac{\partial}{\partial r} p_7\right) c_{si}\, r^2 \mathrm{d}r\mathrm{d}x\mathrm{d}t = 0. \qquad \text{(A.31d)}$$

Since compactly supported continous functions are dense in L^2, we have that X_1 is dense in $L^2(Q_1) \times L^2(Q_1') \times L^2(Q_1) \times L^2(Q_a) \times L^2(Q_c)$. Further, we use

$\iiint_{\Sigma_R} v\,(x,r,t)\; r^2\,\mathrm{d}s(r)\mathrm{d}x\mathrm{d}t \equiv \iint_{Q_1'} v\,(x,R,t)\; R^2\,\mathrm{d}x\mathrm{d}t$ and we obtain the equations of the system adjoint to (2.31):

$$-\alpha_3\left(\frac{\partial p_1}{\partial t}-\frac{\partial p_3}{\partial t}+\alpha_7\frac{\partial p_5}{\partial t}-\alpha_{14}\frac{\partial p_8}{\partial t}\right) \tag{A.32a}$$
$$-\frac{\partial}{\partial x}\left(\alpha_1\frac{\partial p_1}{\partial x}+\alpha_6\frac{\partial p_5}{\partial x}\right)-\frac{\partial \hat{j}}{\partial \varphi_\ell}\left(p_1-p_3+\alpha_7 p_5-\alpha_{14}p_8\right)=0$$

$$\alpha_3\left(\frac{\partial p_1}{\partial t}-\frac{\partial p_3}{\partial t}+\alpha_7\frac{\partial p_5}{\partial t}-\alpha_{14}\frac{\partial p_8}{\partial t}\right) \tag{A.32b}$$
$$-\frac{\partial}{\partial x}\alpha_4\frac{\partial p_3}{\partial x}-\frac{\partial \hat{j}}{\partial \varphi_s}\left(p_1-p_3+\alpha_7 p_5-\alpha_{14}p_8\right)=0$$

$$-\varepsilon_{\ell i}\frac{\partial p_5}{\partial t}-\frac{\partial}{\partial x}\left(\alpha_2\frac{\partial p_1}{\partial x}+\alpha_5\frac{\partial p_5}{\partial x}\right)-\frac{\partial \hat{j}}{\partial c_\ell}\left(p_1-p_3+\alpha_7 p_5-\alpha_{14}p_8\right)=0 \tag{A.32c}$$

$$-\frac{\partial p_7}{\partial t}-\frac{1}{r^2}\frac{\partial}{\partial r}r^2\alpha_8\frac{\partial}{\partial r}p_7=0 \tag{A.32d}$$

Now we reduce the requirement $\partial_\nu v = 0$ on Σ and let it vary freely. Keeping all other requirements, we obtain the additional conditions

$$-\iint_{\Sigma_{ad}}\frac{\partial\varphi_\ell}{\partial\nu}\left(\alpha_1\left(-p_1+p_2\right)+\alpha_6\left(-p_5+p_6\right)\right)\,\mathrm{d}s(x)\mathrm{d}t=0 \tag{A.33a}$$

$$-\iint_{\Sigma_{ad}\cup\Sigma_{bc}}\frac{\partial\varphi_s}{\partial\nu}\alpha_4\left(-p_3+p_4\right)\,\mathrm{d}s(x)\mathrm{d}t=0 \tag{A.33b}$$

$$-\iint_{\Sigma_{ad}}\frac{\partial c_\ell}{\partial\nu}\left(\alpha_2\left(-p_1+p_2\right)+\alpha_5\left(-p_5+p_6\right)\right)\,\mathrm{d}s(x)\mathrm{d}t=0 \tag{A.33c}$$

$$-\iiint_{\Sigma_{R,0}\cup\Sigma_R}\alpha_8\frac{\partial c_{si}}{\partial\nu}\left(-p_7+p_8\right)\,r^2\mathrm{d}s(r)\mathrm{d}x\mathrm{d}t=0 \tag{A.33d}$$

Our requirements for arbitrary $\partial_\nu v$ indicate that

$$p_1=p_2,\quad \text{on } \Sigma_{ad} \tag{A.34a}$$
$$p_3=p_4,\quad \text{on } \Sigma_{ad}\cup\Sigma_{bc} \tag{A.34b}$$
$$p_5=p_6,\quad \text{on } \Sigma_{ad} \tag{A.34c}$$
$$p_7=p_8,\quad \text{on } \Sigma_{R,0}\cup\Sigma_R \tag{A.34d}$$

if and only if we assume $\alpha_i \neq 0$, $i \in \{1,2,4,5,6,8\}$.

In the next step we further relax the conditions and choose $v(T)$ arbitrary instead of $v(T)=0$. We still require that $v(0)=0$ and v to vanish on Σ. Since we have already

dealt with the parts on Q_1 and Q, this leaves us with the terms containing $v(T)$ on Ω and Λ.

$$-\int_{\Omega'}\alpha_3\varphi_\ell(T)\,p_1(T)\,\mathrm{d}x-\int_{\Omega'}-\alpha_3\varphi_\ell(T)\,p_3(T)\,\mathrm{d}x \\ -\int_{\Omega'}\alpha_3\alpha_7\varphi_\ell(T)\,p_5(T)\,\mathrm{d}x-\iint\limits_{\Gamma_{R,i}}\alpha_3\alpha_{14}\left(-\varphi_\ell(T)\right)\,p_8(T)\,r^2\mathrm{d}s(r)\mathrm{d}x=0 \tag{A.35a}$$

$$-\int_{\Omega'}-\alpha_3\varphi_s(T)\,p_1(T)\,\mathrm{d}x-\int_{\Omega'}\alpha_3\varphi_s(T)\,p_3(T)\,\mathrm{d}x \\ -\int_{\Omega'}-\alpha_3\alpha_7\varphi_s(T)\,p_5(T)\,\mathrm{d}x-\iint\limits_{\Gamma_{R,i}}\alpha_3\alpha_{14}\varphi_s(T)\,p_8(T)\,r^2\mathrm{d}s(r)\mathrm{d}x=0 \tag{A.35b}$$

$$-\int_{\Omega}\varepsilon_{\ell i}c_\ell(T)\,p_5(T)\,\mathrm{d}x=0 \tag{A.35c}$$

$$-\iint\limits_{\Lambda}c_{si}(T)\,p_7(T)\,r^2\mathrm{d}r\mathrm{d}x=0 \tag{A.35d}$$

Again, all possible values $v(T)$ are dense in L^2 and $\iint_{\Gamma_{R,i}}v\left(x,r,T\right)\,r^2\,\mathrm{d}s(r)\mathrm{d}x\equiv\int_{\Omega'}v\left(x,R,T\right)\,R^2\,\mathrm{d}x$. Hence we obtain the *final conditions*

$$\alpha_3\,\left(p_1(T)-p_3(T)+\alpha_7p_5(T)-\alpha_{14}p_8(T)\right)=0,\quad\text{on }\Omega' \tag{A.36a}$$

$$-\alpha_3\,\left(p_1(T)-p_3(T)+\alpha_7p_5(T)-\alpha_{14}p_8(T)\right)=0,\quad\text{on }\Omega' \tag{A.36b}$$

$$\varepsilon_{\ell i}p_5(T)=0,\quad\text{on }\Omega \tag{A.36c}$$

$$p_7(T)=0,\quad\text{on }\Lambda \tag{A.36d}$$

Since (A.36a) and (A.36b) coincide, this leaves us with three simplified final conditions:

$$p_1(T)-p_3(T)=0,\quad\text{on }\Omega' \tag{A.37a}$$

$$p_5(T)=0,\quad\text{on }\Omega \tag{A.37b}$$

$$p_7(T)=0,\quad\text{on }\Lambda. \tag{A.37c}$$

Finally, we abandon the constraint $v|_\Sigma=0$:

$$-\iint\limits_{\Sigma_{ad}}\alpha_1\varphi_\ell\,\frac{\partial p_1}{\partial\nu}+\alpha_6\varphi_\ell\,\frac{\partial p_5}{\partial\nu}\,\mathrm{d}s(x)\mathrm{d}t=0 \tag{A.38a}$$

$$\iint\limits_{\Sigma_d}(\bar\varphi_s-\hat\varphi_s)\,\varphi_s\,\mathrm{d}s(x)\mathrm{d}t-\iint\limits_{\Sigma_{ad}\cup\Sigma_{bc}}\alpha_4\varphi_s\,\frac{\partial p_3}{\partial\nu}\,\mathrm{d}s(x)\mathrm{d}t=0 \tag{A.38b}$$

$$-\iint\limits_{\Sigma_{ad}}\alpha_2c_\ell\,\frac{\partial p_1}{\partial\nu}+\alpha_5c_\ell\,\frac{\partial p_5}{\partial\nu}\,\mathrm{d}s(x)\mathrm{d}t=0 \tag{A.38c}$$

$$-\iint\limits_{Q_1'} -\frac{\partial \hat{j}}{\partial c_{si}}\, c_{si}\, p_1 \,\mathrm{d}x\mathrm{d}t - \iint\limits_{Q_1'} \frac{\partial \hat{j}}{\partial c_{si}}\, c_{si}\, p_3 \,\mathrm{d}x\mathrm{d}t - \iint\limits_{Q_1'} -\alpha_7 \frac{\partial \hat{j}}{\partial c_{si}}\, c_{si}\, p_5 \,\mathrm{d}x\mathrm{d}t \tag{A.38d}$$
$$-\iiint\limits_{\Sigma_{R,0}\cup\Sigma_R} \alpha_8\, c_{si}\, \frac{\partial p_7}{\partial \nu}\, r^2 \mathrm{d}s(r)\mathrm{d}x\mathrm{d}t - \iiint\limits_{\Sigma_R} \alpha_{14}\, \frac{\partial \hat{j}}{\partial c_{si}}\, c_{si}\, p_7\, r^2 \mathrm{d}s(r)\mathrm{d}x\mathrm{d}t = 0$$

To complete the adjoint system, we obtain the boundary conditions

$$\alpha_1 \frac{\partial p_1}{\partial \nu} + \alpha_6 \frac{\partial p_5}{\partial \nu} = 0, \quad \text{on } \Sigma_{ad} \tag{A.39a}$$

$$-\alpha_4 \frac{\partial p_3}{\partial \nu} = \begin{cases} \bar{\varphi}_s - \hat{\varphi}_s & \text{on } \Sigma_d \\ 0 & \text{else} \end{cases} \tag{A.39b}$$

$$\alpha_2 \frac{\partial p_1}{\partial \nu} + \alpha_5 \frac{\partial p_5}{\partial \nu} = 0, \quad \text{on } \Sigma_{ad} \tag{A.39c}$$

$$-\alpha_8 \frac{\partial p_7}{\partial \nu} = \begin{cases} \frac{\partial \hat{j}}{\partial c_{si}} \left(p_1 - p_3 + \alpha_7 p_5 - \alpha_{14} p_7\right) & \text{on } \Sigma_R \\ 0 & \text{on } \Sigma_{R,0} \end{cases} \tag{A.39d}$$

Note that if (A.39a) and (A.39c) form a regular system, analogous to (2.27), they can be split into two parts:

$$\alpha_1 \frac{\partial p_1}{\partial \nu} = \alpha_2 \frac{\partial p_1}{\partial \nu} = 0, \quad \text{on } \Sigma_{ad}, \tag{A.40a}$$

$$\alpha_5 \frac{\partial p_5}{\partial \nu} = \alpha_6 \frac{\partial p_5}{\partial \nu} = 0, \quad \text{on } \Sigma_{ad}, \tag{A.40b}$$

In addition, the variational inequality of (A.29)

$$\sum_{i=1}^{l} \chi_i \left(\bar{\lambda}_i - \hat{\mu}_i\right) \left(\lambda_i - \bar{\lambda}_i\right) \tag{A.41}$$
$$-\iint\limits_{Q_1'} \frac{\partial \hat{j}}{\partial \mu}^T \left(\lambda - \bar{\lambda}\right) \left(-\bar{p}_1 + \bar{p}_3 - \alpha_7\, \bar{p}_5 + \alpha_{14}\, \bar{p}_8\, R^2\right) \mathrm{d}x\mathrm{d}t \geq 0 \qquad \forall \lambda \in \mathcal{L}_{ad}$$

has to be fullfilled.

Glossary

Battery

Several cells electrically connected in series or parallel or both. Usually specified in "n s m p" notation, where m denotes parallel cells and n denotes the number of individual or parallel cells in series. Several cells are usually grouped in modules for better handling and manipulation during manufacturing.

C-Rate

A widely used scaling factor unit representing a discharge or charge current, such that a current may be expressed in multiples or fractions of the rated capacity.

Calendar Life

The life expectancy of a battery cell/module/pack during storage.

Capacity

The total amount of charge that a battery cell is capable of containing (usually expressed in the units ampere-hours A h).

Cell

Also: Battery, Battery Cell, Electrochemical Cell. The smallest possible electrochemical cell. Two (or several) electrodes in arbitrary geometrical as well as topological configuration chemically connected in the same electrolyte.

Cycle

A sequence of a charge and discharge of a battery.

Cycle Life

The life expectancy of a battery cell/module/pack when subjected to cycling.

DOD

Depth of Discharge; Typically a measure of the distance (in energy) from a full charge. Also used to describe the energy added or removed during cycling in some situations. Always given as a percentage.

EOL

End of Life; The end of life of a battery, i.e. a point in time when a battery's capacity or power capability has reached a usage specific criterion, e.g. 70 % of its original capacity.

Internal Resistance

The electric resistance (usually in expressed in mΩ) of a battery cell. More specifically, the sum of the ionic and electronic resistances of the cell components.

Module

Several cells electrically connected in series or parallel or both. Usually specified in "n s m p" notation, where m denotes parallel cells and n denotes the number

of individual or parallel cells in series. Modules are building blocks to form a full pack. Usually, modules are equipped with sensors and monitoring logic on cell level.

OCV

Open Circuit Voltage; The difference in potential between the terminals of a cell when the battery is fully rested at a specific temperature (that is, the battery has been subjected to an open circuit for a substantial period of time).

Pack

or Battery Pack. Several Modules connected in series to form a system along with special monitoring and safety related devices, e.g. a BMS, fuses and others.

SOC

State of Charge; A fraction of the total amount of charge that is available in the battery at a given time. Usually given as a percentage.

SOH

State of Health; A measurement of usable life of a battery cell, usually refers to the current capacity and possibly inner resistance.

Specific Energy

Unit energy per mass $\mathrm{W\,h\,kg^{-1}}$; The amount of energy that is theoretically capable of being contained per unit mass.

Specific Power

Unit Power per mass $\mathrm{W\,kg^{-1}}$; The power capability scaled per unit mass

List of Abbreviations

Li^+	Li-Ion
ACF	autocorrelation function
AM	Adaptive Metropolis
BMS	Battery Management System
CC	Constant Current Charge
CCCV	Constant Current Charge with subsequent Constant Voltage Charge
DFN	Doyle–Fuller–Newman model
DOF	Degrees of Freedom
DR	Delayed Rejection
DRAM	Delayed Rejection Adaptive Metropolis
FEM	Finite Element Method
GHG	greenhouse gas
iACT	integrated autocorrelation time
iid	independent and identically distributed
IS	Impedance Spectroscopy
LSQ	Least Squares
MCMC	Markov Chain Monte Carlo
MOAT	"Morris–one–at–a–time"
MOEA-DD	Multiobjective Evolutionary Algorithm based on Dominance and Decomposition
MOGA	Multiobjective Genetic Optimization Algorithm
MPC	Model Predictive Control
MSE	Mean Square Error
nRSME	normalized Root-Mean-Square Error
NSDE	Non-dominant Sorting Differential Evolution
NSGA-III	Non-dominant Sorting Genetic Algorithm III
OCP	Open Circuit Potential
OCV	Open Circuit Voltage
ODE	Ordinary Differential Equation

PCA	Principal Component Analysis
PDE	Partial Differential Equation
PSO	Particle Swarm Optimization
RMSE	Root-Mean-Square Error
RSS	Residual Sum of Squares
RTP	Reference Test Protocol
SA	Sensitivity Analysis
SC	Single Component
SoC	State of Charge
SoH	State of Health
SOHO	Single Objective Hybrid Optimizer
SPM	Single–Particle model
UQ	Uncertainty Quantification

Nomenclature

A_i	Inner surface
brugg_x	Bruggemann coefficient
C_{dl}	Double–layer capacity
c_x	Li^+–concentration in phase x
$c_{x,0}$	Initial Li^+–concentration
$\hat{D}_x$	Diffusivity
D_x	Effective Diffusivity
$d_i(\boldsymbol{\theta})$	Elementary effect of variable $\boldsymbol{\theta}_i$
e	Random number in $(0, 1)$
F	Faraday's constant
$f(\cdot, \theta)$	Model output
F_i	Distribution of effects of $\boldsymbol{\theta}_i$
$\bar{f}\left(\bar{\boldsymbol{\theta}}\right)$	Model output for target parameters
$\bar{f}\left(\bar{\boldsymbol{\theta}}\right)$	Model output for target parameters
$i(t)$	Cell current density
j^*_{BV}	Butler–Volmer current density
k	Exchange current density and reaction rate
$k_{a:c}$	Combined factor k_a/k_c
$k_{a:c}$	Combined factor k_a/k_c
n	Number of sample
n	Number of sample
$q(.\|\theta_n)$	Parameter proposal distribution
Q_1	Space–time cylinder of Ω
Q'_1	Space–time cylinder of Ω'
Q_2	Space–time cylinder of Λ
r	Radial coordinate in particles
R_0	Proposal deviation of $q(.\|\theta_0)$
R_0	Proposal deviation of $q(.\|\theta_0)$
R_a	Particle radius in anode
R_c	Particle radius in cathode
R_g	Universal gas constant
R_n	Proposal deviation of $q(.\|\theta_n)$ at sample n
R_n	Proposal deviation of $q(.\|\theta_n)$ at sample n
T	Final simulation time
t_i	Time at step i of reference model
t_i	Time at step i of reference model
t_j	Time at step j of model under test
t_j	Time at step j of model under test
t^+_ℓ	Transference number of cations
u	Unknowns of the model
U_{OCV}	Equilibrium potential function
$\mathbf{y}, y_i$	Points of measurements
z	Number of transferred electrons
α	Charge transfer coefficient
$\alpha(\cdot, \hat{\theta})$	Acceptance probability
ε	Measurement error
ε_x	Phase x volume fraction
$\varepsilon_{\ell:s}$	Combined factor $\varepsilon_\ell/\varepsilon_s$
$\varepsilon_{\ell+s}$	Combined factor $\varepsilon_\ell + \varepsilon_s$
ϵ_Σ	Small value to add to R_n
ϵ_Σ	Small value to add to R_n
φ_x	Electric potential in phase x

η	Overpotential in j_{BV}^{*}
$\hat{\kappa}\left(c_{\ell}\right)$	Ionic conductivity function
$\kappa\left(c_{\ell}\right)$	Effective ionic conductivity
Λ_a	Anode domain in particles
Λ_c	Cathode domain in particles
Λ	Combined anode and cathode model domain
μ	Sample mean
μ_{ℓ}	Migration coefficient
Ω_a	Anode model domain
Ω_c	Cathode model domain
Ω_s	Separator model domain
Ω	Entire model domain
Ω'	Combined anode and cathode model domain
$\pi(\boldsymbol{\theta})$	Prior probability
σ	Sample or measurement noise standard deviation
$\hat{\sigma}_s$	Electronic conductivity
σ_s	Effective electronic conductivity
θ	Parameter set of interest
$\boldsymbol{\theta}_0$	Initial parameter values
$\boldsymbol{\theta}_0$	Initial parameter values
$\boldsymbol{\theta}_a$	Lower parameter bounds
$\boldsymbol{\theta}_a$	Lower parameter bounds
τ	Integrated autocorrelation time
τ	Integrated autocorrelation time
$\boldsymbol{\theta}_b$	Upper parameter bounds
$\boldsymbol{\theta}_b$	Upper parameter bounds
$\hat{\theta}$	Proposed parameter
$\tilde{\boldsymbol{\theta}}(\boldsymbol{\theta})$	Transformed parameters
$\tilde{\boldsymbol{\theta}}(\boldsymbol{\theta})$	Transformed parameters
$\bar{\boldsymbol{\theta}}$	Target parameters
$\bar{\boldsymbol{\theta}}$	Target parameters
$\mathcal{P}$	Parameter space
ϑ	Temperature

List of Figures

List of Tables

Bibliography

Bakr, M. H., Bandler, J. W., Biernacki, R. M., Chen, S. H., & Madsen, K. (1998, Dec). A trust region aggressive space mapping algorithm for EM optimization. *IEEE Transactions on Microwave Theory and Techniques*, *46*, 2412–2425.
(cited on page 42.)

Bakr, M. H., Bandler, J. W., Madsen, K., & Søndergaard, J. (2001, Dec). An Introduction to the Space Mapping Technique. *Optimization and Engineering*, *2*(4), 369–384.
(cited on page 41.)

Bandler, J., Biernacki, R., Chen, S. H., Grobelny, P., & Hemmers, R. (1994, Dec). Space mapping technique for electromagnetic optimization. *Microwave Theory and Techniques, IEEE Transactions on*, *42*(12), 2536–2544. doi: 10.1109/22.339794
(cited on page 5.)

Berger, T. (2018). *Alterungsmodellierung von Lithium-Ionen-Zellen mit Gauß-Prozess-Regression* (Master Thesis). Graz University of Technology, Graz, Austria.
(cited on page 57.)

Beskos, A., Papaspiliopoulos, O., & Roberts, G. O. (2006, Dec). Retrospective exact simulation of diffusion sample paths with applications. *Bernoulli*, *12*(6), 1077–1098. doi: 10.3150/bj/1165269151
(cited on page 78.)

Bizeray, A. M., Kim, J., Duncan, S. R., & Howey, D. A. (2019). Identifiability and parameter estimation of the single particle lithium-ion battery model. *IEEE Transactions on Control Systems Technology*, *27*(5), 1862-1877. doi: 10.1109/TCST.2018.2838097
(cited on page 5.)

Boukamp, B. A. (1986). A nonlinear least squares fit procedure for analysis of immittance data of electrochemical systems. *Solid State Ionics*, *20*(1), 31–44.
(cited on page 4.)

Broyden, C. G. (1965, Oct). A class of methods for solving nonlinear simultaneous equations. *Mathematics of Computation*, *19*(92), 577–593.
(cited on page 40.)

Buller, S., Thele, M., Doncker, R. W. D., & Karden, E. (2005). Impedance-based simulation models of supercapacitors and Li-ion batteries for power electronic applications. In *Ieee transactions on industry applications* (Vol. 41, pp. 742–747). doi: 10.1109/TIA.2005.847280
(cited on page 16.)

Canova, M. (2016, Jun). *Introduction to Lithium-ion Batteries, Modeling and SOC Estimation.* Lecture Notes. (Center for Automotive Research, The Ohio State University)
(cited on page 3.)

Chawla, N., Bharti, N., & Singh, S. (2019). Recent Advances in Non-Flammable Electrolytes for Safer Lithium-Ion Batteries. *Batteries*, *5*(1). doi: 10.3390/batteries5010019
(cited on pages 1, 2, and 123.)

Conrad, P. R. (2014). *Accelerating Bayesian inference in computationally expensive computer models using local and global approximations* (PhD Thesis). Massachusetts Institute of Technology.
(cited on page 95.)

Craiu, R. V., Rosenthal, J., & Yang, C. (2009). Learn From Thy Neighbor: Parallel-Chain and Regional Adaptive MCMC. *Journal of the American Statistical Association*, *104*(488), 1454-1466. doi: 10.1198/jasa.2009.tm08393
(cited on page 51.)

Deb, K. (2001). *Multi-objective optimization using evolutionary algorithms* (Vol. 16; K. Deb, Ed.). John Wiley & Sons.
(cited on pages 45 and 69.)

Deb, K., & Agrawal, R. (1995). Simulated Binary Crossover for Continuous Search Space. *Complex Systems*, *9*, 115-148.
(cited on pages 45 and 69.)

Deb, K., & Jain, H. (2014, Aug). An Evolutionary Many-Objective Optimization Algorithm Using Reference-Point-Based Nondominated Sorting Approach, Part I: Solving Problems With Box Constraints. *IEEE Transactions on Evolutionary Computation*, *18*(4), 577-601. doi: 10.1109/TEVC.2013.2281535
(cited on page 45.)

Dolgov, S., Anaya-Izquierdo, K., Fox, C., & Scheichl, R. (2018, Oct). Approximation and sampling of multivariate probability distributions in the tensor train decomposition. *arXiv e-prints*, arXiv:1810.01212.
(cited on page 95.)

Dong, T. K., Kirchev, A., Mattera, F., Kowal, J., & Bultel, Y. (2011). Dynamic Modeling of Li-Ion Batteries Using an Equivalent Electrical Circuit. *Journal of The Electrochemical Society*, *158*(3), A326-A336. doi: 10.1149/1.3543710
(cited on page 16.)

Doyle, M., Fuller, T. F., & Newman, J. (1993). Modeling of Galvanostatic Charge and Discharge of the Lithium/Polymer/Insertion Cell. *Journal of The Electrochemical Society*, *140*(6), 1526-1533. doi: 10.1149/1.2221597
(cited on pages 20 and 91.)

Fischer, H.-M. (2013, Dec). *Voltage classes for electric mobility* (Technology and Standardisation review). Frankfurt am Main, Germany: ZVEI - German Electrical and Electronic Manufacturers' Association, Centre of Excellence Electric Mobility.
(cited on page 2.)

Forman, J. C., Moura, S. J., Stein, J. L., & Fathy, H. K. (2012). Genetic identification and fisher identifiability analysis of the Doyle-Fuller-Newman model from experimental cycling of a LiFePO4 cell. *Journal of Power Sources*, *210*(0), 263 - 275. doi: 10.1016/j.jpowsour.2012.03.009
(cited on pages 5, 69, 74, and 75.)

Gelman, A., Roberts, G. O., Gilks, W. R., et al. (1996). Efficient Metropolis jumping rules. *Bayesian statistics*, *5*(599-608), 42.
(cited on page 50.)

Geyer, C. J. (1992). Practical markov chain monte carlo. *Statistical Science*, *7*(4), 473–483.
(cited on pages 81 and 86.)

Greenleaf, M., Li, H., & Zheng, J. P. (2013, Oct). Modeling of Li_xFePO_4 Cathode Li-Ion Batteries Using Linear Electrical Circuit Model. *IEEE Transactions on Sustainable Energy*, *4*(4), 1065-1070. doi: 10.1109/TSTE.2013.2267752
(cited on page 16.)

Guzzella, L., & Amstutz, A. (2005). The QSS toolbox manual [Computer software manual]. Zürich: Institut für Mess-und Regeltechnik, Eidgenössische Technische Hochschule Zürich.
(cited on pages 15 and 60.)

Guzzella, L., & Sciarretta, A. (2007). *Vehicle propulsion systems* (L. Guzzella & A. Sciarretta, Eds.). Springer, Berlin, Heidelberg.
(cited on page 15.)

Haario, H., Laine, M., Mira, A., & Saksman, E. (2006). DRAM: efficient adaptive MCMC. *Statistics and computing*, *16*(4), 339–354.
(cited on pages 6 and 54.)

Haario, H., Saksman, E., & Tamminen, J. (1999). Adaptive proposal distribution for random walk Metropolis algorithm. *Computational Statistics*, *14*(3), 375–396.
(cited on pages 6 and 54.)

Haario, H., Saksman, E., & Tamminen, J. (2001). An adaptive Metropolis algorithm. *Bernoulli*, 223–242.
(cited on pages 6, 50, and 54.)

Hastings, W. K. (1970, Apr). Monte Carlo sampling methods using Markov chains and their applications. *Biometrika*, *57*(1), 97-109. doi: 10.1093/biomet/57.1.97
(cited on pages 6 and 47.)

Hintermüller, M., & Vicente, L. N. (2005, Apr). Space Mapping for Optimal Control of Partial Differential Equations. *SIAM J. on Optimization*, *15*(4), 1002–1025. doi: 10.1137/S105262340342907X
(cited on page 42.)

Hornung, U. (1996). *Homogenization and porous media* (U. Hornung, Ed.). Springer Science & Business Media.
(cited on page 19.)

Hrvanovic, D. (2018). *Aging and State filtering for Lithium-ion cells* (Master Thesis). Graz University of Technology, Graz, Austria.
(cited on page 57.)

Hu, X., Li, S., & Peng, H. (2012). A comparative study of equivalent circuit models for li-ion batteries. *Journal of Power Sources*, *198*, 359 - 367. doi: https://doi.org/10.1016/j.jpowsour.2011.10.013
(cited on pages 5 and 16.)

Jin, N., Danilov, D. L., Van den Hof, P. M., & Donkers, M. (2018). Parameter estimation of an electrochemistry-based lithium-ion battery model using a two-step procedure and a parameter sensitivity analysis. *International Journal of Energy Research*, *42*(7), 2417-2430. doi: 10.1002/er.4022
(cited on pages 5 and 75.)

Karthikeyan, D. K., Sikha, G., & White, R. E. (2008). Thermodynamic model development for lithium intercalation electrodes. *Journal of Power Sources*, *185*(2), 1398 - 1407. doi: DOI:10.1016/j.jpowsour.2008.07.077
(cited on page 22.)

Kim, G.-H., Smith, K., Lee, K.-J., Santhanagopalan, S., & Pesaran, A. (2011). Multi-Domain Modeling of Lithium-Ion Batteries Encompassing Multi-Physics in Varied Length Scales. *Journal of The Electrochemical Society*, *158*(8), A955-A969. doi: 10.1149/1.3597614
(cited on pages 18 and 19.)

Kumar, P., & Bauer, P. (2010, Sep). Parameter extraction of battery models using multiobjective optimization genetic algorithms. In *Proceedings of 14th international power electronics and motion control conference epe-pemc 2010* (pp. T9-106–T9-110). doi: 10.1109/EPEPEMC.2010.5606653
(cited on page 5.)

Langtangen, H. P., & Pedersen, G. K. (2016). *Scaling of Differential Equations*. Springer. doi: 10.1007/978-3-319-32726-6
(cited on page 98.)

Laubichler, C. (2018). *Ageing Modelling of Li-Ion Cells Based on Longitudinal Data* (Master Thesis). Graz University of Technology, Graz, Austria.
(cited on page 57.)

Leuthner, S. (2013). Übersicht zu Lithium-Ionen-Batterien. In *Handbuch lithium-ionen-batterien* (pp. 13–19). Springer Berlin Heidelberg. doi: 10.1007/978-3-642-30653-2_2
(cited on page 3.)

Li, K., Deb, K., Zhang, Q., & Kwong, S. (2015, Oct). An Evolutionary Many-Objective Optimization Algorithm Based on Dominance and Decomposition. *IEEE Transactions on Evolutionary Computation*, *19*(5), 694-716. doi: 10.1109/TEVC.2014.2373386
(cited on page 45.)

Linden, D., & Reddy, T. (2002). *Handbook of batteries* (3rd ed.). McGraw-Hill.
(cited on page 2.)

Lyly, M., Ruokolainen, J., & Järvinen, E. (1999). ELMER – a finite element solver for multiphysics. *CSC-report on scientific computing*, *2000*, 156–159.
(cited on page 20.)

Mancini, R., & Volkwein, S. (2011). *Space mapping techniques for a coupled parameter dependent elliptic parabolic system* (Internal Report). Konstanz, Germany: Universität Konstanz.
(cited on page 27.)

Mathworks matlab [Computer software manual]. (1992). Natick, MA.
(cited on pages 37, 60, and 66.)

Metropolis, N., Rosenbluth, A. W., Rosenbluth, M. N., Teller, A. H., & Teller, E. (1953). Equation of State Calculations by Fast Computing Machines. *The Journal of Chemical Physics*, *21*(6), 1087-1092. doi: 10.1063/1.1699114
(cited on pages 6, 47, 48, 49, 52, and 55.)

Morris, M. (1991). Factorial Sampling Plans for Preliminary Computational Experiments. *Technometrics*, *33*(2), 161–174.
(cited on page 55.)

Newman, J., & Thomas-Alyea, K. E. (2004). *Electrochemical Systems* (3rd ed.). John Wiley & Sons, Inc., Hoboken, New Jersey. doi: ISBN:978-0471477563
(cited on pages 4, 14, 21, and 22.)

Ning, G., & Popov, B. N. (2004). Cycle Life Modeling of Lithium-Ion Batteries. *Journal of The Electrochemical Society*, *151*(10), A1584-A1591. doi: 10.1149/1.1787631
(cited on pages 4 and 21.)

Nyman, A., Ekström, H., & Fontes, E. (2018). *White paper: Modeling the Lithium-Ion Battery* (Tech. Rep.). COMSOL, Inc. (https://www.comsol.com/sf/offers/COMSOL_WhitePapers_Li-IonBattery-20200720.pdf, accessed 05.08.2020)
(cited on page 1.)

Papaspiliopoulos, O., & Roberts, G. O. (2008, Feb). Retrospective Markov chain Monte Carlo methods for Dirichlet process hierarchical models. *Biometrika*, *95*(1), 169-186. doi: 10.1093/biomet/asm086
(cited on page 78.)

Petzl, M., & Danzer, M. A. (2013, Sep). Advancements in OCV Measurement and Analysis for Lithium-Ion Batteries. *IEEE Transactions on Energy Conversion*, *28*(3), 675-681. doi: 10.1109/TEC.2013.2259490
(cited on page 16.)

Pichler, A. (2018). *Efficient Design of Experiment for testing the Ageing of Lithium-Ion Cells* (Master Thesis). Graz University of Technology, Graz, Austria.
(cited on page 57.)

Pichler, F. (2018). *Derivation of a Multi-Scale Battery Model and its High-Performance Computing Implementation* (PhD Thesis). University of Graz.
(cited on pages 21, 22, 69, 76, 83, and 87.)

Pichler, F., & Cifrain, M. (2014). Application-Related Battery Modelling: From Empirical to Mechanistic Approaches. In A. Thaler & D. Watzenig (Eds.), (pp. 53–69). Cham: Springer International Publishing. doi: 10.1007/978-3-319-02523-0_4
(cited on pages 4 and 16.)

Plett, G. (2016). *Equivalent-Circuit Methods* (Battery Management Systems ed., Vol. 2; G. Plett, Ed.). Artech House.
(cited on page 2.)

Ramadesigan, V., Chen, K., Burns, N. A., Boovaragavan, V., Braatz, R. D., & Subramanian, V. R. (2011). Parameter Estimation and Capacity Fade Analysis of Lithium-Ion Batteries Using Reformulated Models. *Journal of The Electrochemical Society*, *158*(9), A1048-A1054. doi: 10.1149/1.3609926
(cited on page 5.)

Randles, J. E. B. (1947). Kinetics of rapid electrode reactions. *Discuss. Faraday Soc.*, *1*, 11-19. doi: 10.1039/DF9470100011
(cited on page 14.)

Reddy, S. R., Scharrer, M. K., Pichler, F., Watzenig, D., & Dulikravich, G. S. (2019). Accelerating parameter estimation in Doyle–Fuller–Newman model for lithium-ion batteries. *COMPEL-The international journal for computation and mathematics in electrical and electronic engineering.*
(cited on pages 5, 9, and 86.)

Robič, T., & Filipič, B. (2005). Evolutionary Multi-Criterion Optimization. In C. C. Coello, A. H. Aguirre, & E. Zitzler (Eds.), (Vol. 3410, pp. 520–533). Berlin, Heidelberg: Springer.
(cited on pages 45 and 46.)

Saltelli, A., Tarantola, S., Campolongo, F., & Ratto, M. (2004). *Sensitivity Analysis in Practice: A Guide to Assessing Scientific Models*. New York, NY, USA: Halsted Press.
(cited on pages 34, 36, and 55.)

Santhanagopalan, S., Guo, Q., Ramadass, P., & White, R. E. (2006). Review of models for predicting the cycling performance of lithium ion batteries. *Journal of Power Sources*, *156*(2), 620 - 628. doi: DOI:10.1016/j.jpowsour.2005.05.070
(cited on pages 4 and 21.)

Santhanagopalan, S., Guo, Q., & White, R. E. (2007). Parameter Estimation and Model Discrimination for a Lithium-Ion Cell. *Journal of The Electrochemical Society*, *154*(3), A198-A206. doi: 10.1149/1.2422896
(cited on pages 5 and 66.)

Scharrer, M. K., Cifrain, M., & Prochazka, W. (2011). Mechanistic PDE Model for Impedance Simulation of Lithium-Ion Cells. In *Kraftwerk Batterie, Aachen.*
(cited on page 10.)

Scharrer, M. K., Haario, H., & Watzenig, D. (2014). Bayesian Inference for Lithium-Ion Cell Parameter Estimation. In A. Thaler & D. Watzenig (Eds.), (pp. 89–109). Cham: Springer International Publishing. doi: 10.1007/978-3-319-02523-0_6
(cited on pages 5, 6, and 9.)

Scharrer, M. K., Messner, S., & Hillbrand, B. (2016). *Validated state observers and state predictors* (Project iCOMPOSE Deliverable No. D3.3). Graz, Austria: Virtual Vehicle Research Center.
(cited on pages 15, 16, 61, and 62.)

Scharrer, M. K., Messner, S., & Szymanski, D. (2014). *Virtual system prototype for the development of the iCEM / virtual safety concept* (Project iCOMPOSE Deliverable No. D3.2). Graz, Austria: Virtual Vehicle Research Center.
(cited on pages 15 and 61.)

Scharrer, M. K., Pichler, F., Cifrain, M., & Watzenig, D. (2014a). Surrogate Parameter Identification for coupled 3D Lithium-Ion Cell Models. In *IGTE 2014.*
(cited on pages 9 and 11.)

Scharrer, M. K., Pichler, F., Cifrain, M., & Watzenig, D. (2014b). Surrogate parameter identification for coupled lithium-ion cell models. *Journal for Computation and Mathematics in Electrical and Electronic Engineering*, *34*(5), 1578–1588. doi: 10.1108/COMPEL-02-2015-0091
(cited on pages 9 and 11.)

Scharrer, M. K., Pichler, F., & Suhr, B. (2012, May). Simulation und Ansätze zur Parameteridentifikation eines 1D elektrochemischen Modells von Lithium-Ionen-Zellen. In *NAFEMS deutschsprachige Konferenz 2012* (pp. 106–109). NAFEMS.
(cited on page 41.)

Scharrer, M. K., Pichler, F., & Watzenig, D. (2021). *Statistical Inference for a High-Fidelity Lithium-Ion Cell Model.* (Accepted for publication in IPSE)
(cited on page 9.)

Scharrer, M. K., Suhr, B., & Watzenig, D. (2012, Sep). Surrogate Parameter Optimization based on Space Mapping for Lithium-Ion Cell Models. In *15th international IGTE symposium on numerical field calculation in electrical engineering* (pp. 368–380). Verlag der Technischen Universität Graz.
(cited on pages 10 and 41.)

Scharrer, M. K., Suhr, B., & Watzenig, D. (2013, Jun). A new Space Mapping Parameter Surrogate Optimization for Lithium-Ion Cell Models. In *4th inverse problems, design and optimization symposium.* IPDO.
(cited on page 10.)

Schmidt, A., Bitzer, M., Imre, A., & Guzzella, L. (2010). Experiment-driven electrochemical modeling and systematic parameterization for a lithium-ion battery cell. *Journal of Power Sources*, *195*(15), 5071 - 5080. doi: DOI:10.1016/j.jpowsour.2010.02.029
(cited on page 5.)

Sobol, I. (1967). On the distribution of points in a cube and the approximate evaluation of integrals. *U.S.S.R Computational Mathematics and Mathematical Physics*, *7*(4), 86–112. doi: https://doi.org/10.1016/0041-5553(67)90144-9
(cited on page 69.)

Solonen, A., Ollinaho, P., Laine, M., Haario, H., Tamminen, J., & Järvinen, H. (2012). Efficient MCMC for Climate Model Parameter Estimation: Parallel Adaptive Chains and Early Rejection. *Bayesian Analysis*, *7*(3), 715–736.
(cited on pages 51 and 78.)

Speltino, C., Domenico, D. D., Fiengo, G., & Stefanopoulou, A. G. (2009). On the Experimental Identification of an Electrochemical Model of a Lithium-Ion Battery: Part II. In *The european control conference.*
(cited on pages 5 and 76.)

Tagade, P., Hariharan, K. S., Basu, S., Verma, M. K. S., Kolake, S. M., Song, T., ... Doo, S. (2016). Bayesian calibration for electrochemical thermal model of lithium-ion cells. *Journal of Power Sources*, *320*, 296 - 309. doi: https://doi.org/10.1016/j.jpowsour.2016.04.106
(cited on page 6.)

Tierney, L., & Mira, A. (1999). Some adaptive Monte Carlo methods for Bayesian inference. *Statistics in Medicine*, *18*(18), 2507-2515. doi: 10.1002/(SICI)1097-0258(19990915/30)18:17/18<2507::AID-SIM272>3.0.CO;2-J
(cited on page 53.)

Tröltzsch, F. (2010). *Optimal Control of Partial Differential Equations: Theory, Methods and Applications*. American Mathematical Society.
(cited on page 105.)

Uddin, K., Perera, S., Widanage, W. D., Somerville, L., & Marco, J. (2016). Characterising Lithium-Ion Battery Degradation through the Identification and Tracking of Electrochemical Battery Model Parameters. *Batteries*, *2*(2). doi: 10.3390/batteries2020013
(cited on page 5.)

United Nations Framework Convention on Climate Change. (2015). *Paris Declaration on Electro-Mobility and Climate Change & Call to Action.* (http://newsroom.unfccc.int/media/521376/paris-electro-mobility-declaration.pdf, accessed 20.01.2020)
(cited on page 1.)

Virtanen, P., Gommers, R., Oliphant, T. E., Haberland, M., Reddy, T., Cournapeau, D., ... Contributors (2019, Jul). SciPy 1.0–Fundamental Algorithms for Scientific Computing in Python. *arXiv e-prints*, arXiv:1907.10121.
(cited on pages 37 and 66.)

Weinan, E., Engquist, B., Li, X., Ren, W., & Vanden-Eijnden, E. (2007). Heterogeneous multiscale methods: a review. *Commun. Comput. Phys*, *2*(3), 367–450.
(cited on page 18.)

Welford, B. P. (1962). Note on a Method for Calculating Corrected Sums of Squares and Products. *Technometrics*, *4*(3), 419–420. doi: 10.1080/00401706.1962.10490022
(cited on page 50.)

Wirgin, A. (2004, Jan). *The inverse crime.* arXiv. (cited 2019 Jun 26)
(cited on pages 6 and 46.)

Wolpert, D. H., & Macready, W. G. (1997). No free lunch theorems for optimization. *IEEE transactions on evolutionary computation*, *1*(1), 67–82.
(cited on pages 45 and 55.)

Zhang, S. S. (2013). Liquid electrolyte lithium/sulfur battery: Fundamental chemistry, problems, and solutions. *Journal of Power Sources*, *231*(0), 153 - 162. doi: http://dx.doi.org/10.1016/j.jpowsour.2012.12.102
(cited on page 5.)